AFWL-TR-
85-92

(2)

AD-A169 133

THE RESPONSE OF SOIL TO IMPULSE LOADS USING THE SPLIT-HOPKINSON PRESSURE BAR TECHNIQUE

Conrad W. Felice

May 1986

DTIC
ELECTE
JUL 0 1 1986
S D
D

Final Report

Approved for public release; distribution unlimited.

AIR FORCE WEAPONS LABORATORY
Air Force Systems Command
Kirtland Air Force Base, NM 87117-6008

E COPY

86 7 1 096

This final report was prepared by the Air Force Weapons Laboratory, Kirtland Air Force Base, New Mexico, under Job Order 627A0101. Captain Conrad W. Felice (NTES) was the Laboratory Project Officer-in-Charge.

When Government drawings, specifications, or other data are used for any purpose other than in connection with a definitely Government-related procurement, the United States Government incurs no responsibility or any obligation whatsoever. The fact that the Government may have formulated or in any way supplied the said drawings, specifications, or other data, is not to be regarded by implication, or otherwise in any manner construed, as licensing the holder, or any other person or corporation; or as conveying any rights or permission to manufacture, use, or sell any patented invention that may in any way be related thereto.

This report has been authored by an employee of the United States Government. Accordingly, the United States Government retains a nonexclusive, royalty-free license to publish or reproduce the material contained herein, or allow others to do so, for the United States Government purposes.

This report has been reviewed by the Public Affairs Office and is releasable to the National Technical Information Service (NTIS). At NTIS, it will be available to the general public, including foreign nations.

If your address has changed, if you wish to be removed from our mailing list, or if your organization no longer employs the addressee, please notify AFWL/NTES, Kirtland AFB, NM 87117 to help us maintain a current mailing list.

This technical report has been reviewed and is approved for publication.

CONRAD W. FELICE
Captain, USAF
Project Officer

DAVID H. ARTMAN, JR
Major, USAF
Chief, Applications Branch

FOR THE COMMANDER

CARL L. DAVIDSON, Colonel, USAF
Chief, Civil Engineering Research Div

DO NOT RETURN COPIES OF THIS REPORT UNLESS CONTRACTUAL OBLIGATIONS OR NOTICE ON A SPECIFIC DOCUMENT REQUIRES THAT IT BE RETURNED.

UNCLASSIFIED

SECURITY CLASSIFICATION OF THIS PAGE

REPORT DOCUMENTATION PAGE

1a. REPORT SECURITY CLASSIFICATION Unclassified	1b. RESTRICTIVE MARKINGS
2a. SECURITY CLASSIFICATION AUTHORITY	3. DISTRIBUTION/AVAILABILITY OF REPORT Approved for public release; distribution unlimited.
2b. DECLASSIFICATION/DOWNGRADING SCHEDULE	
4. PERFORMING ORGANIZATION REPORT NUMBER(S) AFWL-TR-85-92	5. MONITORING ORGANIZATION REPORT NUMBER(S)
6a. NAME OF PERFORMING ORGANIZATION Air Force Weapons Laboratory 6b. OFFICE SYMBOL (If applicable) NTES	7a. NAME OF MONITORING ORGANIZATION
6c. ADDRESS (City, State and ZIP Code) Kirtland Air Force Base, NM 87117	7b. ADDRESS (City, State and ZIP Code)
8a. NAME OF FUNDING/SPONSORING ORGANIZATION 8b. OFFICE SYMBOL (If applicable)	9. PROCUREMENT INSTRUMENT IDENTIFICATION NUMBER
8c. ADDRESS (City, State and ZIP Code)	10. SOURCE OF FUNDING NOS. PROGRAM ELEMENT NO. 63311F; PROJECT NO. 627A; TASK NO. 01; WORK UNIT NO. 01
11. TITLE (Include Security Classification) THE RESPONSE OF SOIL TO IMPULSE LOADS USING THE SPLIT-HOPKINSON PRESSURE BAR TECHNIQUE	
12. PERSONAL AUTHOR(S) Felice, Conrad W.	
13a. TYPE OF REPORT Final Report 13b. TIME COVERED FROM Mar 82 TO Jun 85	14. DATE OF REPORT (Yr., Mo., Day) 1986 May 15. PAGE COUNT 320
16. SUPPLEMENTARY NOTATION	

17. COSATI CODES			18. SUBJECT TERMS (Continue on reverse if necessary and identify by block number)
FIELD	GROUP	SUB. GR.	Compacted Soil, High Strain-Rate, Split-Hopkinson, Pressure Bar
08	13		

19. ABSTRACT (Continue on reverse if necessary and identify by block number)

The split-Hopkinson pressure bar (SHPB) technique has been adapted to measure the dynamic response of soil to impulse loads. The SHPB technique is relatively simple and can significantly extend the range of stresses and strain-rates that can be applied beyond the capabilities of current equipment used for dynamic laboratory soil investigations. This capability will assist in satisfying the demand for soil property data which more closely reflects environments related to weapon effects problems.

The various considerations involved in designing an SHPB experiment and evaluating the data with soil as a specimen are discussed in detail. Soils have several characteristics which complicate their use as specimens in an SHPB experiment: low wave speeds, nonlinear hysteretic behavior, and low unconfined compressive strength compared to the applied loads. Insight is provided as to how these factors affect experimental accuracy and data reliability.

(over)

20. DISTRIBUTION/AVAILABILITY OF ABSTRACT UNCLASSIFIED/UNLIMITED ☒ SAME AS RPT ☐ DTIC USERS ☐	21. ABSTRACT SECURITY CLASSIFICATION Unclassified
22a. NAME OF RESPONSIBLE INDIVIDUAL Capt C. W. Felice	22b. TELEPHONE NUMBER (Include Area Code) (505) 846-6471 22c. OFFICE SYMBOL NTES

DD FORM 1473, 83 APR EDITION OF 1 JAN 73 IS OBSOLETE.

UNCLASSIFIED

SECURITY CLASSIFICATION OF THIS PAGE

19. ABSTRACT (Continued)

It has been shown herein that the assumptions necessary to obtain meaningful data from an SHPB experiment can be satisfied when using compacted soil specimens constrained to a nearly uniaxial strain state. Also the ability to replicate experimental results has been established. In addition, the dynamic soil stress-strain response was found to be governed principally by the initial gas porosity of the specimen and no strain-rate dependency was exhibited at strains less than the initial gas porosity. A compliment of stress-strain curves are presented for specimens prepared at several combinations of moisture and density with applied stresses and strain-rates up tp 520 MPa and 4000/s^{-1}, respectively.

ACKNOWLEDGMENTS

The author would like to extend his appreciation to Professor J. M. Olsen for the advice and guidance he provided throughout this research effort. In addition, I would like to acknowledge the ideas, comments, criticisms, and support of the many people who contributed to the successful completion of this dissertation. In particular, special gratitude is due Dr. E. S. Gaffney for his infinite patience during the many hours he provided advice and assistance, and to Dr. J. A. Brown for providing his expertise, and time in the laboratory, without which this effort would not have been possible. To these gentleman I am deeply indebted.

Acknowledgment is also due the Air Force Weapons Laboratory for its support of this research effort, in particular, to Dr. M. A. Plamondon, Technical Advisor to the Civil Engineering Research Division. I would also like to thank the Air Force Office of Scientific Research for providing financial support.

And to my wife Laura, my sincere and heartfelt gratitude for the patience, understanding and encouragement she provided throughout the several years

QUALITY INSPECTED 1

Codes
Dist | Avail and/or Special
A-1

which were required for the completion of this effort. And finally to my daughter Allyson, who endured the absence of her father many times in order to make this possible.

TABLE OF CONTENTS

ACKNOWLEDGMENTS iii

LIST OF FIGURES viii

LIST OF TABLES xv

1. INTRODUCTION 1

2. DEVELOPMENT OF THE SPLIT-HOPKINSON PRESSURE BAR EXPERIMENT 5

2.1 The Hopkinson Pressure Bar 5
2.2 The Davies Bar 8
2.3 The Kolsky Bar 11
2.4 Theory of Measurement 14
2.5 Contributions of Recent Investigators 29
2.6 Application of the SHPB to Soils 39

3. EXPERIMENTAL APPARATUS AND MATERIAL 42

3.1 Experimental Apparatus 42
3.2 Soil Characteristics 49
3.3 Specimen Preparation 50
3.4 Specimen Confining System 57

4. EXPERIMENTAL ASSUMPTIONS AND DATA ANALYSIS 60

4.1 Experimental Assumptions 60
4.1.1 Uniform Distribution of Stress 60
4.1.2 Wave Dispersion 62
4.1.3 Stress Variation Over the Cross Section of the Bar 67
4.1.4 Specimen-Bar Interface Friction 68
4.2 Data Reduction Procedure 70
4.2.1 Raw Data 71
4.2.2 Processed Data 71

5. PRESENTATION OF EXPERIMENTAL RESULTS 87

5.1 Experimental Results 87
5.2 Stress-Strain Response 91
5.3 Uniaxial Strain Path 94

5.4 Experimental Replication..... 95
5.5 Soil Behavior..... 103

6. DISCUSSION OF EXPERIMENTAL RESULTS..... 113

6.1 Experimental Assumptions..... 113
6.1.1 Uniform Distribution of Stress..... 114
6.1.2 Wave Dispersion..... 120
6.1.3 Stress Variation Over the Cross Section of the Bar..... 121
6.1.4 Specimen-Bar Interface Friction..... 126
6.2 Experimental Replication..... 129
6.3 Soil Behavior..... 132
6.4 Strain in Excess of Initial Gas Porosity..... 138
6.4.1 Loss of Soil and Moisture..... 140
6.4.2 Compression of Pore Water..... 143
6.4.3 Radial Expansion of the Confining Cylinder and Specimen..... 143
6.4.4 Strain Correction..... 144
6.5 Strain-Rate Dependence..... 146
6.6 Conditions of Experiment..... 151
6.7 Application of the SHPB Technique..... 152

7. CONCLUSIONS AND RECOMMENDATIONS..... 156

7.1 Conclusions..... 156
7.2 Recommendations..... 158

Appendices

A. MATHEMATICS OF THE DISPERSION CORRECTION PROCEDURE.. 162

B. GAS GUN AND INSTRUMENTATION..... 170

C. DERIVATION OF THE RELATIONSHIP BETWEEN THE STRIKER BAR IMPACT VELOCITY AND THE MAGNITUDE OF THE APPLIED STRESS WAVE..... 186

D. EXPERIMENTAL PROCEDURE CHECKLIST..... 189

E. SUPPORTING TABLES..... 192

F. PROCEDURE AND RESULTS OF MOISTURE/DENSITY VARIATION STUDY..... 204

G. REDUCE CODE..... 212

H. SPECIMEN MOISTURE/DENSITY RELATIONSHIPS TO THE HARVARD MINIATURE COMPACTION CURVE..... 238

I. PLOTTED EXPERIMENTAL RESULTS WITH SUMMARY DATA..... 242

J. GROSS STRAIN CORRECTION..... 292

REFERENCES..... 298

LIST OF FIGURES

Figure		Page
2.1.	The Hopkinson bar (Hopkinson, 1914).....	6
2.2.	The Davies bar (adapted from Davies, 1948).....	9
2.3.	The Kolsky bar (adapted from Kolsky, 1949).....	13
2.4.	Forces acting on a bar in longitudinal motion...	15
2.5.	Specimen in place between pressure bars.....	20
2.6.	Derivation of reflection and transmission coefficients.....	22
2.7.	Representation of elastic wave interaction in the specimen and pressure bars caused by the loading stress wave.....	23
2.8.	Particle velocity history at the specimen-bar interfaces, experiment 115.....	25
2.9.	Strain-rate-time response for experiment 115....	27
2.10.	Strain-time response for experiment 115.....	28
2.11.	Interface stress averaging.....	30
2.12.	Solution to the fundamental mode of vibration of the dispersion equation (adapted from Davies, 1948).....	36
2.13.	Comparison of the exact solution (solid line) and the polynomial approximation to the fundamental mode of vibration of the dispersion equation.....	38
3.1.	The Split-Hopkinson pressure bar apparatus.....	43
3.2.	Split-Hopkinson pressure bar system arrangement (Nagy and Muelenhaupt, 1983).....	44
3.3.	Split-Hopkinson pressure bar schematic.....	45

3.4. Particle size distribution curve (o by sieve and Δ by hydrometer..... 51

3.5. Results from Harvard miniature compaction procedure..... 52

3.6. Hydraulic press used for static compaction..... 54

3.7. Spacer rings, confining cylinder, and plungers.. 55

3.8. Confining cylinder with specimen positioned between the pressure bars..... 59

4.1. Uncorrected incident and reflected (inverted) stress waves..... 63

4.2. Comparison of uncorrected and corrected reflected stress waves (waves have been inverted)..... 64

4.3. Corrected incident and reflected (inverted) stress waves..... 65

4.4. Uncorrected stress waves for a 6.35 mm specimen, experiment 115..... 72

4.5. Uncorrected stress waves for a 12.7 mm specimen, experiment 134..... 73

4.6. Uncorrected and corrected stress waves for a 6.35 mm specimen, experiment 115..... 74

4.7. Uncorrected and corrected stress waves for a 12.7 mm specimen, experiment 134..... 75

4.8. Stress waves for a 6.35 mm specimen corrected and time-shifted to the specimen-bar interfaces, experiment 115..... 76

4.9. Stress waves for a 12.7 mm specimen corrected and time-shifted to the specimen-bar interfaces, experiment 134..... 77

4.10. Strain-rate-time response for a 6.35 mm specimen, experiment 115..... 79

4.11. Strain-rate-time response for a 12.7 mm specimen, experiment 134..... 80

4.12. Strain-time response for a 6.35 mm specimen, experiment 115..... 81

4.13. Strain-time response for a 12.7 mm specimen, experiment 134..... 82

4.14. Stress-time response for a 6.35 mm specimen, experiment 115..... 83

4.15. Stress-time response for a 12.7 mm specimen, experiment 134..... 84

4.16. Stress-strain response for a 6.35 mm specimen, experiment 115..... 85

4.17. Stress-strain response for a 12.7 mm specimen, experiment 134..... 86

5.1. Stress-strain response for experiment 55..... 90

5.2. Stress-strain response for experiment 132..... 92

5.3. Replicate experiments for 6.35 mm specimens at an applied stress of approximately 250 MPa .. 97

5.4. Replicate experiments for 6.35 mm specimens at an applied stress of approximately 400 MPa... 98

5.5. Replicate experiments for 6.35 mm specimens at an applied stress of approximately 520 MPa... 99

5.6. Replicate experiments for 12.7 mm specimens at an applied stress of approximately 250 MPa... 100

5.7. Replicate experiments for 12.7 mm specimens at an applied stress of approximately 400 MPa... 101

5.8. Replicate experiments for 12.7 mm specimens at an applied stress of approximately 520 MPa... 102

5.9. Stress-strain response for 6.35 mm specimens to a range of applied stresses..... 104

5.10. Stress-strain response for 12.7 mm specimens to a range of applied stresses..... 105

5.11. Comparison of stress-strain response based on specimen length to an applied stress of approximately 250 MPa..... 107

5.12. Comparison of stress-strain response based on specimen length to an applied stress of approximately 400 MPa..... 108

5.13. Comparison of stress-strain response based on specimen length to an applied stress of approximately 520 MPa..... 109

5.14. Comparison of stress-strain response for 6.35 mm specimens based on moisture content to an applied stress of approximately 250 MPa... 111

5.15. Comparison of stress-strain response for 12.7 mm specimens based on moisture content to an applied stress of approximately 400 MPa... 112

6.1. Stress-strain response for experiment 134..... 115

6.2. Stress-time response of the specimen-bar interfaces, experiment 134..... 116

6.3. Average specimen stress-time response and the difference between the stress-time response of the specimen-bar interfaces, experiment 134..... 117

6.4. Comparison of stress-strain response using the uncorrected and corrected stress waves..... 122

6.5. Incident stress wave modeled with n = 17 and n = 9 Fourier terms..... 125

6.6. Stress-strain response computed from stress waves modeled with n = 17 and n = 9 Fourier terms..... 127

6.7. One-dimensional soil stress-strain response (adapted from Dass and Bratton, 1983)..... 133

6.8. Comparison of computed specimen strain and initial gas porosity..... 139

6.9. Comparison of computed specimen strain and component corrected strain..... 145

6.10. Comparison of computed specimen strain and gross corrected strain..... 147

6.11. Stress-strain-rate plot for 6.35 mm specimens compacted at optimum conditions..... 148

6.12. Stress-strain-rate plot for 12.7 mm specimens compacted at optimum conditions..... 149

B.1. Gas gun (Nagy and Muelenhaupt, 1983)..... 172

B.2. Gas gun calibration curve..... 174

B.3. Laser velocity measuring system..... 176

B.4. Electro-hydraulic control block diagram and monitor unit circuits (Nagy and Muelenhaupt, 1983)..... 178

B.5. Front view of electro-hydraulic control and monitor unit..... 179

B.6. Rear view of electro-hydraulic control and monitor unit..... 180

B.7. Signal conditioner amplifier (Nagy and Muelenhaupt, 1983)..... 183

B.8. Wiring diagram for signal conditioner input connector, half bridge operation (Nagy and Muelenhaupt, 1983)..... 185

F.1. Density variation for specimen 1..... 206

F.2. Density variation for specimen 2..... 207

F.3. Density variation for specimen 3..... 208

F.4. Moisture variation for specimen 1..... 209

F.5. Moisture variaiton for specimen 2..... 210

F.6. Moisture variaiton for specimen 3..... 211

H.1. Moisture/density relationship to the Harvard miniature compaction curve for specimens compacted dry of optimum..... 239

H.2. Moisture/density relationship to the Harvard miniature compaction curve for specimens compacted near optimum..... 240

H.3. Moisture/density relationship to the Harvard miniature compaction curve for specimens compacted wet of optimum..... 241

I.1. Stress-strain response for experiment 31..... 244

I.2. Stress-strain response for experiment 32..... 245

I.3. Stress-strain response for experiment 38..... 246

I.4. Stress-strain response for experiment 39..... 247
I.5. Stress-strain response for experiment 40..... 248
I.6. Stress-strain response for experiment 41..... 249
I.7. Stress-strain response for experiment 42..... 250
I.8. Stress-strain response for experiment 55..... 251
I.9. Stress-strain response for experiment 56..... 252
I.10. Stress-strain response for experiment 57..... 253
I.11. Stress-strain response for experiment 58..... 254
I.12. Stress-strain response for experiment 59..... 255
I.13. Stress-strain response for experiment 60..... 256
I.14. Stress-strain response for experiment 61..... 257
I.15. Stress-strain response for experiment 62..... 258
I.16. Stress-strain response for experiment 71..... 259
I.17. Stress-strain response for experiment 72..... 260
I.18. Stress-strain response for experiment 73..... 261
I.19. Stress-strain response for experiment 74..... 262
I.20. Stress-strain response for experiment 75..... 263
I.21. Stress-strain response for experiment 76..... 264
I.22. Stress-strain response for experiment 112..... 265
I.23. Stress-strain response for experiment 113..... 266
I.24. Stress-strain response for experiment 114..... 267
I.25. Stress-strain response for experiment 115..... 268
I.26. Stress-strain response for experiment 116..... 269
I.27. Stress-strain response for experiment 117..... 270
I.28. Stress-strain response for experiment 118..... 271
I.29. Stress-strain response for experiment 119..... 272

I.30. Stress-strain response for experiment 131..... 273
I.31. Stress-strain response for experiment 132..... 274
I.32. Stress-strain response for experiment 133..... 275
I.33. Stress-strain response for experiment 134..... 276
I.34. Stress-strain response for experiment 135..... 277
I.35. Stress-strain response for experiment 136..... 278
I.36. Stress-strain response for experiment 137..... 279
I.37. Stress-strain response for experiment 138..... 280
I.38. Stress-strain response for experiment 139..... 281
I.39. Stress-strain response for experiment 145..... 282
I.40. Stress-strain response for experiment 146..... 283
I.41. Stress-strain response for experiment 147..... 284
I.42. Stress-strain response for experiment 148..... 285
I.43. Stress-strain response for experiment 162..... 286
I.44. Stress-strain response for experiment 163..... 287
I.45. Stress-strain response for experiment 164..... 288
I.46. Stress-strain response for experiment 165..... 289
I.47. Stress-strain response for experiment 166..... 290
I.48. Stress-strain response for experiment 167..... 291
J.1. Linear regression fit to data for specimens compacted at conditions near optimum..... 294

LIST OF TABLES

Table		Page
6.1.	Fourier Coefficients, Values for R/Λ, and C_n/C_0 for the Incident Wave of Experiment 134	124
6.2.	Component Contribution to Specimen Strain	142
E.1.	Initial Specimen Parameters	193
E.2.	Moisture Loss Between the Time a Specimen is Prepared and the Time it is Positioned Between the Bars	195
E.3.	Experimental Results	196
E.4.	Specimen Seating Strain	198
E.5.	Computed Radial Displacements Due to Applied Load	199
E.6.	Mass of Soil Lost During the Experiment	201
E.7.	Measured Moisture Content Changes Before and After the Experiment	202
J.1.	Strain Correction Data	295
J.2.	Strain Correction Results	297

1. INTRODUCTION

The response of soil to high amplitude, short duration, impulse loads characteristic of the airblast and ground motion from a weapon explosion is an important problem in protective construction design and analysis (Calhoun and Kraft, 1966; Schindler, 1968). A means of understanding the soil response is through laboratory investigation. However, the laboratory environment must be able to reflect the type of confinement, magnitude of stress change, and the time scale of loading expected in the problem (Whitman, 1970).

A reasonable assumption is that the soil response in the superseismic region of an airblast will be approximately one-dimensional (Crawford, Higgins, and Bultmann, 1974). The time scale of loading is essentially instantaneous (Crawford et al., 1974). Peak stresses can be in excess of 1000 MPa (Brode, 1984). To model the soil response to this type of loading, uniaxial strain devices have been developed (e.g., Schindler, 1968). Current devices can apply stresses up to 400 MPa with loading times on the order of 0.3 milliseconds (e.g., Jackson, Ehrgott, and Rohani, 1980).

Over the last thirty-five years the split-Hopkinson

presure bar (SHPB) technique has been used as a tool for investigating the response of metals, rocks, ceramics, foams, and other materials to short duration compressive impulse loads (e.g., Lindholm, 1964; Hodge and Wasley, 1969; Christensen, Swanson, and Brown, 1972). Some of the SHPB devices in use can apply stresses in excess of 1000 MPa with loading times on the order of 0.04 milliseconds (Gaffney and Brown, 1984). Until recently, the SHPB technique has not been readily applied to the field of soil mechanics. Because of the ability to apply high stresses at a high rate of loading, the adaption of the SHPB technique to measure the dynamic response of soil seems to be a natural extension. The objective of this research has been to determine whether the SHPB technique can be effectively used to measure the dynamic response of soil.

The use of soil as specimens in a SHPB experiment is not a trivial matter because soils hava very low wave speeds ($\cong$ 300 m/s) in comparison to the traditional materials tested in the SHPB (e.g., steel, 5000 m/s). Soils, also exhibit nonlinear hysteretic behavior which will cause the amplitude of a stress wave to attenuate as it propagates through it (Hendron and Auld, 1968). In addition, the relatively low unconfined compressive strength of the soil (e.g., < 0.1 MPa) creates difficulties in controlling boundary conditions.

This dissertation is organized into seven chapters. Chapter 2 presents the development of pressure bar experimentation from its inception by Hopkinson (1914), through the contributions of Davies (1948), and the introduction of the SHPB method by Kolsky (1949). Also presented is the basic theory of measurement used in reducing the experimental data, as well as contributions to the method made by recent investigators, and the methods application to soil mechanics.

Chapter 3 describes the SHPB apparatus, the characteristics of the soil, and how the specimens were prepared. The assumptions of the experiment and their bearing on experimental results as well as the data reduction procedure have been addressed in chapter 4. Chapter 5 presents the experimental results in terms of the soil stress-strain response, and establishes that the response is nearly one of uniaxial strain. In addition, the ability to replicate experimental results is demonstrated and the observed soil behavior at different compaction conditions to a range of applied stresses are presented. Chapter 6 establishes that the experimental assumptions can indeed be satisfied when using soil specimens in a SHPB experiment. The results presented in chapter 5 are also analyzed to evaluate the dominant parameter governing the observed stress-strain response and a strain-rate independence is established for specimen

strains less than the initial gas porosity. In addition, specimen conditions that may lead to erroneous stress-strain response and an evaluation of the SHPB experiment are presented. Chapter 7 presents the conclusions drawn from the analyses and provides recommendations for further research. Ten appendices have been included to supplement and support the discussions in the main text.

2. DEVELOPMENT OF THE SPLIT-HOPKINSON PRESSURE BAR EXPERIMENT

2.1 The Hopkinson Pressure Bar

In 1914, Bertram Hopkinson devised a method to experimentally study the mechanical behavior of solids in response to short duration impulse loads. The main components of the apparatus constructed by Hopkinson were a long cylindrical steel bar, a time piece, and a ballistic pendulum (see figure 2.1). As shown in figure 2.1, the cylindrical steel bar was suspended by threads, such that it was free to swing in a vertical plane and remain parallel to its original position. The time piece was the same diameter as the cylindrical bar and attached to it by magnetic attraction.

The experiment was initiated by the impact of a lead bullet or the detonation of gun cotton, near the end of the cylindrical bar opposite the end to which the time piece was attached. The impact produced a compressive stress wave that was assumed to propagate down the length of the bar and through the joint between the bar and time piece without distortion. The stress distribution over the cross section of the bar was assumed to be uniform. Upon reaching the end of the time piece, the compressive stress

1-GUN COTTON CHARGE
2-STEEL ROD
3-TIME PIECE
4-BALLISTIC PENDULUM
5-RECORDING DEVICES

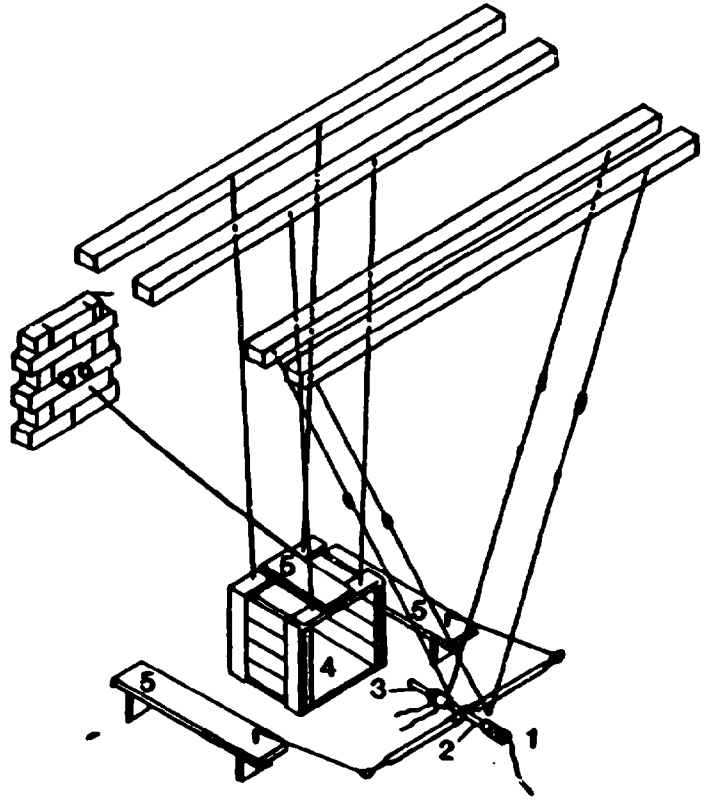

Figure 2.1. The Hopkinson bar (Hopkinson, 1914).

wave was assumed to reflect as a tensile wave. The joint between the bar and the time piece could not sustain a tensile force greater than the magnetic force connecting them. Hence, when the tensile force across the joint exceeded the magnetic force, the time piece would separate from the bar with a given amount of momentum. This momentum was measured by the ballistic pendulum. The momentum trapped in a given length time piece corresponded to the area under the stress-time curve between points of equal pressure, separated by the time required for the wave to travel the length of the time piece twice. By measuring the momentum delivered to different length time pieces, the area under the stress-time curve for different time intervals could be obtained allowing a complete stress-time curve to be constructed. However, the precise form of the stress-time curve could not be ascertained. This is because the commencement of the different intervals was not known. Although the precise form of the stress-time curve could not be determined, the maximum stress and the total duration of impact could always be evaluated.

Despite its innovative approach, Hopkinson's method suffered from several experimental, as well as theoretical, limitations. Experimentally, the force necessary to separate the bar and time piece was unknown. Also, the available intrumentation could not detect the

commencement of the time interval over which the momentum was measured. Theoretically, it was assumed that the applied stress would be uniform over the cross section of the bar and that the stress wave would propagate down the bar without distortion. These limitations were addressed and overcome through an extensive study of the Hopkinson bar method by Davies (1948).

2.2 The Davies Bar

Davies (1948) made several changes to the original experimental method developed by Hopkinson. The generated stress wave produced both longitudinal and radial displacements as it propagated down the bar. Davies developed a means of measuring the displacements electrically through a bar condenser unit mounted on the free end of the pressure bar (see figure 2.2). The condenser unit was initially charged to a high voltage that would be constant for small time intervals. The displacements caused a change in capacitance of the condenser unit, producing an electrical signal that was displayed as a function of time on a cathode ray oscillograph. Using elastic wave theory, Davies translated the electrical records into a precise stress-time curve. The electrical recording system avoided the use of a time piece, and alleviated the associated experimental problems. Therefore, with the introduction of electrical

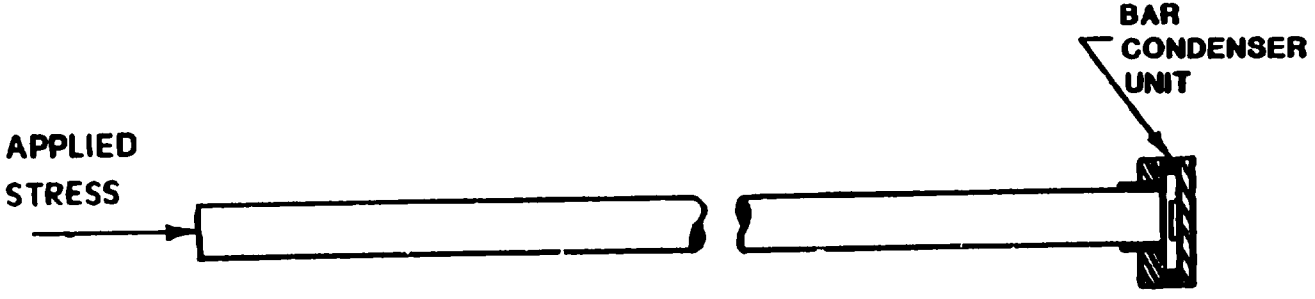

Figure 2.2. The Davies bar (adapted from Davies, 1948).

data recording, the experimental limitations associated with Hopkinson's original experimental method are avoided.

As part of the same study, Davies (1948) described the phenomenon of wave dispersion and established the accuracy of the experimental results when assuming one-dimensional wave propagation in the pressure bar. One-dimensional elastic wave theory assumes that a propagating wave will travel without change of form, at a constant velocity (C_0), that is independent of wavelength (Λ). The constant longitudinal velocity (C_0) can be expressed as $C_0^2 = E/\rho$, where E is Young's modulus and ρ is mass density. This assumption is only true if Λ of the propagating wave is long compared to the radius (R) of the bar. The equation governing the longitudinal vibrations of a infinitely long circular cylinder (referred to in the literature as the dispersion equation), developed independently by Pochhammer (1876) and Chree (1889), shows that the one-dimensional assumption will only be approximate, as the velocity of wave propagation will depend on Λ.

The compressive stress wave in a pressure bar experiment is composed of many frequencies. Evidence of this will be shown in section 4.1. Because the wave velocity (C_n) will depend on Λ, each frequency component will travel at a different C_n. With some frequency components travelling faster than others, the wave will

change form or disperse as it progagates. The amount a wave disperses will effect the uniformity of stress distribution over the cross section of the bar. The more a wave disperses, the less uniform the stress distribution. Measurements in the experiment are made at the surface of the pressure bar (see figure 2.2). Therefore, if the surface measurements do not represent the behavior over the cross section of the bar, the accuracy of the experiment is reduced.

By using the dispersion equation, Davies (1948) showed that the oscillations in the recorded displacement history were attributable to dispersion and not experimental inaccuracies. He also established the error in measuring the displacement history at the surface of the pressure bar to be $\pm$ 3 percent, provided that $R/\Lambda < 0.1$.

2.3 The Kolsky Bar

With the experimental and theoretical foundations of the method established, Kolsky (1949) modified the apparatus to permit dynamic material properties to be determined by indirect measurments. Kolsky sandwiched a thin cylindrical specimen (i.e., having an aspect ratio, $l/d \cong 0.1$, where l is the specimen length, and d is the specimen diameter) between two pressure bars. The pressure bars were fitted with condenser microphones for data

recording. He then applied an impact load such that a compressive stress wave propagated toward the specimen (see figure 2.3). When the propagating stress wave reaches the specimen, a portion of it will be reflected as a tensile wave and a portion will be transmitted through the specimen. The amplitudes of the reflected and transmitted waves will depend on the physical properties of the specimen as well as those of the pressure bars. By assuming a uniform distribution of stress and strain along the longitudinal axis of the specimen, Kolsky was able to develop relationships between the incident and transmitted displacements (recorded at the respective condenser microphones mounted on the bars) and the average stress, strain, and strain-rate in the specimen. These equations will be derived in section 2.4. This experimental method is now known as the Kolsky method, or the split-Hopkinson pressure bar (SHPB) method.

By using thin specimens, Kolsky attempted to avoid the complication of axial inertia. Radial inertia effects were accounted for through a numerical correction that assumed a frictionless specimen-bar interface. The effects of axial and radial inertia in a SHPB experiment are important because they act to oppose the equilibration of stress within the specimen. Kolsky determined that by using a thin layer of lubrication between the specimen, and the bars, the specimen-bar interfaces could be assumed

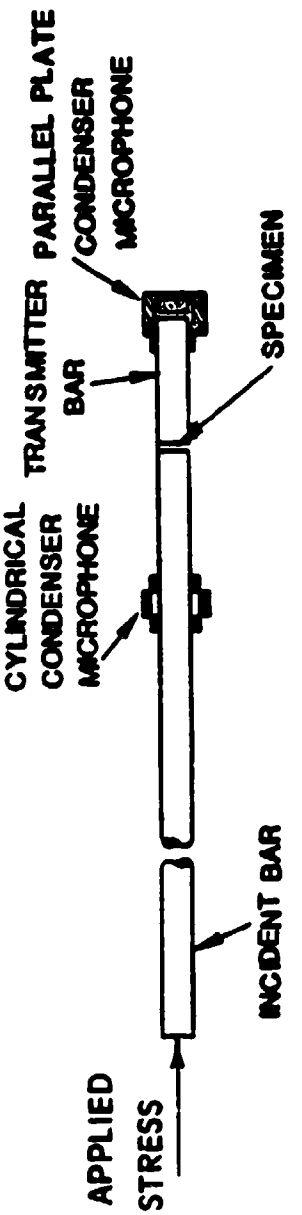

Figure 2.3. The Kolsky bar (adapted from Kolsky, 1949).

to be frictionless.

2.4 Theory of Measurement

Assuming that a wave generated from a disturbance produced in an isotropic elastic bar propagates parallel to the longitudinal axis of the bar such that it can be considered to be a plane wave, the general form of the wave equation will be one-dimensional. In the one-dimensional case, the elements of the bar will extend and contract with no lateral displacement of the axis of the bar (Kolsky, 1963). A one-dimensional condition is idealized in figure 2.4. The assumptions of the one-dimensional condition are: (1) each plane cross section will remain plane while in motion, (2) the stress over the cross section will be uniform, and (3) that the wavelength of the wave will be long compared to the cross sectional dimension of the bar (Kolsky, 1963).

Isolating a small element of the bar, dx, with cross sectional area A, the stress at section A-A will be σ and the stress at section B-B will be $\sigma + (\partial\sigma / \partial x)\, dx$. Taking the x-axis as the direction of wave propagation, the components of Newton's second law of motion ($F = m\, a$, where F is force, m is mass, and a is acceleration) can be written as;

$$F = \left[\sigma + \frac{\partial \sigma}{\partial x}\, dx - \sigma\right] A \,, \qquad (2.1)$$

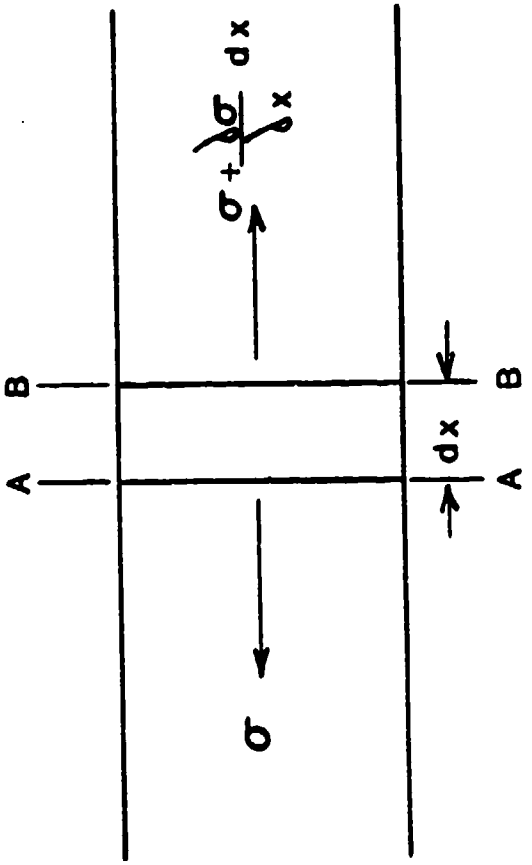

Figure 2.4. Forces acting on a bar in longitudinal motion.

$$F = \frac{\partial \sigma}{\partial x} dx\, A \ , \tag{2.2}$$

$$m = \rho\, A\, dx \ , \tag{2.3}$$

$$a = \frac{\partial^2 U}{\partial t^2} \ , \tag{2.4}$$

where ρ is the mass density of the bar and U is displacement. Combining terms yields;

$$\frac{\partial \sigma}{\partial x} dx\, A = \rho\, A\, dx \frac{\partial^2 U}{\partial t^2} \ . \tag{2.5}$$

Equation (2.5) reduces to;

$$\frac{\partial \sigma}{\partial x} = \rho \frac{\partial^2 U}{\partial t^2} \ . \tag{2.6}$$

Using Hooke's law for an isotropic elastic solid in uniaxial stress;

$$\sigma = E\varepsilon \ , \tag{2.7}$$

and rewriting ε in terms of displacement as;

$$\varepsilon = \frac{\partial U}{\partial x} \ , \tag{2.8}$$

equation (2.7) can be written as;

$$\sigma = E \frac{\partial U}{\partial x} \ . \tag{2.9}$$

Taking the partial derivative of equation (2.9) with respect to x yields;

$$\frac{\partial \sigma}{\partial x} = E \frac{\partial^2 U}{\partial x^2} \quad . \tag{2.10}$$

Substituting the expression for $\partial\sigma / \partial x$ from equation (2.10) into equation (2.6) yields;

$$\frac{\partial^2 U}{\partial t^2} = \frac{E}{\rho} \frac{\partial^2 U}{\partial x^2} \quad . \tag{2.11}$$

Substituting $C_o^2 = E/\rho$ into equation (2.11) provides an expression for the propagation of longitudinal waves of infinite wavelength along a bar;

$$\frac{\partial^2 U}{\partial t^2} = C_o^2 \frac{\partial^2 U}{\partial x^2} \quad . \tag{2.12}$$

The solution of equation (2.12) is attributed to d'Alembert, and may be given as (Timoshenko and Goodier, 1970);

$$U = f(x - C_o t) + g(x + C_o t) \quad , \tag{2.13}$$

where f and g are arbitrary functions, with f representing a wave travelling in the positive x-direction and g representing a wave travelling in the negative x-direction.

If a wave is considered to travel only in the negative x-direction, equation (2.13) can be written as;

$$U = g(x + C_o t) \quad . \tag{2.14}$$

Differentiating equation (2.14) with respect to x yields;

$$\frac{\partial U}{\partial x} = g' \quad , \tag{2.15}$$

where the prime denotes the derivative with respect to the argument. Differentiating equation (2.14) with resect to t yields;

$$\frac{\partial U}{\partial t} = C_o \, g' \quad . \tag{2.16}$$

Combining equations (2.15) and (2.16) yields;

$$\frac{\partial U}{\partial t} = C_o \frac{\partial U}{\partial x} \quad . \tag{2.17}$$

Substituting Hooke's law (equation 2.9) into equation (2.17) yields;

$$\frac{\partial U}{\partial t} = \frac{C_o \sigma}{E} \quad . \tag{2.18}$$

Substituting ρC_o^2 for E, equation (2.18) can be rewritten as:

$$\frac{\partial U}{\partial t} = \frac{\sigma}{\rho \, C_o} \quad . \tag{2.19}$$

By substituting v for the particle velocity ($\partial U / \partial t$), equation (2.19) simplifies to;

$$\sigma = \rho \, C_o \, v \quad . \tag{2.20}$$

The product ρC_o is commonly referred to as the characteristic impedance of the material (Rinehart, 1975).

The procedure followed in deriving the equation for particle velocity is similar to that of other authors (e.g., Kolsky, 1963; Rinehart, 1975; Zukus, Nicholas, Greszczuk, and Curran, 1982).

A diagram of the SHPB near the specimen is shown in figure 2.5. The stress waves σ_i (incident wave) and σ_r (reflected wave) act on interface 1 and σ_t (transmitted wave) acts on interface 2. Before any reflections occur, the particle velocity of the incident bar is given as;

$$v_i = \frac{\sigma_i}{\rho c_o} \quad . \tag{2.21}$$

If the characteristic impedance, or area of the specimen, is different than that of the pressure bars, a portion of the compressive stress wave at interface 1 will be reflected as a tensile wave and that portion of the stress wave which the specimen is able to support is transmitted through the specimen. When the portion of the stress wave propagating through the specimen reaches interface 2, the wave is once again partitioned, with a portion being reflected back into the specimen and a portion being transmitted into the transmitter bar. The reflected wave at interface 2 is compressive; hence, it will continue to traverse the specimen, increasing in amplitude with each transit. The characteristic impedance of the specimen, relative to the characteristic impedance of the pressure bars, and any difference in area will govern the increase

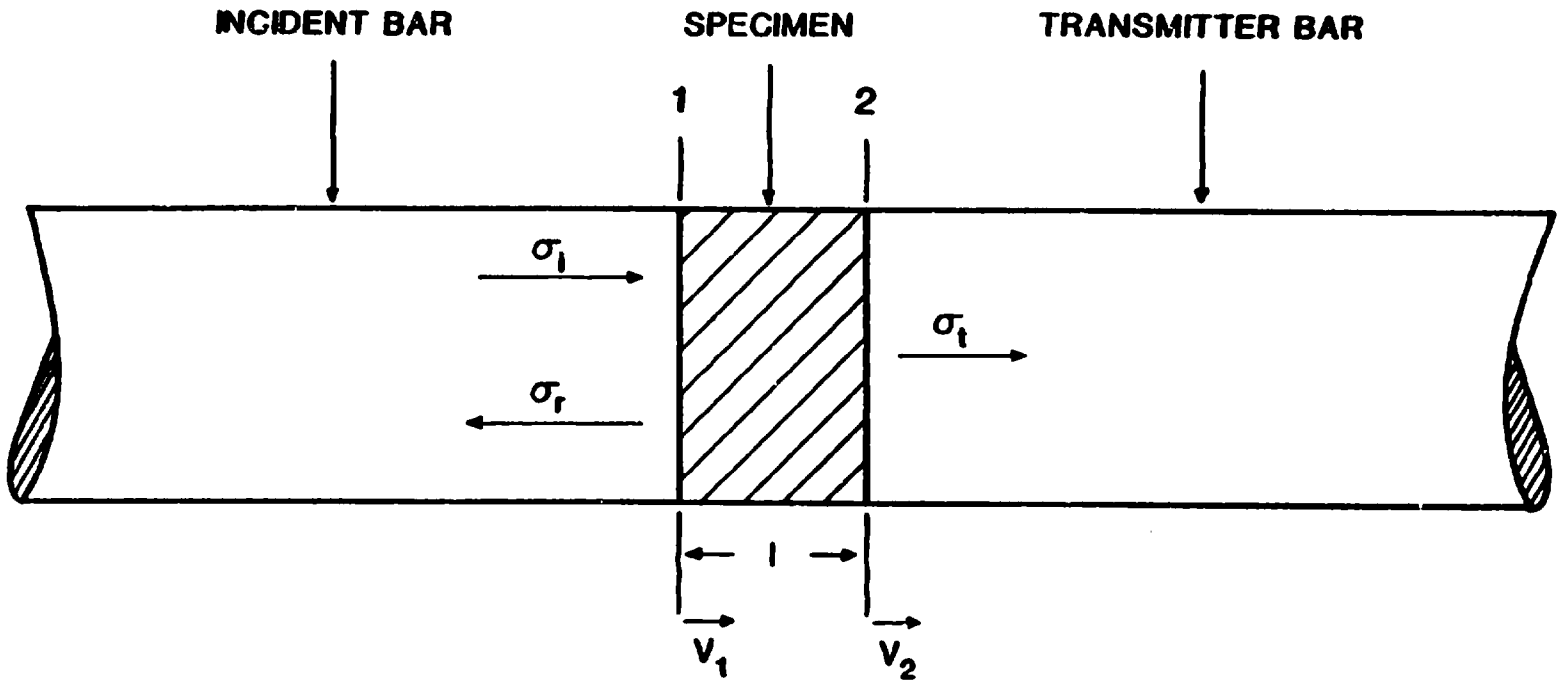

Figure 2.5. Specimen in place between pressure bars.

in amplitude. The result of these internal reflections is that the net particle velocity of interface 1 will increase, and then decrease with time, while the net stress on interface 1 will decrease, and then increase with time. The net particle velocity of interface 2 will increase with time, as will the net stress on interface 2.

The equations for the reflection and transmission coefficients for a wave impinging on an interface are derived in figure 2.6. Figure 2.7 illustrates the process of elastic wave propagation exercising the repeated application of the reflection and transmission coefficients. The process is terminated at the point of stress equilibrium with the incident wave. This figure was prepared with the assumption that the wavelength of the incident wave is infinite. For illustrative purposes, it was also assumed that the density of the specimen was one-half that of the pressure bars and the wave velocity (C_o) in the specimen and pressure bars is equal, thus the characteristic impedance of the specimen is one-half that of the pressure bars. The pressure bars are considered to be of a sufficient length to avoid the necessity of considering reflections from their ends. An implicit assumption for using equations (4) and (5) derived in figure 2.6 is that $d\sigma/d\varepsilon$ is constant for the specimen material. However, when a specimen deforms plastically, as does the soil specimens in this research, $d\sigma/d\varepsilon$ is not

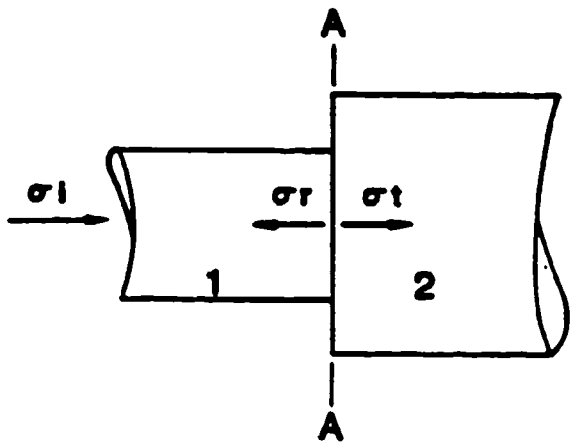

At interface A - A,

$$\Sigma F = 0, \qquad (\sigma_i + \sigma_r) A_1 = \sigma_t A_2, \tag{1}$$

$$\text{Continuity} \qquad v_i - v_r = v_t. \tag{2}$$

From equation (2.20), equation (2) can be written as,

$$\frac{\sigma_i}{\rho_1 c_1} - \frac{\sigma_r}{\rho_1 c_1} = \frac{\sigma_t}{\rho_2 c_2}. \tag{3}$$

Solving equation (3) for σ_t, and substituting the result into equation (1), a solution for σ_r in terms of σ_i can be expressed as follows,

$$\sigma_r = \frac{A_2\rho_2 c_2 - A_1\rho_1 c_1}{A_2\rho_2 c_2 + A_1\rho_1 c_1}\,\sigma_i. \tag{4}$$

By following the same procedure and solving equation (3) for σ_r, and substituting the result into equation (1), a solution for σ_t in terms of σ_i can be expressed as,

$$\sigma_t = \frac{2A_1\rho_2 c_2}{A_2\rho_2 c_2 + A_1\rho_1 c_1}\,\sigma_i. \tag{5}$$

Figure 2.6. Derivation of reflection and transmission coefficients.

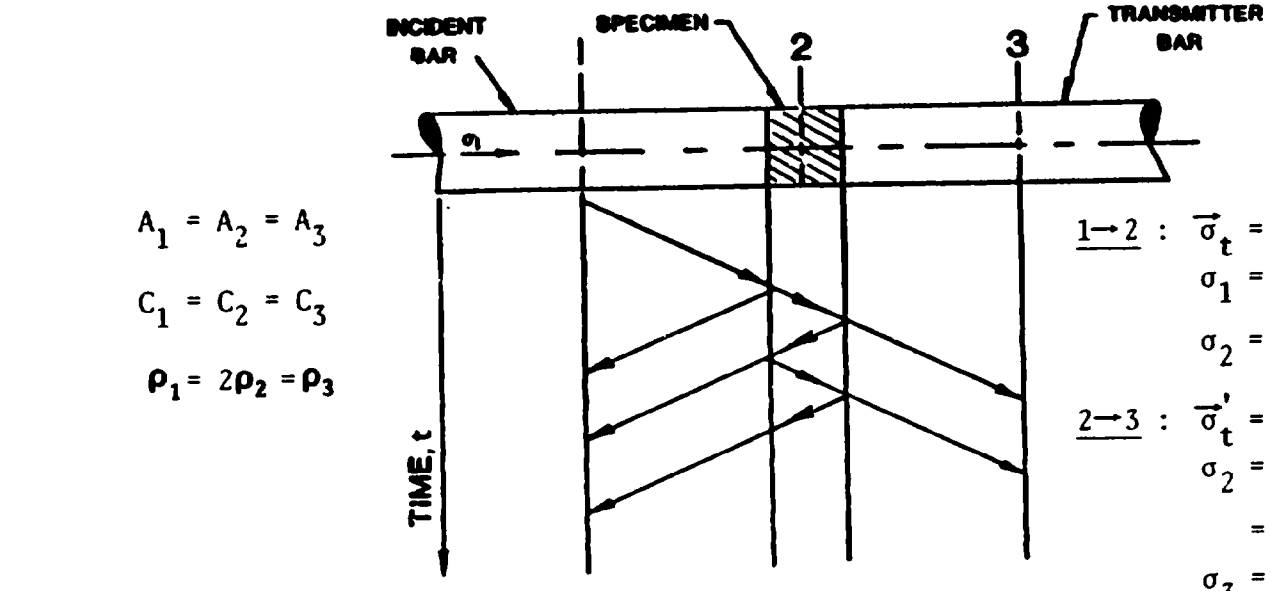

$A_1 = A_2 = A_3$

$C_1 = C_2 = C_3$

$\rho_1 = 2\rho_2 = \rho_3$

$1 \rightarrow 2$: $\vec{\sigma}_t = (2/3)\sigma_i$ and $\overleftarrow{\sigma}_r = -(1/3)\sigma_i$

$\sigma_1 = \sigma_i - (1/3)\sigma_i = (2/3)\sigma_i$

$\sigma_2 = (2/3)\sigma_i$

$2 \rightarrow 3$: $\vec{\sigma}'_t = (4/3)\sigma_2$ and $\overleftarrow{\sigma}'_r = (1/3)\sigma_2$

$\sigma_2 = (2/3)\sigma_i + (2/3)(1/3)\sigma_i$

$= (8/9)\sigma_i$

$\sigma_3 = (4/3)(2/3)\sigma_i = (8/9)\sigma_i$

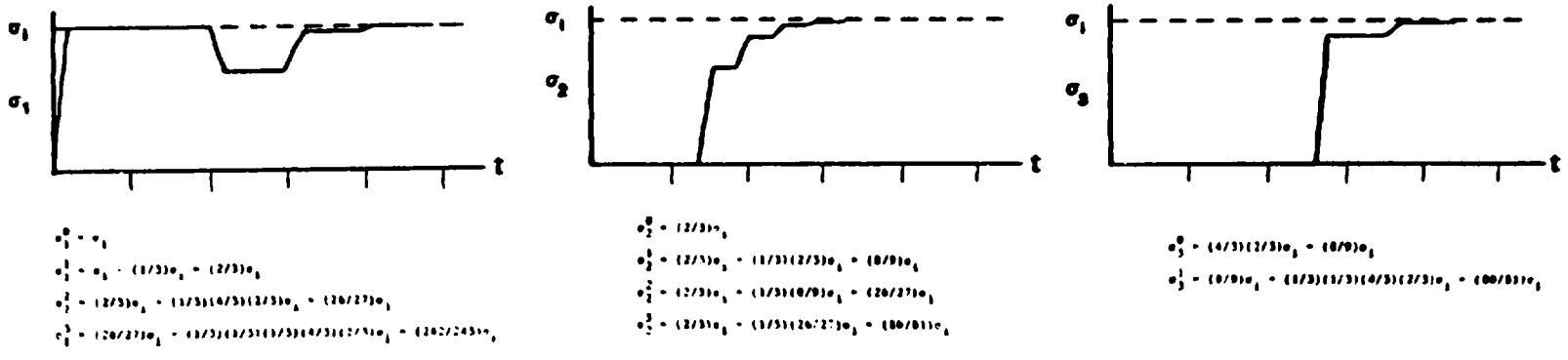

Figure 2.7. Representation of elastic wave interaction in the specimen and pressure bars caused by the loading stress wave.

constant but will be dependent on the velocity at which the wave propagates in the specimen.

The net particle velocity of interface 1 will be;

$$v_1 = v_i - (- v_r) \quad , \tag{2.22}$$

or;

$$v_1 = \frac{\sigma_i - (-\sigma_r)}{\rho C_o} \quad , \tag{2.23}$$

and the particle velocity of interface 2;

$$v_2 = \frac{\sigma_t}{\rho C_o} = v_t \quad . \tag{2.24}$$

Representative particle velocities for interfaces 1 and 2 with soil as the specimen are shown in figure 2.8. By taking the difference of the particle velocities at each interface, the rate at which the specimen is straining can be computed as;

$$\dot{\varepsilon} = \frac{(v_i - (- v_r) - v_t)}{l} \quad , \tag{2.25}$$

or;

$$\dot{\varepsilon} = \frac{(\sigma_i - (- \sigma_r) - \sigma_t)}{\rho C_o l} \quad . \tag{2.26}$$

The strain experienced by the specimen at any time t, can be computed by taking the integral of the strain-rate;

$$\varepsilon = \int_0^t \dot{\varepsilon} \, dt \quad . \tag{2.27}$$

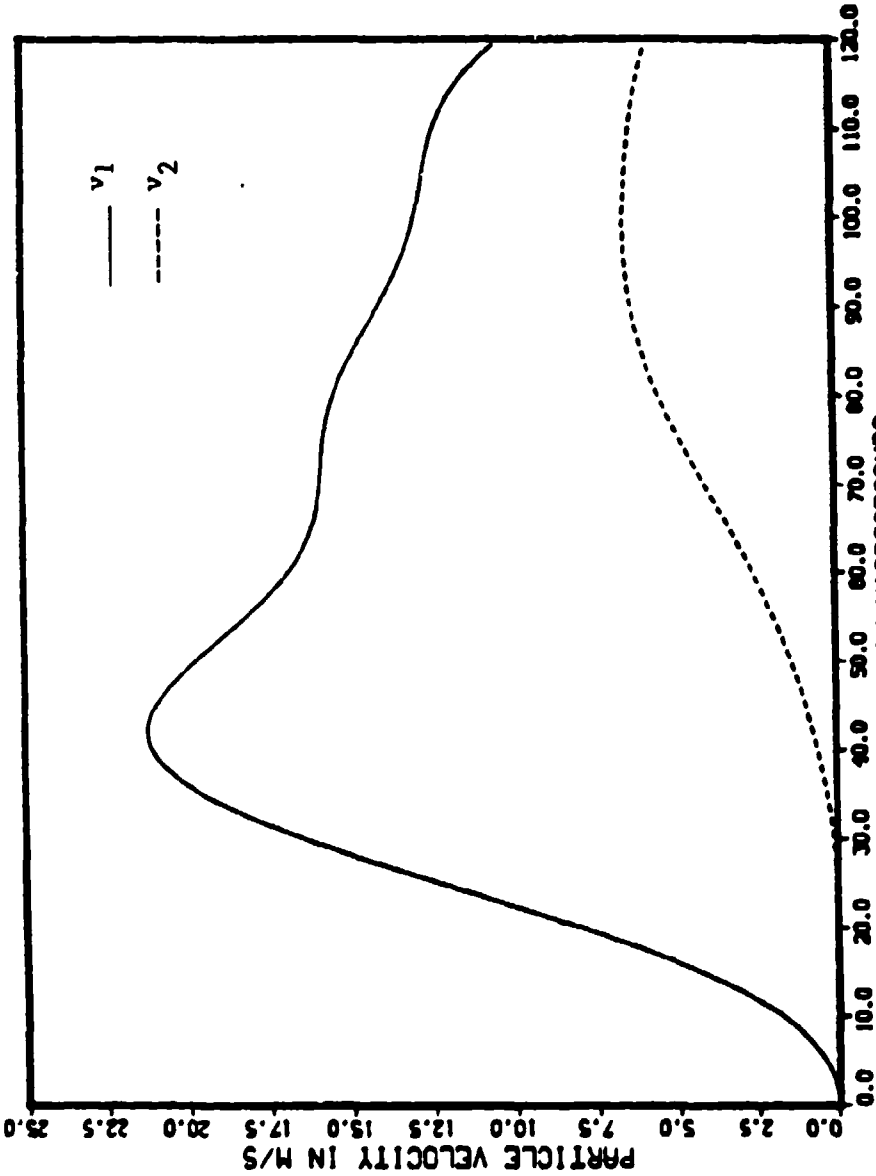

Figure 2.8. Particle velocity history at the specimen-bar interfaces, experiment 115.

Figures 2.9 and 2.10 show typical results for $\dot{\varepsilon}$ and ε, respectively, as computed from equations (2.26) and (2.27). If the specimen is straining uniformly then the values obtained from equations (2.26) and (2.27) will be exact. However, the specimen will not usually experience uniform straining over its length. Therefore, the computed strain-rate and strain can only be considered average values for the specimen.

The stresses at interfaces 1 and 2 can be determined in a similar fashion. The force at interfaces 1 and 2 will be;

$$F_1 = (\sigma_i + (- \sigma_r)) A_1 = \sigma_t' A_2 , \qquad (2.28)$$

$$F_2 = (\sigma_t' + (- \sigma_r')) A_2 = \sigma_t A_1 , \qquad (2.29)$$

where σ_t' is the stress transmitted into the specimen, σ_r' is the stress reflected at interface 2, A_1 is the area of the pressure bars, and A_2 is the area of the specimen. The stress at each interface is then;

$$\sigma_1 = \frac{(\sigma_i + (- \sigma_r)) A_1}{A_2} , \qquad (2.30)$$

$$\sigma_2 = \frac{\sigma_t A_1}{A_2} , \qquad (2.31)$$

and the average stress in the specimen will be;

$$\sigma_{avg} = \frac{\sigma_1 + \sigma_2}{2} , \qquad (2.32)$$

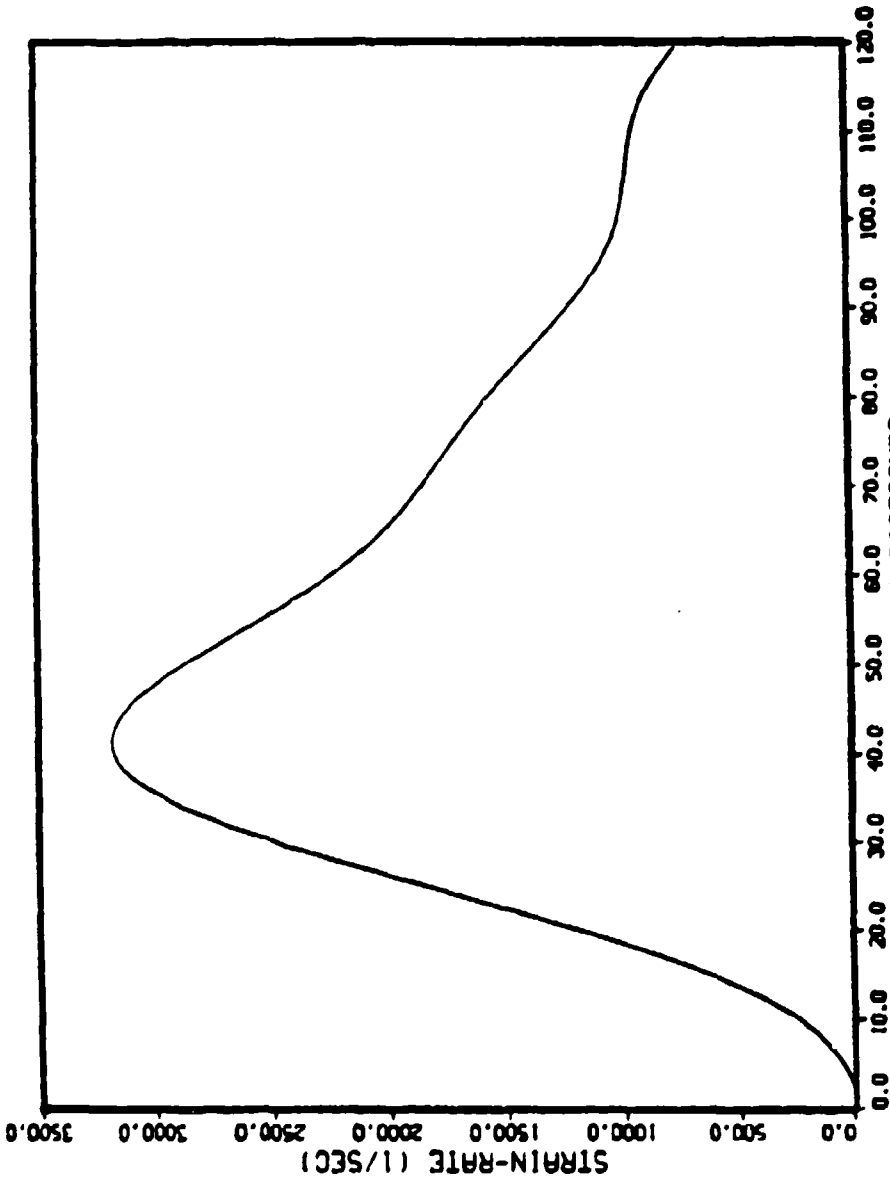

Figure 2.9. Strain-rate-time response for experiment 115.

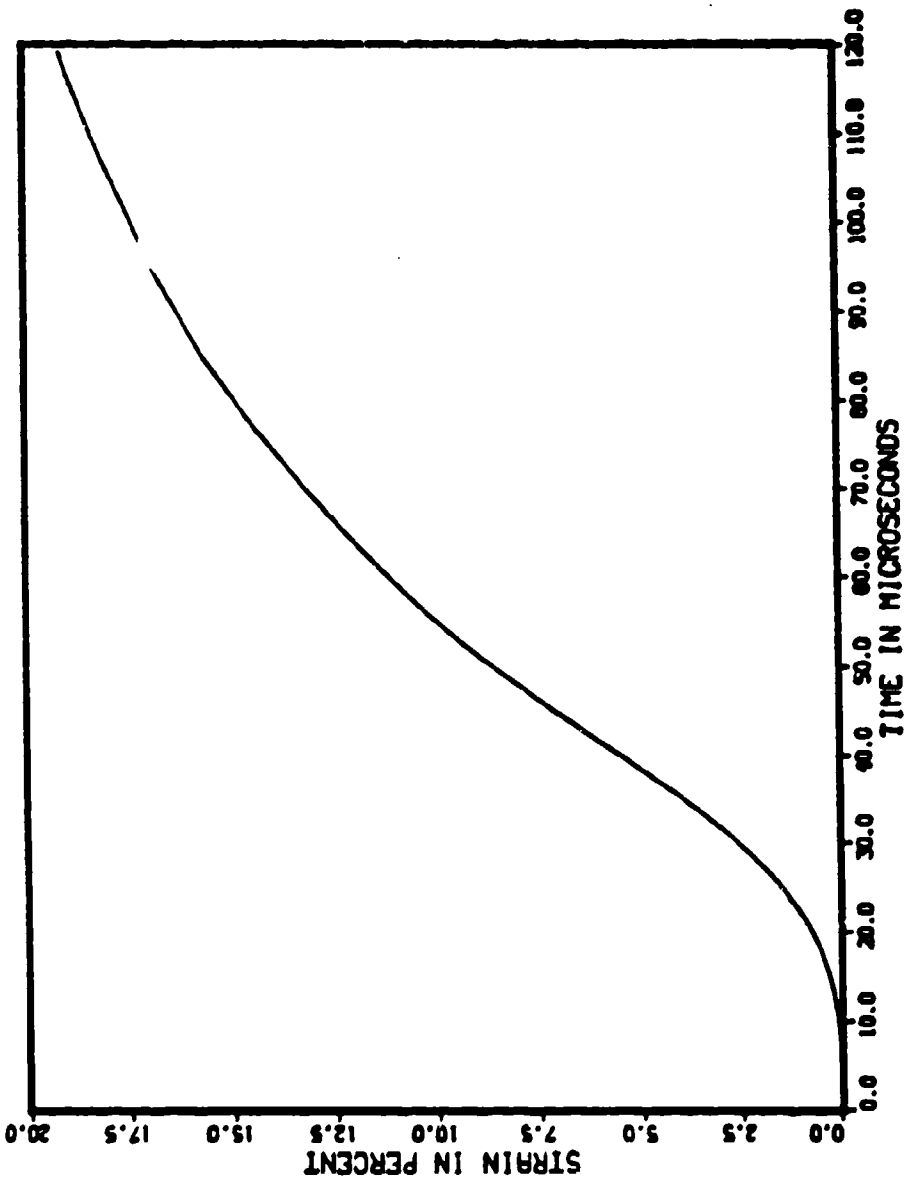

Figure 2.10. Strain-time response for experiment 115.

or;

$$\sigma_{avg} = \frac{(\sigma_i + (- \sigma_r) + \sigma_t) A_1}{2 A_2} \quad . \qquad (2.33)$$

Figure 2.11 shows a graphic representation of the averaging procedure and its result.

2.5 Contributions of Recent Investigators

Since the modification made by Kolsky to the original Hopkinson bar experimental configuration, the only significant change has been the introduction of strain gauges for data recording. The use of strain gauges was first reported by Hauser, Simmons, and Dorn (1961). Replacement of the condenser microphones with strain gauges avoids the requirement of differentiating the displacement records as a continuous strain history can now be recorded.

To simplify equations (2.26), (2.27), and (2.33) some investigators have assumed the stress along the axis of the specimen to be uniform (e.g., Lindholm, 1964). From this assumption it follows that;

$$\sigma_1 = \sigma_2 \quad , \qquad (2.34)$$

$$\sigma_t = \sigma_i + (- \sigma_r) \quad , \qquad (2.35)$$

Substitution of equation (2.35), into equation (2.33)

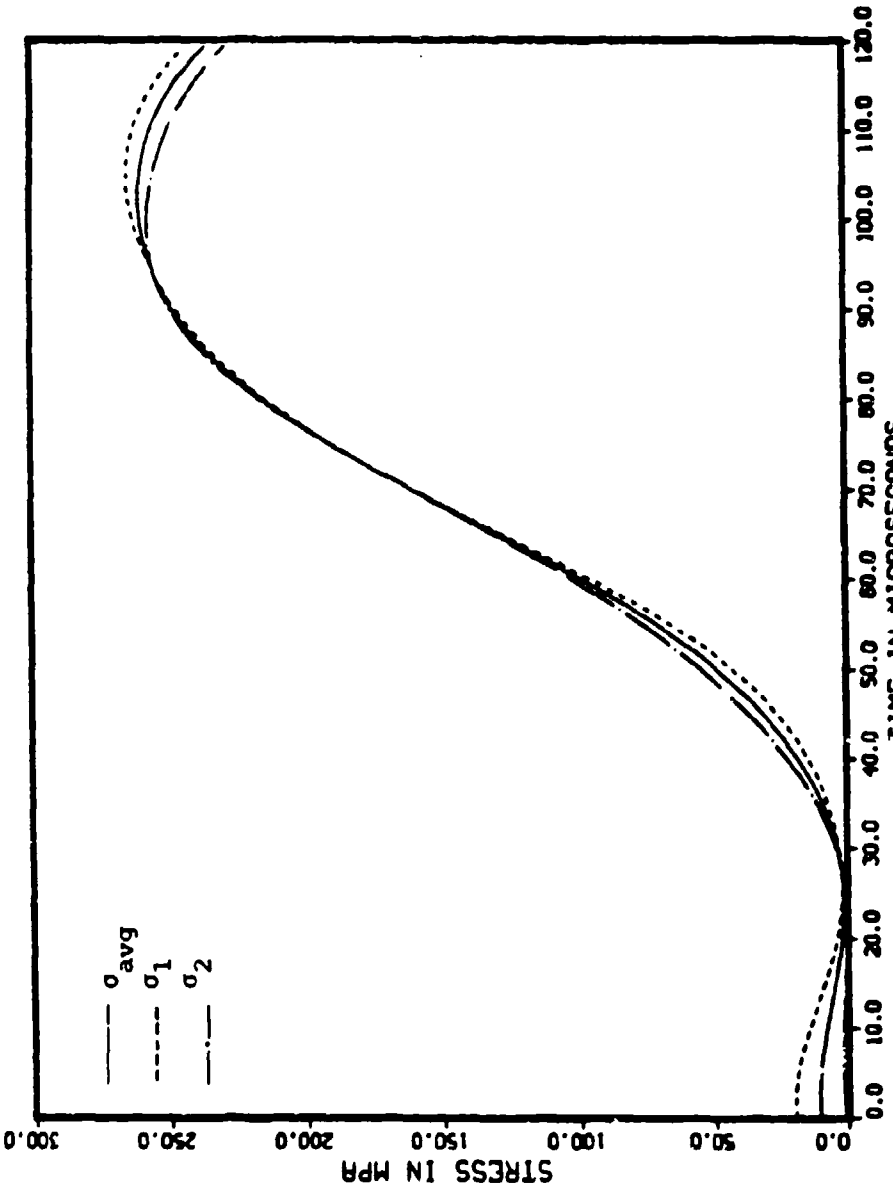

Figure 2.11. Interface stress averaging.

yields;

$$\sigma_{avg} = \frac{\sigma_t \, A_1}{A_2} \, . \tag{2.36}$$

Similarly, substitution of equation (2.35), into equation (2.26), and (2.27) yields;

$$\dot{\varepsilon} = \frac{-2\,(-\sigma_r)}{l\rho C_o} \, , \tag{2.37}$$

$$\varepsilon = \frac{-2}{l\rho C_o} \int_0^t (-\sigma_r)\, dt \, . \tag{2.38}$$

Because equations (2.36), (2.37), and (2.38) require an additional assumption beyond those necessary for the experiment, they were not used in this investigation. Instead, all computations of specimen stress, strain, and strain-rate have been performed using equations (2.26), (2.27), and (2.33). A discussion of the experimental assumptions is presented in section 4.1.

A critical analysis was made of the Kolsky technique, and its assumptions by Davies and Hunter (1963). Their experimental technique was essentially the same as that used by Kolsky. However, by using an analytic method, a criterion was developed to estimate if the assumptions of the experiment are satisfied, principally the uniform stress condition (see section 4.1).

Davies and Hunter (1963) determined that to minimize the effects of friction, the specimen aspect ratio should

be approximately unity. The criterion to estimate when stress equilibrium in the specimen has been achieved is based on the duration of the applied stress wave (T) and the characteristic velocity at which the wave propagates through the specimen ($C_s^2 = E_s/\rho_s$, where E_s is the slope of the tangent to the stress-strain curve at a point ($d\sigma/d\varepsilon$) and ρ_s is the density of the specimen). The characteristic velocity (C_s) is that given by the Taylor-von Karmen theory for a plastically deforming specimen (von Karmen, 1942; Taylor, 1958). Combining energy principles with the Taylor-von Karmen theory, the derived criterion for estimating when stress equilibrium in the specimen has been achieved is given as (Davies and Hunter, 1963);

$$\frac{d\sigma}{d\varepsilon} > \frac{\pi^2 \rho_s l^2}{T^2} \quad . \tag{2.39}$$

Davies and Hunter (1963) recommended that when this inequality is violated, equilibrium has not been reached and the stress-strain data may be in error.

The SHPB experimental environment was studied numerically by Bertholf and Karnes (1974). They used a two-dimensional, finite-difference, elastic-plastic, wave propagation computer code to investigate the response of an aluminum specimen. The aluminum specimen was modeled as a strain-rate independent material. The code, TOODY, was developed by Bertholf and Benzley (1968). The main

objectives of their research were: (1) to examine the validity of the SHPB experimental assumptions (i.e., in particular, inertia and friction), (2) to establish bounds for the experimental parameters, (3) to evaluate the corrections proposed by previous investigators, and (4) to determine how the material response is influenced when the experimental assumptions are violated (see section 4.1) (Bertholf and Karnes, 1974).

Bertholf and Karnes (1974) determined that the SHPB experiment could be used to accurately, and reliably determine material response at high rates of loading, provided that certain precautions were taken to minimize the effects of inertia and friction. It was shown that the effects of inertia and friction between the specimen and the bars could lead to the conclusion that the material response was rate dependent (i.e., inertia and friction affected the degree to which stress and strain uniformity in a specimen could be achieved), especially for the case of relatively thin specimens (i.e., small aspect ratios). Their numerical computations showed that the influence of inertia on experimental data could be minimized by bounding the maximum specimen strain-rate such that (Bertholf and Karnes, 1974);

$$D\dot{\varepsilon}_{max} = 5 \times 10^{3} \text{ cm } s^{-1} , \qquad (2.40)$$

where the loading wave is a ramp and;

$$\frac{T_r}{D} > 16 \ \mu s \ cm^{-1} , \qquad (2.41)$$

where T_r is the rise-time of the loading wave and D is the diameter of the pressure bars. In addition they showed that if sufficient care is taken to lubricate the ends of the specimen-bar interfaces, the influence of friction on experimental results can be minimized. Their investigation also determined that the criterion proposed by Davies and Hunter to determine if the reduced data may be in error, was indeed reasonable.

Since Davies' pioneering work several investigators have throughly examined the dispersive nature of wave propagation in elastic bars (e.g., Curtis, 1960; Yeung Wye Kong, Parsons, and Cole, 1974). However, only recently has a numerical procedure to account for wave dispersion been developed that can easily be incorporated into the standard SHPB data reduction technique (Follansbee and Frantz, 1983; Follansbee and Frantz, 1984). This technique has been adapted for use in this research.

As mentioned in section 2.2, the generated stress wave is not composed of a single frequency but, instead, a spectrum of frequencies, with each frequency travelling at its own respective phase velocity (C_n) and wavelength (Λ). Due to this frequency variation, oscillations develop in the propagating stress wave which have no counterpart in the applied stress wave (Curtis, 1960). The

nature of the wave oscillations can be described mathematically through the use of the dispersion equation (see section 2.2). The dispersion equation can be written in the form (Wasley, 1973);

$$\frac{2g}{R}(h^2 + k^2)J_1(gR)J_1(hR) - (h^2 - k^2)^2 J_0(gR)J_1(hR) \quad (2.42)$$

$$- 4 k^2 ghJ_0(hR)J_1(gR) = 0 \quad ,$$

where

$$g^2 = \frac{\rho p^2}{\lambda + 2\mu} - k^2 \quad ,$$

$$h^2 = \frac{\rho p^2}{\mu} - k^2 \quad ,$$

J_0 is a Bessel function of the first kind of order zero, J_1 is a Bessel function of the first kind of order one, R is the radius of the bar, k is the wave number ($2\pi/\Lambda$), λ and μ are Lame's constants, p is the circular frequency, and ρ is the bar density. The solution to the first mode of vibration of the dispersion equation is shown in figure 2.12 for a material with a Poisson's ratio of 0.29.

The plot of the fundamental mode of the dispersion equation shows that a high frequency wave will travel slower than a low frequency wave (see figure 2.12). Hence, as a wave propagates, the higher frequency components of the wave will lag behind the lower frequency components causing a change in the original shape of the wave. This wave dispersion as related to the SHPB experiment

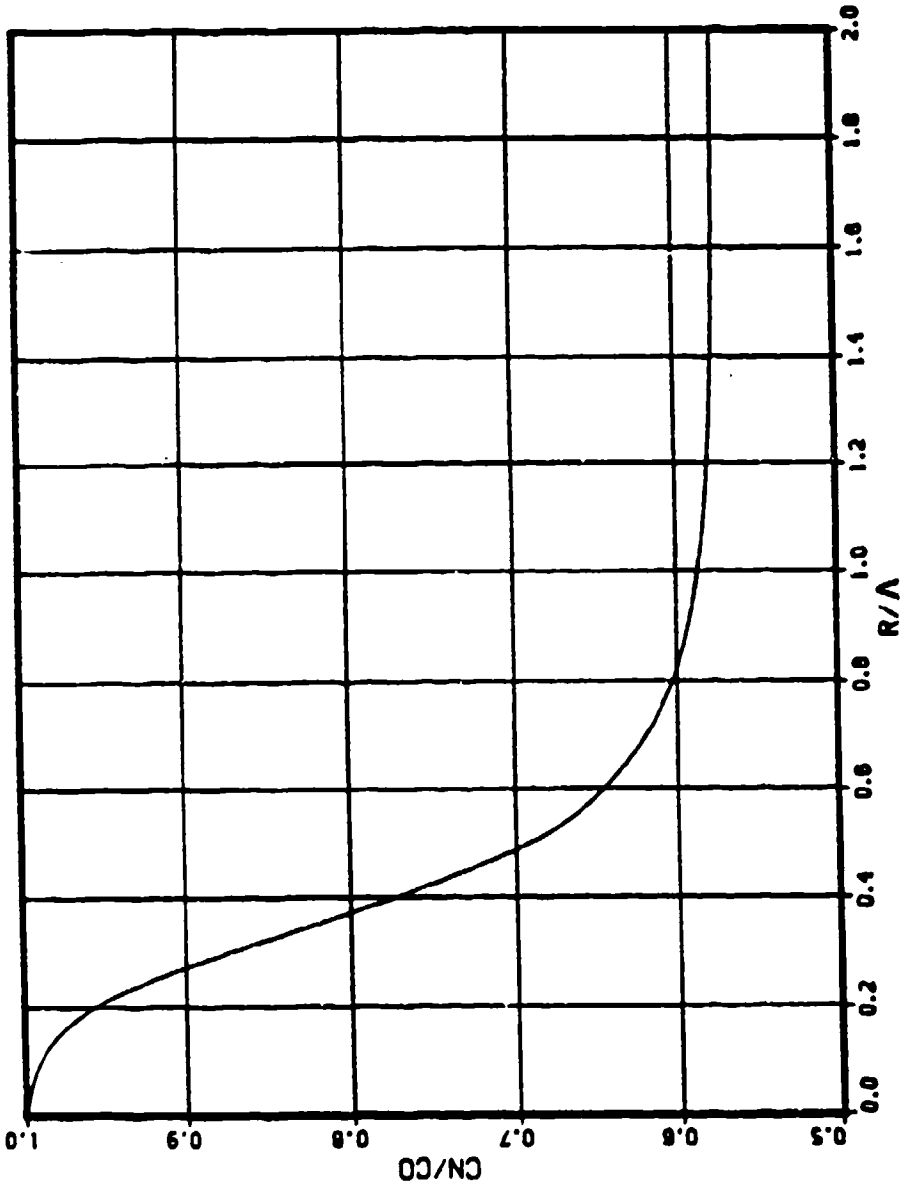

Figure 2.12. Solution to the fundamental mode of vibration of the dispersion equation (adapted from Davies, 1948).

increases the difficulty in interpreting specimen behavior as deduced from the standard data reduction technique (Follansbee and Frantz, 1983).

An assumption of the dispersion correction procedure is that only the fundamental mode of vibration is excited during the SHPB experiment. This assumption is supported by the work of Davies (1948) and Follansbee and Frantz (1983). Based on this assumption, the fundamental mode of vibration of the dispersion equation has been approximated by fitting the data with an equation of the form (Follansbee and Frantz, 1983);

$$\frac{C_n}{C_0} = 0.5764 + \frac{0.4236}{22\left[\frac{R}{\Lambda}\right]^4 + 12.8\left[\frac{R}{\Lambda}\right]^3 - 2.77\left[\frac{R}{\Lambda}\right]^2 + 0.92\left[\frac{R}{\Lambda}\right]^{1.5} + 1} \qquad (2.43)$$

Figure 2.13 compares the approximation to the solution of the dispersion equation for the fundamental mode of vibration. Also, the applied stress wave has been represented as a Fourier cosine series;

$$f(t) = \frac{A_0}{2} + \sum_{n=1}^{\infty} D_n \cos(n\omega_0 t - \Phi), \qquad (2.44)$$

where A_0 is the amplitude of the largest frequency component, ω_0 is the lowest frequency component, D_n is the amplitude of frequency component $n\omega_0$, and Φ is the phase angle. The phase angle is the component used to correct the waveform for dispersion. A complete mathematical description of the dispersion correction procedure is

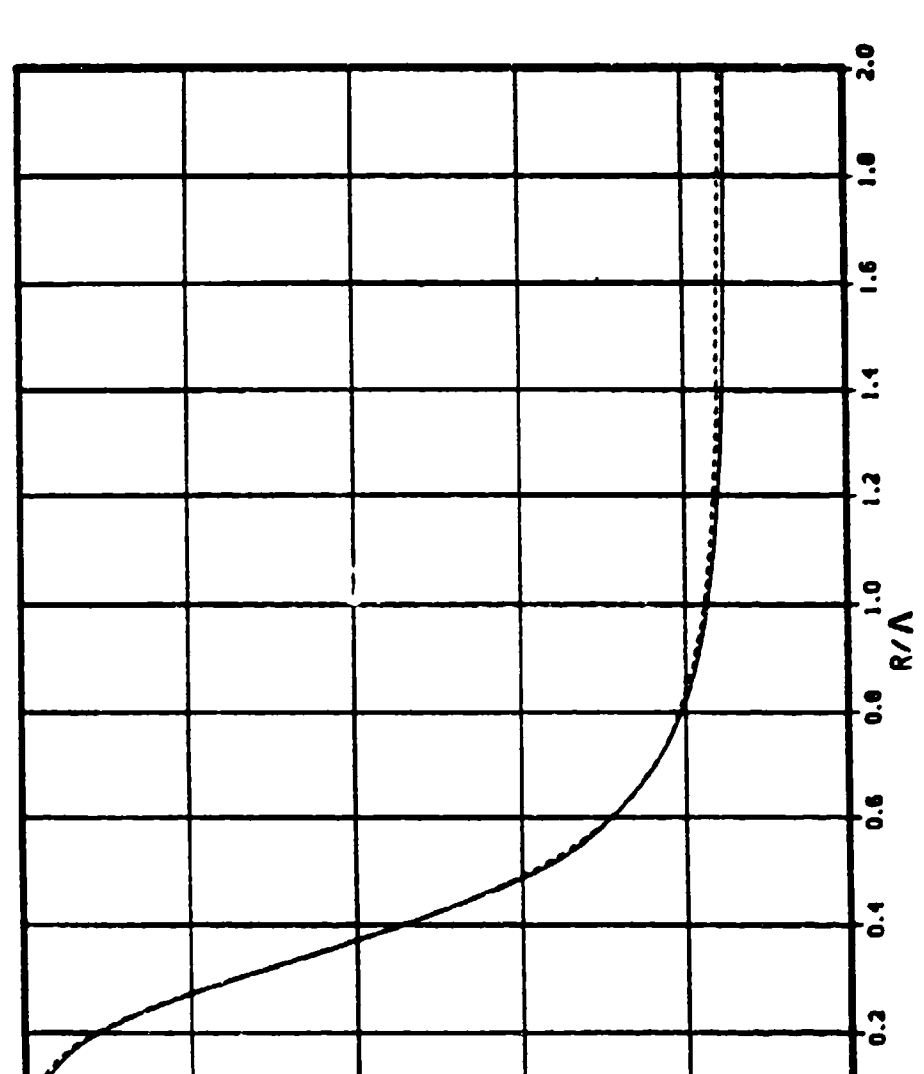

Figure 2.13. Comparison of the exact solution (solid line) and the polynomial approximation to the fundamental mode of vibration of the dispersion equation.

presented in appendix A.

2.6 Application of the SHPB to Soils

In 1967 Fletcher and Poorooshasb presented a paper on their work with the SHPB using thin clay specimens. The purpose of their study was to investigate the response of a kaolin clay to loads of low magnitude, applied at high rates. The largest magnitude load was less than 1 MPa and the average strain-rate was 200 s^{-1}. The loading stress wave was initiated by a steel ball accelerated to the desired impact velocity by rolling it down a ramp.

Their results showed that the response of the clay was influenced by the preconsolidation pressure at which it was prepared. At applied loads greater than the preconsolidation pressure, a peak stress was achieved that was greater than the preconsolidation pressure. After reaching the peak, the specimen stress fell rapidly to a level at which the clay appeared to flow at a constant stress. For applied loads less than the preconsolidation pressure, the peak stress achieved was equal to the applied stress. Once this stress level was reached, the clay flowed at that stress with no loss of strength, in contrast to the specimens where the applied stress was greater than the preconsolidation pressure.

In their paper, no details are presented as to whether or not the assumptions of the experiment were

satisfied (see section 4.1). The equations they present to determine the specimen stress and strain assume that the stress is uniform across the specimen. This assumption needs to be questioned for soil specimens.

A more recent investigation into the response of soils using the SHPB has been conducted by Gaffney, Brown, and Felice (1985). The soil was a clayey sand obtained from the CARES-Dry site, located on Luke Air Force Base, Arizona. The specimens were prepared by static compaction in thick-walled confining cylinders. Four specimens were prepared at a moisture content of 3.5 percent and a wet density of 1.77 g/cm^3 . Two nominal specimen lengths were used, 13 mm, and 25 mm. The initial volume of air contained in the specimen was approximately 29 percent of the total specimen volume. The applied stresses for the experiments ranged up to 500 MPa.

In addition to the SHPB experiments, gas gun experiments at high strain-rates (> 5000 s^{-1}) and quasi-static experiments (strain-rates on the order of (5×10^{-3} s^{-1}) were also conducted. Through comparison of the results obtained over a range of strain-rate regimes, it was concluded that for strain-rates below 5000 s^{-1} the response of the soil with a moisture content of 3.5 percent was independent of strain-rate. It was noted that in the SHPB experiments, the specimens retained some volume of air and that the soil response may be

significantly different if all the air voids had been closed (Gaffney et al., 1985).

The same SHPB apparatus used by Gaffney et al. (1985) was also used for this investigation.

3. EXPERIMENTAL APPARATUS AND MATERIAL

3.1 Experimental Apparatus

A photograph of the SHPB apparatus used in this research is shown in figure 3.1. Figure 3.2 presents a diagrammatic representation of the apparatus. Figure 3.3 presents an enlarged schematic of the incident and transmitter pressure bars showing the specimen positioning and the location of the strain gauges. The apparatus is the property of the Geophysics Group at the Los Alamos National Laboratory, Los Alamos, New Mexico. The main components of the system are the gas gun, the reaction frame, and the incident and transmitter pressure bars (additional components are noted in figure 3.2).

The incident and transmitter pressure bars are constructed of Vascomax 350 CVM maraging steel that has been heat treated to sustain a yield stress of about 2 GPa. Each pressure bar is 60.3 mm in diameter and 1.22 m in length. The bars ride in adjustable teflon bearings that allow unrestricted motion in the horizontal plane. The teflon bearings do not restrict the passage of the stress wave (Lindholm, 1964). Adjustments of the teflon bearings for system alignment are made through four-wedge supported mounting rings. The entire system is supported

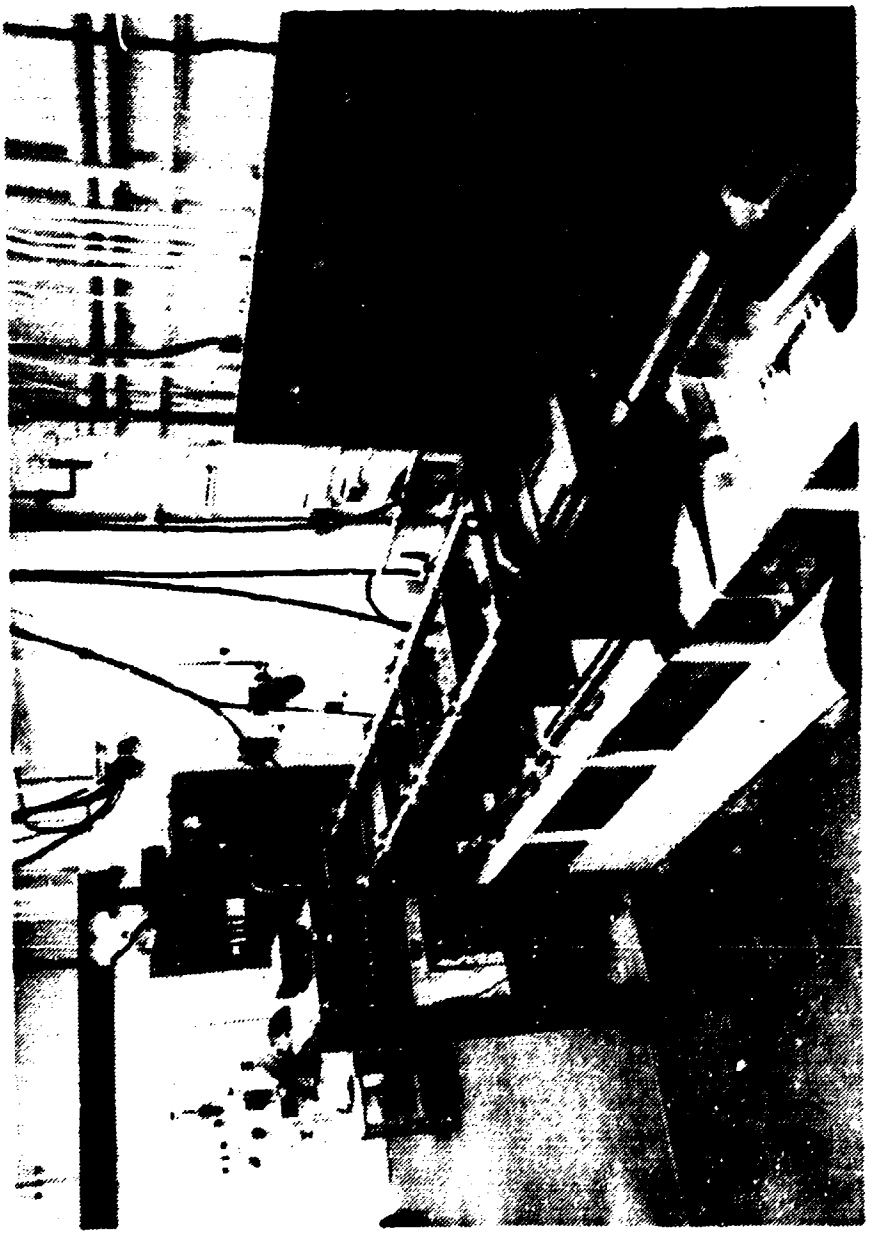

Figure 3.1. The Split-Hopkinson pressure bar apparatus.

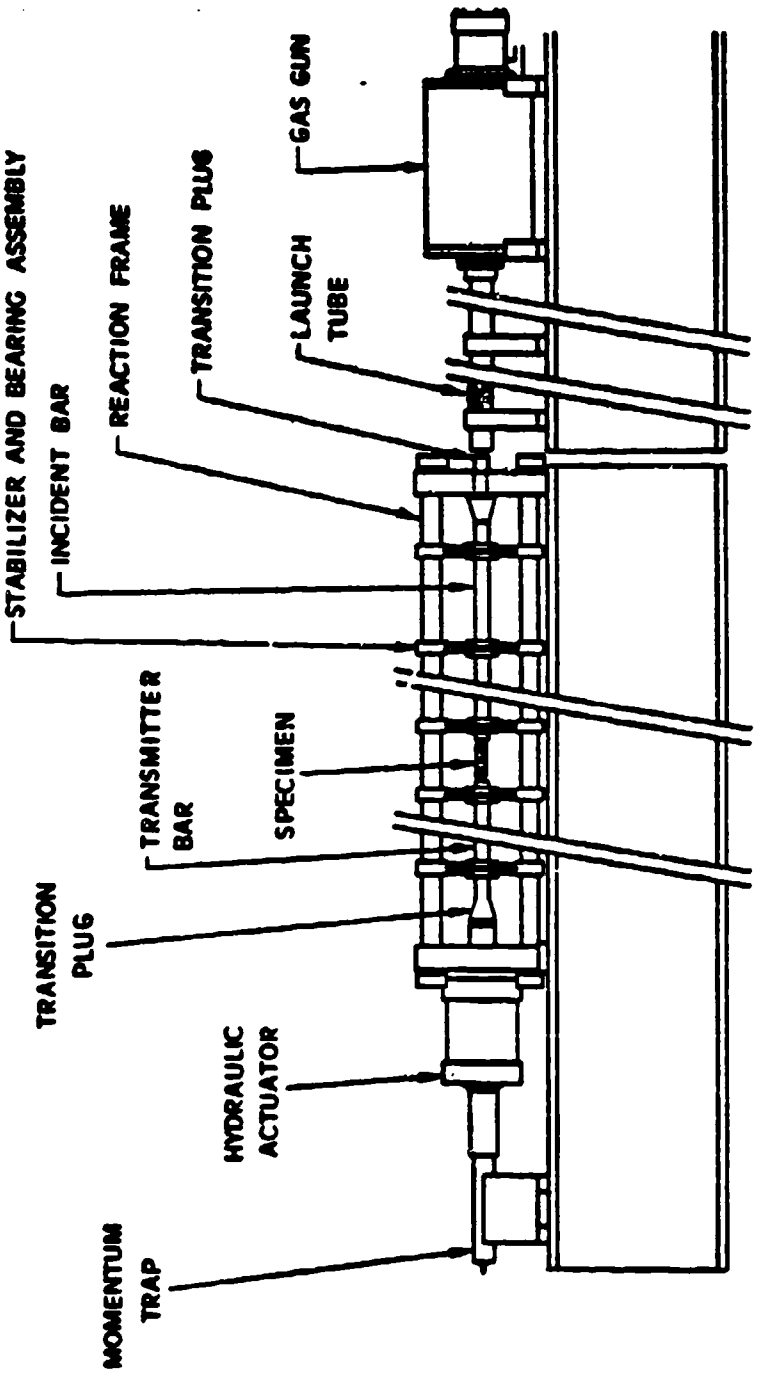

Figure 3.2. Split-Hopkinson pressure bar system arrangement (Nagy and Muelenhaupt, 1983)

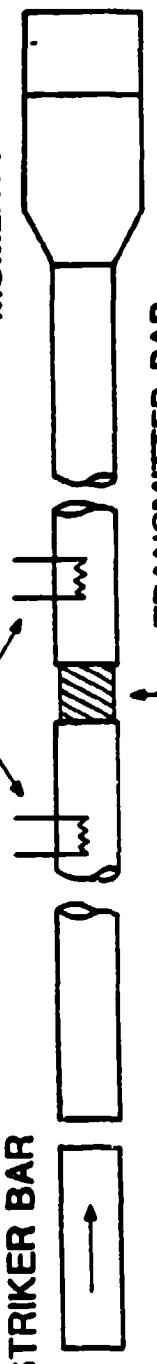

Figure 3.3. Split-Hopkinson pressure bar schematic.

by a massive four-column reaction frame mounted on a steel I-beam.

The applied stress wave is initiated by the impact of the striker bar on the incident bar. The striker bar is constructed of the same material and has a slightly larger diameter (60.5 mm) than the pressure bars. Three striker bar lengths were available, 0.127, 0.254, and 0.508 m. To minimize misalignment during impact and increase the rise time of the applied stress wave, the impact end of the striker bar is slightly rounded (Follansbee and Frantz, 1983). The striker bar is accelerated down the launch tube to the appropriate impact velocity by the gas gun. The amplitude of the applied stress wave is proportional to the impact velocity of the striker bar which is controlled by the gas gun breech pressure (Nagy and Muelenhaupt, 1983). A description of the gas gun is presented in appendix B along with the correspondence between breech pressure and the striker bar impact velocity. In appendix C the relationship between the impact velocity of the striker bar and the amplitude of the applied stress wave is derived. The end of the launch tube is vented so that the gas driving the striker bar is expelled before impact. This is done to avoid multiple impacts by the striker bar on the incident bar. Just prior to impact, the striker bar velocity is measured by three sets of diode lasers and photodetectors mounted in the end of the launch tube. The

laser velocity measuring system is described in appendix B.

The applied stress wave in the bars is monitored by resistance strain gauges mounted on the radial surface of the pressure bars (see figure 3.3). The strain gauges (Micro-Measurement No. EA-06-125AV-120 with extra long foil tabs) are mounted in pairs on opposite sides of the respective pressure bars and connected in a half-bridge configuration to nullify bending strains. The strain gauges are bonded (bonding agent is CA120SL Bean adhesive) to the pressure bars at mid-length. The positioning of the strain gauges on the incident bar is particularly critical because it is necessary to obtain continuous records of the incident and reflected waves without overlap.

The data recorded from strain gauge bridges are filtered and preamplified and then routed to a data acquisition system. The data are recorded by CAMAC (IEEE-583) based waveform digitizers. The incident and transmitter bar records were recorded on separate channels with 8-bit resolution at a rate of 0.5 microseconds per data point for all but experiments 31 and 32 where the data collection rate was 0.25 microseconds per data point. The duration of data recording is 8 milliseconds per channel. Positioning of this data collection window such that only the data of interest is gathered is controlled by a timing signal generated by the laser velocity

measuring system (see appendix B). The data are read by a Digital Equipment Corporation LSI-11/02 microcomputer and stored on a flexible disk. The data are then transferred by magnetic tape to a CRAY-1S mainframe computer located at the Air Force Weapons Laboratory, Kirtland Air Force Base, New Mexico for complete data processing. Additional information on the SHPB instrumentation is presented in in appendix B.

An additional feature of this particular SHPB is that a static preload of up to 200 MPa can be applied to the specimen. This is accomplished by a hydraulic ram located at the downstream end of the transmitter bar (see figure 3.2). A tapered transition plug is used to transfer the load from the hydraulic ram system. Another transition plug is located at the impact end of the incident bar which is fabricated with a large diameter shoulder to support the static preload that is applied to the specimen (see figure 3.2). It is tapered to match the diameter of the incident bar where they contact. The transition plugs are constructed of the same material as the pressure bars and the striker bar. A static preload was not applied to the specimens in this research.

Appendix D includes a detailed outline of the procedure followed when conducting a SHPB experiment.

3.2 Soil Characteristics

The soil used for the experiments described herein was sampled in bulk quantities from a test pit in an undisturbed area of the McCormick Ranch test site located on Kirtland Air Force Base, New Mexico. The site has been used for explosive testing by the Department of Defense since the early 1960s. The geology of the site consists of some surface playa underlain by unconsolidated eolian sand, alluvium, and lacustrine deposits 15 to 30 m thick (Bedsun, 1983). The water table is estimated to lie at a depth of 60 to 90 m (Bedsun, 1983).

In order that the soil be as free of organic material as possible, the surface vegetation was scraped away and the sample taken from a depth of 1 to 2 m. After arriving at the University of Utah soils laboratory, the samples were mixed to break apart large clumps and to achieved a uniform mixture. The following tests were then performed to determine the soil properties: (1) mechanical sieve and hydrometer analyses to determine grain-size distribution, (2) Atterberg limits, (3) hygroscopic moisture determination, and (4) specific gravity. These tests were conducted in accordance with the American Society for Testing and Materials standards (ASTM, 1982). The moisture/density relationship was determined by the Harvard miniature compaction procedure using three layers with 25, 40 pound tamps per layer. An x-ray diffraction

study was also performed to determine the soil constitutive minerals. This study was conducted at the Los Alamos National Laboratory, Los Alamos, New Mexico.

The results of these tests showed the soil to be a nonplastic, clayey silty sand (see figure 3.4) with a specific gravity of 2.67 and hygroscopic moisture content of 2.9 percent. The constitutive minerals and their percentages are, quartz, 60 percent, feldspar, 30 percent, with traces of hornblende, illite, montmorillonite, cristobalite, and calcite. A carbonate test showed the percentage of calcite to be approximately 2 percent.

3.3 Specimen Preparation

The majority of specimens were prepared near the optimum moisture content (13.3 %) and dry density (1.87 g/cm^3) as determined by the Harvard miniature compaction procedure (see figure 3.5). A complete tabulation of the initial specimen parameters for each specimen is presented in table E.1 of appendix E. To achieve as uniform conditions among specimens as possible, the soil was mixed in batches sufficient to prepare a minimum of five experimental specimens. Before the addition of water, the soil was passed through a No. 4 sieve (4.75 mm opening), weighed and placed in a large flat pan. The correct amount of moisture was added by using a spray bottle so that an even distribution could be obtained. The soil was then

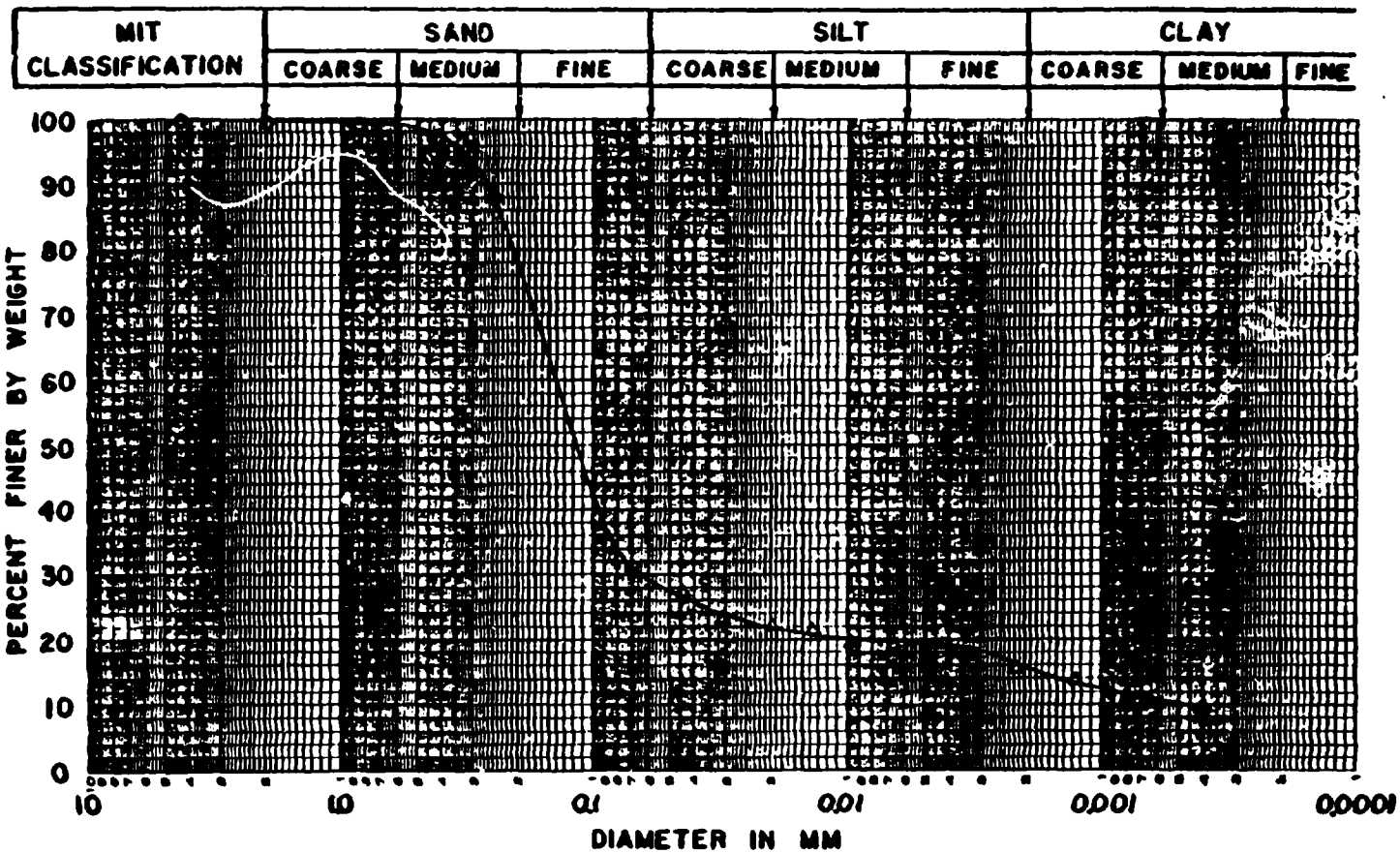

Figure 3.4. Particle size distribution curve (0 by sieve, Δ by hydrometer).

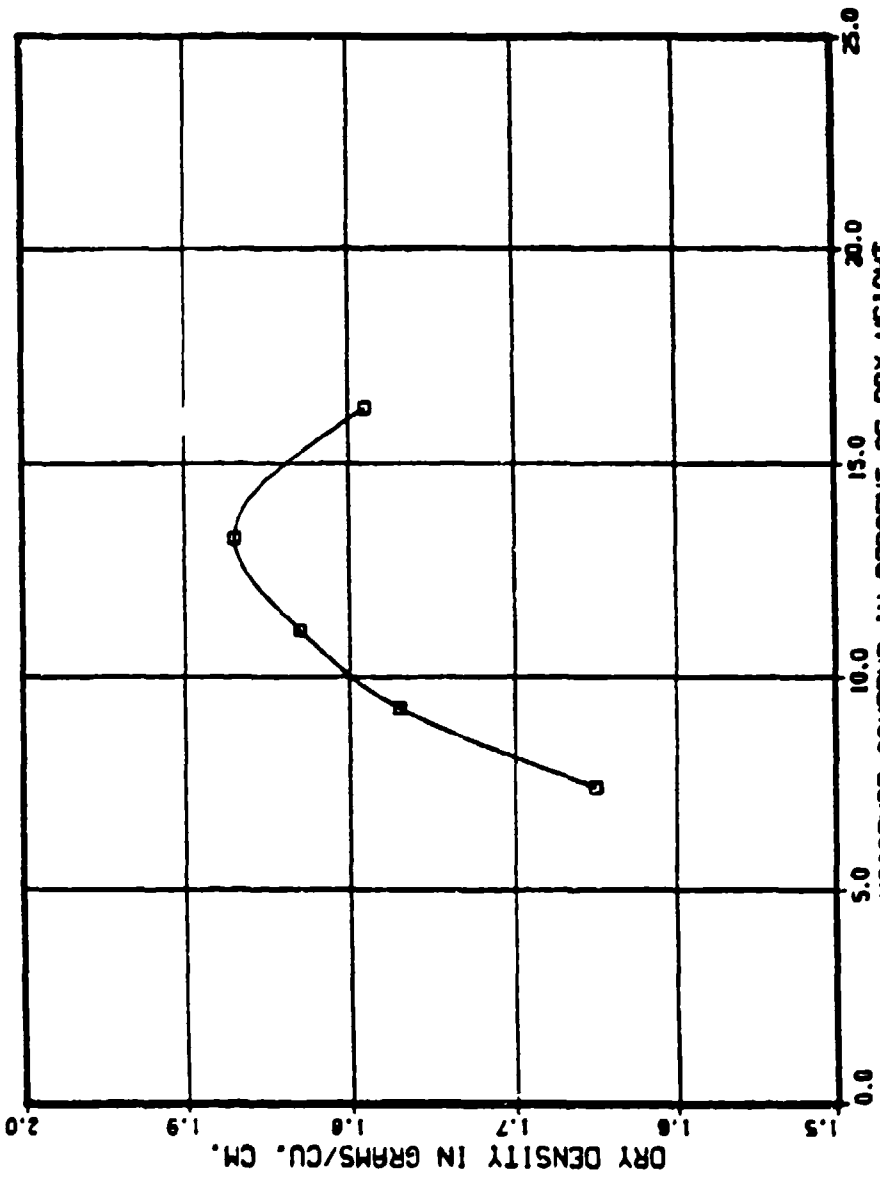

Figure 3.5. Results from Harvard miniature compaction procedure.

mixed throughly. After mixing, a damp cover was placed over the soil for a period of 20 minutes to allow the soil-water mixture to equilibrate. Following the equilibration period, the soil was again mixed to assure that an even mixture was obtained.

The individual experimental specimens were then prepared by removing the appropriate soil mass from the batch mix to yield a given volume when compacted. At this time a small specimen of the batch mix was taken for a moisture content determination. The standard laboratory techniq[illegible] r moisture content determination was followed (ASTM-[illegible]216-80). The specimens were statically compacted in the confining cylinders by using a hydraulic press (see figure 3.6) with spacer rings (see figure 3.7) to control the specimen length (i.e., density). A description of the specimen confining system is presented section 3.4. Two nominal specimen lengths were used 12.7 mm and 6.35 mm. These lengths were chosen based on the work of Gaffney and Brown (1984). They reported that for specimen lengths greater than 13 mm difficulty was encountered in obtaining a transmitted stress signal.

Each specimen was then sealed in a plastic bag to minimize any moisture loss that might occur prior to the experiment. Eight tests were conducted to quantify the amount of moisture loss to be expected between the time the specimen was prepared and the time the experiment was

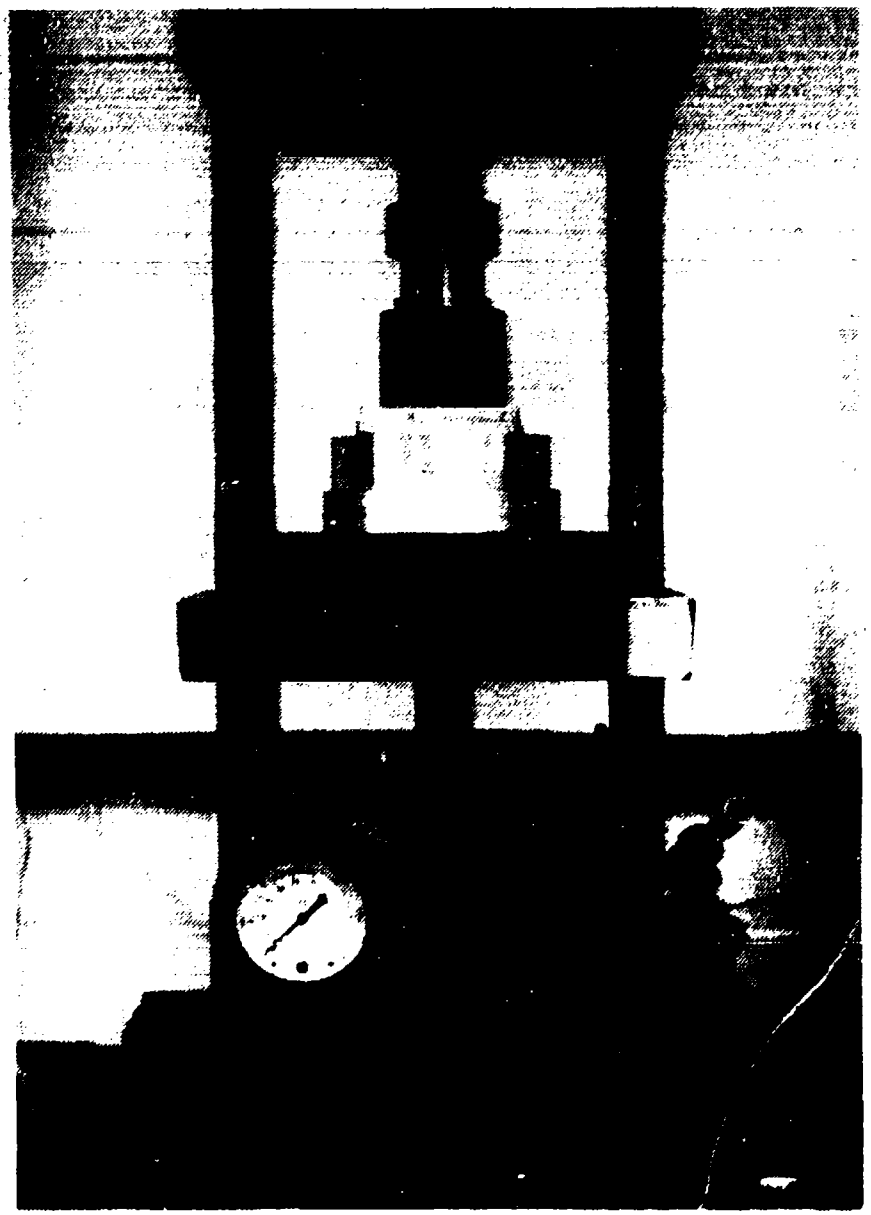

Figure 3.6. Hydraulic press used for static compaction.

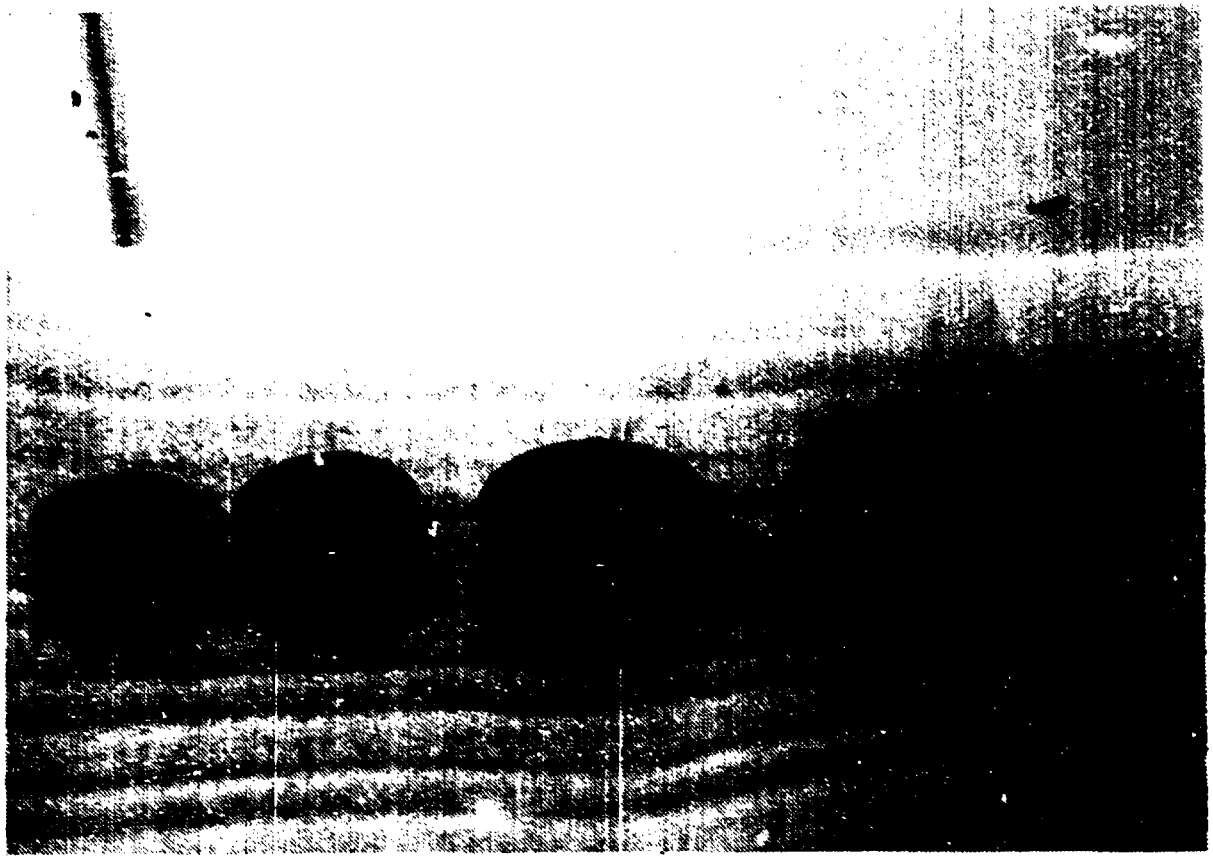

Figure 3.7. Spacer rings, confining cylinder, and plungers.

performed. The results showed an average loss was 5.4 percent of the total moisture with a standard deviation of 1.8. These results are believed to be representative of the pre-experiment moisture losses for the specimens prepared near optimum compaction conditions. The result for each test is presented in table E.2 of appendix E.

The same preparation procedure was followed for specimens prepared on the wet and dry side of optimum conditions.

Prior to performing the experiment, the specimen was removed from the plastic bag and the length of the specimen was measured inside the confining cylinder. This was accomplished by lowering a depth gauge from the lip of the cylinder to the surface of the specimen on both ends of the cylinder. Hence, by knowing the depth to the specimen surface on each end of the cylinder, and the length of the cylinder, the specimen length could be computed. At the completion of each experiment, the specimen length was again measured. The specimen was then extruded from the confining cylinder and a portion of the specimen used to determine the postexperiment moisture content.

Whenever a specimen of soil is compacted there will exist moisture and density variations over its length. A limited experimental study was conducted to evaluate the extent of these variations for specimens compacted using

the static compaction technique. The nominal length of the specimens prepared for this study was 12 cm. The experimental procedure and results are presented in appendix F. The results indicate that in general, a specimen will have the highest density at its ends and the lowest density at its center. The moisture content will vary from a high at the center to lower at the ends.

Although the specimen lengths used in the moisture and density variation study greatly exceeded the specimen lengths used for the SHPB experiments, the results can readily be interpolated. In short sections near the center of the specimen, the variations in density and moisture were less than 2 and 4 percent, respectively. During compaction, these variations are affected by friction between the soil and the confining cylinder. For long specimens a greater area will exist over which friction forces can act. Hence, friction will influence moisture/density variations to a greater degree in longer specimens than it will in short. Therefore, these values can be considered upper bounds for the short specimens used in the SHPB experiments.

3.4 Specimen Confining System

To achieve a nearly uniaxial strain environment for the experiments, the soil specimen was compacted in a thick-walled confining cylinder. The condition of uniaxial

strain will be confirmed in section 5.3. The concept of confining a SHPB specimen such that it will experience a condition of nearly uniaxial strain was first presented by Bhushan and Jashman (1978).

The nominal dimensions of the confining cylinder are 60.3 mm inside diameter, 102 mm outside diameter, and 44.5 mm in length. The confining cylinder served several purposes; first, to contain the soil specimen itself, and second, because the specimen will experience a state of nearly uniaxial strain, the effects of radial inertia are avoided. The confinement also prevented specimen distortion or barrelling during the experiment.

When the confining cylinder containing the specimen was placed between the pressure bars approximately 19.0 mm of the cylinder overlapped the bars on each end (see figure 3.8). To determine if the confining cylinder was transferring any stress to the transmitter bar, a test was conducted with the bars separated a distance of 3.0 mm and the confining cylinder placed over the air gap. The 3.0 mm distance was greater than the anticipated displacement of the incident bar. If the confining cylinder did indeed transfer stress to the transmitter bar, a signal would be recorded at the transmitter bar strain gauge; if not, the strain gauge record should be flat. The results indicated that the confining cylinder did not transfer any measurable stress to the transmitter bar.

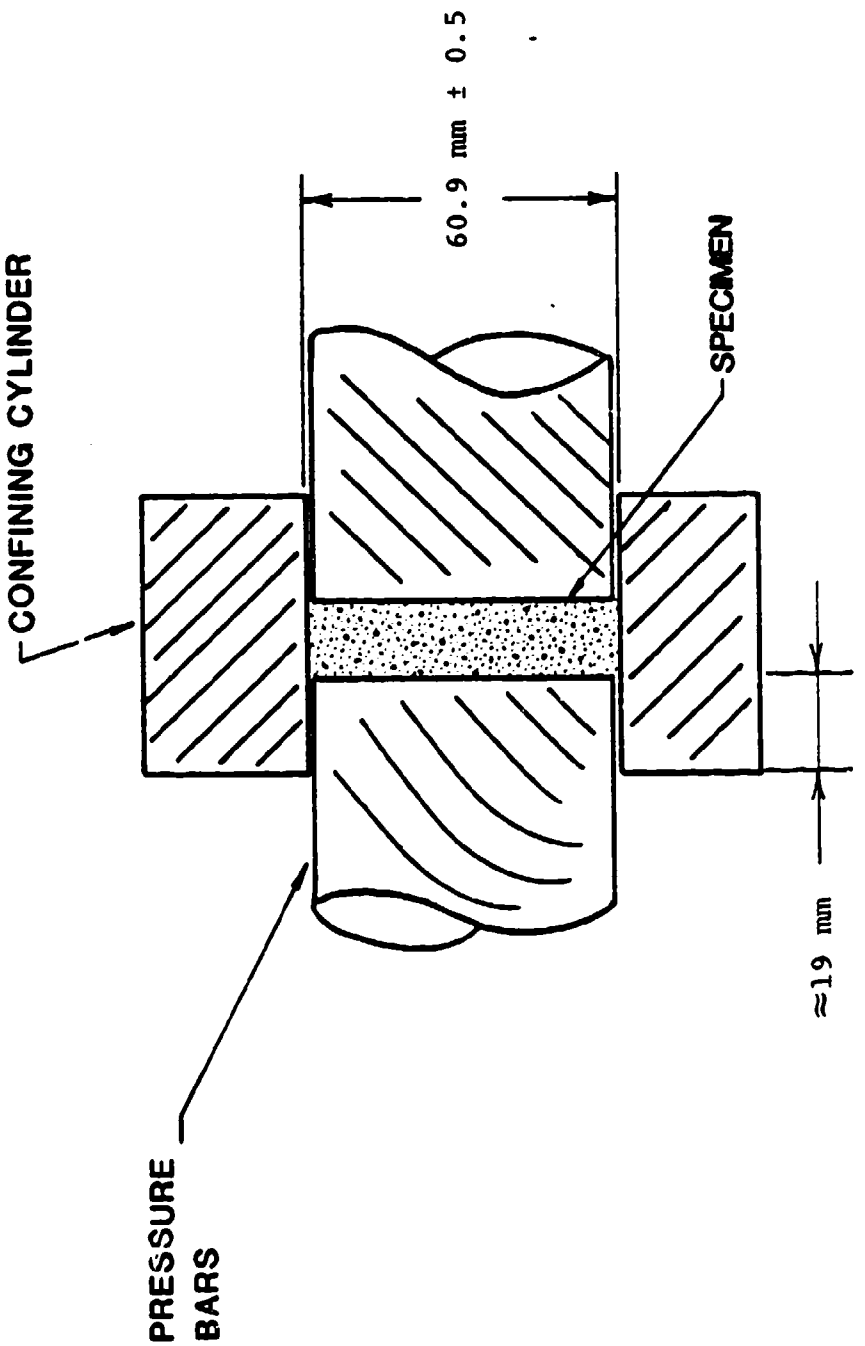

Figure 3.8. Confining cylinder with specimen positioned between the pressure bars.

4. EXPERIMENTAL ASSUMPTIONS AND DATA ANALYSIS

4.1 Experimental Assumptions

The limitations of the SHPB experimental method are dependent on how well the assumptions required to reduce the data are satisfied. These assumptions are:

(1) there is a uniform distribution of axial and radial stress over the length of the specimen,

(2) the waves in the pressure bars propagate without dispersion,

(3) the stress state over the cross sectional area of the pressure bars is one-dimensional, and

(4) the interfaces between the pressure bars and the specimen are frictionless.

These are the basic assumptions made Kolsky (1949). Each assumption and its bearing on the experimental results will be described.

4.1.1 Uniform Distribution of Stress

As the stress wave first enters the specimen axial and radial inertia forces act to oppose the equilibration of stress. This establishes a stress gradient between the two faces of the specimen. If the wave-transit time in the specimen is small compared to the duration of the applied

stress wave, many reflections can take place within the specimen. The stress gradient will diminish, resulting in a nearly uniform distribution of stress over the length of the specimen. If there is insufficient time for the stress in the specimen to equilibrate, the experiment is one of wave propagation rather than one of uniform stress. Should this be the case, a constitutive equation would be required to study the phenomena. This defeats the purpose of the experiment as it is the the constitutive equation that is sought in the first place. Hence, if care is exercised in selecting specimen geometry and the duration of the applied stress wave, the SHPB experiment provides a method of obtaining a material relationship without the disadvantages of having to undertake a wave propagation analysis.

This assumption is perhaps the most difficult to satisfy when using soil specimens in a SHPB experiment. Because soils exhibit nonlinear hysteretic behavior and have low wave speeds (e.g., $\cong 300$ m/s) there may be insufficient time for the stress gradient between the two faces of the specimen to diminish. Therefore, to satisfy the uniform stress assumption the specimen aspect ratio will have to be small and the duration of the applied stress wave long.

4.1.2 Wave Dispersion

The stress wave initiated by the impact of the striker bar on the incident pressure bar is initially very complex. This is due in part to friction at the striker bar-incident bar interface, as well as the appearance of spherical and dilatational waves (Follansbee and Frantz, 1983). These end effects disappear at about 10 bar diameters from the point of impact (Wasley, 1973, and Yeung Wye Kong et al., 1974).

Figure 4.1 shows the waves as recorded by the incident bar strain gauge in a test in which no specimen was placed between the incident and transmitter bars. The incident and transmitter bars were separated such that the specimen-incident bar interface was a free end. In this configuration, the applied stress wave upon reaching the free end is reflected as a tensile wave with amplitude equal, but opposite in sign to the applied wave. If the wave does not disperse during propagation, the two waves should be identical. Clearly, wave dispersion does occur as the period of the oscillations of the reflected wave are greater than those of the incident wave.

Figures 4.2 and 4.3 demonstrate the application of the dispersion correction (see appendix A) to the waves generated in the SHPB test with the specimen-incident bar interface as a free end (see section 2.5). Figure 4.2 compares the reflected stress wave as recorded at the

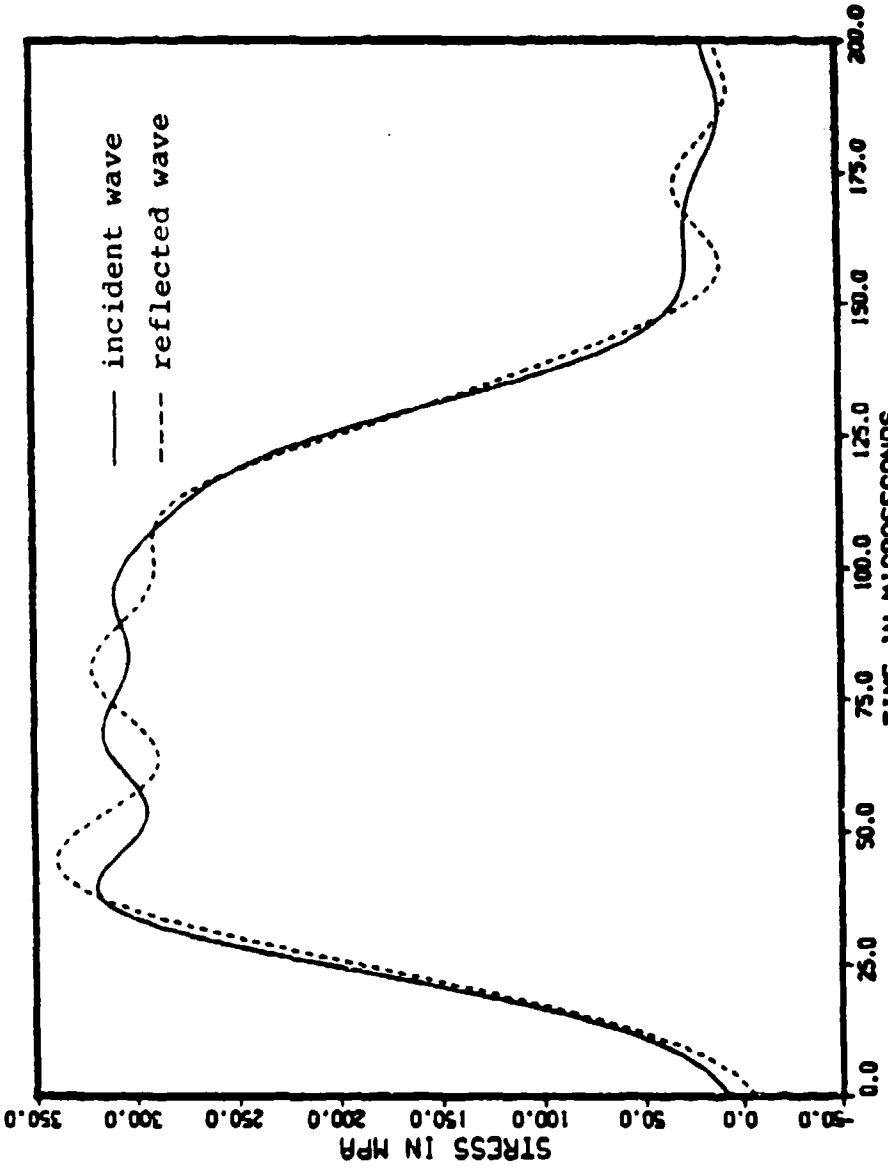

Figure 4.1. Uncorrected incident and reflected (inverted) stress waves.

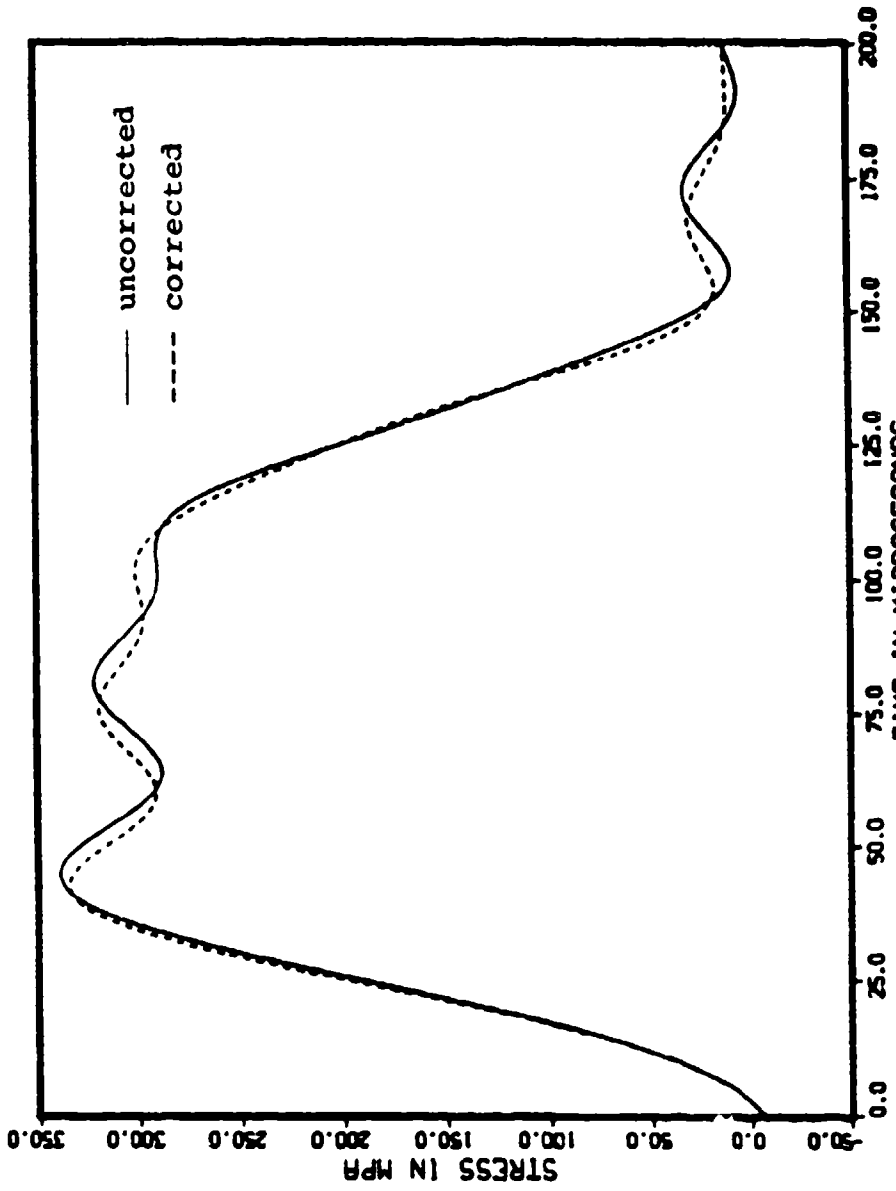

Figure 4.2. Comparison of uncorrected and corrected reflected stress waves (waves have been inverted).

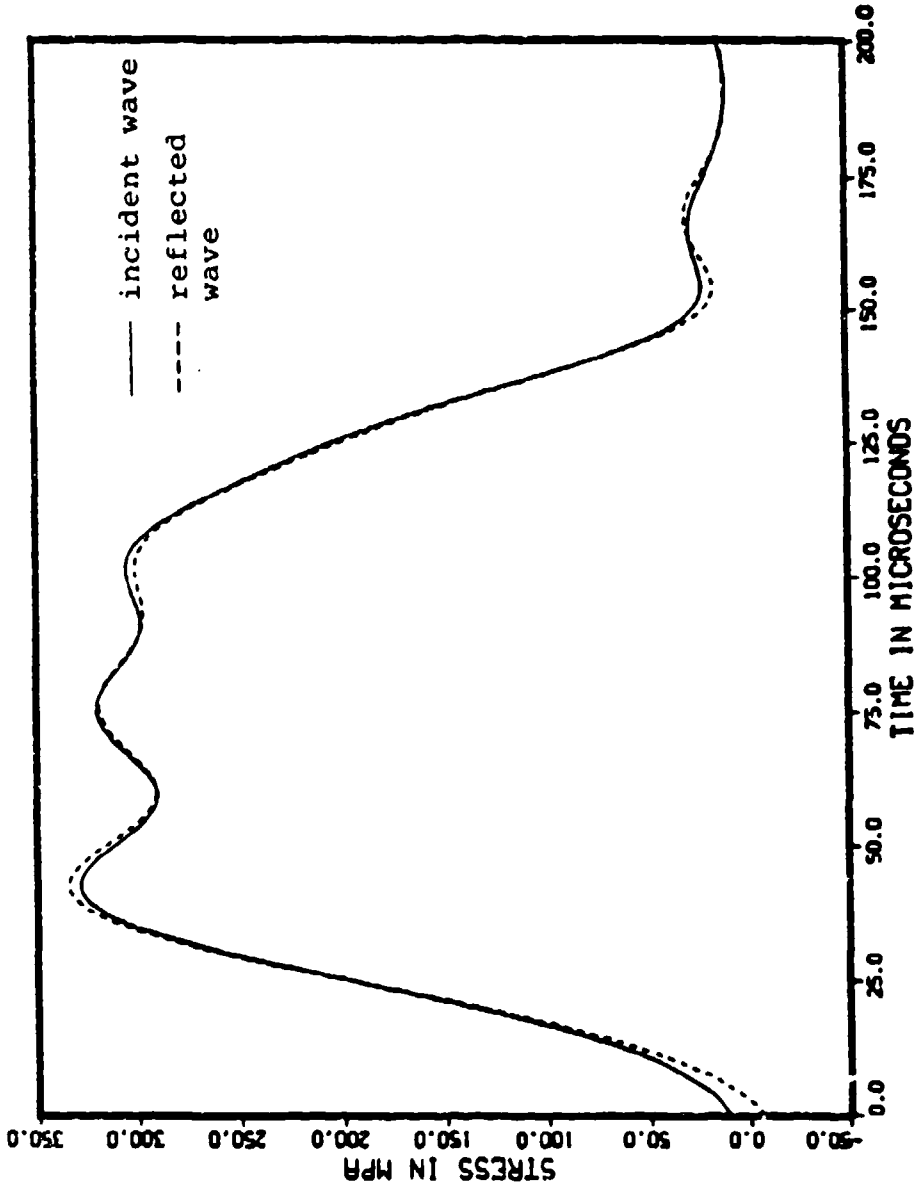

Figure 4.3. Corrected incident and reflected (inverted) stress waves.

strain gauge location with the dispersion corrected wave as reconstructed at the specimen-incident bar interface. It is evident that the dispersion correction has effectively compressed the reflected wave during the reconstruction. This is to be expected as the phase angle will decrease for negative values of Δx (see appendix A, equation A.26). In figure 4.3 the dispersion corrected incident and reflected stress waves as reconstructed at the specimen-incident bar interface are shown. From figure 4.3 it can be seen there is a correspondence of the peaks and valleys of the two waves. This correspondence was not evident between the uncorrected stress waves at the recorded strain gauge position (see figure 4.1). This correspondence supports the assumption that only the fundamental mode of vibration is excited in the SHPB experiment (Follansbee and Frantz, 1983). If other modes of vibration had been present, the procedure of performing the dispersion correction based on obtaining the waves' component phase velocity and wavelength from the fundamental mode would not have been successful (Follansbee and Frantz, 1983).

Figure 4.1 clearly shows that wave dispersion does occur, while figure 4.3 shows that the Follansbee and Frantz (1983) correction procedure can be used to account for the phenomenon. If dispersion is not accounted for in the reduced experimental data, large oscillations will appear in the stress-strain curve which can mask trends and

increase the difficulty in interpreting specimen response (see section 6.1.2).

4.1.3 Stress Variation Over the Cross Section of the Bar

The information required to evaluate the strain-rate-time, strain-time, and stress-time response of a specimen in a SHPB experiment is obtained from strain gauges mounted on the surface of the pressure bars (see figure 3.3). If this recorded information is not consistent with the stress-time response the pressure bar is experiencing over its cross sectional area, the resulting computations may be seriously in error. Hence, a significant condition that must be present in any SHPB experiment is that the longitudinal stress and displacement be nearly constant over the cross sectional area of the bar.

A prediction of the dispersion equation is that the longitudinal stress and displacement will vary over the cross sectional area of the pressure bars, and that the variation will be dependent on the ratio R/Λ (Davies, 1948). Therefore, errors are unavoidable if one-dimensional wave analysis is used to reduce the data. The significance of the error and its impact on interpreting experimental results was investigated by Davies (1948). Using the limiting condition of $R/\Lambda = 0$ as an error baseline (i.e., theoretically at $R/\Lambda = 0$ the longitudinal displacement

and stress are constant over the cross sectional area of the bar), Davies was able to establish that for $R/\Lambda < 0.1$, the displacement recorded at the surface of the pressure bar would differ from that at the bars longitudinal axis by $\pm$ 3 percent (Davies, 1948).

In this research the diameter of the pressure bars are larger than those used by past investigators by at least a factor of 2 and in some cases a factor of 3. For example, in the experiments performed by Lindholm (1964) the diameter of the pressure bars were 1.9 cm. A concern in using the larger bars is that the behavior over the cross section will deviate from one-dimensional condition that is assumed; hence increasing the error in the computations beyond that established by Davies. Any additional error and its affect on the computed specimen stress-strain response has been addressed in section 6.1.3.

4.1.4 Specimen-Bar Interface Friction

In the traditional SHPB experiment, a specimen with a diameter slightly less than that of the bars is placed between them (Lindholm, 1964). This is to allow the specimen to expand radially during the experiment while not exceeding the diameter of the pressure bars. As stress is applied to the specimen, radial shear stresses are created between the pressure bars and the specimen. This has been commonly referred to as "end effects" or "friction

effects." A result of these effects is that the specimen tends to be clamped at the specimen-bar interfaces (Green and Perkins, 1969). This prevents the specimen from expanding uniformly; hence, barreling of the specimen is often observed. This may result in a strengthing effect being observed in the stress-strain response (Betholf and Karnes, 1974). In addition, these effects may greatly increase the degree of nonuniformity of stress and strain in the specimen (Bertholf and Karnes, 1974).

To reduce the effects of friction it is common practice to apply a film of lubrication to the ends of the pressure bars in contact with the specimen. The results of the numerical study conducted by Bertholf and Karnes (1974) have shown this to be an acceptable method to miminize the effects of friction on stress-strain response. However, the effects of friction cannot be considered independently of specimen geometry, i.e., aspect ratio (Rand, 1967). Rand (1967) has shown that decreasing the specimen aspect ratio will have the same effect as increasing the coefficient of friction between the specimen and the pressure bars. Again as a result of the work of Bertholf and Karnes (1974), a specimen aspect ratio of 0.5 is thought to be an optimum.

However, for soil specimens an aspect ratio of 0.5 may be too restrictive due to the same concerns mentioned in section 4.1.1 (i.e., low wave speed and nonlinear hysteretic behavior). Therefore the aspect ratio for a soil

specimen must be large enough so that friction effects are minimized but small enough to permit stress equilibration within the duration of the applied stress wave. A method to retain a small aspect ratio while avoiding friction effects is to contain a soil specimen in a confining cylinder. The confining cylinder prevents barreling and excessive radial strain so that the specimen is in a state of nearly uniaxial strain (see section 5.4). Hence, friction effects on specimen stress-strain response is minimized (see section 6.1.4).

4.2 Data Reduction Procedure

This section will present the steps used in the data reduction procedure to compute the average specimen strain-rate-time, strain-time, and stress-time response. The steps are:

(1) data input,

(2) correct each wave for dispersion,

(3) compute the average specimen strain-rate-time, strain-time, and stress-time response using equations (2.26), (2.27), and (2.33), and

(4) output processd data.

To perform the computations required in the data reduction procedure a computer program (REDUCE) was developed. A flowchart and listing of REDUCE is presented in appendix G along with an example of the output for

experiment 134.

4.2.1 Raw Data

Examples of the raw data recorded by the strain gauges for the two nominal specimen lengths are shown in figures 4.4 and 4.5. Figures 4.6 and 4.7 compare the raw data of figures 4.4 and 4.5 with the data after the dispersion correction procedure has been performed. Because the raw data are recorded at some distance away from the specimen-bar interfaces, and the equations used in the computations are only valid at the specimen-bar interfaces, each wave must be corrected for the dispersion that occurs between the strain gauge and the specimen-bar interface.

4.2.2 Processed Data

Figures 4.8 and 4.9 illustrate the waves of figures 4.4 and 4.5 after correction for dispersion and time shifting to the specimen-bar interfaces. The incident and reflected waves are shifted to the specimen-incident bar interface so that they will start at the same moment. The transmitted wave will be shifted to the specimen-transmitter bar interface but with a delay which depends on the wave velocity in the specimen. As the distance between the specimen-bar interface and the strain gauge is the same for both pressure bars, Δx, each wave is time shifted by $\Delta x/C_0$, where C_0 (4900 m/s) is the wave

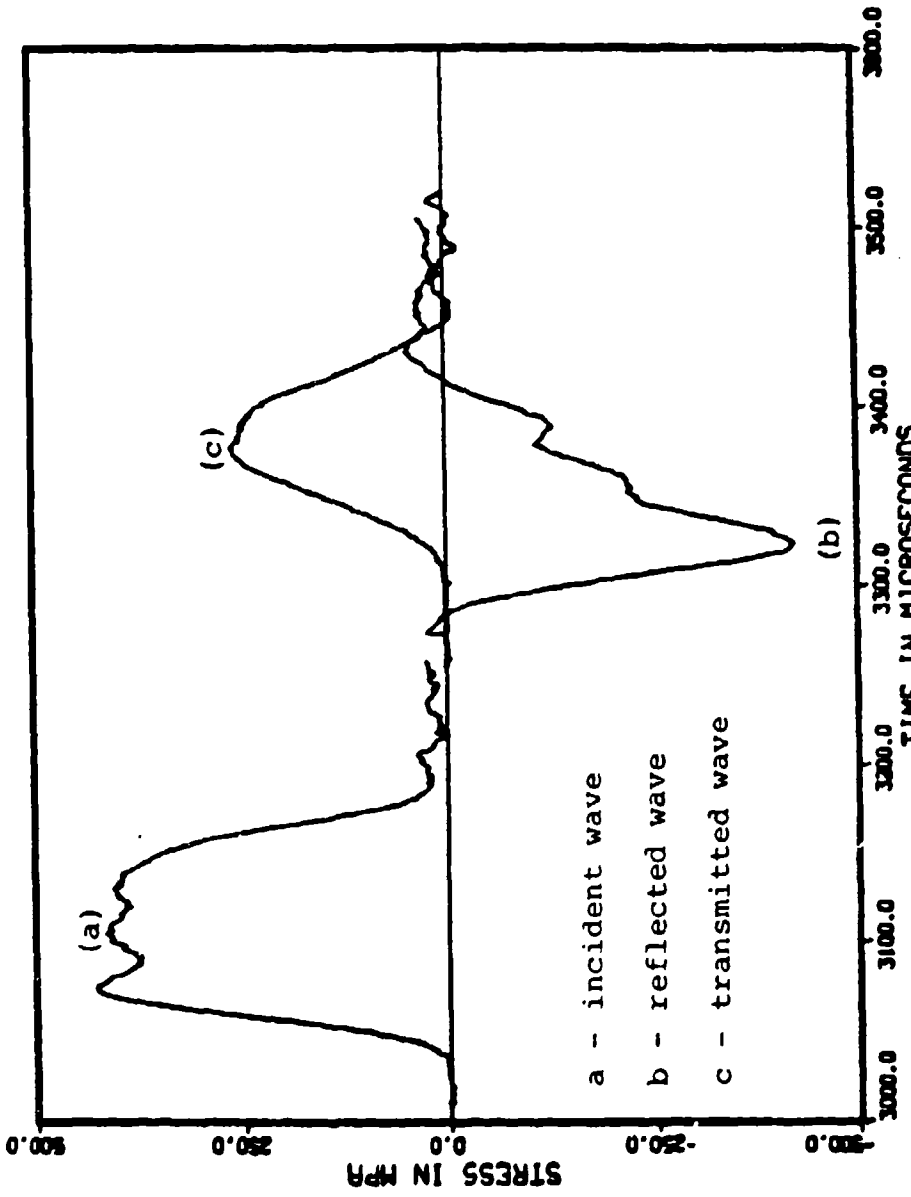

Figure 4.4. Uncorrected stress waves for a 6.35 mm specimen, experiment 115.

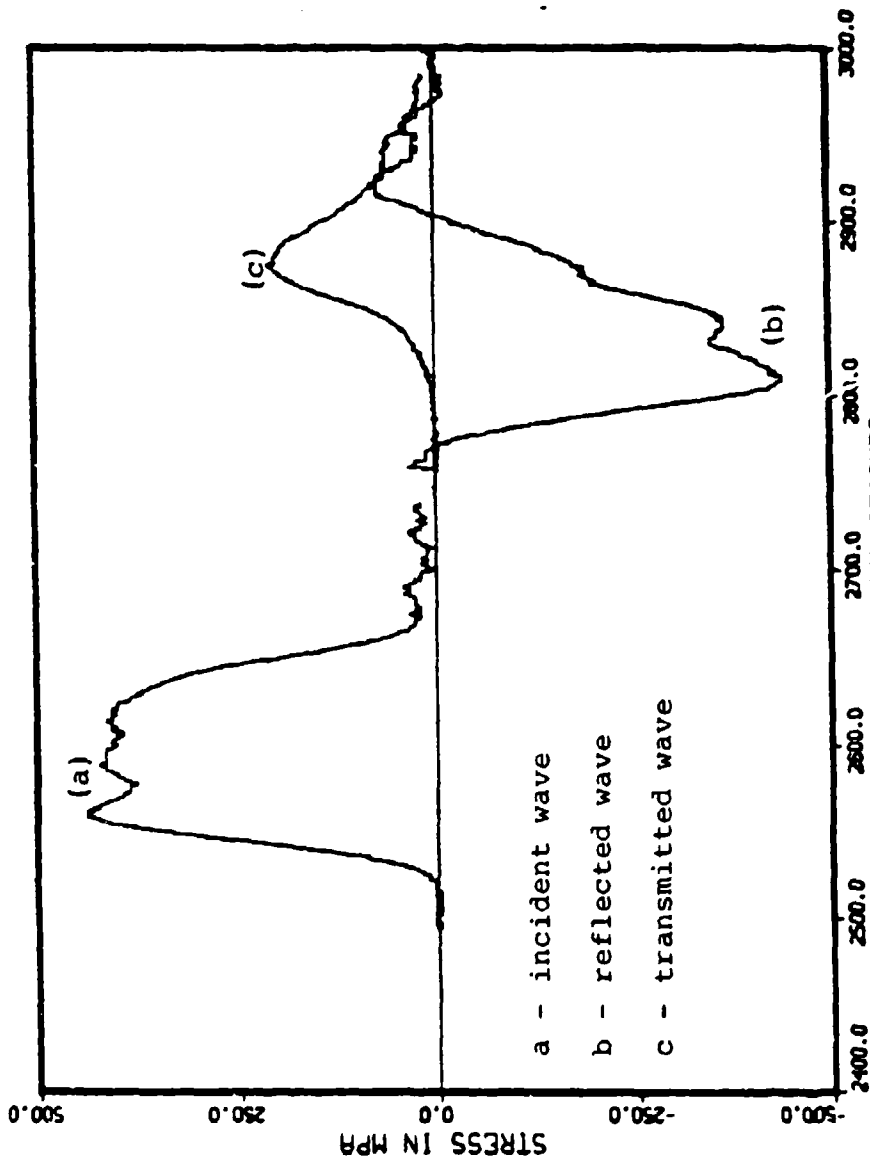

Figure 4.5. Uncorrected stress waves for a 12.7 mm specimen, experiment 134.

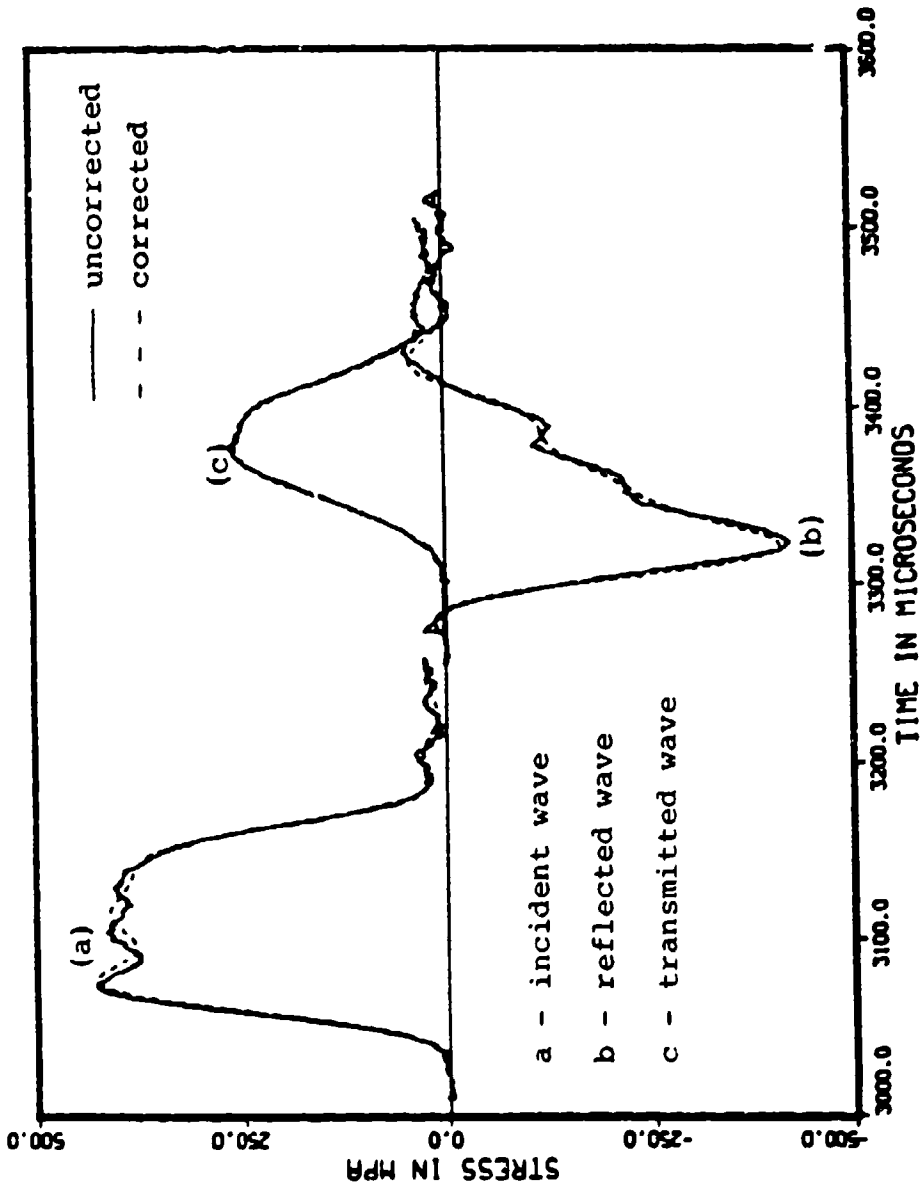

Figure 4.6. Uncorrected and corrected stress waves for a 6.35 mm specimen, experiment 115.

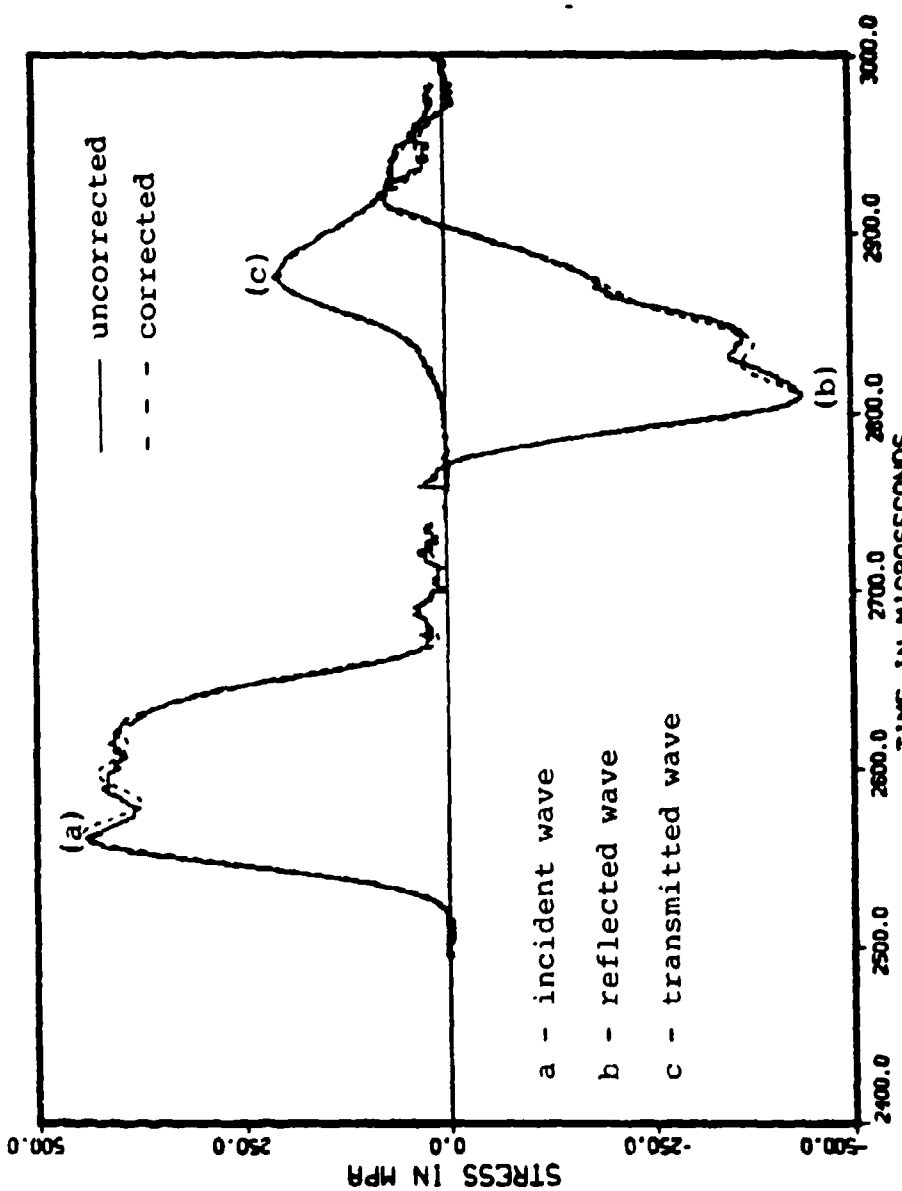

Figure 4.7. Uncorrected and corrected stress waves for a 12.7 mm specimen, experiment 134.

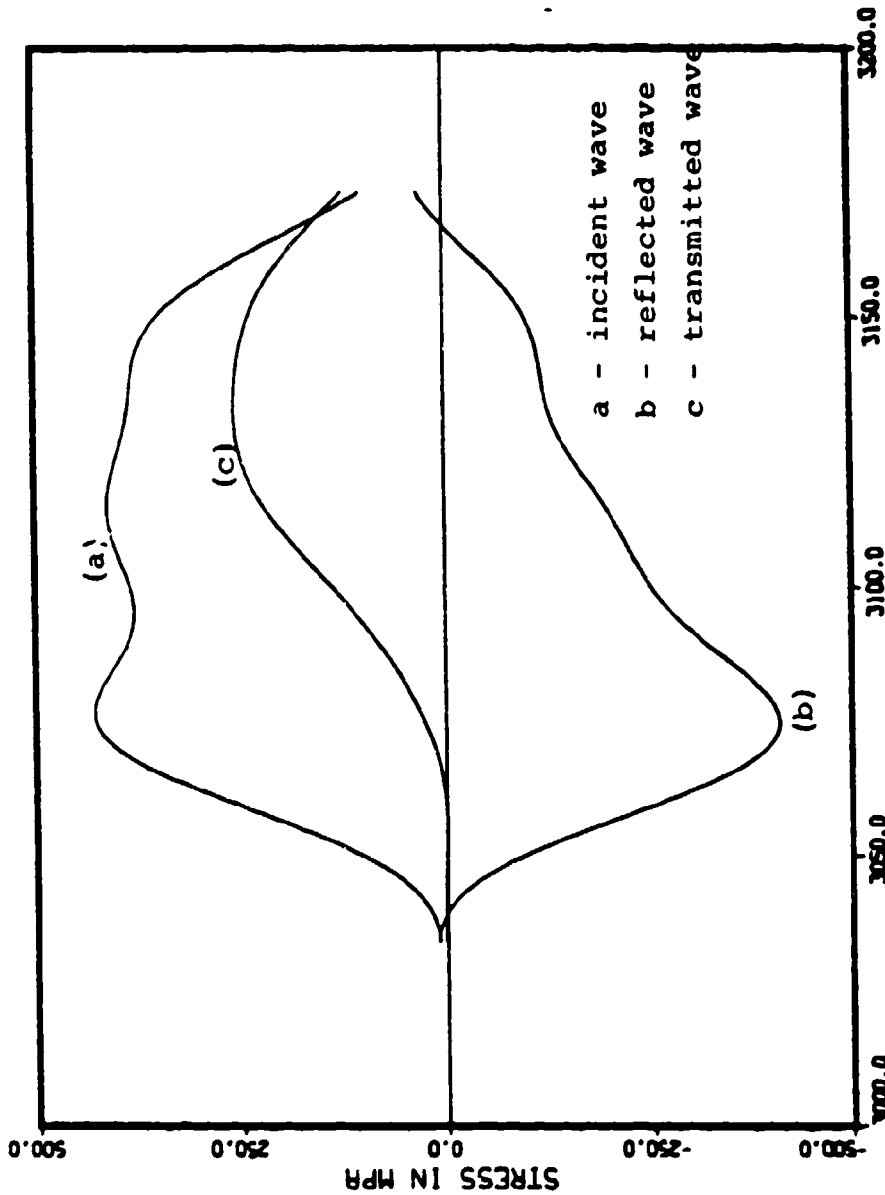

Figure 4.8. Stress waves for a 6.35 mm specimen corrected and time shifted to the specimen-bar interfaces, experiment 115.

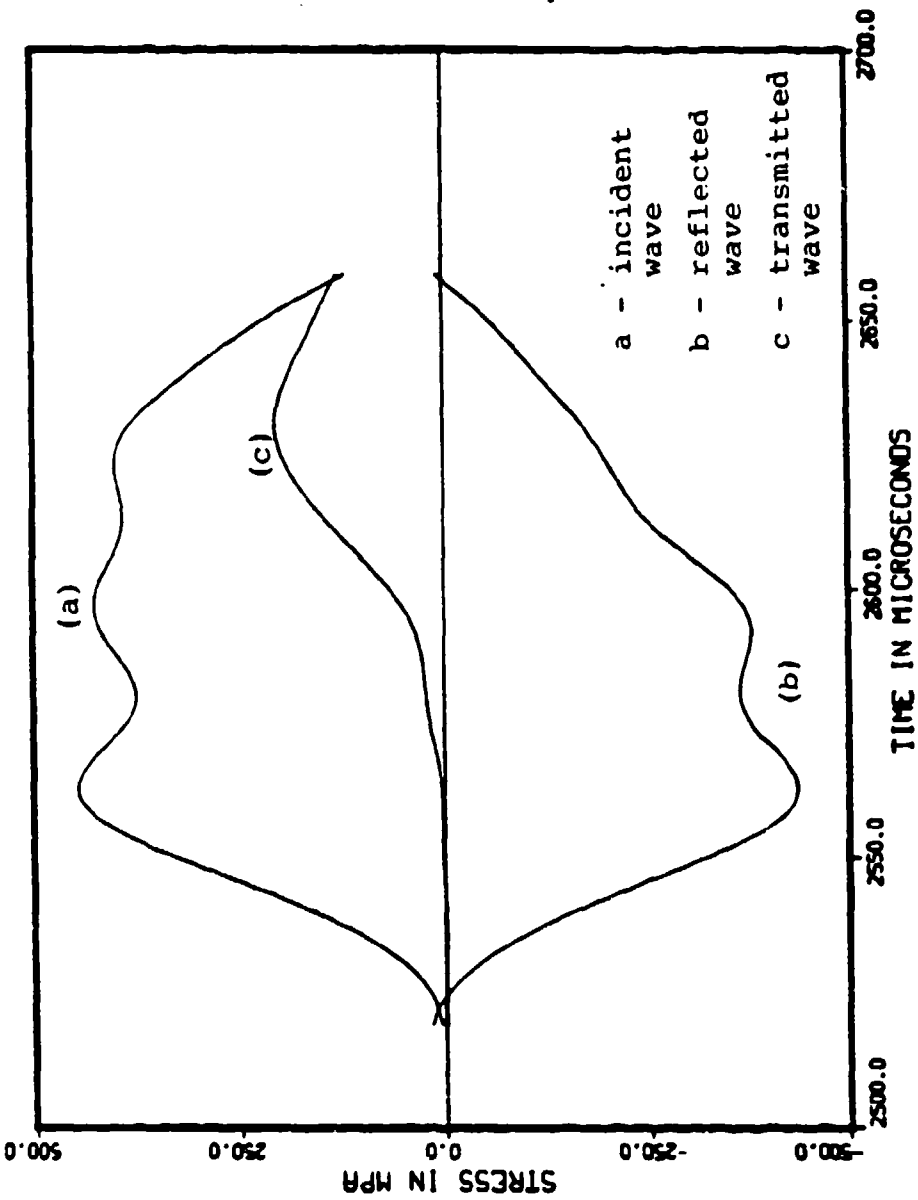

Figure 4.9. Stress waves for a 12.7 mm specimen corrected and time shifted to the specimen-bar interfaces, experiment 134.

velocity in the pressure bars.

Examples of the average strain-rate-time, strain-time, stress-time, and stress-strain response as computed by REDUCE for the two nominal specimen lengths are shown in figures 4.10 through 4.17.

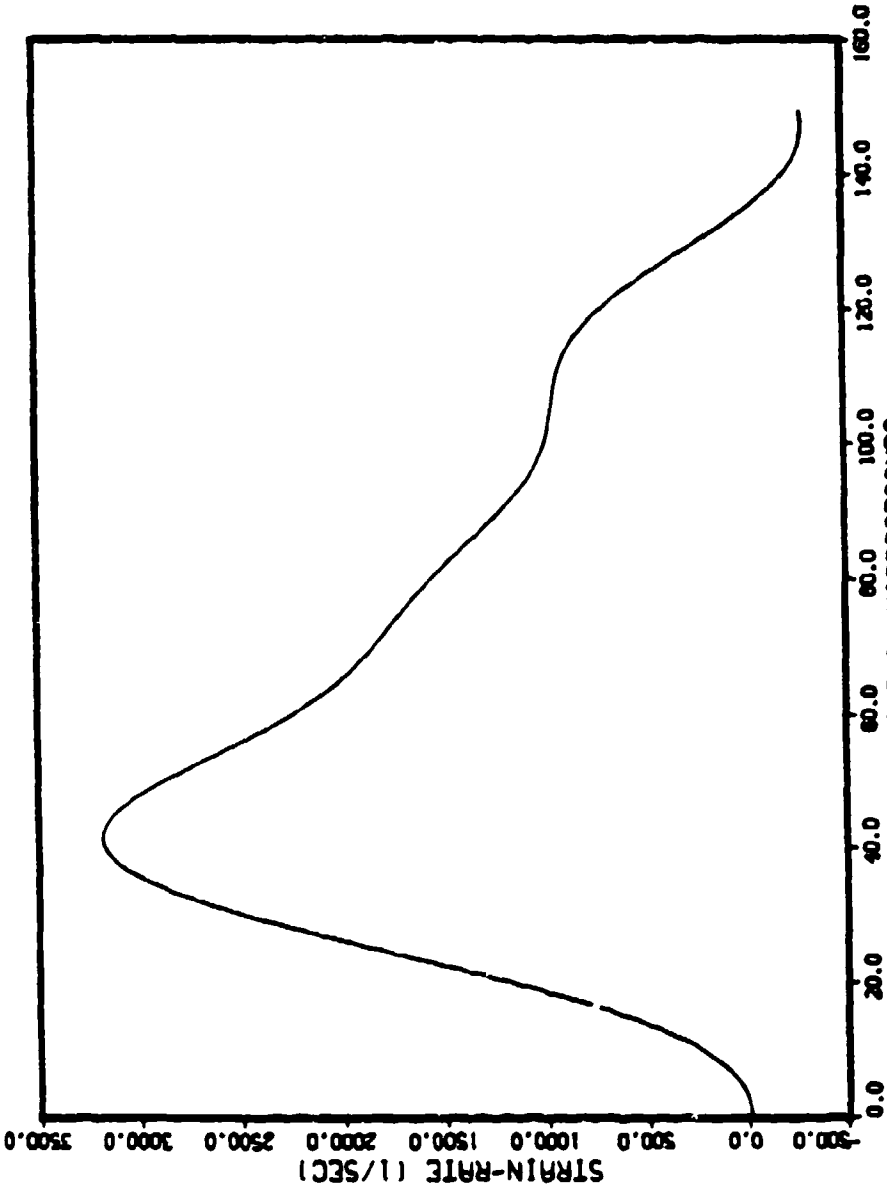

Figure 4.10. Strain-rate-time response for a 6.35 mm specimen, experiment 115.

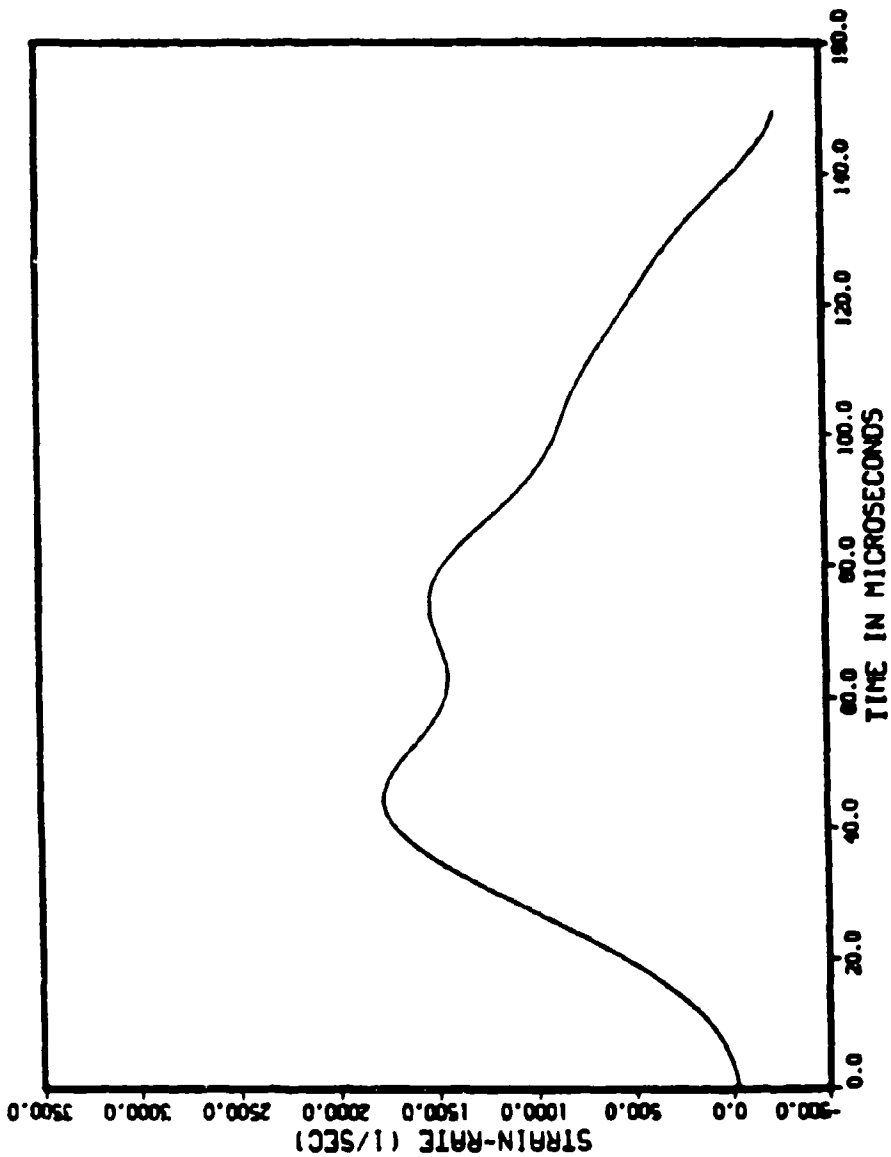

Figure 4.11. Strain-rate-time response for a 12.7 mm specimen, experiment 134.

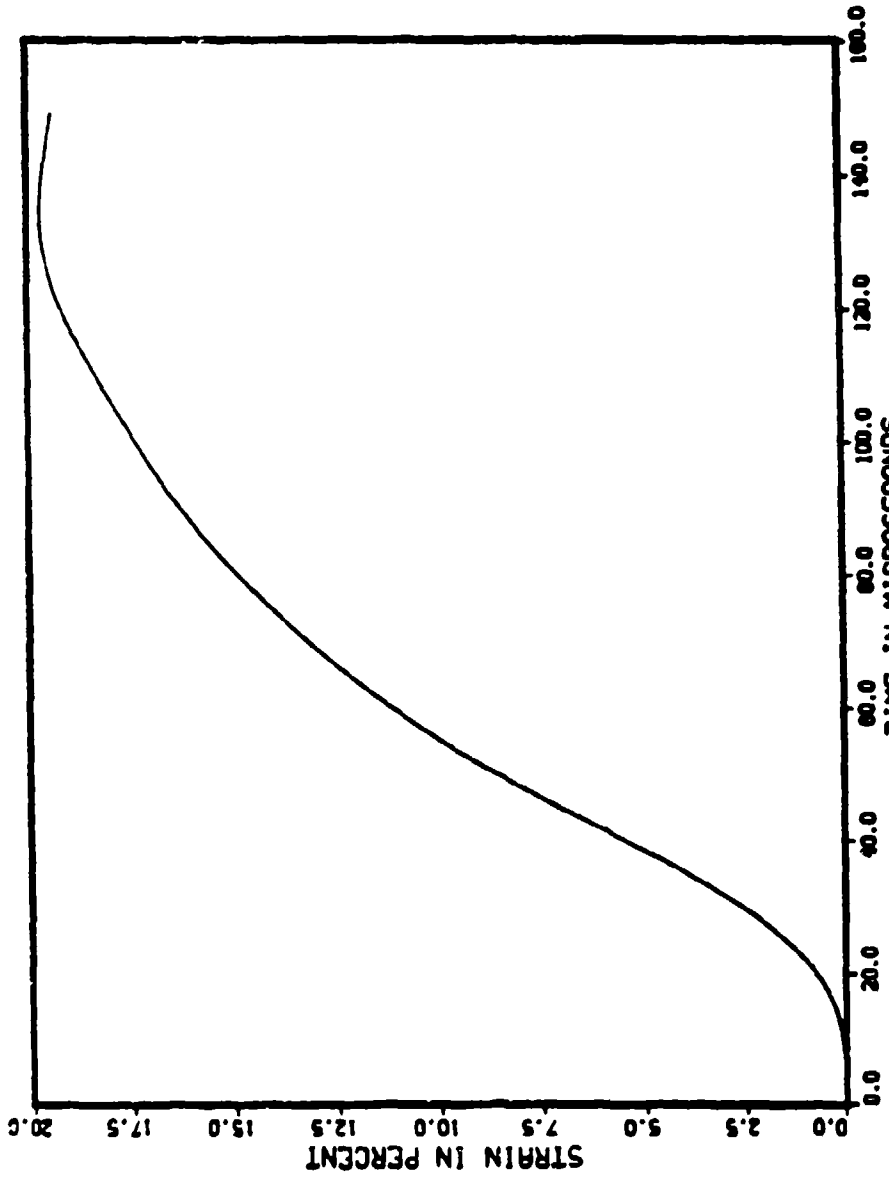

Figure 4.12. Strain-time response for a 6.35 mm specimen, experiment 115.

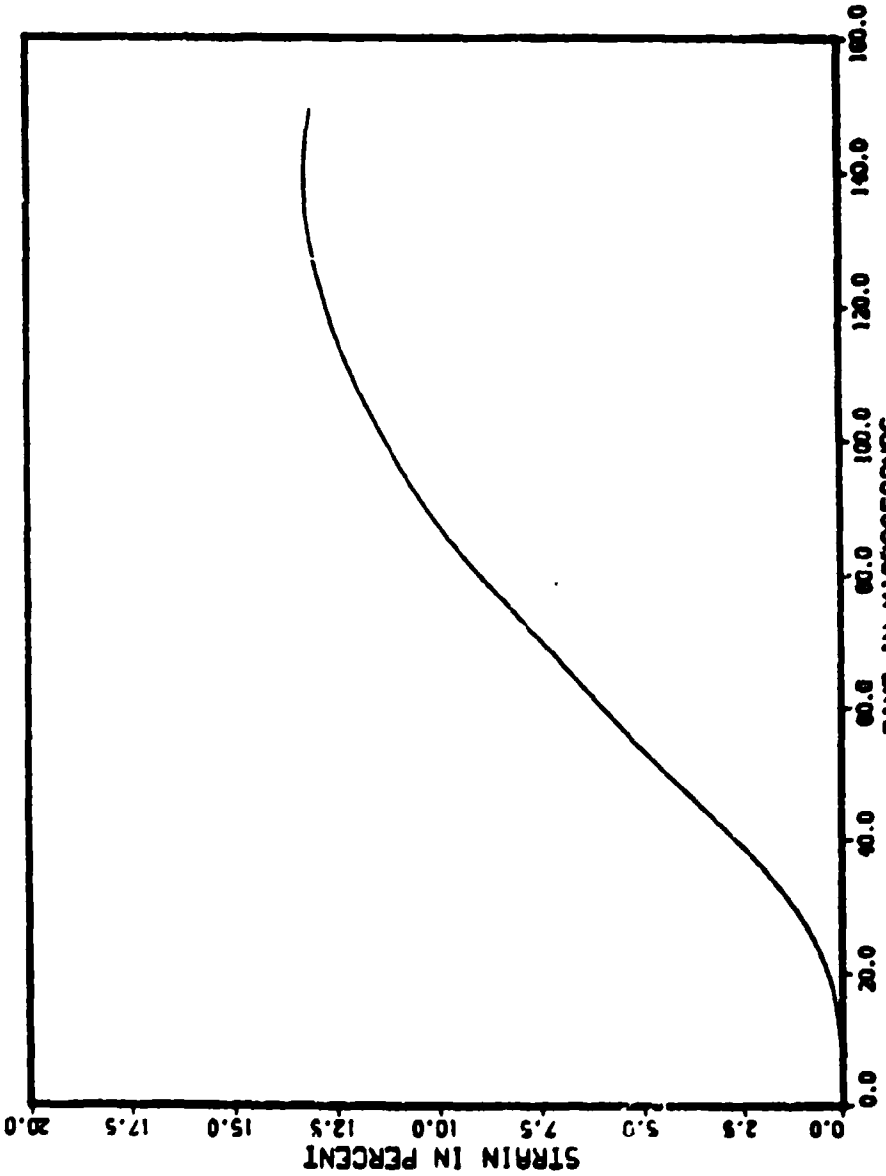

Figure 4.13. Strain-time response for a 12.7 mm specimen, experiment 134.

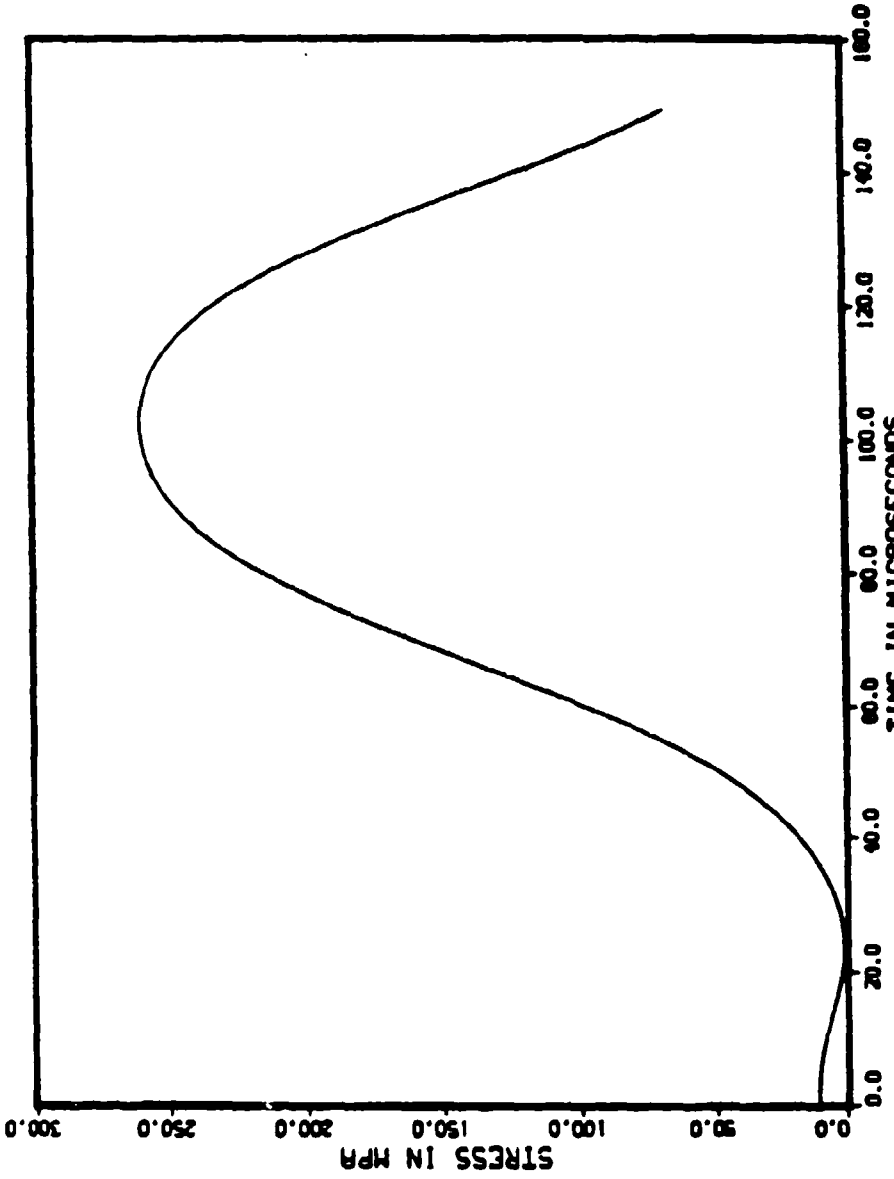

Figure 4.14. Stress-time response for a 6.35 mm specimen, experiment 115.

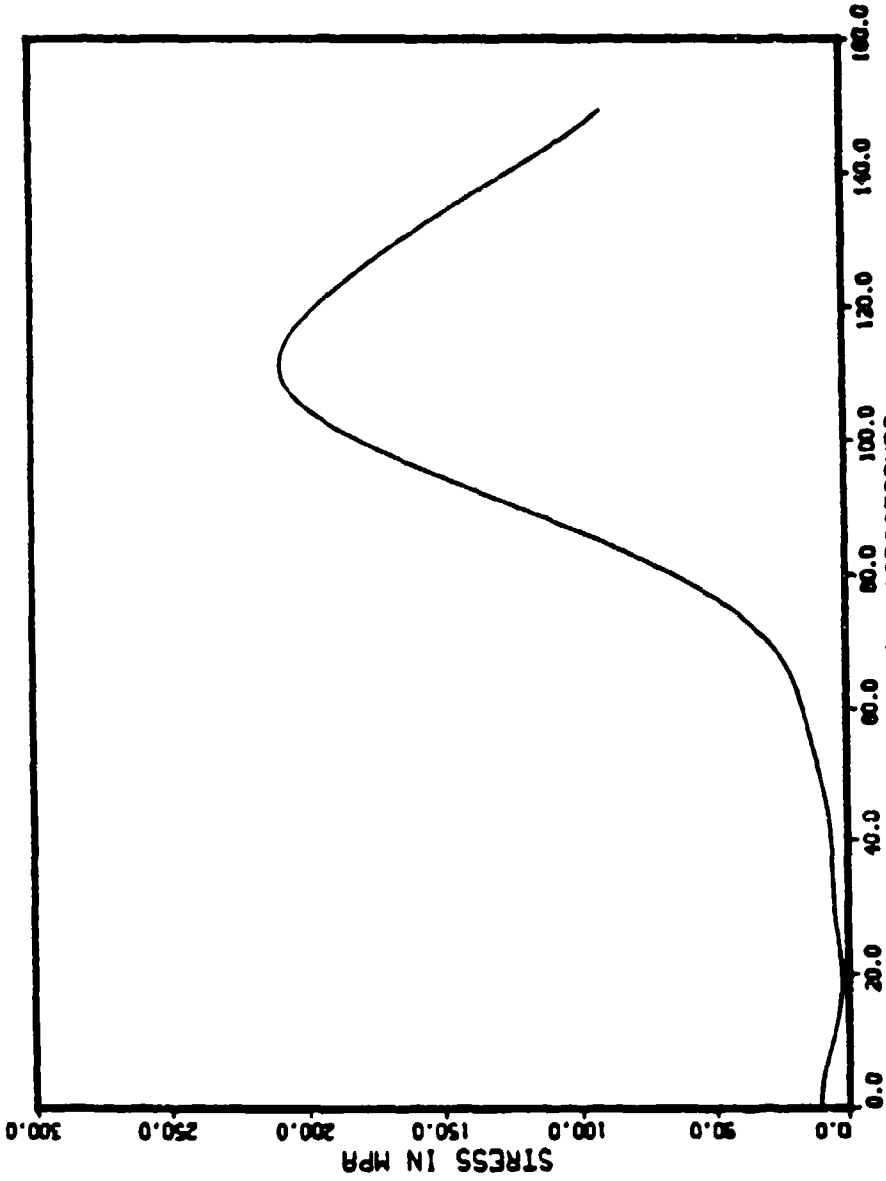

Figure 4.15. Stress-time response for a 12.7 mm specimen, experiment 134.

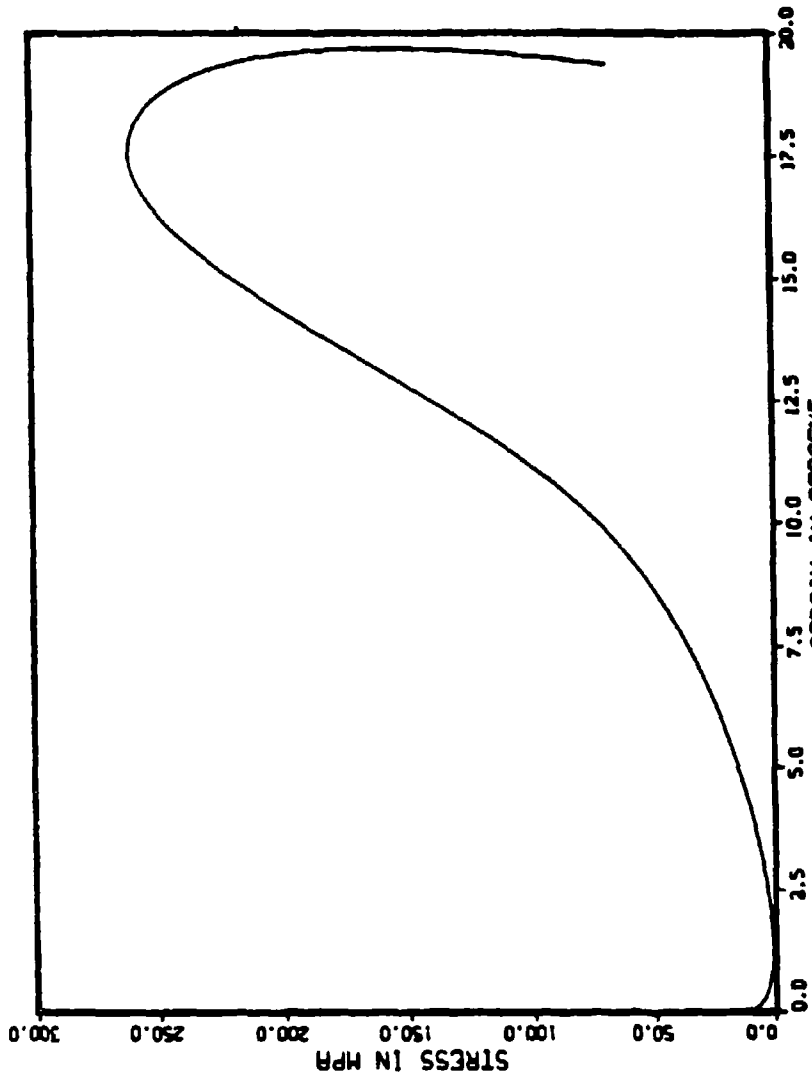

Figure 4.16. Stress-strain response for a 6.35 mm specimen, experiment 115.

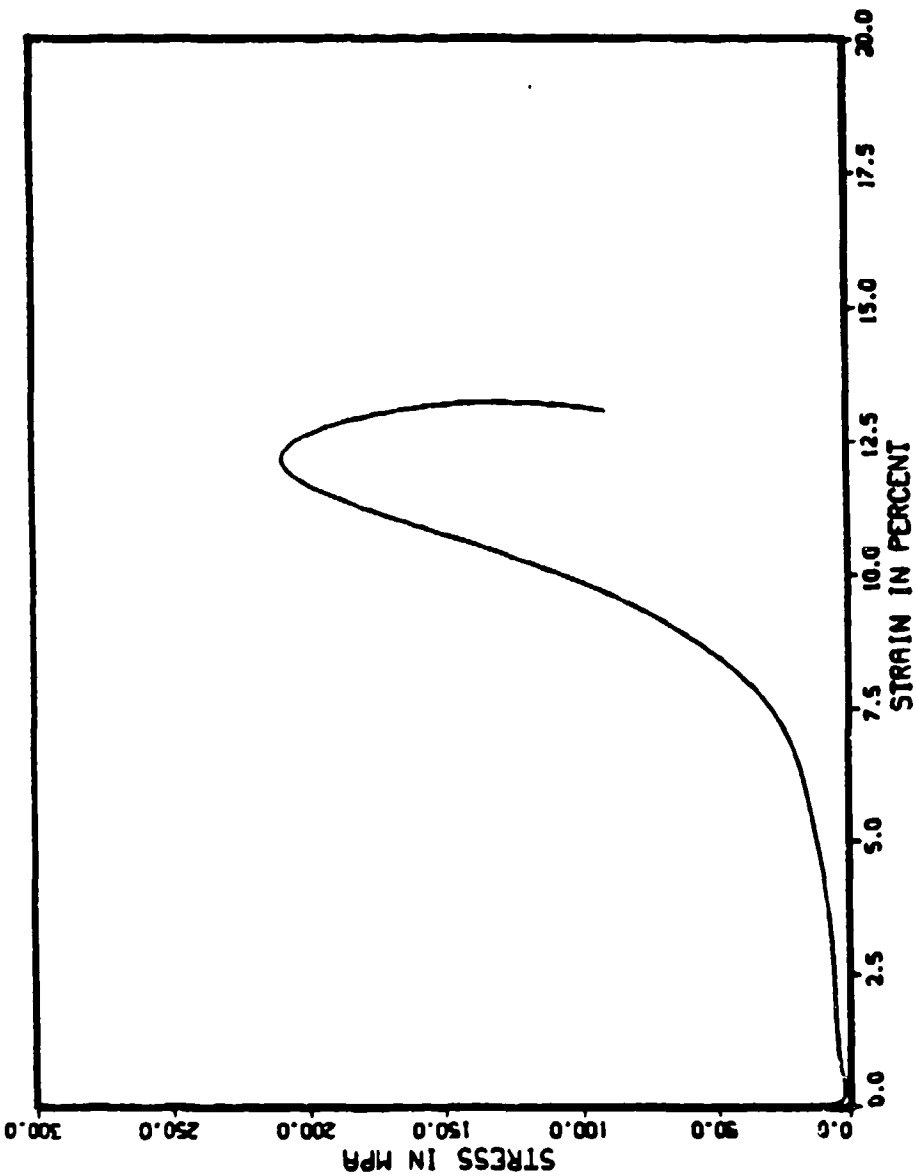

Figure 4.17. Stress-strain response for a 12.7 mm specimen, experiment 134.

5. PRESENTATION OF EXPERIMENTAL RESULTS

5.1 Experimental Results

In this research 50 experiments were conducted on compacted sand specimens. The compaction moisture and density combinations ranged from dry of optimum to wet of optimum conditions as determined by the Harvard miniature compaction procedure (see figure 3.5). The majority of experiments were performed with specimens prepared at or near optimum conditions. In most cases, a minimum of two experiments were conducted at each combination of specimen moisture content and density. The moisture/density data points for each group (i.e., specimens prepared dry, near, and wet of optimum) and their relationship to the Harvard miniature compaction curve are presented in appendix H. The applied stresses and maximum strain-rates for the experiments ranged from 130 MPa to 760 MPa, and from 500 s^{-1} to 5000 s^{-1}, respectively. The applied stress, peak stress, strain at peak stress, and strain-rate at peak stress for each experiment are tabulated in table E.3 of appendix E.

Three different length striker bars were available to generate the applied stress wave, 0.127, 0.254, and 0.508 m. Several experiments were performed with the 0.508 m striker bar; however, the incident wave and the

reflected wave were found to overlap. Hence, the termination of the incident wave and the commencement of the reflected wave could not be resolved. Dispersion of the incident wave was determined to be the cause of the overlap, and not the incorrect placement of the incident bar strain gauge. It was shown in section 4.1.2 that for positive values of Δx, the phase angle will increase causing the propagating wave to be stretched. The data from these experiments were not reduced. No experiments were attempted with the 0.127 m striker bar as the specimen would not be able to reach equilibrium within the duration of the stress wave ($\cong$50 microseconds). Hence, the 0.254 m striker was selected to initiate the stress wave for all the experiments reported herein.

Although 50 experiments were performed, only the results of 27 are used for the purpose of comparison. In the process of preparing the SHPB apparatus for firing, a seating strain was applied to the specimen. The amount of seating strain sustained by a specimen varied from experiment to experiment. This was an artifact of the SHPB apparatus and required a change in the experimental procedure so that the inherent variability was accounted for in the data reduction procedure. The cause of this difficulty and the procedure that was developed to measure the variable seating strain is discussed in section 6.2.

The procedure to measure the seating strain was

applied to experiment 112 and every experiment thereafter (see section 6.2). Accurate seating strains are necessary to determine the change in specimen length and phase relationships (e.g., initial gas porosity). A knowledge of these parameters is essential as they will influence a specimens response to a given stress. If accurate assessments are to made concerning for example experimental replication, the initial parameters of the specimens being compared must be similar. This is particularly critical for soil specimens. Hence, in the experiments where seating strains were not measured (i.e., 31 through 76), the results are not suitable for the purpose of comparison.

The average seating strain experienced by the specimens in experiment 112 through 167 was 7.5 percent with a standard deviation of 3.8. The results are tabulated in table E.4 of appendix E. For the experiments where the seating strain was not measured, the initial specimen length was adjusted by 7.5 percent for use in the computations. Figure 5.1 shows the stress-strain response for experiment 55 using the specimen length that was measured just before it was placed between the bars and the adjusted length. It is evident that the overall reponse is not affected by adjusting the specimen length by 7.5 percent. However, the correct response to use for comparison is not known. It will be shown throughout this

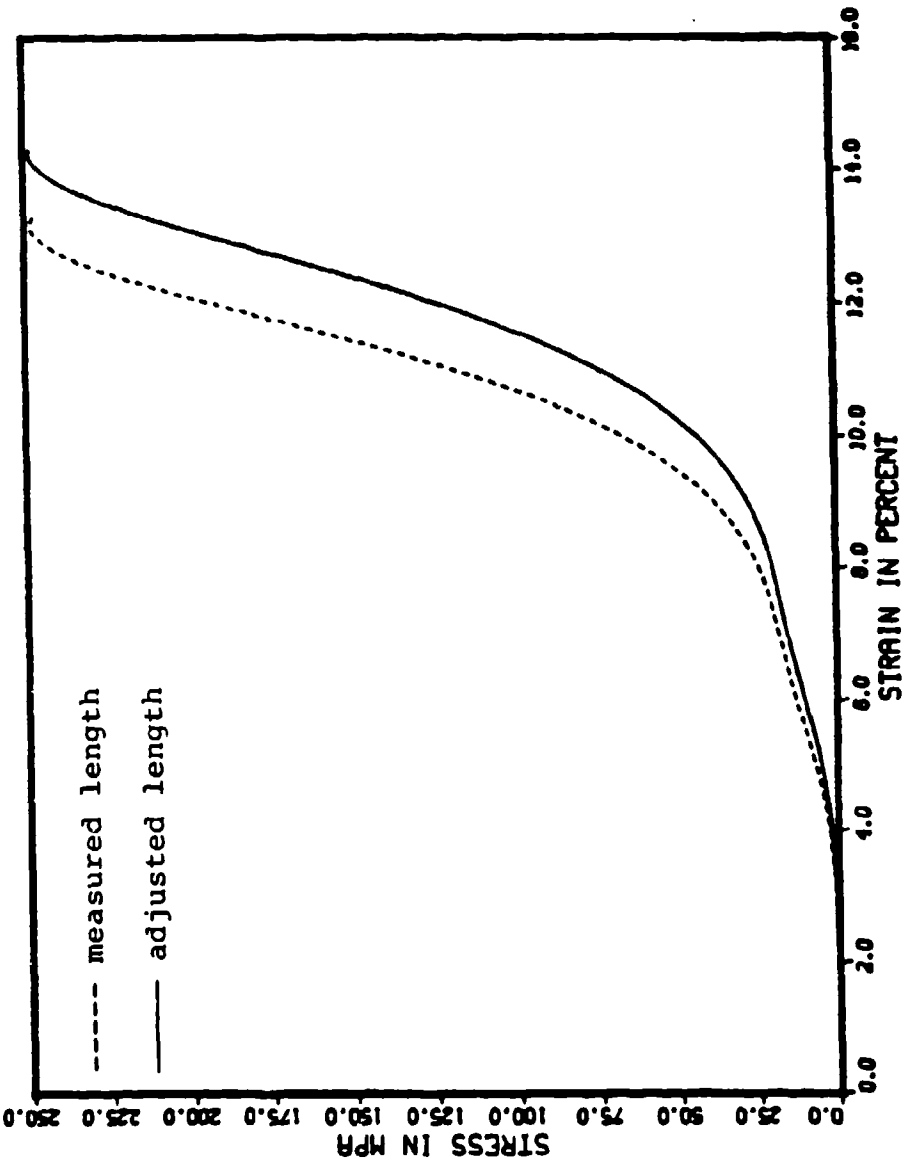

Figure 5.1. Stress-strain response for experiment 55.

chapter the response is not inconsistent with the response obtained in experiments where the seating was measured. Hence, although the specimen stress-strain response for experiments 31 through 76 is consistent, they are not suitable for the purpose of comparison. The computed stress-strain response and summary information for each of the 50 experiments are presented in appendix I.

5.2 Stress-Strain Response

Figure 5.2 shows the stress-strain response for a 12.7 mm specimen to an applied stress of 400 MPa. The response is representative for both specimen lengths subjected to the applied stresses used in this research.

The stress-strain curve can be divided into three regions which describe the overall specimen response. The first, region O to A, is where inertia effects act to oppose the equilibration of stress. The extent of this region can be estimated by using the criterion of Davies and Hunter (1963) as well as experimentally (see section 6.1.1). At A the specimen is considered to be in quasi-equilibrium and the deformation nearly homogeneous. Region A to B is characterized by particle rearrangment into a denser packing and closing of the air voids. The strain at B is equal to the initial gas porosity of the specimen. At this point there are theoretically no air voids remaining.

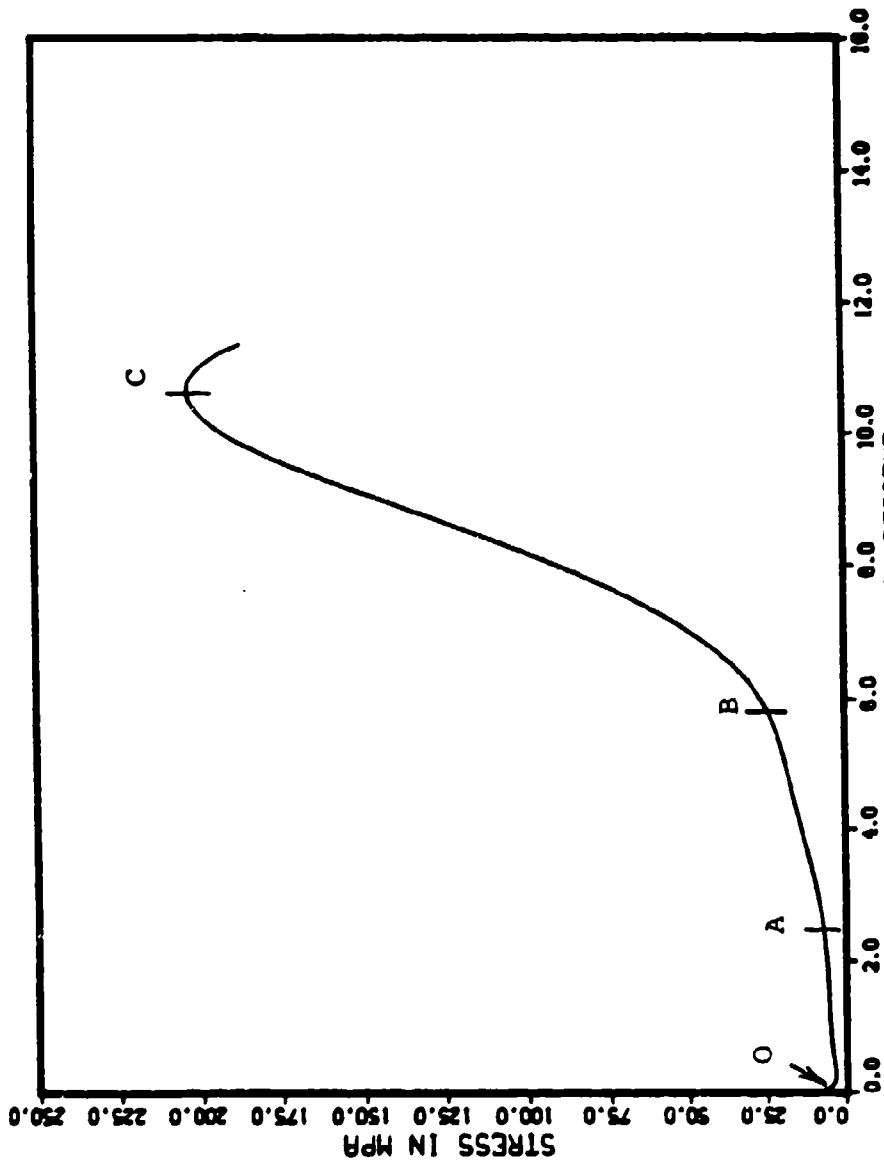

Figure 5.2. Stress-strain response for experiment 132.

The initial gas porosity of the specimen is computed as the volume of air contained in the specimen divided by the total volume of the specimen. In dynamic uniaxial strain experiments on partially saturated sand where the stress changes are large, the pore air will be highly compressed, and then dissolved in the pore water (Whitman, 1970). This behavior is characteristic of the response observed in region A to B. With no pore air remaining (zero gas porosity), the specimen will be fully saturated (point B). Under these conditions the compressive resistance of the water will greatly exceed the compressive resistance of the soil skeleton (Whitman, 1970). When this occurs, the specimen will become strongly resistant to additional deformation. This behavior governs the response in the region B to C.

In the unloading region of the curve (i.e., beyond point C), the specimen in many of the experiments continued to acculumate strain (e.g., see figures 4.16 and 4.17). The cause of the additional strain accumulation may be that the specimen can retain some memory of its loading. Another cause might be the extrusion of material. The potential for loss of material during the experiment is discussed in section 6.4. The unloading region of the curve will not be used in the analyses.

5.3 Uniaxial Strain Path

A nearly uniaxial strain state is forced upon the specimen by the fact that it is contained in a confining cylinder. This condition may be verified by comparing the radial strain experienced by the confining cylinder and maximum longitudinal strain experienced by the specimen. The radial strain was estimated by computing a maximum radial deflection of the confining cylinder using thick-walled cylinder theory. The equation used to compute the radial deflection of a thick-walled cylinder subject to internal pressure was (Seely and Smith, 1952);

$$\Delta R = \frac{P\ R_1}{E}\left[\frac{R_2^2 + R_1^2}{R_2^2 - R_1^2} + \nu\right] \quad , \qquad (5.1)$$

where R_1 is the inside radius of the cylinder, R_2 is the outside radius of the cylinder, P is the internal pressure, E (10 GPa) is Young's modulus of the confining cylinder, and ν (0.3) is Poisson's ratio for the confining cylinder. The internal pressure was taken as the peak stress experienced by the specimen. This assumes that Poisson's ratio for the soil is 0.5. The assumption is reasonable if the soil is near saturation as the pore water will be highly resistant to volume change (Whitman, 1970) In nearly all the experiments conducted the specimens were completely saturated at peak stress. The computed radial strain is thought to be an upper bound as

the internal pressure is not distributed over the entire length of the confining cylinder due to some overlap on the pressure bars (see figure 3.8). The results of the computations are presented in table E.5 in appendix E.

The computed radial strain of the confining cylinder for all experiments did not exceed 1 percent. Comparing the radial strain of the confining cylinder (ε_r) to the maximum longitudinal strain (ε_l) experienced by the specimen (see table E.3 in appendix E), it was found that;

$$\varepsilon_r < 0.06\,\varepsilon_l \quad , \tag{5.2}$$

for all experiments except one (experiment 137), where the radial strain was 9 percent of the longitudinal strain. Hence, by comparison, the specimen can be considered to be in a state of nearly uniaxial strain during the experiment.

5.4 Experimental Replication

If the SHPB technique is to prove useful for evaluating dynamic soil response, the reproducibility of experimental results must be established. This section will present the results of replicate experiments on different length specimens subjected to a range of applied stresses.

Replicate experiments were conducted at the nominal applied stresses of 250, 400, and 520 MPa and specimen

lengths of 6.35, and 12.7 mm. The variation in the applied stresses did not exceed ± 8 percent. The results are presented in figures 5.3 through 5.8. The applied stress is given in parenthesis next to the experiment identification.

From figures 5.3 through 5.8 the experimental results can be considered to be reproducible. It can be seen that in nearly all cases the slopes of the stress-strain curves, the peak stress, and the strain at peak stress for the replicated experiments are directly comparable (the computed values of peak stress are tabulated in table E.3 in appendix E). However, there are several discrepancies to be noted. In figure 5.5 both specimens behaved similarily up to 275 MPa. At that point, the specimen in experiment 162 began to accumulate strain with very small changes in stress, whereas the specimen in experiment 163 continued to accumulate stress with very small changes in strain. The initial specimen lengths, phase relationships, and applied stresses were virtually identical for both specimens (see table E.1 in appendix E for phase relationships and table E.3 in appendix E for applied stresses). In figure 5.7, the stress-strain response for each specimen is very similar except that each begins to stiffen at different strains.

These discrepancies may be attributed to several factors. One is the difficulty in preparing specimens with

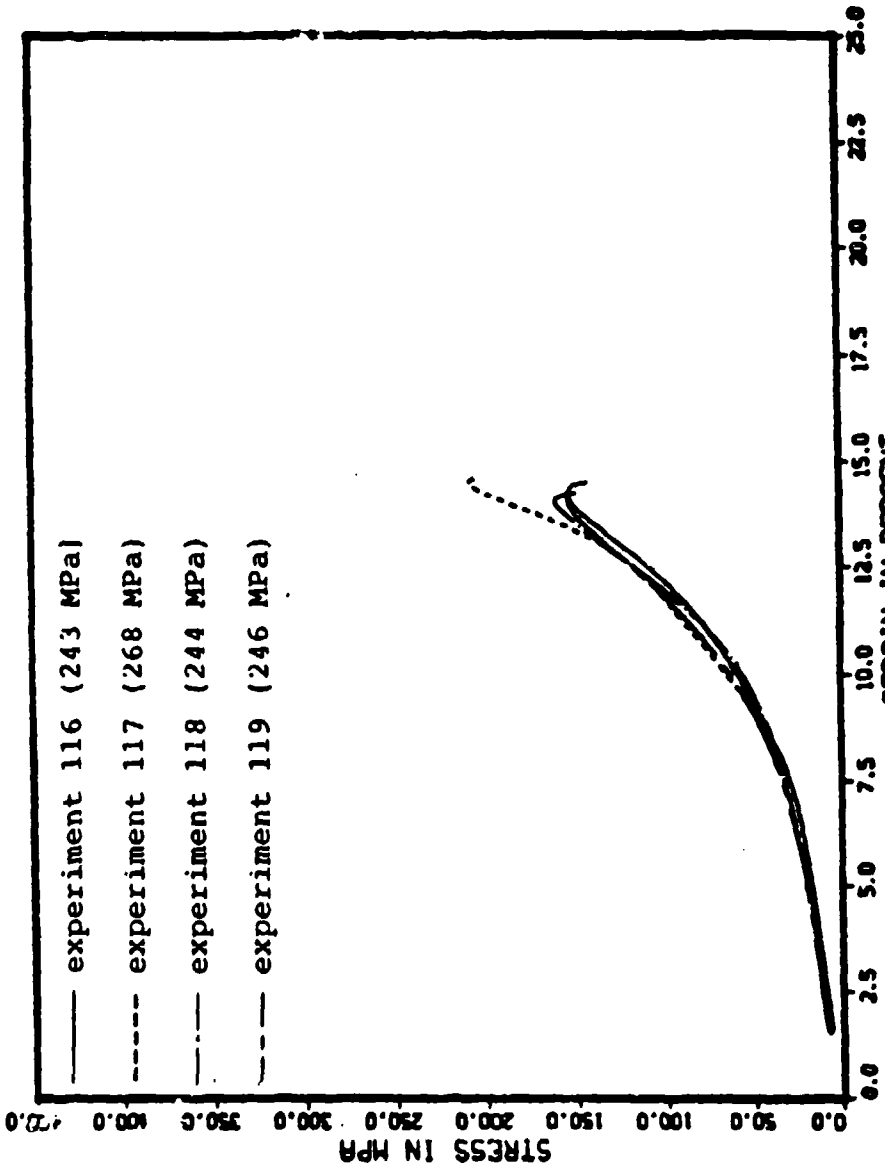

Figure 5.3. Replicate experiments for 6.35 mm specimens at an applied stress of approximately 250 MPa.

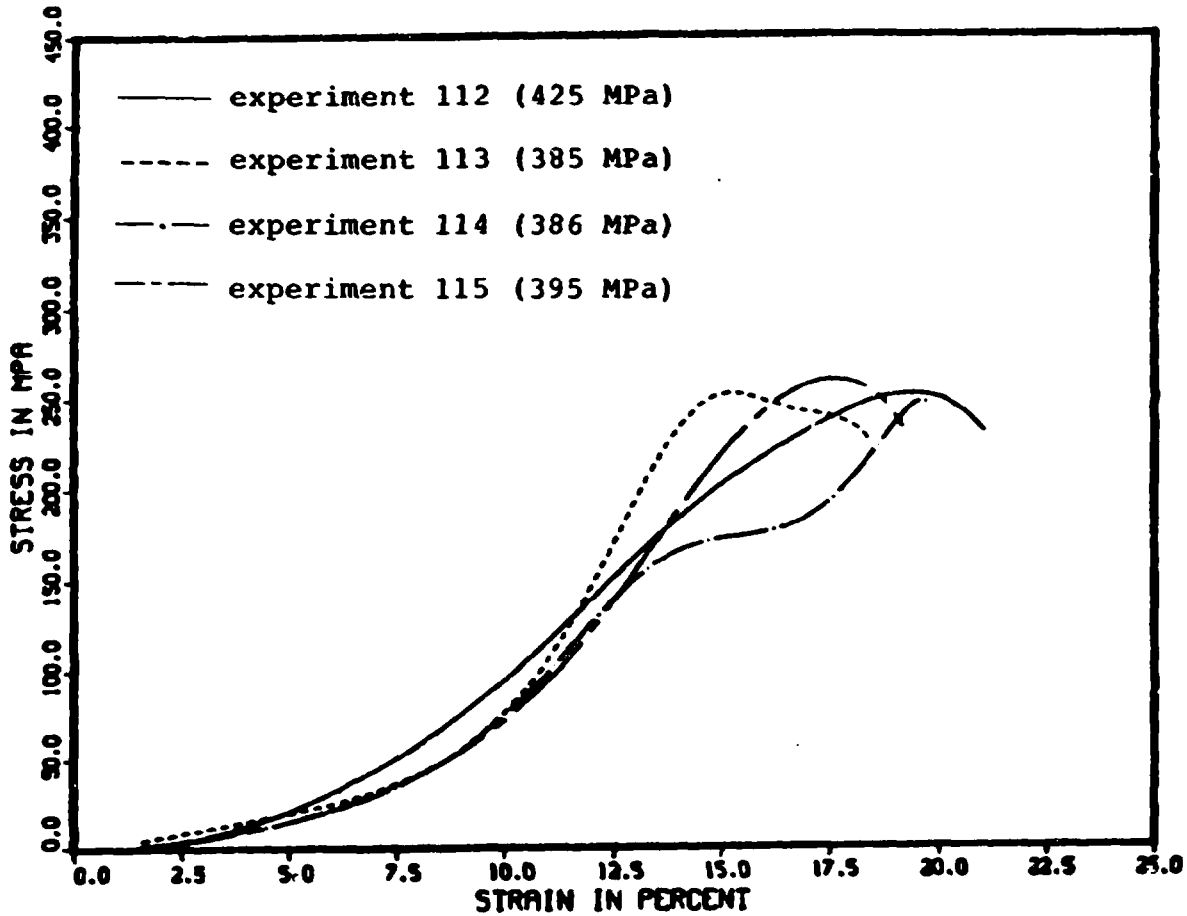

Figure 5.4. Replicate experiments for 6.35 mm specimens at an applied stress of approximately 400 MPa.

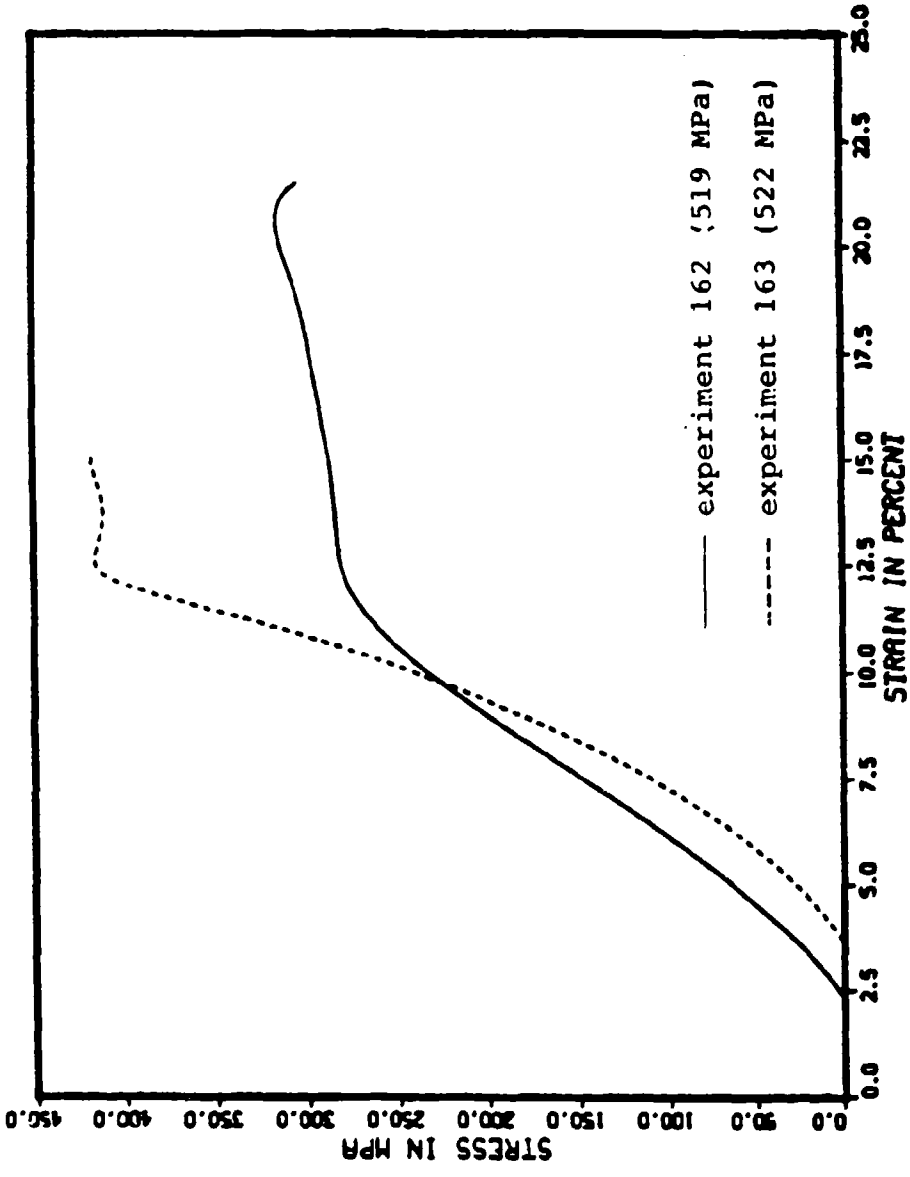

Figure 5.5. Replicate experiments for 6.35 mm specimens at an applied stress of approximately 520 MPa.

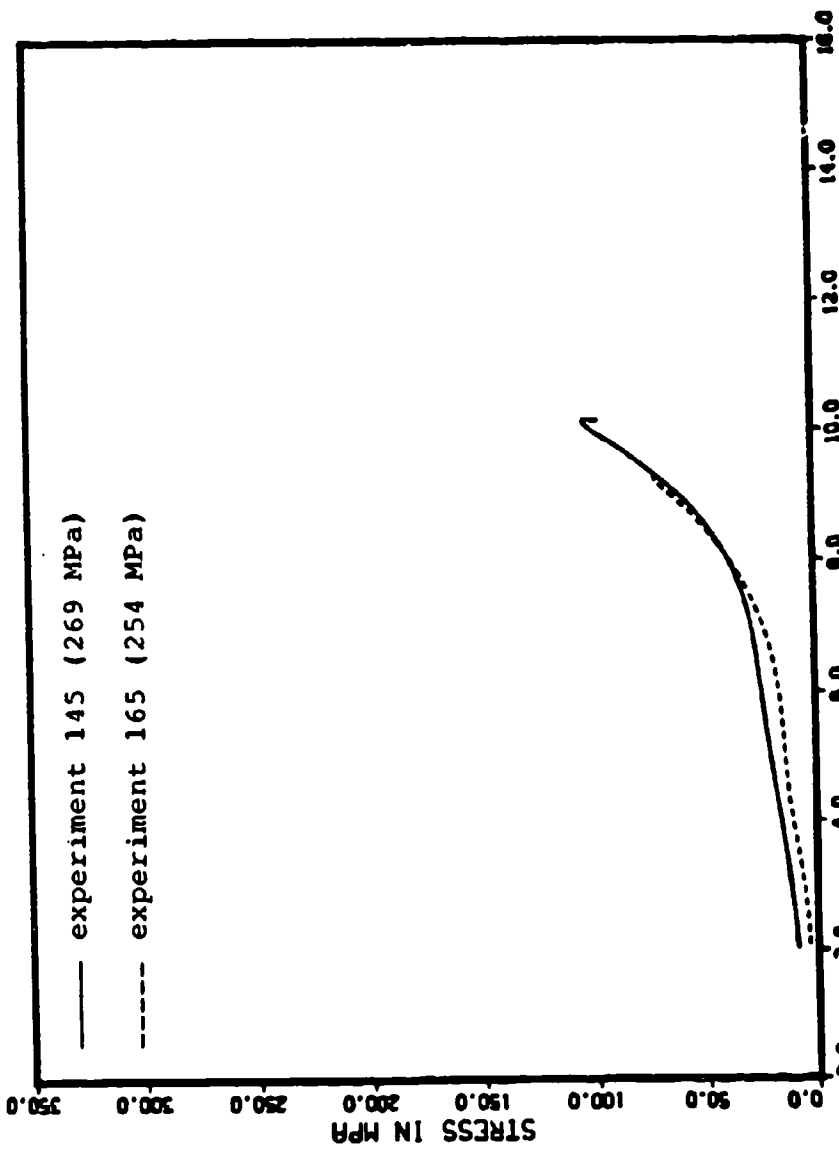

Figure 5.6. Replicate experiments for 12.7 mm specimens at an applied stress of approximately 250 MPa.

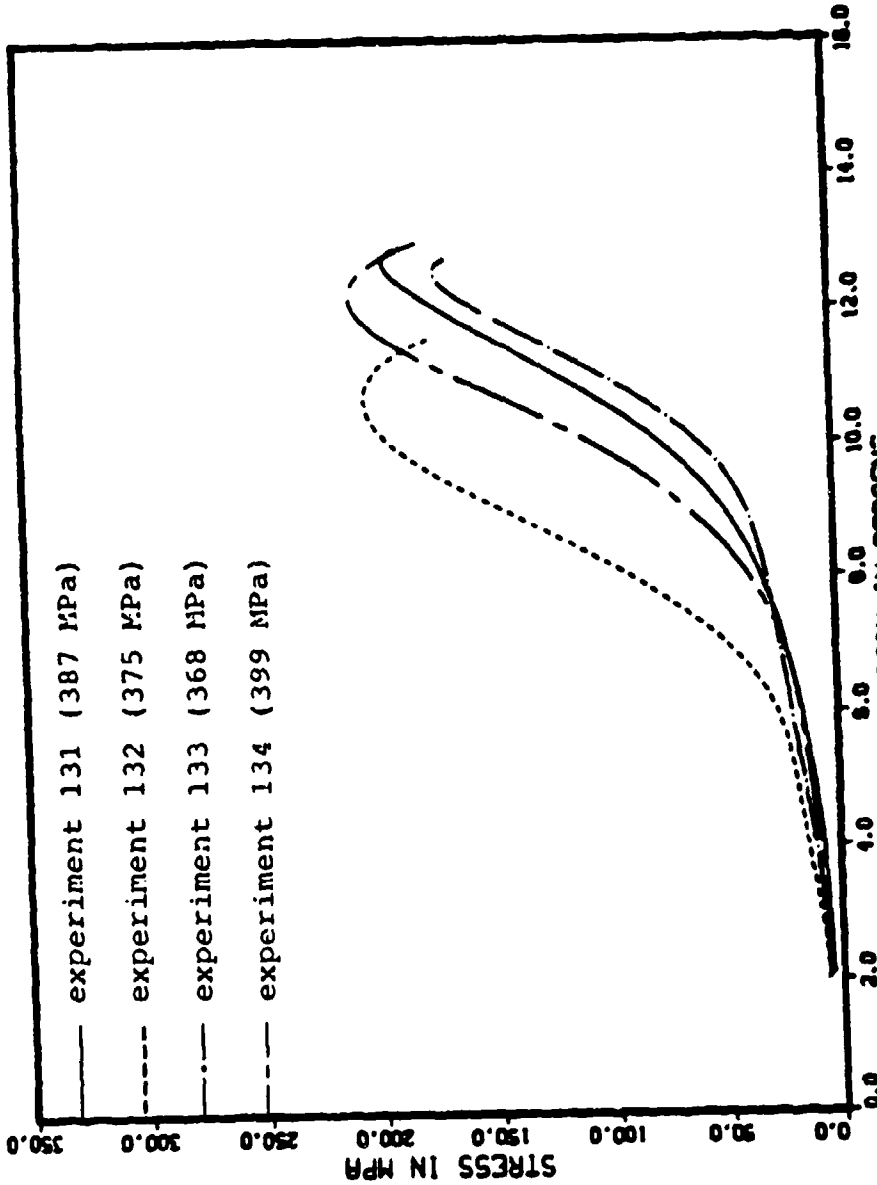

Figure 5.7. Replicate experiments for 12.7 mm specimens at an applied stress of approximately 400 MPa.

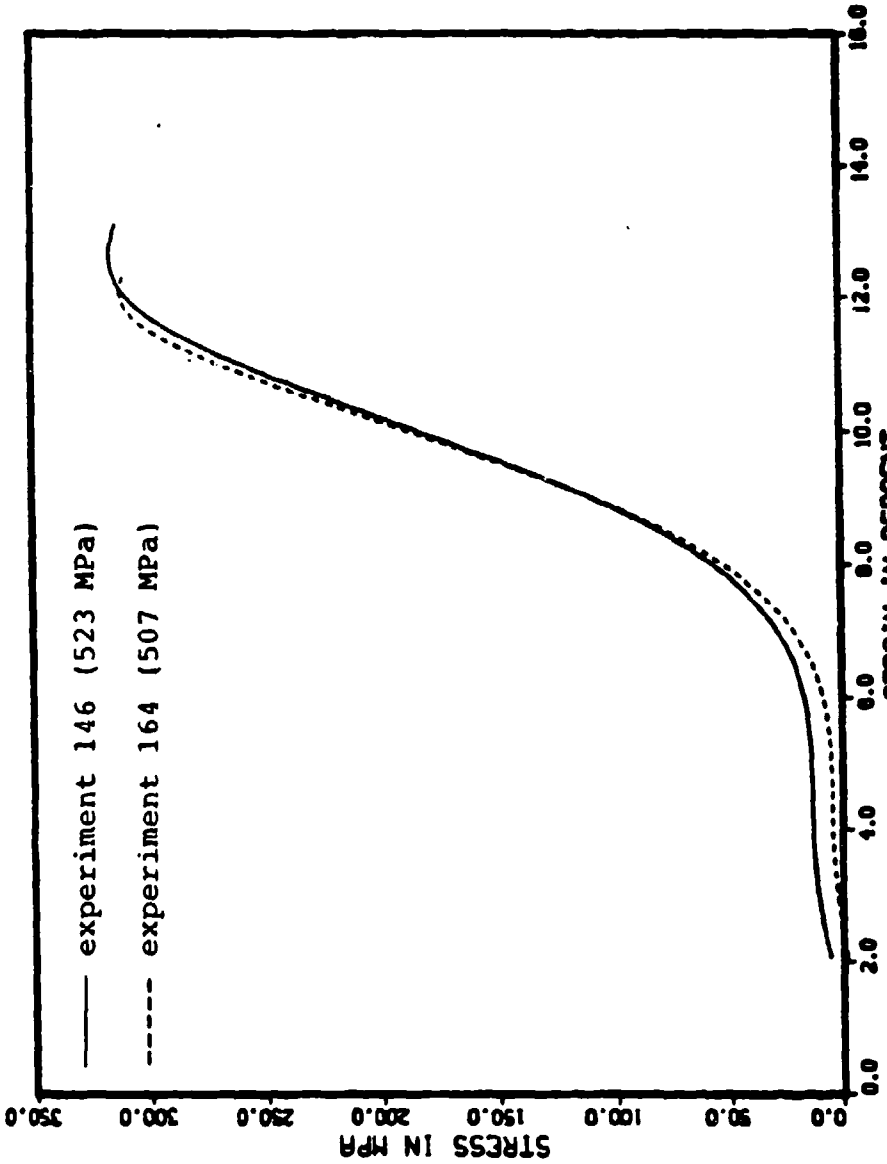

Figure 5.8. Replicate experiments for 12.7 mm specimens at an applied stress of approximately 520 MPa.

identical properties (i.e., moisture, density, etc.). A second is that as the seating strain cannot be controlled with great precision it is difficult to have specimens with identical phase relationships. Third, it is difficult to achieve duplicate impact velocities due to a variable friction force between the launch tube and the striker bar. These potential sources of difficulty in replicating experimental results are discussed in section 6.2. Another factor that might hamper the replication of experimental results is that soil and or moisture might be escaping through the annular region between the confining cylinder and the pressure bars during the experiment (see figure 3.8). A discussion of soil and moisture loss is presented in section 6.4.

5.5 Soil Behavior

Three methods of analysis will be used to describe the observed soil behavior: (1) by comparison of the stress-strain response of specimens with similar lengths to a range of applied stresses, (2) by comparing the response of specimens with different lengths to the same applied stress, and (3) by comparing the response of specimens with similar lengths but prepared at different initial moisture contents to the same applied stress.

Figures 5.9 and 5.10 show the typical stress-strain response for the nominal specimen lengths of 6.35 mm and

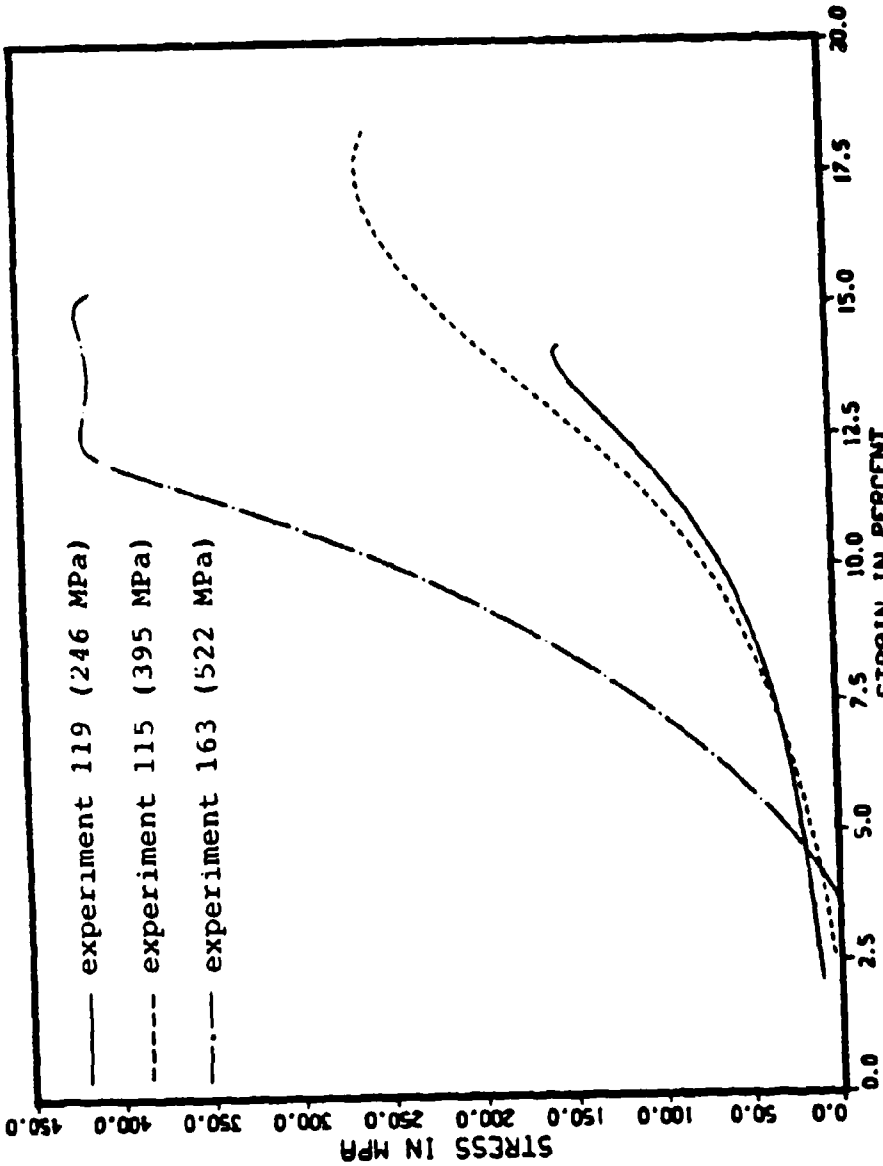

Figure 5.9. Stress-strain response for 6.35 mm specimens to a range of applied stresses.

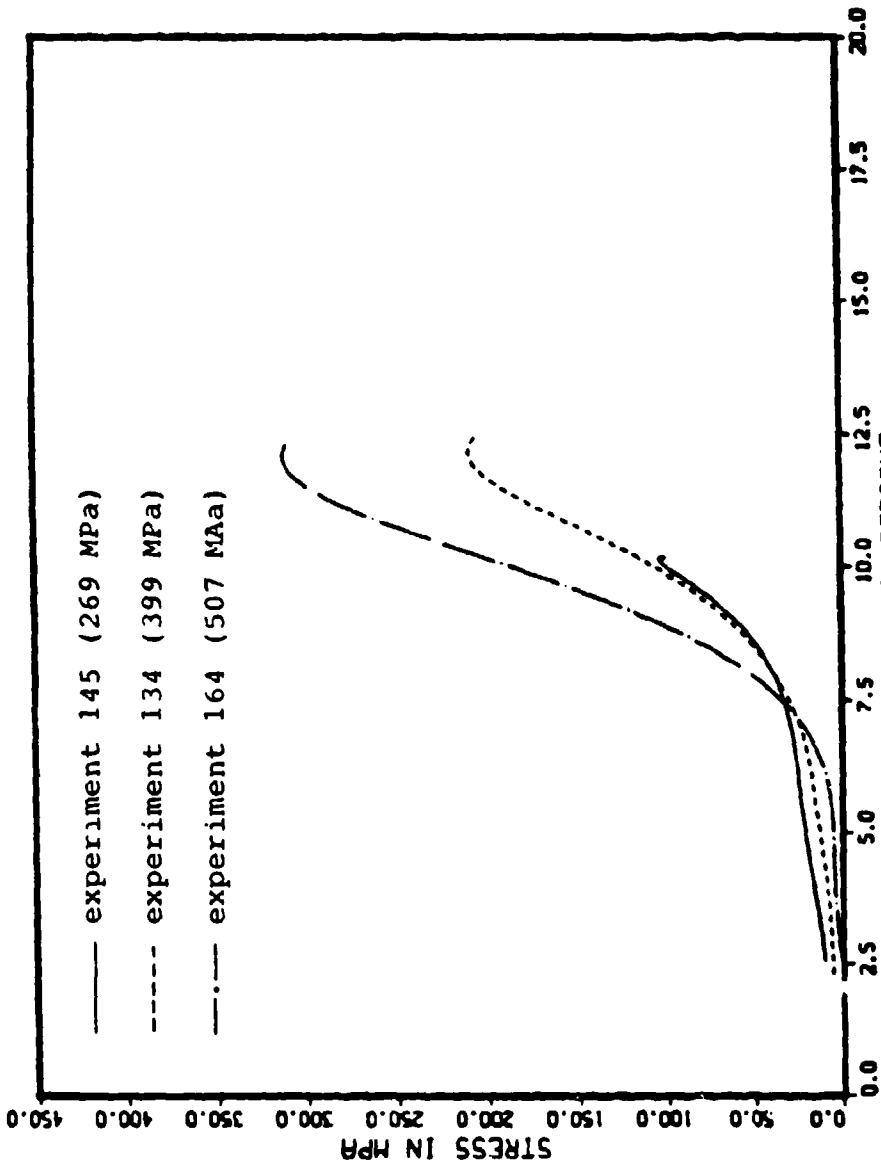

Figure 5.10. Stress-strain response for 12.7 mm specimens to a range of applied stresses.

12.7 mm respectively, to a range of applied stresses. It can be observed that the average stress experienced by the specimen increased with increasing applied stress independent of the specimen length. For both specimen lengths, the stress-strain response is very similar for applied stresses up to 400 MPa with some increase in stiffness observed at the higher applied stress. For all applied stress levels, the specimens began to stiffen at strains approximately equal to the initial gas porosity. For both specimen lengths and at all applied stresses, the strain at peak stress experienced by the specimen exceeded the initial gas porosity of the material.

Figures 5.11, 5.12, and 5.13 compare the stress-strain response of specimens to the same approximate applied stress but with different specimen lengths. The nominal applied stresses are 250, 400, and 520 MPa respectively. From figures 5.11 and 5.12 it can be seen that the strain experienced by the shorter specimens exceeded those of the longer specimens. Also the longer specimens showed greater stiffness at lower strains than the shorter specimens. This apparent discrepancy in response between the two specimen lengths may be explained by examining the initial gas porosity for each specimen.

To observe how moisture content variations affect stress-strain response, specimens were prepared at the following nominal moisture contents; 7, 13, and 15

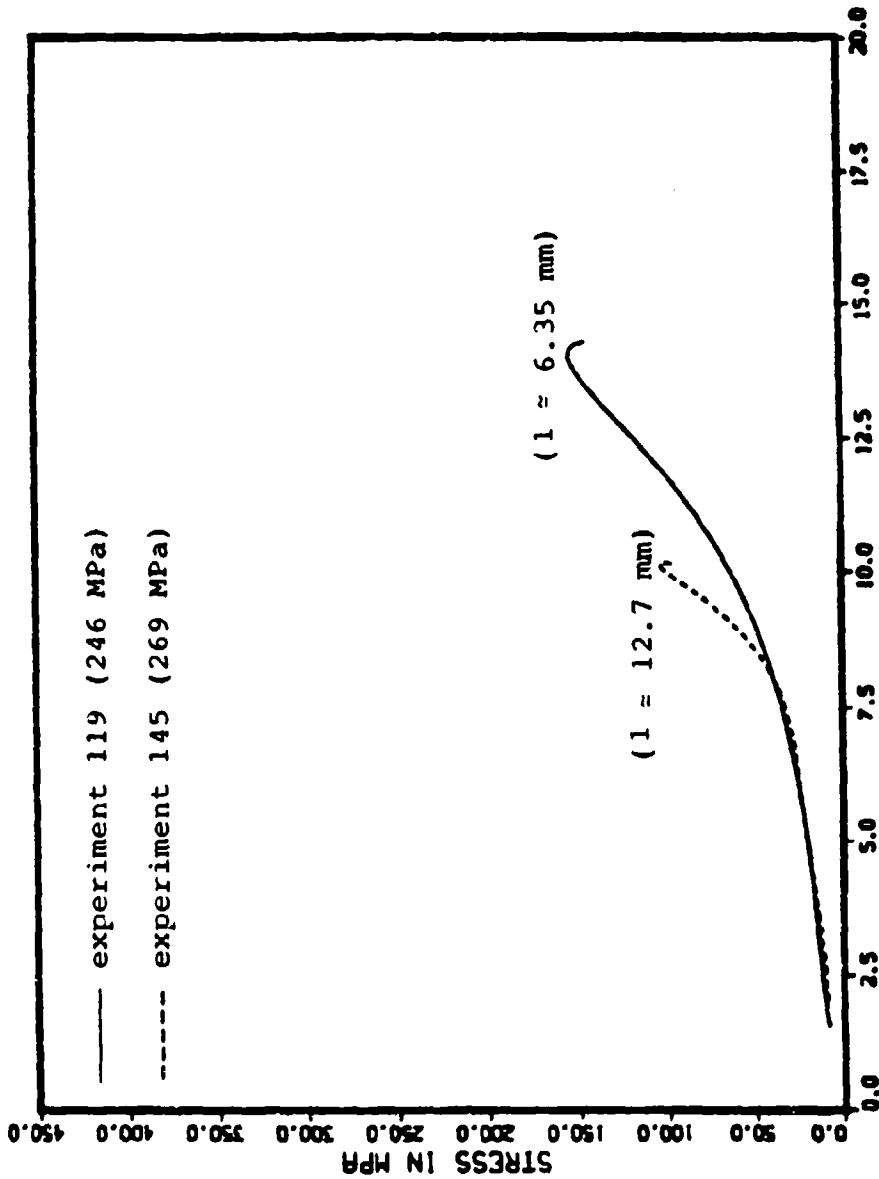

Figure 5.11. Comparison of stress-strain response based on specimen length to an applied stress of approximately 250 MPa.

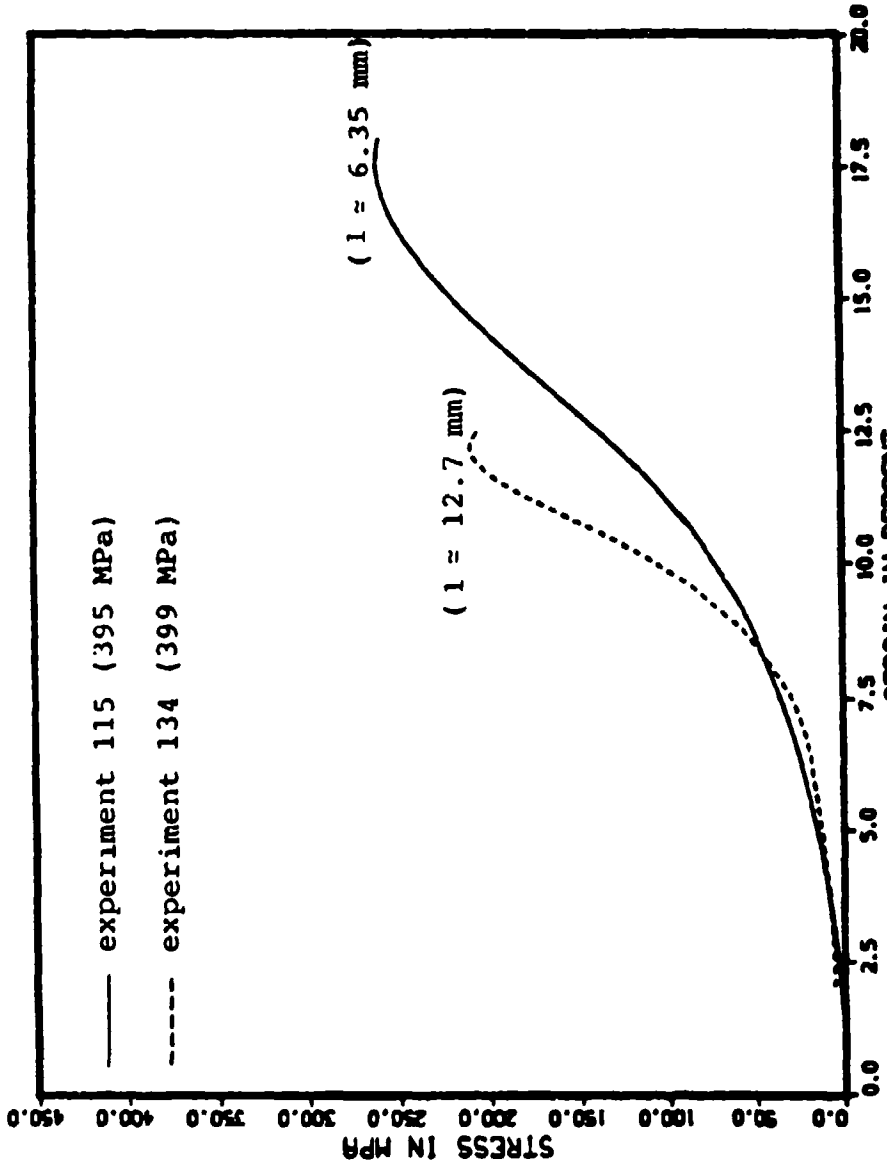

Figure 5.12. Comparison of stress-strain response based on specimen length to an applied stress of approximately 400 MPa.

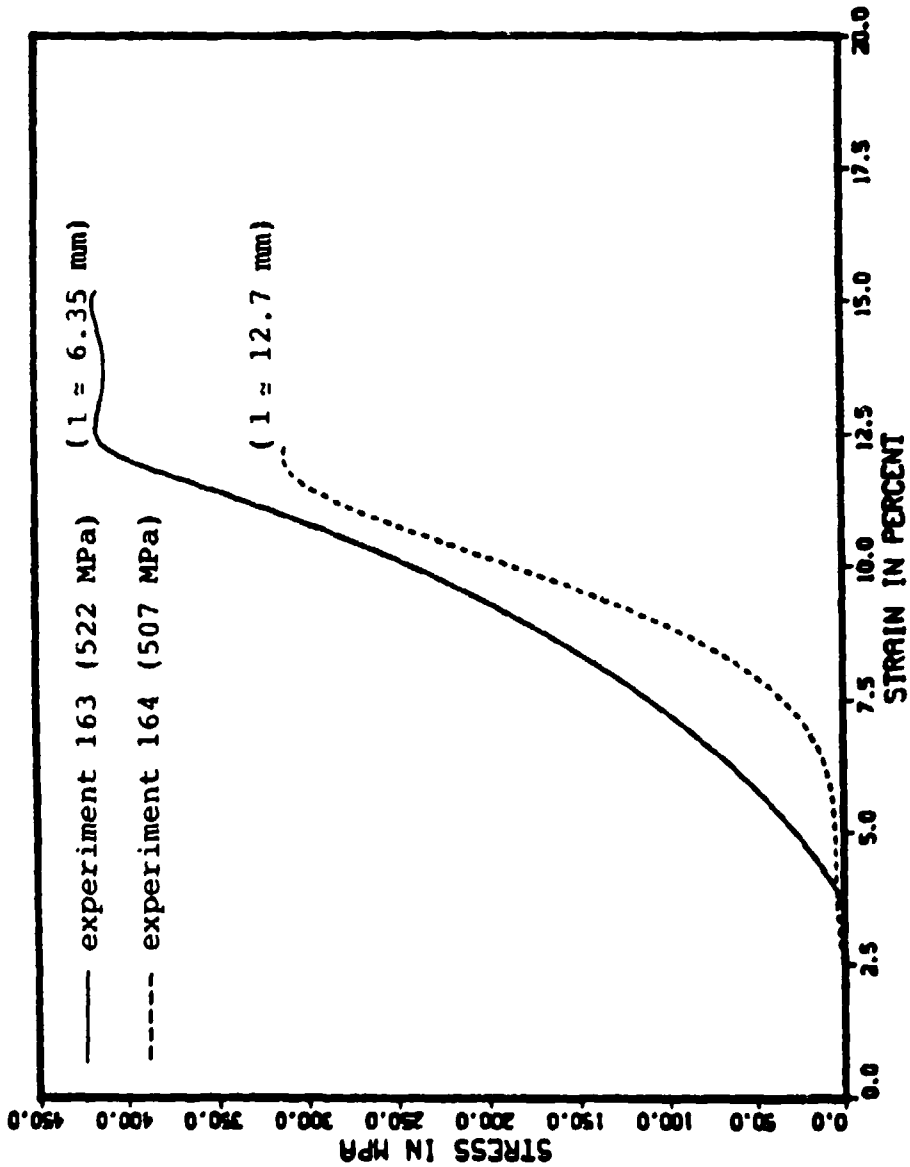

Figure 5.13. Comparison of stress-strain response based on specimen length to an applied stress of approximately 520 MPa.

percent. Figure 5.14 shows the effect of moisture content on the stress-strain response of 6.35 mm specimens to an applied stress of 250 MPa, and figure 5.15 shows the response of 12.7 mm specimens to an applied stress of 400 MPa.

These figures show that the average stress experienced by the specimens increased while the strain at peak stress decreased with increasing moisture content. As with the other stress-strain curves shown, there is a marked break in slope near a strain equal to the initial gas porosity. This change in slope is not observed for the 12.7 mm specimen with the lowest moisture content (experiment 135); however, the maximum strain (16 percent) did not approach the initial gas-filled porosity of 23.4 percent. Also, the specimens became somewhat stiffer with increasing moisture content, at least at strains in excess of the initial gas porosity. At strains less than the initial gas porosity this observation is less clear.

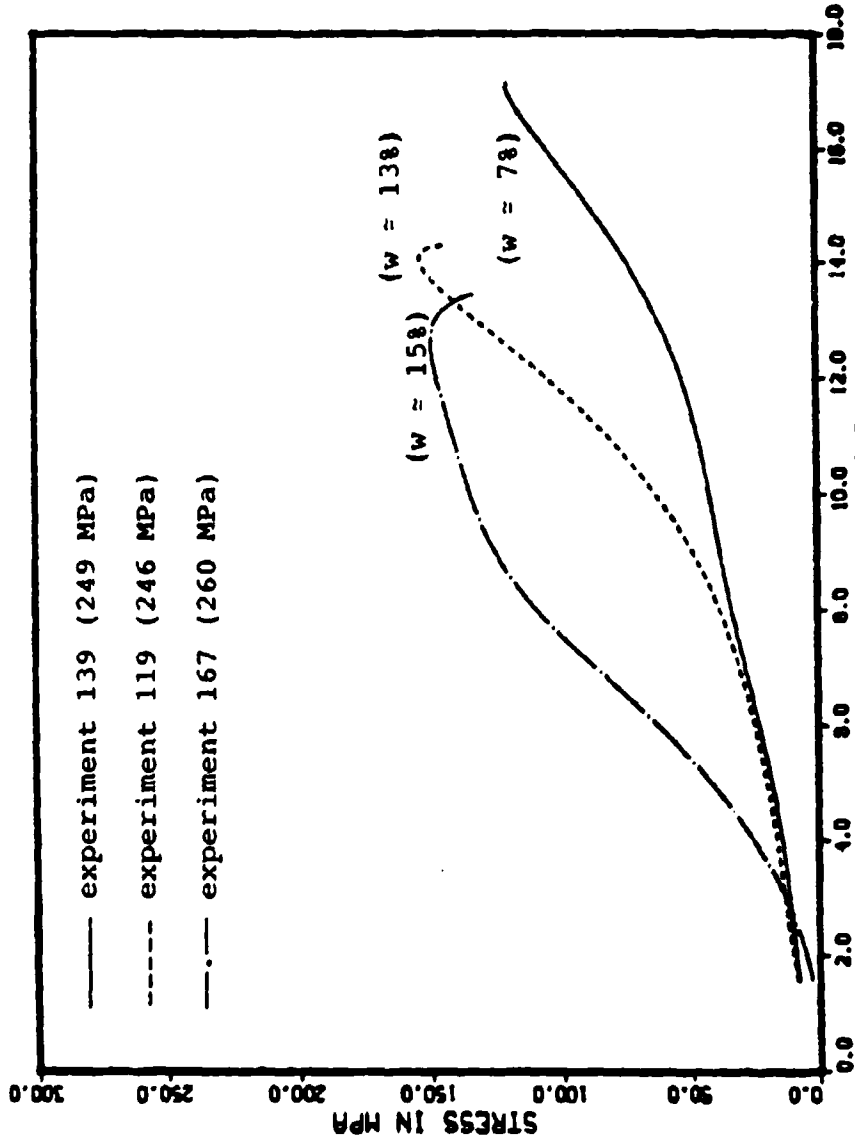

Figure 5.14. Comparison of stress-strain response for 6.35 mm specimens based on moisture content (w) to an applied stress of approximately 250 MPa.

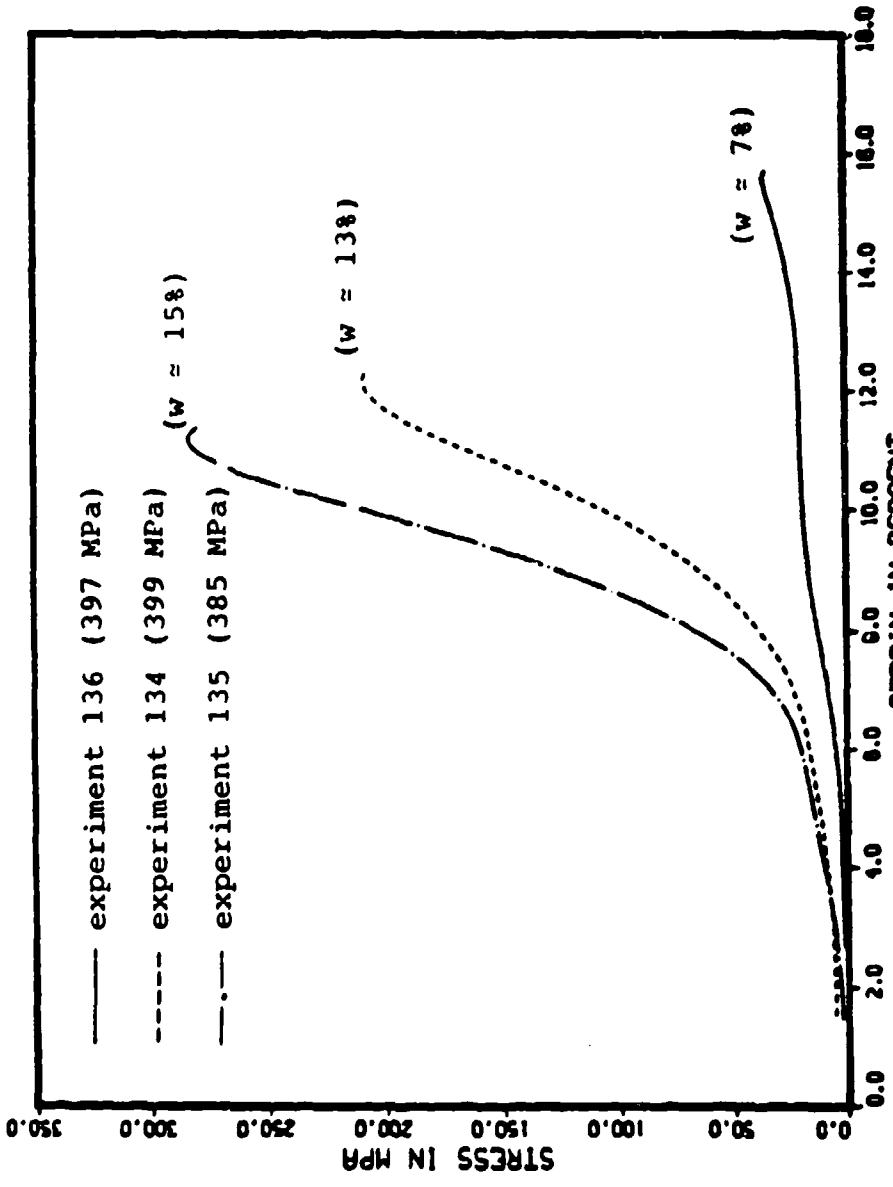

Figure 5.15. Comparison of stress-strain response for 12.7 mm specimens based on moisture content (w) to an applied stress of approximately 400 MPa.

6. DISCUSSION OF EXPERIMENTAL RESULTS

In chapter 4 the experimental assumptions that need to be satisfied in order to obtain meaningful data were presented. Chapter 5 presented the stress-strain response for sand specimens compacted to different moisture/density conditions and subjected to a range of applied stresses. The stress-strain response was computed using the theory established in chapter 2 and the reduction procedure outlined in chapter 3. This chapter will establish that the experimental assumptions stated in chapter 4 can be satisfied when using soil specimens and will address the discrepancies noted in section 5.5 concerning stress-strain response. In addition, the specimen conditions that were necessary to satisfy the assumptions and those that could contribute to erroneous soil response will be discussed. Also, the advantages of the SHPB experiment over similar methods to determine one-dimensional dynamic soil properties will be addressed.

6.1 Experimental Assumptions

From the strain gauge data collected during a SHPB experiment it is assumed that the stress, strain, and strain-rate response in the specimen at any time can be

computed by averaging the forces and particle velocities at the specimen-bar interfaces. For the computations to be meaningful the assumptions of the experiment must be satisfied (see section 4.1). The degree to which the assumptions are satisfied using soil specimens and large diameter pressure bars will be analyzed.

6.1.1 Uniform Distribution of Stress

Using the criterion developed by Davies and Hunter (1963);

$$\frac{d\sigma}{d\varepsilon} > \frac{\pi^2 \rho_s l^2}{T^2} , \qquad (2.39)$$

an estimate can be established as to when stress uniformity might be achieved in a SHPB specimen. The inequality is conservative because its derivation is based on a lower permissible value for the propagation velocity of waves in the specimen (Davies and Hunter, 1963). Because unloading waves generated in the experiment will travel faster than the plastic waves in the specimen, quasi-equilibrium will be reached sooner than indicated by the inequality (Davies and Hunter, 1963).

Figures 6.1, 6.2, and 6.3 show results of experiment 134. Using equation (2.39), the stress-strain curve (figure 6.1), the appropriate specimen length (1.259 cm), density (2.12 g/cm^3), and T ($\cong$130 microseconds) stress equilibrium is estimated to be reached at 42 microseconds.

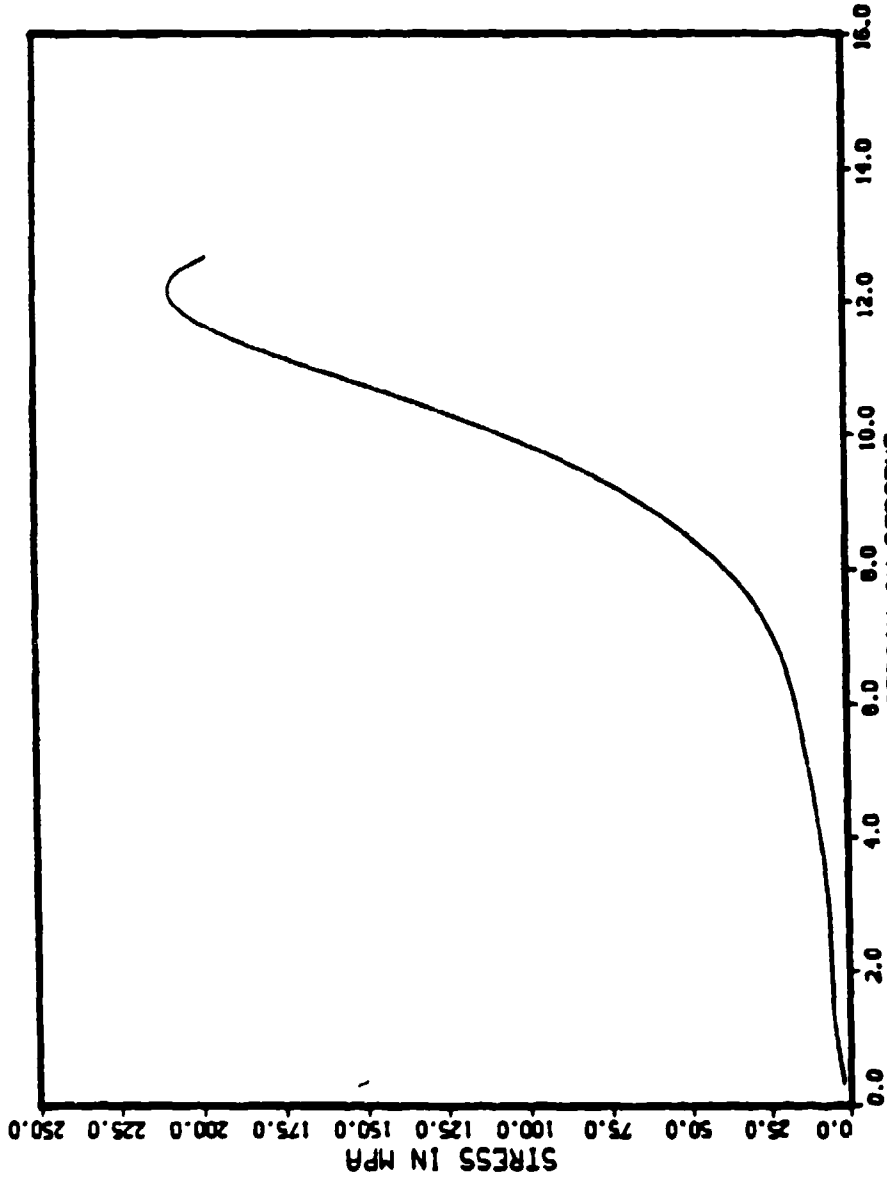

Figure 6.1. Stress-strain response for experiment 134.

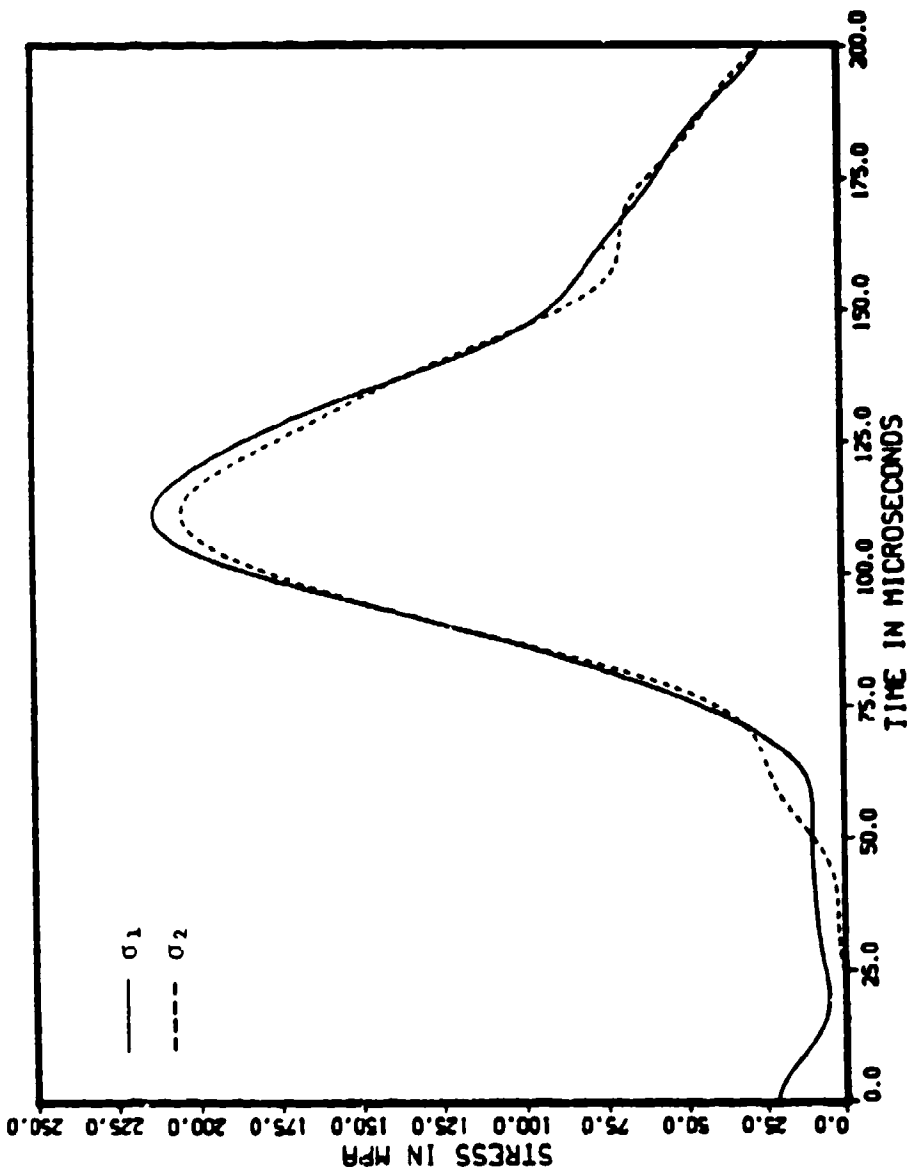

Figure 6.2. Stress-time response of the specimen-bar interfaces, experiment 134.

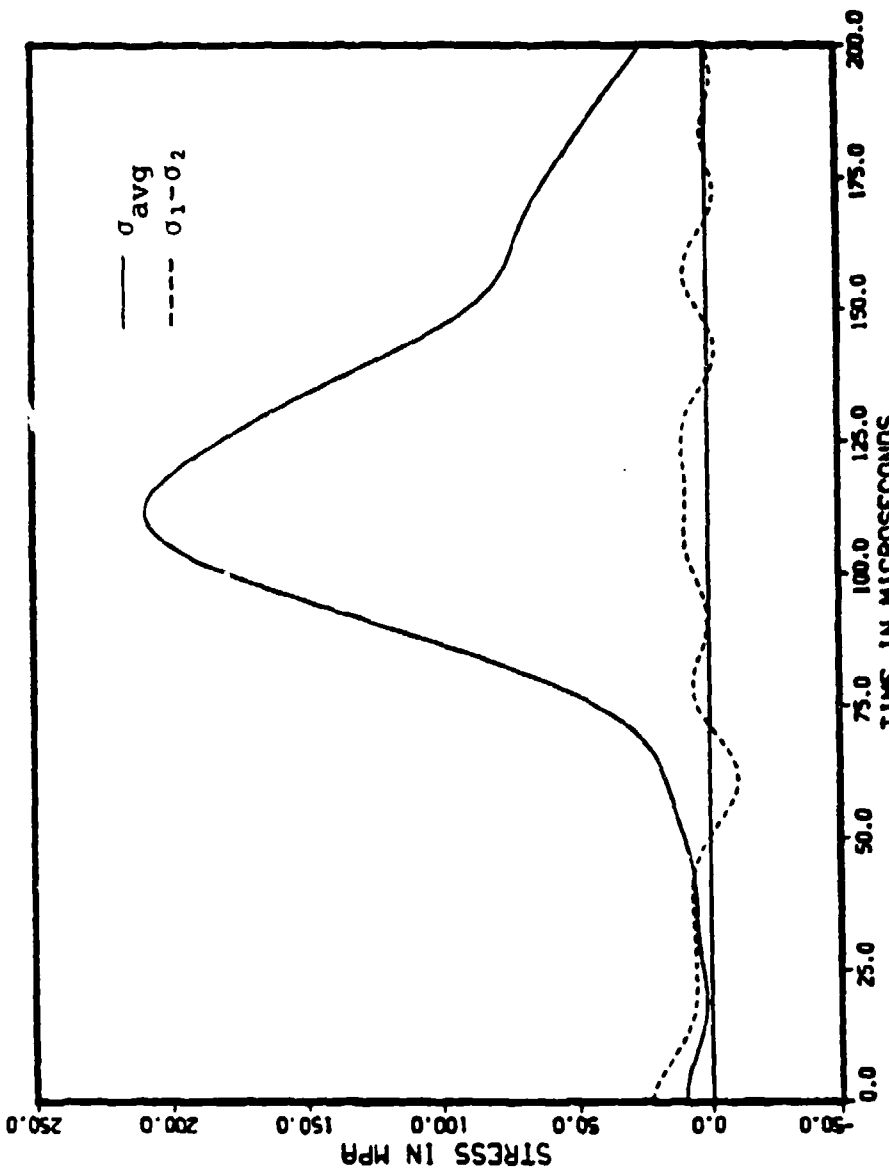

Figure 6.3. Average specimen stress-time response and the difference between the stress-time response of the specimen-bar interfaces, experiment 134.

The values for specimen length and density are given in table E.1 of appendix E and T is approximated from figure 4.5. Numerical values for the slope of the stress-strain curve for experiment 134 are given in the example computer output in appendix G. Figure 6.2 shows the stress histories at the specimen-bar interfaces. From figure 6.2 it can be seen that after about 25 microseconds the stresses at the two interfaces begin to converge to approximately the same value and are indeed equal at 50 microseconds. The stress difference across the specimen as a function of time and the average stress-time response is shown in figure 6.3. If inertia forces were absent, the stress difference, would be zero. It can be seen that after 25 microseconds the stress difference is very small relative to the average stress from which it can be concluded that the stress gradient in the specimen has diminished.

The experimental evidence presented in figures 6.2 and 6.3 support the estimate computed from the Davies and Hunter (1963) criterion as to when stress uniformity is achieved in a SHPB soil specimen. Hence, the Davies and Hunter criterion can be used to estimate when stress uniformity is likely to be achieved in a soil specimen.

In contrast to the criterion of Davies and Hunter (1963) which provided a reasonable estimate to the time required for the specimen to reach equilibrium, the

criterion of Bertholf and Karnes (1974) is violated in every experiment by at least a factor of 2 (see section 2.5). For example, a maximum strain-rate of 1800 s^{-1} was computed for experiment 134. Substituting 1800 s^{-1} into equation (2.40) along with the diameter of the bar (6.03 cm) yields;

$$D\dot{\varepsilon}_{max} = 10800 \text{ cm } s^{-1} , \tag{6.3}$$

and subtituting the rise-time ($\cong$ 45 microseconds) of the loading wave into equation (2.41) yields;

$$\frac{T_r}{D} = 7.5 \text{ } \mu s \text{ } cm^{-1}. \tag{6.4}$$

The rise-time of the loading wave can be approximated from figure 4.5. To satisfy the Bertholf and Karnes (1974) criterion the specimen strain-rate and loading wave rise-time would have to be less than 800 s^{-1} and greater than 90 microseconds, respectively.

The purpose of the Bertholf and Karnes (1974) criterion was to bound the experimental parameters such that the influence of inertia would be minimized. Although the experiments in this research did not satisfy the criterion, it has been shown that stress equilibrium will be achieved, satisfying the uniform stress assumption.

The influence of inertia and its affect on the ability of a soil specimen to reach stress equilibrium has been investigated experimentally, and the results compared

with the estimates computed from the criterion of Davies and Hunter (1963) and Bertholf and Karnes (1974). Experimentally it has been demonstrated that the stress at the specimen-bar interfaces will be approximately equal within the rise-time of the incident stress wave. This means that the first 1 to 2 percent strain the specimen sustains must be disregarded as stress equilibrium within the specimen has not been achieved. It has been shown that the criterion of Davies and Hunter provides a reasonable estimate as to when stress uniformity is achieved in the specimen by direct comparsion to the experimental results. In contrast to the criterion of Davies and Hunter, the bounds on the experimental parameters established by Bertholf and Karnes are too restrictive when applied to soil specimens.

6.1.2 Wave Dispersion

Davies (1948) showed that oscillations in the recorded stress waves were attributable to dispersion and could be predicted (see sections 2.4 and 4.1.2). However, until recently there has been no technique that could easily be incorporated into the standard SHPB data reduction procedure to account for this phenomenon (Follansbee and Frantz, 1983). Consequently, the oscillations in the raw data were retained and a smoothing technique applied to the reduced data. Although the

smoothing of reduced SHPB data is an accepted practice (e.g., Rand, 1967), a systematic method of accounting for the dispersive nature of a propagating wave is preferable.

The effects of dispersion on the experimental results obtained in this research was investigated by conducting a test with the end of the incident bar being a free end (see section 4.1.2). The correction procedure was shown to account for the wave dispersion occuring between the strain gauge location and the free end of the incident bar.

Figure 6.4 illustrates the effect of dispersion on the appearance of the stress-strain curve for experiment 2'.. Here it can be seen that the dispersion corrected curve is smoother and easier to interpret. For instance, it would have been difficult to correlate the sudden increase in stiffness to the condition of zero air voids had the dispersion correction procedure not been employed. Hence, an effect of dispersion on experimental results is to mask trends.

6.1.3 Stress Variation Over the Cross Section of the Bar

The diameter of the pressure bars used in this research was significantly larger than that used in past SHPB experimentation. A consequence of using a larger diameter bar is that the stress-time history over the cross sectional area of the pressure bar may not be

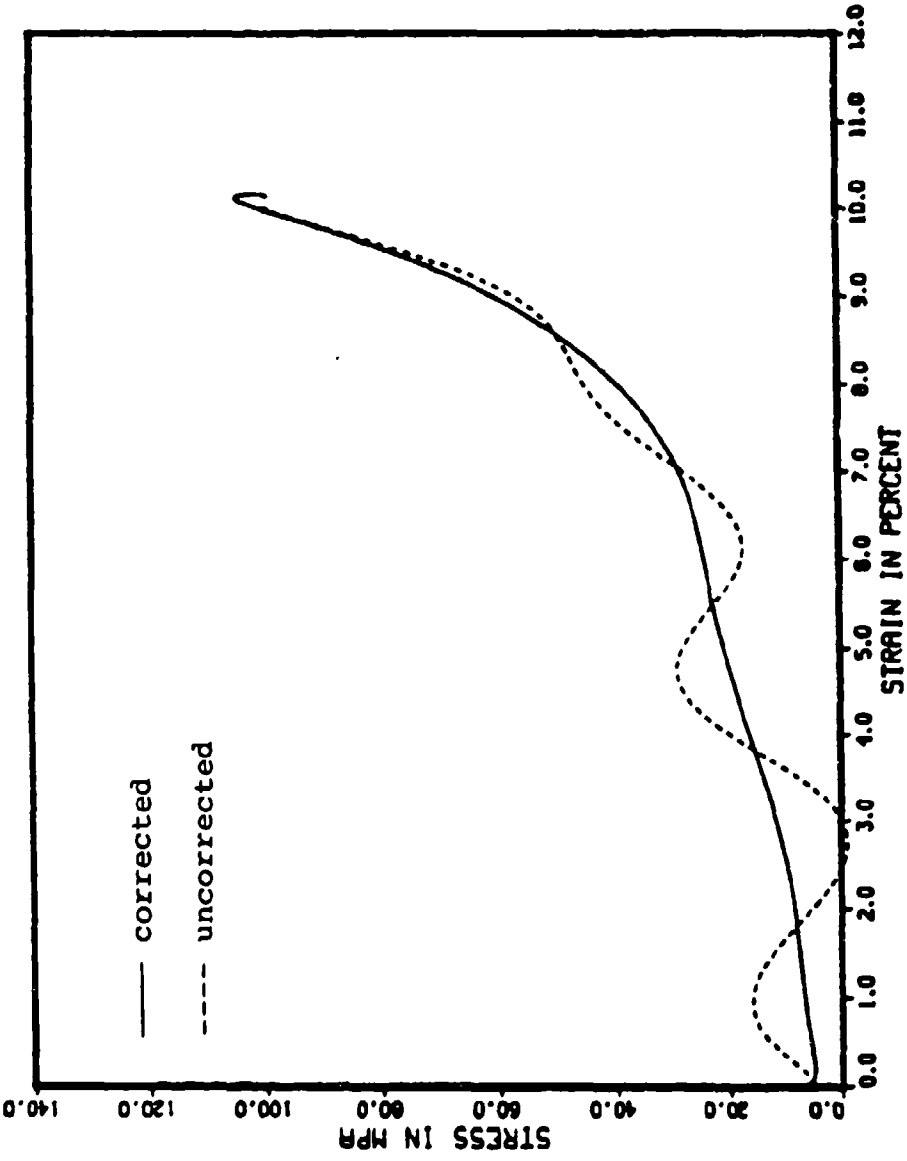

Figure 6.4. Comparison of stress-strain response using the uncorrected and corrected stress waves.

constant. Hence, measurements made at the surface of the bar might not be representative of the behavior over its cross section. In the work of Davies (1948) he showed that if $R/\Lambda < 0.1$ the displacements at the bar surface would differ from those along the axis of the bar by $\pm$ 3 percent.

In order to investigate the degree to which the criterion established by Davies is satisfied for the SHPB used in this research, the incident wave for experiment 134 was decomposed into its respective Fourier components. Table 6.1 lists the values n, R/Λ, C_n/C_o, and the ratios of the amplitudes of the Fourier component $n\omega_o(D_n)$ to the largest magnitude Fourier component (A_o).

For $n < 9$, the value R/Λ is less than 0.1, and the magnitude of the Fourier component (D_n) is approximately 6 percent of the largest magnitude Fourier component (A_o). These computations illustrate that the high frequency Fourier components of the wave are damped out quickly which tends to support a nearly uniform stress-time distribution over the cross sectional area of the bar. However, $n = 17$ is required to model the experimentally observed wave; therefore, the error in the computations will be in excess of $\pm$ 3 percent.

Figure 6.5 shows the incident wave modeled with $n = 17$, and $n = 9$ along with their difference. The difference was taken as a qualitative indicator of the

Table 6.1

Fourier Coefficients, Values for R/Λ , and C_n/C_o for the Incident Wave of Experiment 134

n	R/Λ	C_n/C_o	D_n/A_o (a)
1	0.01170	0.99966	0.89275
2	0.02340	0.99918	0.65881
3	0.03500	0.99864	0.41980
4	0.04670	0.99804	0.18439
5	0.05840	0.99733	0.02868
6	0.07020	0.99646	0.12833
7	0.08200	0.99538	0.13652
8	0.09380	0.99402	0.11074
9	0.10570	0.99229	0.05668
10	0.11770	0.99012	0.02368
11	0.12980	0.98743	0.05596
12	0.14210	0.98408	0.05409
13	0.15450	0.98002	0.04164
14	0.16730	0.97505	0.02027
15	0.18030	0.96911	0.01707
16	0.19380	0.96196	0.02908
17	0.20770	0.95353	0.02016
18	0.22220	0.94358	0.00962
19	0.23750	0.93186	0.01329
20	0.25370	0.91817	0.00912

a) Ao = 25.32032.

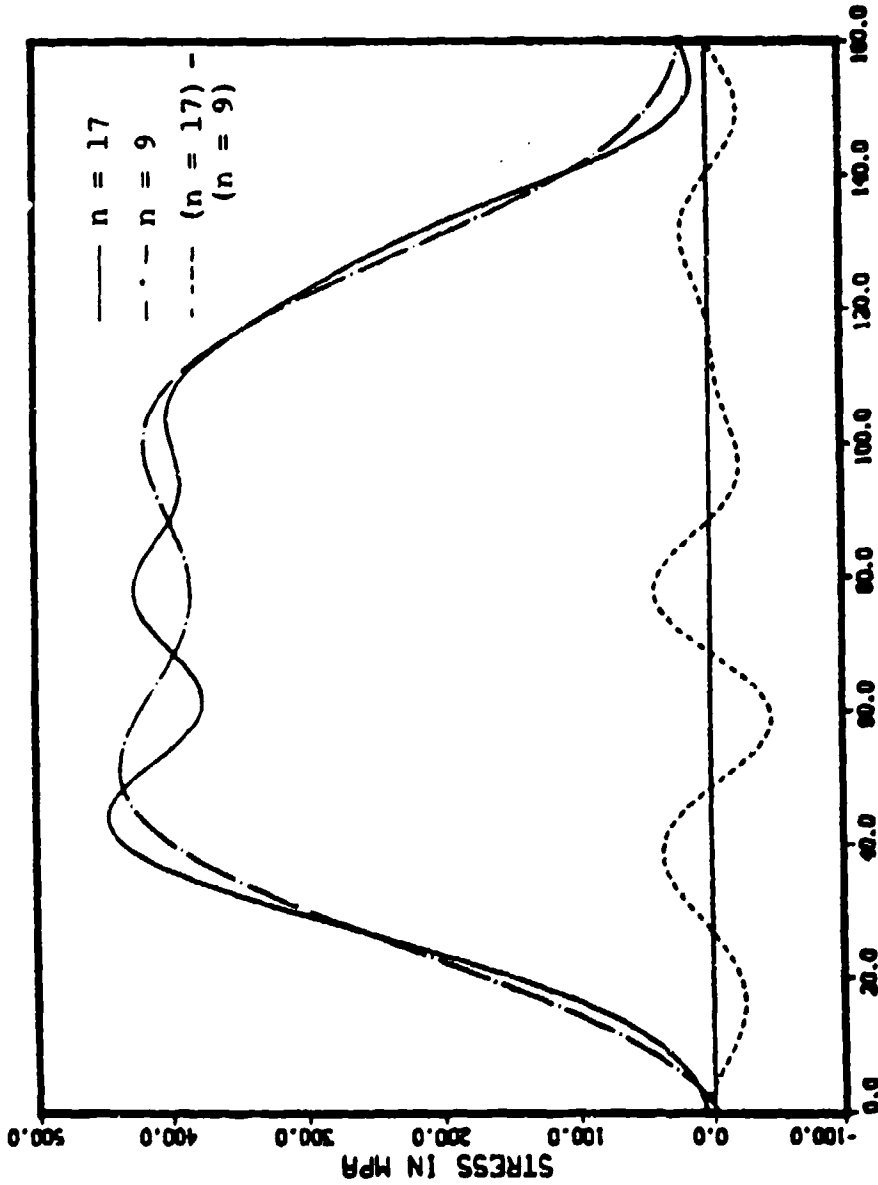

Figure 6.5. Incident stress wave modeled with n = 17 and n = 9 Fourier terms.

error in excess of ± 3 percent. A quantitative measure can be computed by summing the absolute values of the Fourier coefficients for n equal 10 to 17 and dividing by the summation of the Fourier coefficients for n equal 0 to 17.

$$\frac{\sum_{n=10}^{17} D_n}{A_0 + \sum_{n=1}^{17} D_n} = 0.068 \quad . \tag{6.5}$$

This relative error will be an upper bound as D_n is computed from A_n and B_n which can be opposite in sign. Hence, as a worst case the computational error will be approximately ± 10 percent.

Figure 6.6 shows the difference in the computed average stress-strain response between using n = 17 and n = 9. It can be seen that the stress-strain response is not significantly altered; hence ± 10 percent can be considered to be an upper bound on the error when assuming one-dimensional wave analysis to reduce the data obtained using 60.3 mm diameter pressure bars.

6.1.4 Specimen-Bar Interface Friction

The numerical work of Bertholf and Karnes (1974) has shown that friction between the specimen and the pressure bars can affect specimen response, particularly for relatively thin specimens. Interface friction affects specimen response in two ways: (1) a greater stress will be required to produce a given strain, and (2) the

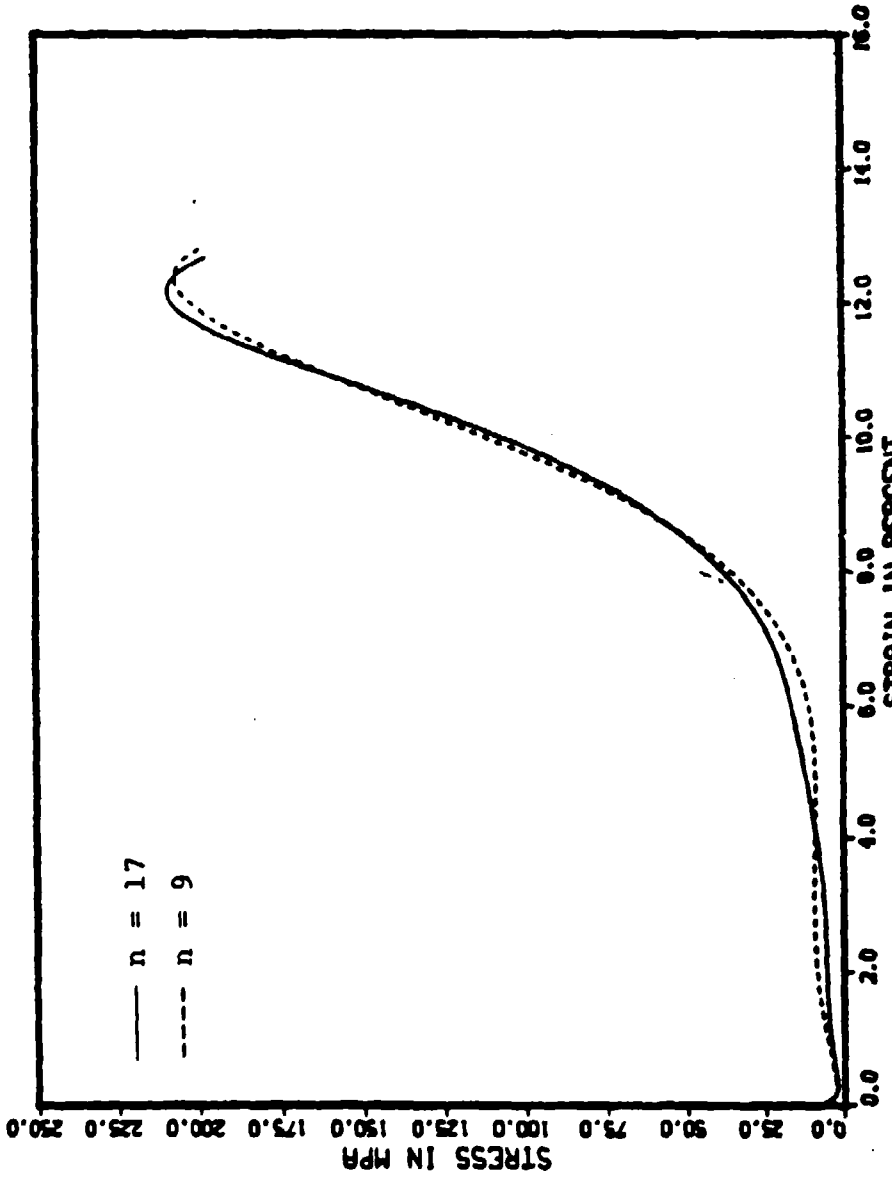

Figure 6.6. Stress-strain response computed from stress waves modeled with n = 17 and n = 9 Fourier terms.

specimen will barrel. From their work they concluded that the effects of friction could be minimized if the specimen-bar interfaces were lubricated and a specimen aspect ratio of approximately 0.5 selected.

All the specimens in this research were the same diameter as the pressure bars and placed in a confining cylinder which prevented excessive barreling and hence negligible shear stresses between the specimen and the pressure bars. This was verified in section 5.3 where it was shown that the specimen did sustain some radial strain but for all experiments was less than 1 percent.

The results of section 5.5 can be used to examine the effect of friction on specimen stress-strain response. In figures 5.11, 5.12, and 5.13 the stress-strain response is compared for different length specimens to the nominal applied stresses of 250, 400, and 520 MPa, respectively. These figures are useful because the specimen lengths are different by a factor of two; hence if friction effects exist their stress-strain response should not be the same.

In all three figures the stress-strain response for the different length specimens is nearly identical up to their initial gas porosities (see also section 6.4). For strains in excess of the initial gas porosity the specimen response is governed principally by the pore water. This is evident from the results presented throughout chapter 5. In all three figures the peak stress of the shorter

specimens exceeded that of the longer by at least 25 percent. As the specimen does sustain some radial strain (see section 5.3) this phenomenon may be due to friction. However, to be conclusive, experiments need to be conducted on specimens with as similar initial gas porosities as possible.

Hence, for soil specimens with lengths different by a factor of two and aspect ratios less than 0.2, friction is not observed to influence the stress-strain response at strains less than the initial gas porosity. From this conclusion it can be determined that the optimum aspect ratio of 0.5 is too restrictive when applied to soil specimens and that by maintaining a condition of nearly uniaxial strain, aspect ratios less than 0.5 can be used with the effects friction on stress-strain response held to a minimum.

6.2 Experimental Replication

The replicate experiments shown in section 5.4 were conducted to evaluate the degree to which the results of an experiment could be reproduced. In this research, several aspects of the experimental process have been identified as hindering complete experimental reproducibility with compacted sand specimens.

In attempting to achieve replicate experimental results, each specimen was prepared according to the same

procedure. The procedure for preparing each specimen has been presented in section 3.3. However, regardless of following a consistent procedure for preparation, variations in specimen parameters oxisted from specimen to specimen. For example, the optimum moisture content for the soil was 13.3 percent (see section 3.3), the moisture content for the specimens prepared near optimum ranged from 10.4 to 13.9 percent. The results shown in section 5.4 have demonstrated that the initial parameters will govern the specimen stress-strain response. Additional evidence will be presented in section 6.3. If complete experimental replication is to be achieved, then each specimen must have the same initial parameters. This requirement has been difficult to attain for the compacted specimens prepared in this research. Therefore, some discrepancies in the results are inevitable.

Due to the nature of the specific SHPB used for this research and the compressibility of the specimens, the seating strains produced by positioning the specimen between the bars could not be controlled with great precision. After the specimen was positioned between the bars, and a tight contact between system components checked, the hydraulic actuator was used to position the momentum trap (see figure 3.2). During this process, a variable stress was applied through the transmitter bar to the specimen causing it to compress. The range of this

stress was from 2 to 8 MPa. A measure of the seating strain was obtained by recording the displacement the momentum trap caused by the movement of the hydraulic actuator (see section 5.1). However the inability to control the amount of seating strain made it difficult to have two specimens with similar lengths and phase relationships (e.g., initial gas porosity). This increased the difficulty in achieving complete experimental replication and contributed to the observed discrepancies. (e.g., see figures 5.5 and 5.7).

How well the experimental results can be replicated are also dependent on how consistently the load is applied. In section 3.1 it was noted that the magnitude of the applied load was proportional to the impact velocity of the striker bar which is controlled by the breech pressure in the gas gun. To determine the required gas gun breech pressure to produce a given striker bar impact velocity, a theoretical velocity-breech pressure calibration curve was developed. The velocity-breech pressure calibration curve for the 0.254 m striker bar and its construction are presented in section B.2 of appendix B. Over the period of time the experiments were conducted, it was found that the breech pressure to produce a given impact velocity differed from that which was predicted from the theoretical curve. The variation has been attributed to a variable friction force between the launch

tube and the striker bar. To minimize the effects of friction, the launch tube was periodically swabbed out and treated with a light coating of lubricating oil. Also a dust cover was fabricated for the vent holes on the launch tube so that contamination could be reduced when the system was inactive. Regardless of these efforts, it was difficult to achieve duplicate impact velocities with a given breech pressure.

In spite of the above mentioned difficulties, experimental replication can be achieved when using soil specimens in a SHPB experiment. This has been demonstrated convincingly by figures 5.3, 5.6 and 5.8.

6.3 Soil Behavior

In one-dimensional compression the general stress-strain response exhibited by soil is S-shaped. For small stresses changes, yielding is observed with the stress-strain curve concave to the strain axis. For large stress changes, the behavior is characterized by stiffening with the stress-strain curve being concave to the stress axis. This behavior is shown in figure 6.7. The soil is a dry desert alluvium taken from a site near Yuma, Arizona (Dass and Bratton, 1983). The general specimen stress-strain response observed in this research (see section 5.5) is consistent with this description and is similar to that found by other investigators who performed

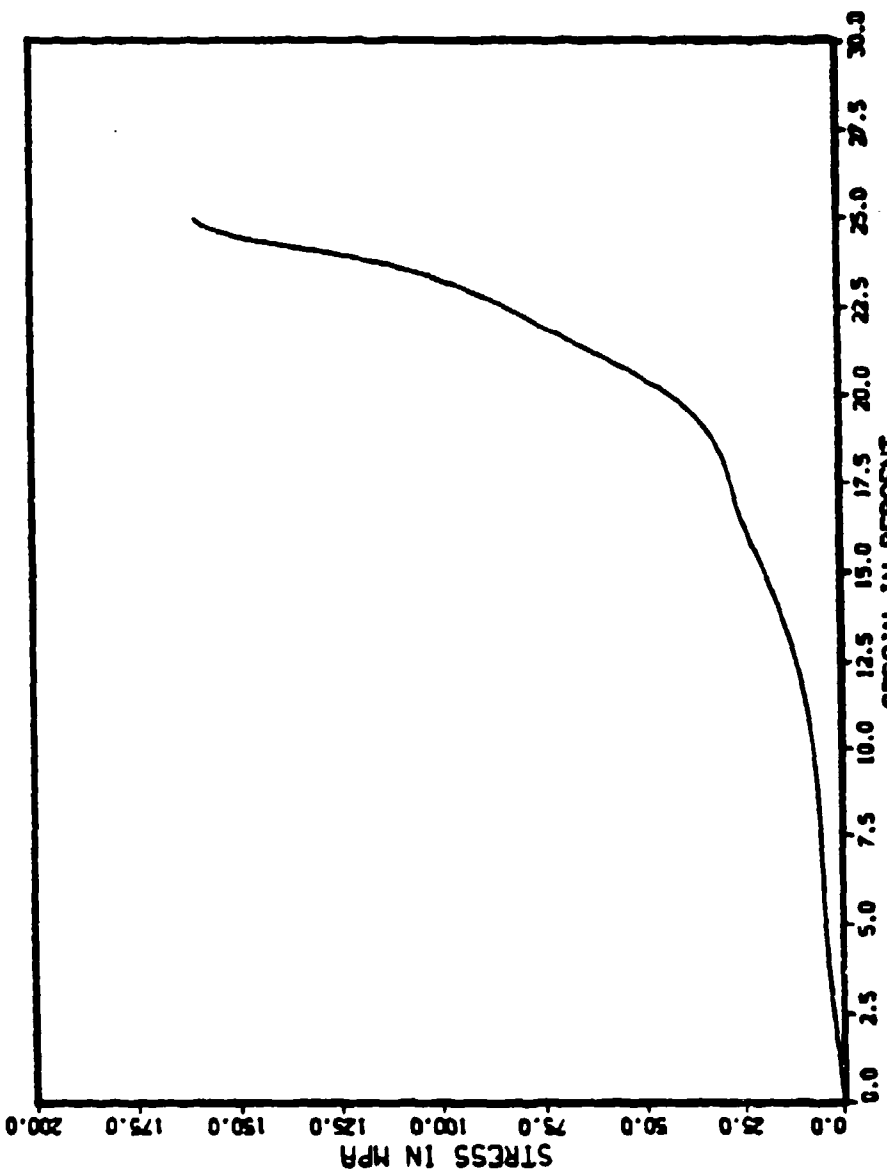

Figure 6.7. One-dimensional soil stress-strain response (adapted from Dass and Bratton, 1983).

uniaxial strain experiments on similar soils but at lower loading rates (Jackson, 1968; Calhoun and Kraft, 1966).

In section 5.5 three observations were made concerning figures 5.9 and 5.10: (1) the peak stress increases with increasing applied stress, (2) the specimens began to stiffen significantly at a strain near the initial gas porosity, and (3) the strain at peak stress consistently exceeded the initial gas porosity. The first observation is consistent with anticipated behavior, i.e., as the applied stress is increased the peak stress sustained by the specimen should also increase. The second observation was also anticipated and will be analyzed below. The third observation was not anticipated and will be analyzed in section 6.4.

In figures 5.9 and 5.10, at strains less than the initial gas porosity the compressibility of the specimens is nearly constant. In figure 5.9 the stress-strain response for the specimen of experiment 163 does not adhere to this behavior. However, the initial gas porosity of the specimen was 50 percent less than that of the other two so that a stiffer response at a lower strain is to be expected. At strains in excess of the initial gas porosity, the compressibility of the specimens is again nearly constant but with a value greater than the initial compressibility. For example in figure 5.10 the tangent modulus for experiment 134 at 4 percent strain is 0.2 GPa

whereas at 11 percent it is 1.5 GPa. It should be noted that the tangent modulus at 11 percent strain is nearly equal to the bulk modulus of water which is approximately 2 GPa. Between these zones of nearly constant compressibility lies a transition zone that can be identified through the initial gas porosity. In this zone the response of the specimen is shifted from being governed by the soil mass to being governed by the pore water. Hence, the initial gas porosity of a specimen can be used as an indicator to determine a change in the response governing mechanism. It is also of interest to note that a similar response has been observed for McCormick Ranch sand subjected to high hydrostatic compression (Mazanti and Holland, 1970).

Figures 5.11, 5.12, and 5.13 compared the response of different length specimens to a range of applied stresses. In section 5.5 the discrepancies between the response for the two specimen lengths were noted and an examination of the specimens initial gas porosities were proposed as a means to explain them. In figures 5.11 and 5.12 the initial gas porosity of the longer specimens were approximately 50 percent less than that of the shorter specimens (i.e., 6.2 pecent as compared to 9.0 percent, respectively for figure 5.10 and 5.8 percent as compared to 10.6 percent, respectively for figure 5.11). Hence, greater stiffness at lower strains is to be expected for

the longer specimens. In addition, smaller strains should be expected for specimens with lower initial gas porosities. In figure 5.13 the situation is reversed with the initial gas porosity of the shorter specimen less than of the longer (i.e., 4.8 percent as compared to 7.5 percent, respectively). Hence, the behavior shown in figure 5.13 is consistent with the conclusion that the specimen stress-strain response is governed by the initial gas porosity. In addition, it can be concluded that the stress-strain response of specimens with different lengths to the same applied stress will be similar if their initial gas porosities are similar.

Figures 5.14 and 5.15 compare the stress-strain response of specimens with similar lengths but prepared at different moisture contents to the same nominal applied stress. The response shown in these figures for both specimen lengths is consistent with the exception of the specimen of experiment 167. However, as was the case for experiment 163 discussed above, the initial gas porosity of the specimen is approximately 50 percent lower than the other two specimens. Hence the response is not inconsistent with what has already been presented. For the specimens prepared near and wet of optimum, the stress-strain response is consistent with the results presented throughout chapter 5; hence their analysis will follow what has already been discussed. Of interest in

figures 5.14 and 5.15 is the response of the specimens that were prepared at moisture/density conditions dry of optimum.

In figures 5.14 and 5.15 the experiments where the specimens were prepared dry of optimum were 135 and 139. It was mentioned in section 5.5 that a change in slope was not observed for the specimen of experiment 135 and that the strain did not approach the initial gas porosity. It can also be seen that the slope of the stress-strain curve is nearly constant which indicates that the compressibility of the soil skeleton can be considered to be nearly constant and that the compression of the air voids is directly proportional to changes in stress.

A difference is observed in the response of the specimens prepared at the moisture/density conditions dry of optimum for the two specimen lengths. In the 12.7 mm specimen (experiment 135), which had a gas porosity of 23.4 percent, very little build up of stress was experienced at the maximum strain of 16 percent. For the 6.35 mm specimen (experiment 139), which had a gas porosity of 17.7 percent, a substantially higher stress was built up as the strain approached this value. Two factors may be responsible for this difference in behavior. First, the density of the 6.35 mm specimen (1.98 g/cm^3) is greater than that of the 12.7 mm specimen (1.87 g/cm^3). Second, the initial gas porosity of the of the

6.35 mm specimen is lower than that of the 12.7 mm specimen. As the effect of density variations on specimen response was not investigated it can not be concluded that one factor is more dominate than the other. However, the respone of the 6.35 mm specimen is consistent with the response of other specimens where the strain approached or slightly exceeded the initial gas porosity (e.g., experiment 119); hence supporting the conclusion that the initial gas porosity is a governing parameter in determining specimen stress-strain response.

6.4 Strain in Excess of Initial Gas Porosity

As discussed in section 5.2 the initial gas porosity is an approximate upper bound on the strain that a specimen can sustain. However, the results presented in section 5.5 showed that for nearly every experiment, the strain sustained by the specimen exceeded the initial gas porosity (see figure 6.8). There are several factors which may be working together to account for this discrepency:

(1) loss of soil and or moisture,

(2) compression of the pore water as the specimen becomes saturated, and

(3) radial expansion of the confining cylinder and specimen.

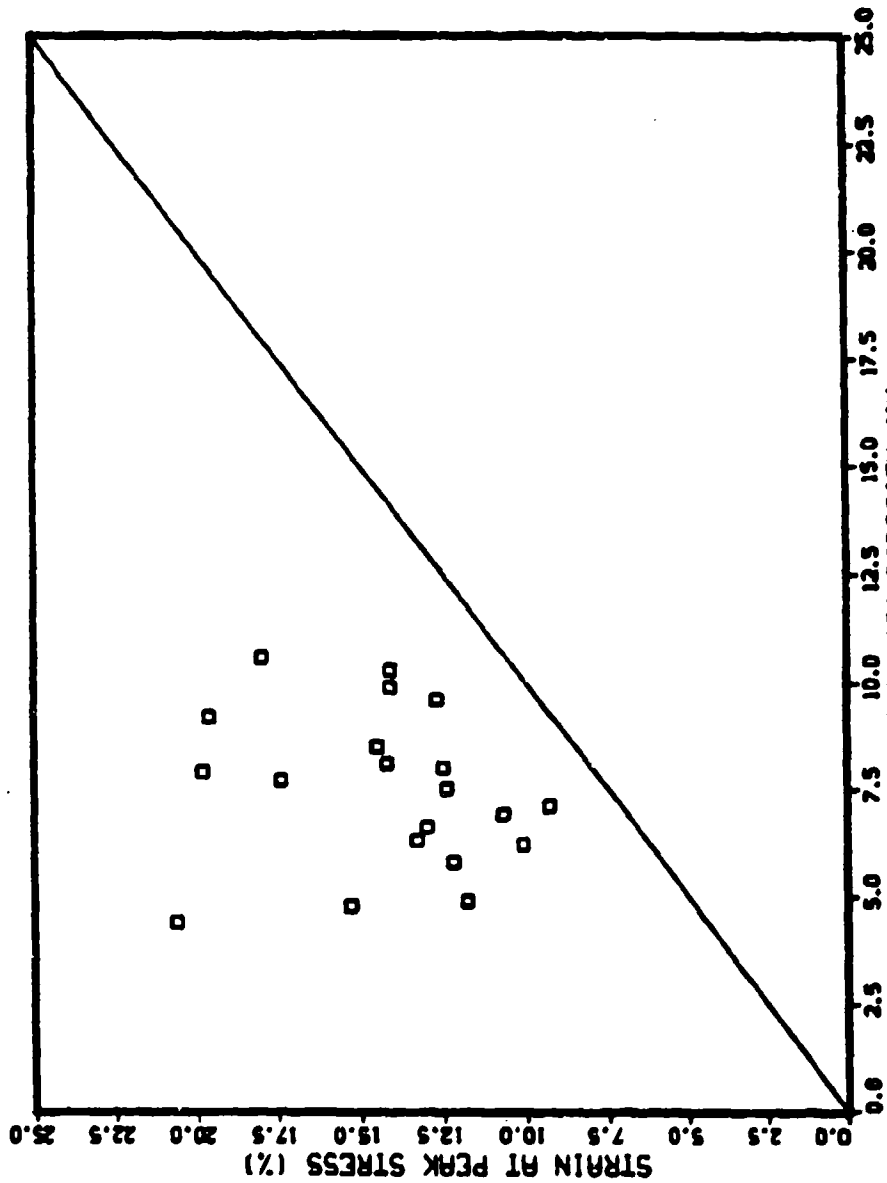

Figure 6.8. Comparison of computed specimen strain and initial gas porosity.

6.4.1 Loss of Soil and Moisture

Soil and moisture loss are possible because the diameter of the bars and the inside diameter of the confining cylinder are not equal. Although the tolerance is very small (see figure 3.8), soil and moisture loss can occur through the annular region between them. The mechanism for the loss is that a pressure gradient is set up between specimen-bar interfaces and the atmosphere.

At the specimen-incident bar interface a portion of the initial compressive stress wave is reflected as a tensile wave due to the lower impedance of the specimen relative to the bar. This tensile wave travels back down the incident bar toward the end at which the impact occurred. As the impact end of the incident bar is now a free end, the tensile wave is reflected as a compressive wave travelling once again toward the specimen, hence, reloading the specimen. For the SHPB experiment the specimen response of interest is that due to the initial stress wave.

This multiple impact situation, complicates the ability to quantify the amount of soil and moisture lost, as the quantity lost during each impact is indeterminate. In addition, the specimen may sustain additional strain during the second impact, making it meaningless to compare a measured strain with the computed strain which results from the initial stress wave.

An attempt to measure the mass of soil lost was made in several experiments. The mass of soil lost was determined by recording the combined mass of the confining cylinder and specimen before it was positioned between the bars and just after it was removed, at the completion of the experiment, and then taking the difference. The maximum and minimum soil loss was computed to be 7.9 and 1.7 g, respectively. The results are tabulated in table E.6 of appendix E. These measurements overestimate the amount of soil lost because the specimen is subjected to multiple impacts.

Because a moisture content was determined at the time the specimen was prepared and immediately after the experiment, a measure of the amount of moisture loss sustained by the specimen can be computed. The maximum and minimum moisture losses were computed to be 27.6 and 1.7 percent of the initial moisture content, respectively. The moisture loss for each experiment is tabulated in table E.7 of appendix E. If all the moisture loss is assumed to occur during the first impact, the specimen can sustain an additional strain proportional to the volume of moisture lost. Using this assumption, the strain contribution from moisture loss for each experiment has been computed and the results tabulated in table 6.2. These strains will be overestimates for the same reason the measured soil loss was an overestimate.

Table 6.2

Component Contribution to Specimen Strain

Experiment No.	Gas Porosity (%)	Water Compression (%)	Moisture Loss (%)	Radial Strain (%)	Sum (%)	Strain at Peak Stress (%)	Balance (%)
112	7.9	1.8	2.6	0.5	12.8	19.8	7.0
113	7.7	1.8	3.9	0.5	13.9	17.4	3.5
114	9.2	1.8	3.8	0.5	15.3	19.6	4.3
115	10.6	1.7	2.2	0.6	15.1	18.0	2.9
116	8.1	1.2	2.6	0.3	12.2	14.2	2.0
117	8.5	1.4	1.5	0.4	11.8	14.5	2.7
118	10.3	1.2	1.9	0.4	13.8	14.1	0.3
119	9.9	1.1	1.7	0.3	13.0	14.1	1.1
131	9.6	1.5	1.8	0.4	13.3	12.7	-0.6
132	6.9	1.6	1.5	0.4	10.4	10.7	0.3
133	8.0	1.4	2.7	0.4	12.5	12.5	0.0
134	5.8	1.7	1.9	0.5	9.9	12.2	2.3
135	23.4	0.2	1.3	0.1	25.0	15.6	-9.4
136	5.2	2.4	6.5	0.6	14.7	11.2	-3.5
137	8.5	2.1	5.7	0.5	16.8	6.3	-10.5
138	4.9	1.6	1.9	0.4	8.8	11.8	3.0
139	17.7	0.6	1.3	0.2	19.8	17.2	-2.6
145	6.2	0.9	0.9	0.2	8.2	10.1	1.9
146	6.3	2.2	1.5	0.7	10.7	13.3	2.6
147	6.6	1.2	2.3	0.3	10.4	13.0	2.6
148	7.4	1.1	2.8	0.2	11.5	15.2	3.7
162	4.4	2.4	2.5	0.7	10.0	20.6	10.6
163	4.8	2.9	1.9	0.9	10.5	15.3	4.8
164	7.5	2.2	1.8	0.7	12.2	12.4	0.2
165	7.1	0.7	1.1	0.2	9.1	9.3	0.2
166	4.4	1.2	2.4	0.3	8.3	13.3	5.0
167	4.2	1.5	2.4	0.4	8.5	12.6	4.1

6.4.2 Compression of Pore Water

In most engineering applications, water is considered to be an incompressible fluid. At the stresses applied in this research (> 100 MPa), this assumption will be invalid. The compression of the pore water will contribute to the strain sustained by the specimen.

The specific volume of water at a variety of temperatures subjected to a range of applied stresses has been tabulated in the Handbook of Physical Constants (Sydney, 1966). These values have been used to compute the strain contribution due to the compression of the pore water. The computation results are presented in table 6.2. The stress used in the computations was taken as the peak stress sustained by the specimen.

6.4.3 Radial Expansion of the Confining Cylinder and Specimen

It has been shown in section 5.3 that the specimens are constrained to a state of nearly uniaxial strain because of the small amount of radial strain that occurs. However small, the radial strain will make some contribution to the overall specimen strain. The method by which the radial strain of the confining cylinder and specimen has been computed and the assumption used in the computations have already been presented in section 5.3. The strain contribution is computed by accounting for the

change in specimen area resulting from the radial displacement. The radial strain contribution to specimen strain in each experiment is tabulated in table 6.2.

6.4.4 Strain Correction

Table 6.2 sums the strain contributions from water compression, moisture loss, and radial strain and compares it to the specimen strain at peak stress. These data are plotted in figure 6.9. It can be seen that in all but a few experiments a balance of strain still remains. Had sufficient information been obtained to compute the strain contribution from soil loss the remaining balance for each experiment would be less.

Due to the uncertainty in the evaluation of the strain contributions from the above mentioned factors, a gross strain adjustment, to account for the excess between strain at peak stress, and the initial gas porosity has been computed. The details of the computations are presented in appendix J. The gross strain correction requires none of the assumptions made in the computations of the strain contribution from moisture loss, pore water compression, or radial expansion. It is based solely on the peak stress sustained by the specimen. In addition, the strain contribution of soil loss is also included.

The results show that the strain balance from the gross correction is less than that computed by summing the

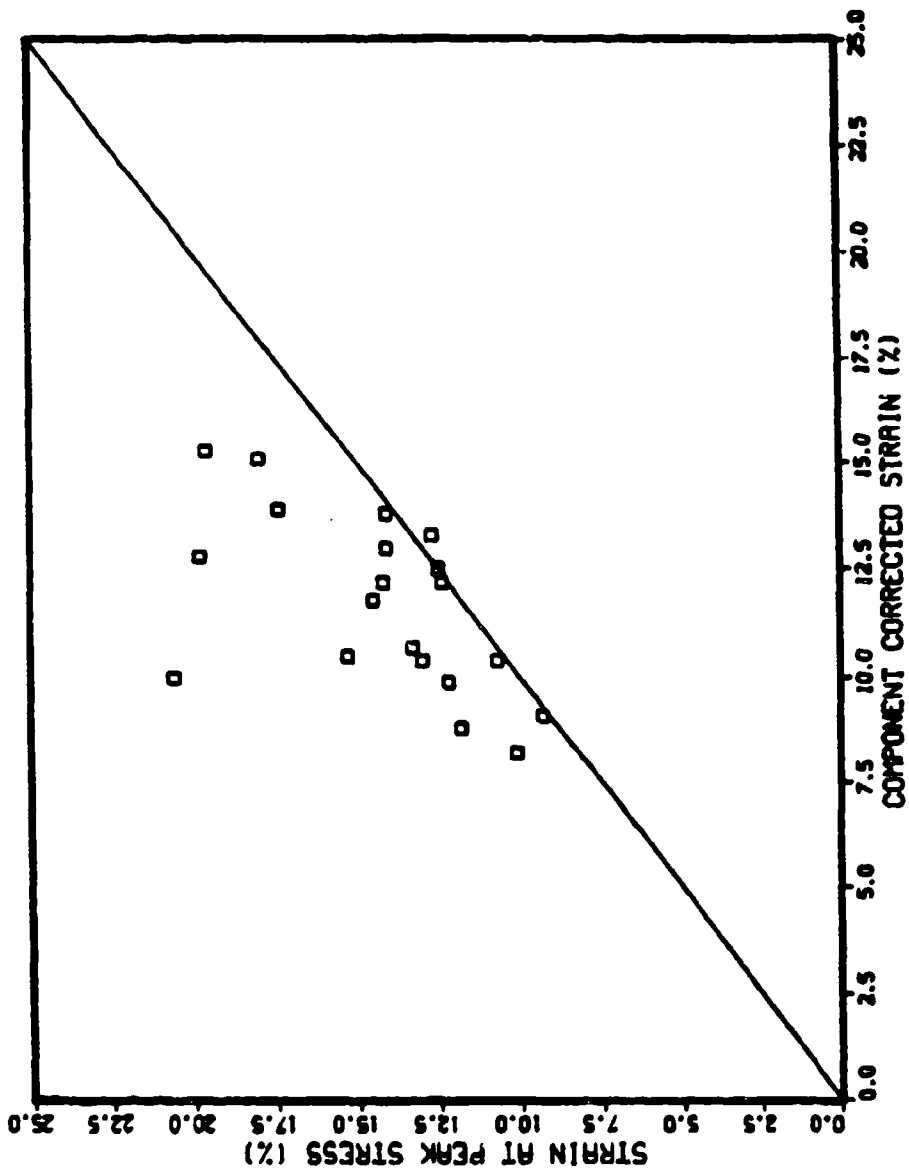

Figure 6.9. Comparison of computed specimen strain and component corrected strain.

individual components indicating that the strain contribution due to soil loss can be significant (see figure 6.10). Regardless of the method used, an accounting of the excess between the strain at peak stress and the initial gas porosity can be made.

6.5 Strain-Rate Dependence

To determine the strain-rate sensitivity of the compacted sand, stress-strain-rate curves at constant strains were constructed for each nominal specimen length. The data were taken from experiments conducted at the nominal applied stresses of 250 MPa and 400 MPa. The results are presented in figures 6.11 and 6.12 for the 6.35 mm and the 12.7 mm long specimens compacted at moisture and density conditions near optimum, respectively. The details of the construction are as follows.

For each experiment, the stress and strain-rate for a given strain was recorded. For the 6.35 mm specimens the range of strains was from 5 percent to 14 percent, and for the 12.7 mm specimens the range of strains was from 5 percent to 10 percent. The stress-strain-rate data points from the experiments for a given strain are then grouped according to the applied stress at which the experiment was conducted and then plotted. From figures 6.11 and 6.12 it can be seen that considerable scatter results. To simplify the presentation, the group of stress-strain-rate data

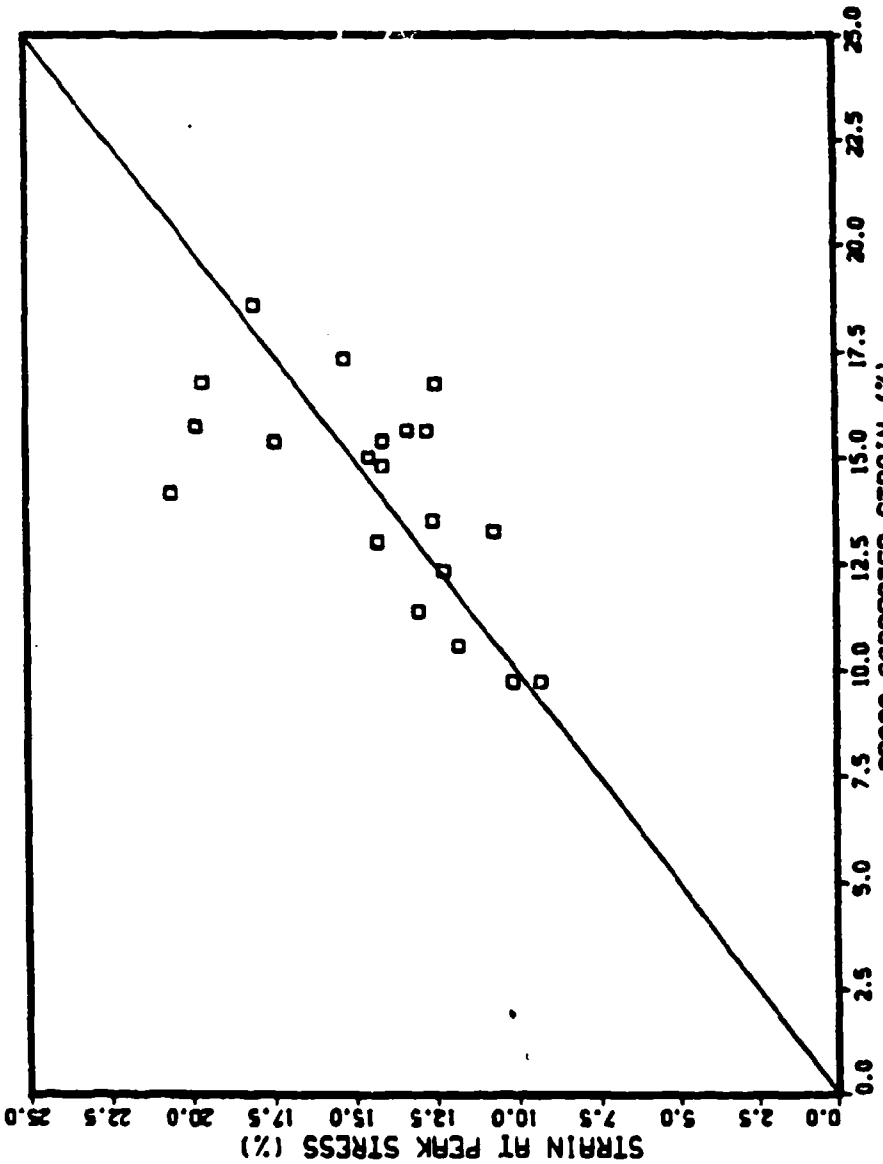

Figure 6.10. Comparison of computed specimen strain and gross corrected strain.

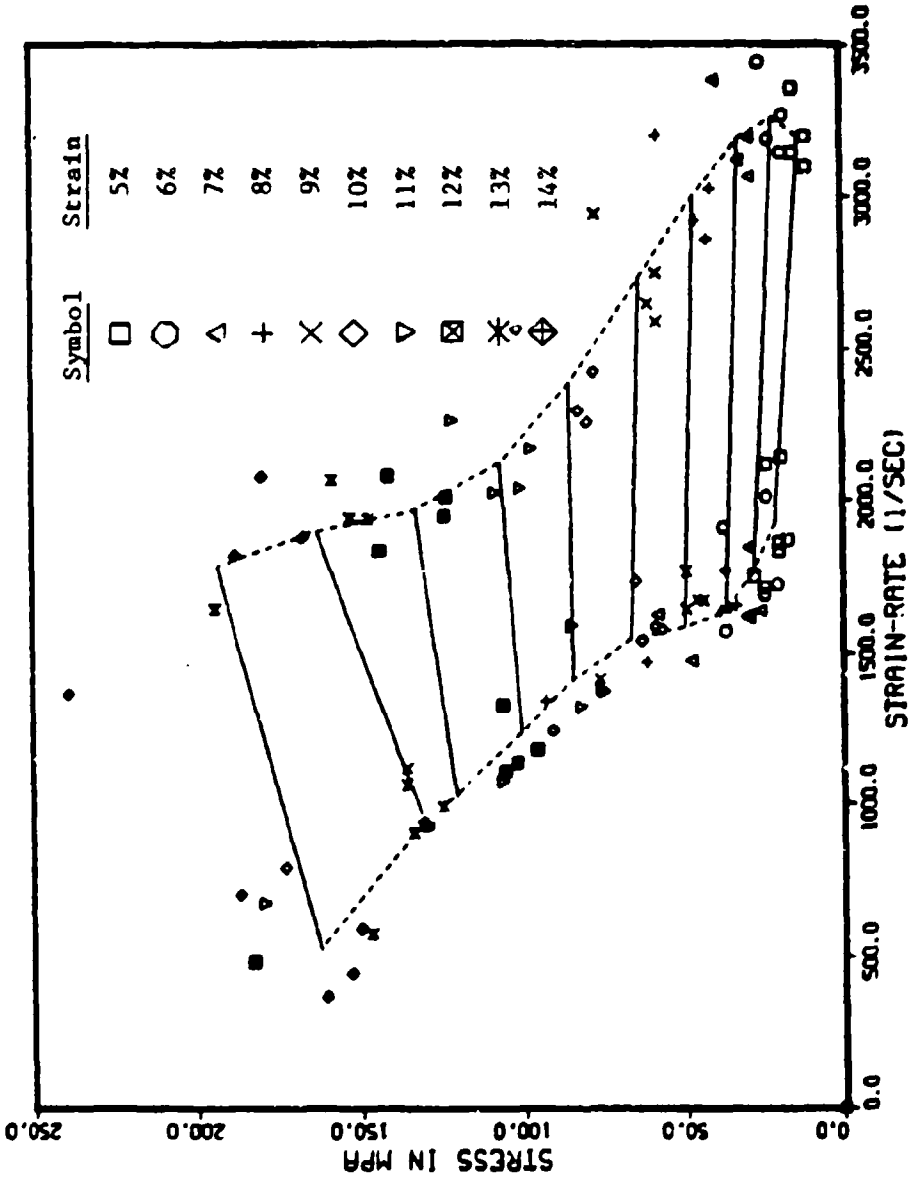

Figure 6.11. Stress-strain-rate plot for 6.35 mm specimens compacted at optimum conditions.

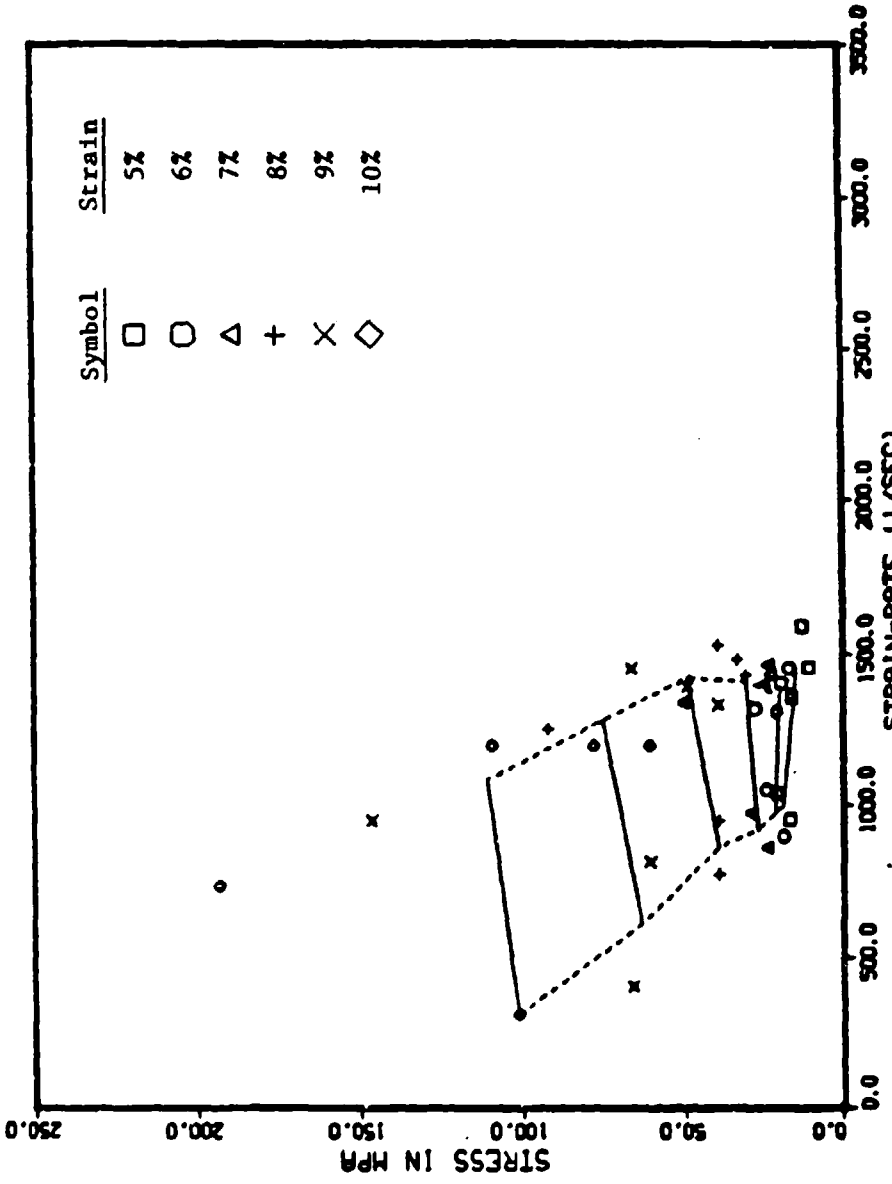

Figure 6.12. Stress-strain-rate plot for 12.7 mm specimens compacted at optimum conditions.

points for a given strain and nominal applied stress were averaged. In figures 6.11 and 6.12 , the dashed lines are the average stress-strain-rate trajectories for a given applied stress. The solid lines connect points of constant strain between the stress-strain-rate trajectories.

In this type of plot, the degree to which the compacted sand is strain-rate dependent can be judged by the slope of the constant strain curves connecting the stress-strain-rate trajectories. If the slope is zero, it can be concluded that the compacted sand response is not strain-rate dependent. The results shown in figures 6.11 and 6.12 indicate the response of the compacted sand is not dependent on strain-rate for strains below the initial gas porosity. This is consistent with the results reported by Gaffney et al. (1985) who found no strain-rate dependence in a drier but otherwise similar soil for total strains less than the initial gas porosity.

It was observed in figures 6.11 and 6.12 that the stress which produced a given strain did not increase with increased strain-rate, indicating that the specimen response was not dependent on strain-rate for strains less than the initial gas porosity. However, this apparent strain-rate independence should be viewed with caution for two reasons, first, the constant strain curves used to show this apparent strain-rate independance are only rough averages developed from a few data points, and second, the

factors identified to account for the discrepancy between the strain at peak stress and initial gas porosity cannot be quantified with the necessary accuracy to determine what their effect on the apparent strain-rate dependency might be.

6.6 Conditions of Experiment

In order to satisfy the assumptions of the experiment (see sections 4.1 and 6.1) the soil specimens were prepared with aspect ratios less than or equal to 0.2 and contained in a confining cylinder. The small aspect ratios were necessary to satisfy the uniform stress assumption while the containment facilitated the control of boundary conditions.

If the specimens had been longer stress equilibrium would not have been achieved during the early portion of the experiment. Had this been the case, a greater portion of the stress-strain curve would have had to be discarded as inertial forces would have dominated the response. Therefore, soil specimens in the SHPB experiments are restricted to small aspect ratios. It may be possible to use greater aspect ratios if the duration of the applied stress wave is extended (e.g., by using a longer striker bar).

In the traditional SHPB experiment the specimen is in a state of nearly uniaxial stress. Because the unconfined

strength of soil (e.g., < 0.1 MPa) is insignificant compared to the applied stresses (e.g., > 100 MPa), reproducing the traditional SHPB experiment with soil specimens is not feasible. Hence, some means of radial confinement is required. Three degrees of radial support can be considered: minimal, intermediate, and stiff. Providing minimal support would most closely approximate the uniaxial stress state in the traditional experiment. However, even the flimsiest of containment systems would provide a radial restraint that would be significant relative to the unconfined strength of the soil. If an intermediate confinement is used, radial stress and strain histories would have to be known to evaluate specimen response. Therefore, the use of minimal or intermediate containment systems would complicate the data analysis. In contrast to the first two, a stiff confinement system is easy to implement and has the advantage that it constrains the specimen to a nearly uniaxial strain path (see section 5.3) which can be easily duplicated at both higher and lower strain-rates.

6.7 Applications of the SHPB Technique

In recent years complex constitutive models have been developed for use in numerical computations to predict the response of soil in the region close to a high yield weapon explosion (e.g., Rubin and Sandler, 1977). These models are

used in large computer codes to study ground-shock problems of both the free-field and soil-structure interaction types (Nelson, Baron, and Sandler, 1971). If these models are to accurately predict field response they must be fit to data which reflect the type of confinement, magnitude of stress change, and time scale of stress application to be expected (Whitman, 1970). These requirements have placed demands on experimentalists to develop laboratory procedures that will reflect field conditions and provide data for the evaluation of the material constants which appear in the models (Nelson et al., 1971).

The soil test most often selected to duplicate the loading condition in the overpressure region associated with weapons effects is the uniaxial strain test. For the past 30 years the dynamic uniaxial strain device has been used to investigate the fundamental nature of soil behavior to rapidly applied loads. Although current devices can apply stresses up to 400 MPa with loading times of 0.3 milliseconds the need for a laboratory test that more closely simulates the environment near a weapon explosion is clear. The SHPB technique is a means to satisfy the demand for more reliable data in support of a wide variety of weapon effects problems.

It is common practice to extrapolate laboratory data to evaluate the material constants which appear in a constitutive model that will be used to represent the soil

behavior to an explosive event. As the SHPB technique can be used to evaluate material response to stresses and strain-rates that are closer to in situ conditons, extrapolation can be avoided and the material constants determined directly. This can lead to a decrease in the time required to evaluate the adequacy of a model to a particular problem as well as a better model because the constants can be evaluated from data that more closely duplicates field conditions. In addition, a reduction in field costs may also be realized as extra in situ measurements can be avoided if the laboratory data can provide a closer approximation of the anticiapted field conditions.

The flyer plate experiment is a particular example where the data from a SHPB experiment would prove useful. The purpose the flyer plate experiment is to develop a technique for field calibrating soil stress and motion instrumentation in the pressure range of 100 to 1000 MPa. In this experiment a planar impact is applied to an instrumented soil test bed by an explosively driven metal plate such that the loading path is approximately uniaxial strain. To calibrate the instrumentation the soil must be properly characterized such that the material model will accurately predict the stress and motion fields. The SHPB technique is the most appropriate means to evaluate the required material properties as precise and accurate

measurements can be made over the stress range of interest.

The SHPB technique can also be used to extend the knowledge of dynamic soil response in several other areas. In section 6.4 it was described that during the experiment the specimen was subjected to multiple impacts. This phenomenon may be exploited to investigate soil response to multiple loadings in rapid succession without altering the specimen properties in between loadings. Hence, providing a laboratory means to investigate soil response to a successive impulse loading envirommment. Another area of interest is the effect of confinment on soil response. By varying the degree of radial support to a soil specimen the effect of confinment on the soil stress-strain response can be evaluated. Such information would be valuable to the understanding of soil response to airblast loading during the transition from the superseismic region to the outrunning region. Also the SHPB technique is capable of providing information on stress attenuation and changes in waveform with distance and their influence on stress-strain response as a function of stress level.

7. CONCLUSIONS AND RECOMMENDATIONS

7.1 Conclusions

The analyses contained in this research permit the following conclusions regarding the use of the SHPB experimental method to measure the dynamic response of soil.

(1) For compacted sand specimens constrained to a nearly uniaxial strain state, the assumptions necessary to obtain meaningful data from a SHPB experiment can be satisfied. It has been shown that stress uniformity over the length of the specimen is achieved and that the criterion of Davies and Hunter (1963) can be used to estimate the time it occurs. The criterion of Bertholf and Karnes (1974) was violated for nearly every experiment and determined to be to restrictive when applied to soil specimens. Wave dispersion was shown to occur and increase the difficulty in interpreting experimental results. However, the effects of wave dispersion can be minimized through the correction procedure developed by Follansbee and Frantz (1983). The error in assuming stress uniformity over the cross sectional area of the bar was determined to be in excess of the $\pm$ 3 percent determined by Davies (1948)

when $R/\Lambda < 0.1$ but less than $\pm$ 10 percent. Friction effects were minimized by confining the specimen and were found not to influence stress-strain response for specimens different in length by a factor of two.

(2) Experimental replication can be achieved. However, every precaution must be taken to prepare specimens with similar phase relationships (e.g., initial gas porosity) and to conduct the experiments following the same procedure if discrepancies in the results are to be avoided. The factors that were found to complicate experimental replication are: preparing specimens with similar initial parameters (e.g., initial gas porosity), the inablity to control seating strain which altered a specimens initial parameters, difficulty in achieving duplicate impact velocities, and soil and moisture loss through the annular region between the confining cylinder and pressure bars.

(3) The stress-strain response is governed principally by the initial gas porosity of the specimen. At strains less than the initial gas porosity the specimen compresses, closing the air voids. At a strain near the initial gas porosity the specimen begins to stiffen significantly. The initial gas porosity was taken as an upper bound on the strain a specimen could sustain. However, in some experiments, the specimen continued to strain beyond the initial gas porosity. The factors

accounting for the excess strain were identified as: soil and moisture loss, compression of the pore water, and radial expansion of the confining cylinder and specimen. This was verified by an overall strain correction and by summing the strain attributed to each factor.

(4) The specimens prepared near optimum conditions were insensitive to strain-rate at strains less than the initial gas porosity. At strains in excess of the initial gas porosity a strain-rate dependency is apparent. Pore water pressure is likely to play a role in this change, but how is not clear.

It is concluded that the SHPB experimental method can be used to determine the dynamic response of soil. Although a few limitations are associated with using soil specimens in a SHPB experiment, there are no serious obstacles that will prevent them from being overcome. The SHPB method is a relatively simple experiment and can significantly extend the range of stresses and strain-rates that can be applied beyond the capabilities of current equipment used for dynamic soil investigations.

7.2 Recommendations

The success of this research effort provides a justification for the expanded use of the SHPB technique for evaluating dynamic soil response. Consequently, it is

recommended that study be initiated in three areas: (1) alternative measurements, (2) containment systems, and (3) modification to equipment.

As a supplement to the traditional measurement techniques which have been described in chapters 2 and 3, the feasibility of sensing the stress waves directly on the specimen-bar interfaces should be explored. For foam specimens such a technique has been employed that uses quartz crystals mounted on the ends of the pressure bars in contact with the specimen (Hodge and Wasley, 1969).

The soil containment system used in this research has presented several difficulties the most important of which is that loss of soil and moisture cannot be prevented. Therefore it would be advantageous to have a system that would prevent such losses. Also such a system would allow unloading behavior to be investigated. In addition, if a confining cell similar to those used for triaxial testing could be built that would be able to apply confining stresses of several hundred megapascals, a means would be available to investigate dynamic shear response. Such a containment system would extend the capabilities of the method when using soil specimens considerably. As a mimimum however, measurements of radial stresses and strain should be attempted. This information alone would be very valuable in deriving constitutive models for general deformation paths.

The final area in which recommendation will be made concerns experimental equipment. Two main problems were encountered in using the equipment described in chapter 3 when using soil specimens: (1) the inability to accurately control seating strains, and (2) only stresses in excess of 200 MPa could be applied with any degree of consistency.

The first difficulty can be eliminated by the introduction of controls sensitive to small changes in stress. These would be beneficial for two reasons. First, an increased control on seating strains could be established and second, a preload could be precisely controlled to simulate geostatic overburden stresses.

The second problem may be overcome by using a striker bar with a characteristic impedance less than that of the steel pressure bars. As the applied stress is proportional to the characteristic impedance of the striker bar (see appendix C) a reduction in the impedance will cause a smaller stress to be applied for the same impact velocity. For example, if the striker bar is constructed of aluminum which has a characteristic impedance nearly three times less than that of steel, for the same impact velocity the applied stress would be reduced by nearly a factor of three.

A final recommendation concerning equipment pertains to the pressure bars. The ratio of the characteristic

impedances for the soil specimens and the pressure bars used in this research was approximately 60 to 1. Although the uniform stress assumption was not seriously compromised, stress equilibrium in the specimen would have been achieved sooner if the impedance mismatch had been smaller. Also the constancy of strain-rate could have been inproved if the characteristic impedance of the pressure bars had been closer to that of the soil (Rand, 1967). Therefore it is recommended that pressure bars be constructed of material other than steel. Potential candidates may be aluminum and possibly some type of plastic.

APPENDIX A

MATHEMATICS OF THE DISPERSION CORRECTION PROCEDURE

A.1 General

The procedure for correcting a waveform for dispersion can be broken down into four basic operations (Follansbee and Frantz, 1983):

(1) transformation of the original waveform to a Fourier series,

(2) computation of the phase velocity for each frequency component,

(3) computation of the adjustment to the phase angle based on position,

(4) reconstruction of the original waveform with adjusted phase angles.

A.2 Transformation to a Fourier Series

The general expression for a Fourier series can be written as follows (Wiley and Barrett, 1982);

$$f(t) = \frac{A_0}{2} + \sum_{n=1}^{\infty} A_n \cos n\omega_0 t + B_n \sin n\omega_0 t \quad , \qquad (A.1)$$

where f(t) is a periodic function, ω_0 is the wave frequency defined as;

$$\omega_0 = \frac{2\pi}{T} \quad , \qquad (A.2)$$

where T is the period of the wave, and A_0, A_n, and B_n are the Fourier coefficients which can be expressed as;

$$A_o = \frac{2}{T}\int_0^T f(t)\ dt \quad , \tag{A.3}$$

$$A_n = \frac{2}{T}\int_0^T f(t)\ \cos\ n\omega_o t\ \ dt, \tag{A.4}$$

$$B_n = \frac{2}{T}\int_0^T f(t)\ \sin\ n\omega_o t\ \ dt. \tag{A.5}$$

Upon evaluation of the Fourier coefficients A_o, A_n, and B_n, the general Fourier series (equation A.1) is transformed to a pure Fourier cosine series. The reduction of the general Fourier series involving the sum of a sine and cosine term is accomplished by first multiplying the sum;

$$A_n \cos\ n\omega_o t + B_n \sin\ n\omega_o t \quad , \tag{A.6}$$

by,

$$\frac{\sqrt{A_n + B_n}}{\sqrt{A_n + B_n}} \quad , \tag{A.7}$$

to yield,

$$\sqrt{A_n + B_n}\left[\frac{A_n}{\sqrt{A_n + B_n}} \cos\ n\omega_o t + \frac{B_n}{\sqrt{A_n + B_n}} \sin\ n\omega_o t\right] . \tag{A.8}$$

By establishing the new variables;

$$D_n = \sqrt{A_n + B_n} \quad , \tag{A.9}$$

which is the resultant amplitude of the frequency

component $n\omega_0 t$, and;

$$\cos\Phi = \frac{A_n}{\sqrt{A_n + B_n}} , \qquad (A.10)$$

$$\sin\Phi = \frac{B_n}{\sqrt{A_n + B_n}} , \qquad (A.11)$$

where Φ is the phase angle which is a measure of the lead or lag of the nth harmonic in reference to the sine or cosine wave of the same frequency (Wiley and Barrett, 1982). Expression (A.8) can be rewritten as;

$$D_n (\cos\Phi \cos n\omega_0 t + \sin\Phi \sin n\omega_0 t). \qquad (A.12)$$

Applying the following trigonometric substitution to expression (A.12) (Selby, 1975);

$$\cos a \cos b + \sin a \sin b = \cos (a - b) , \qquad (A.13)$$

yields,

$$D_n \cos (n\omega_0 t - \Phi). \qquad (A.14)$$

Substituting expression (A.14) into equation (A.1), yields a pure Fourier cosine series of the form;

$$f(t) = \frac{A_0}{2} + \sum_{n=1}^{\infty} D_n \cos (n\omega_0 t - \Phi) . \qquad (A.15)$$

There is one note on the computation Φ. Instead of computing Φ as;

$$\Phi = \tan^{-1} \frac{B_n}{A_n} \quad , \qquad (A.16)$$

Φ will be computed as;

$$\Phi = \cos^{-1} \frac{A_n}{D_n} \quad . \qquad (A.17)$$

This is because the range of the arctangent is $\pm\pi/2$, hence for some phase angles (e.g., $3\pi/4$) an incorrect value would be returned. The range of the arccosine is 0 to π. To maintain the proper sign of the phase angle in the computations; if $B_n < 0$, the resultant phase angle will be the inverse sign of the value obtained in equation (A.17).

A.3 Computation of Phase Velocity

The propagation velocity of a wave at a given frequency is called its phase velocity (C_n). C_n can be written in terms of cyclic frequency (f) and wavelength (Λ) as;

$$C_n = f_n \Lambda \quad , \qquad (A.18)$$

which can be related to the natural frequency (ω_o) through;

$$2\pi f_n = n\omega_o \quad , \qquad (A.19)$$

as,

$$C_n = \frac{n\omega_0 \Lambda}{2\pi} \quad . \qquad (A.20)$$

Equation (A.20) can be written in dimensionless form by rearranging and dividing both sides of the equation by $C_0 R$ to yield.

$$\frac{2\pi C_n R}{\Lambda C_0} = \frac{R\, n\, \omega_0}{C_0} \quad . \qquad (A.21)$$

The terms on the right side of equation (A.21) are all known quantities. The only unknown in equation (A.21) is C_n. A value for C_n can be computed using the polynomial approximation (equation 2.43 to the fundamental mode of the dispersion equation (equation 2.42). The two variables in the polynomial approximation are C_n/C_0, and R/Λ. By computing C_n/C_0 for a given value of R/Λ, the quantities on each side of equation (A.21) can be compared. Hence, by iterating through values of R/Λ, a value for C_n/C_0 can be computed such that the two sides of equation (A.21) will be equal. Once equality has been established, C_n can be computed directly.

A.4 Phase Angle Adjustment Based On Position

From the dispersion equation (equation 2.42) it has been determined that C_n is dependent on Λ (Davies, 1948). This causes a wave to disperse as it propagates because the high frequency components will lag behind the low frequency components. Follansbee and Frantz (1983) have

derived a relationship based on the phase angle (Φ) to account for the dispersion that occurs as a wave propagates a distance Δx. The derivation of the phase angle correction is shown below.

The term inside the brackets of equation (A.15) can be rewritten in terms of position as;

$$n\omega_0 t - \Phi = n\omega_0 \left[t + \frac{\Delta x}{C_0} - \frac{\Delta x}{C_n} \right] , \qquad (A.22)$$

where $\Delta x/C_n$ is the time for a given component to travel a distance Δx. Rewriting the terms of equation (A.22) yields;

$$n\omega_0 t - \Phi = n\omega_0 \left[t + \frac{\Delta x}{C_0} \left[1 - \frac{C_0}{C_n} \right] \right] , \qquad (A.23)$$

$$n\omega_0 t - \Phi = n\omega_0 t - \frac{n\omega_0 \Delta x}{C_0} \left[\frac{C_0}{C_n} - 1 \right] . \qquad (A.24)$$

The phase angle can now be computed as a function of position according to;

$$\Phi' = \frac{n\omega_0 \Delta x}{C_0} \left[\frac{C_0}{C_n} - 1 \right] . \qquad (A.25)$$

A.5 Wave Reconstruction

The last operation in the dispersion correction procedure is wave reconstruction. Essentially this entails adding or subtracting the phase angle adjustment computed for a given position Δx, from equation (A.25) to the

phase angle computed at the original position x, computed from equation (A.17);

$$\Phi'' = \Phi' + \Phi \quad . \tag{A.26}$$

The value for Φ is then substituted into equation (A.15) for Φ, and the wave reconstructed with the effects of dispersion accounted for.

APPENDIX B

GAS GUN AND INSTRUMENTATION

B.1 Gas Gun Operation

A schematic of the gas gun used to propel the striker bar down the launch tube is shown in figure B.1. The three chamber arrangement is prepared for firing by pressurizing with nitrogen gas according to the following procedure.

(1) The set pressure chamber is filled to set the piston assembly and prevent any leakage of gas to the launch tube.

(2) The firing pressure chamber is filled to a pressure not to exceed the pressure in the set pressure chamber so that the risk of accidental firing is reduced.

(3) The breech is filled to a pressure such that when the nitrogen gas is released, the striker bar will be propelled down the launch tube at a predetermined velocity. The required pressure to produce a given velocity is determined from the velocity-breech pressure calibration curve for the striker bar used. To assist in experimental replication, the breech is fitted with a pressure transducer that is connected to a digital volt meter to accurately establish pressurization levels.

(4) Firing is accomplished by venting the set pressure chamber which allows the gas in the firing pressure chamber to release the piston assembly. This breaks the seal between the gun and launch tube causing the breech pressure to be released behind the striker bar propelling it down the launch tube.

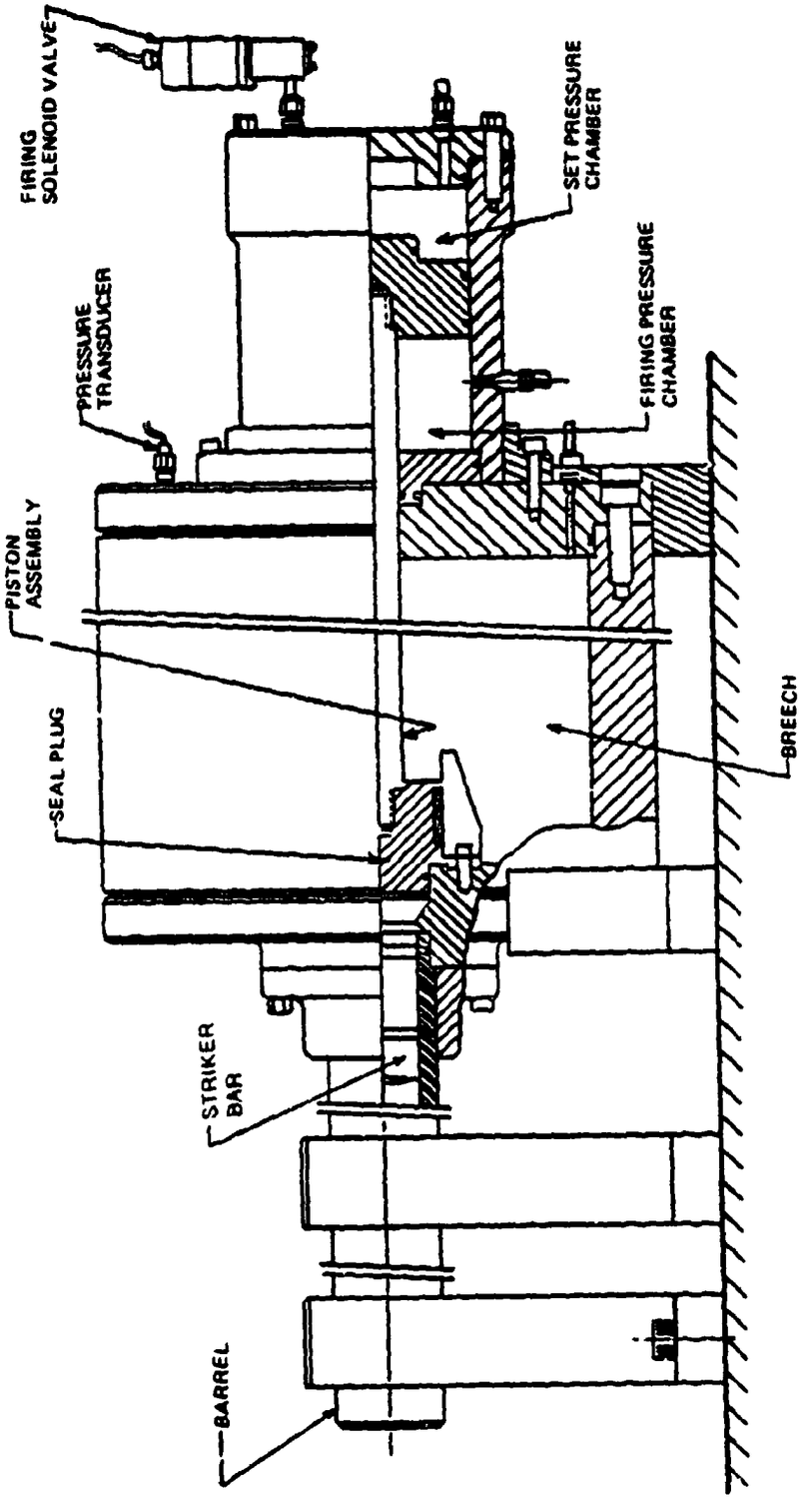

Figure B.1. Gas gun (Nagy and Muelenhaupt, 1983).

B.2 Velocity-Breech Pressure Calibration

The impact velocity of the striker bar as a function of gas gun breech pressure can be determined from the following equation (Nagy and Muelenhaupt, 1983);

$$V(x) = \frac{2P_0 V_0}{m(\gamma - 1)} \left[1 - \left[1 + \frac{\Delta X}{V_0} \right]^{1-\gamma} \right] \qquad (B.1)$$

where

$V(x)$ is the projectile velocity at distance x,

X is the distance traveled while the pressure is applied,

P_0 is the initial breech pressure,

V_0 is the breech volume (65,500 cm^3),

m is the mass of the projectile, and

γ is the ratio of specific heats for the driving gas.

The calibration curve is shown in figure B.2

B.3 Velocity Measuring System

The velocity measuring system consists of three diode lasers with focusing lenses and three photodetectors. The lasers are model OL5100 3mW continuous wave lasers that operate at 8000 to 8200 angstroms in the infrared and are manufactured by Optical Information Systems. The focusing lenses are SELFOC-Micro Lens (SML) made by Nippon Sheet Glass Company Incorporated. The photodetectors are manufactured by Hewlett-Packard. A photograph of the

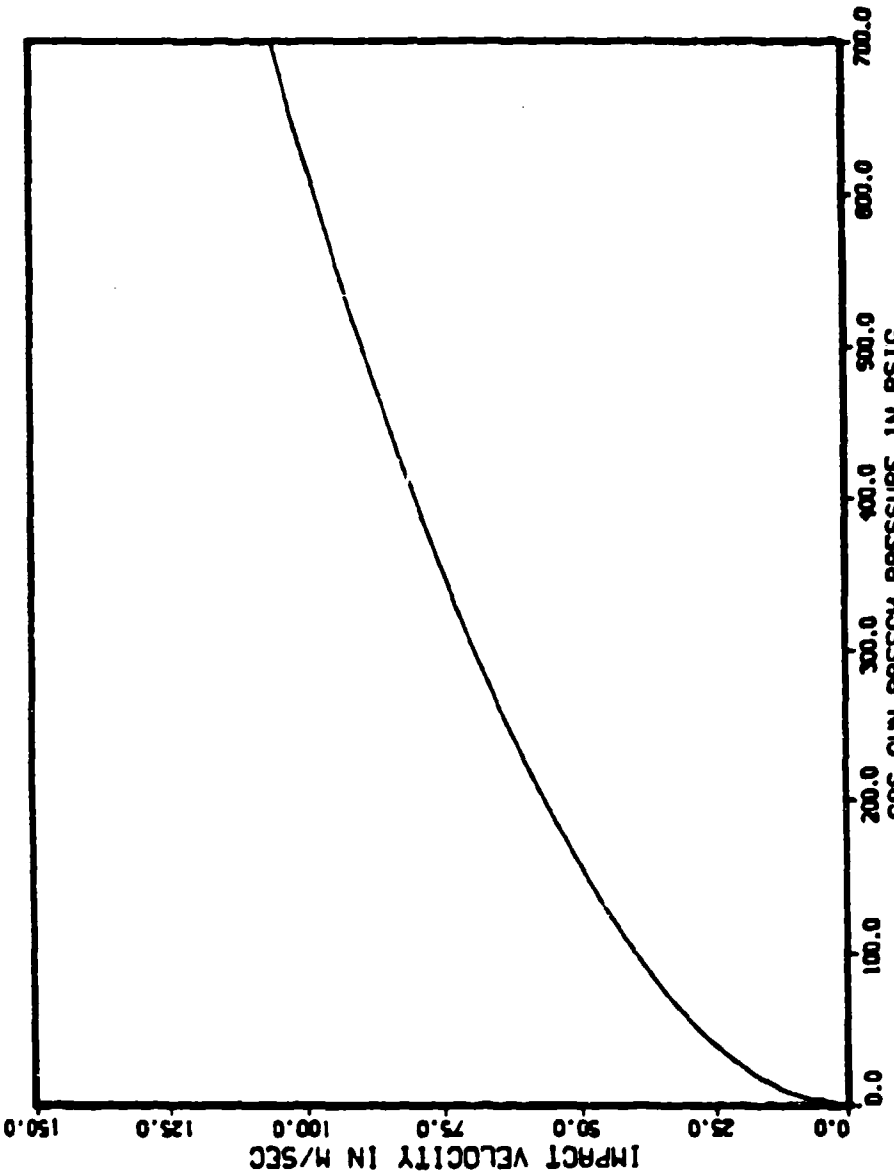

Figure B.2. Gas gun calibration curve.

velocity measuring system detached from the launch tube is shown in figure B.3.

The lasers with the focusing lenses and photodetectors are mounted in sets across from each other. Each set is separated a distance of 1.27 cm from the other. As the striker bar passes the first set, a multichannel clock is started. Each successive set stops a channel of the clock; hence, recording the time for the striker bar to travel across each of the two 1.27 cm intervals. By measuring the travel time across a given distance, the striker bar velocity for each interval is computed. The striker bar velocity for the experiment is then obtained by averaging the striker bar velocity of the two intervals.

In addition to measuring the striker bar velocity, the velocity measuring system is also used to locate within an 8 millisecond window the recording of the strain gauge data by the digitizers. This is accomplished by initiating a time delay as the striker bar passes the last set of lasers and photodetectors. The time delay is set according to the desired striker bar impact velocity. As the digitizers are continuously running, the time delay establishes a termination point for data collection, such that only the strain gauge data of interest are captured within the 8 millisecond window.

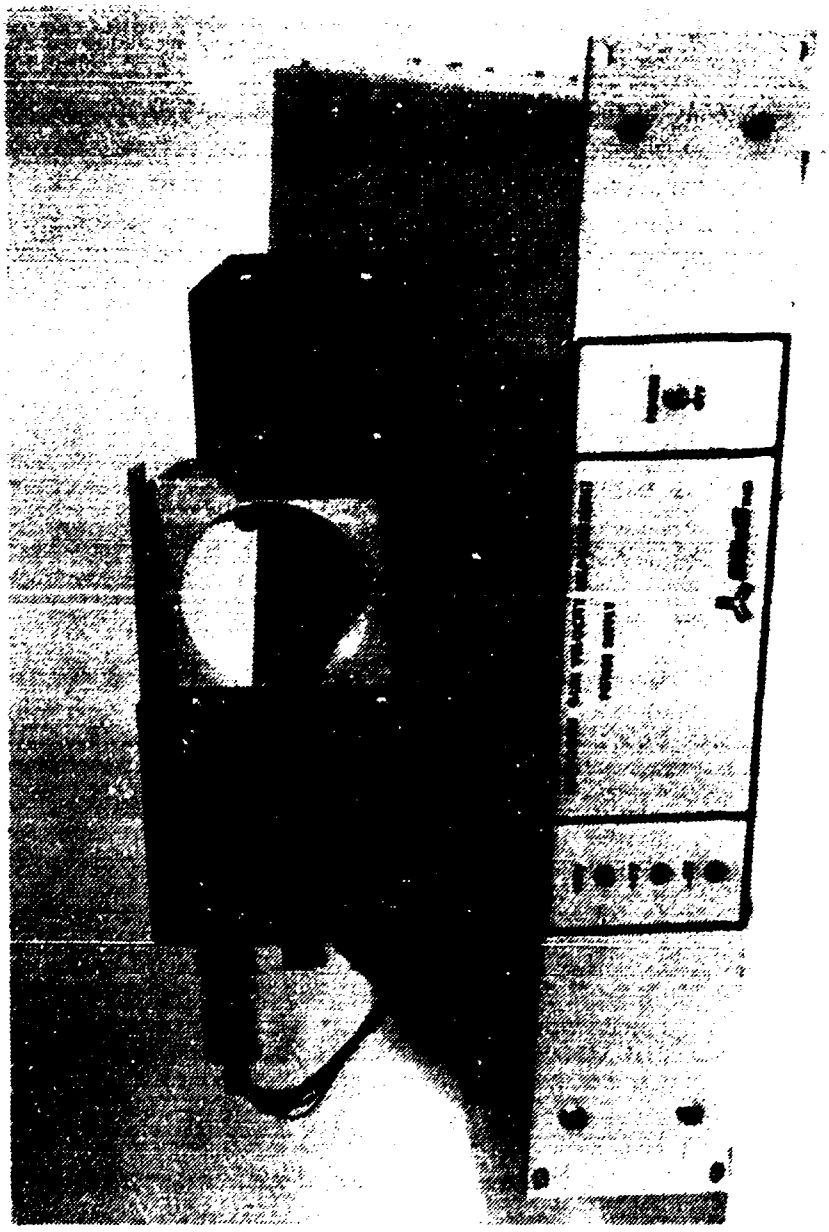

Figure B.3. Laser velocity measuring system.

B.4 Electro-Hydraulic Control and Monitor Unit

The primary circuits of the electro-hydraulic control and monitor unit are shown in figure B.4. The symbols J1 through J15 refer to ports on the rear of the electro-hydraulic control unit. Front and rear views of the electro-hydraulic control unit are shown in figures B.5 and B.6, respectively. A brief description of each major component will be presented.

B.4.1 Carrier Oscillator (A1)

This system component provides the carrier signal for the transducer bridges and the demodulation in the transducer preamplifiers (Nagy and Muelenhaupt, 1983). Also incorporated is an adjustable field-effect transistor amplitude control circuit that limits the variations in carrier level to approximately 0.01 percent (Nagy and Muelenhaupt, 1983).

B.4.2 Transducer Preamplifiers (A2,A3)

There are two carrier preamplifiers, one for axial load (A2), and one for firing pressure (A3). Each one amplifies the signal from its respective transducer and demodulates it to produce two analog signals (Nagy and Muelenhaupt, 1983). Each amplifier operates with a carrier-driven Wheatstone bridge circuit.

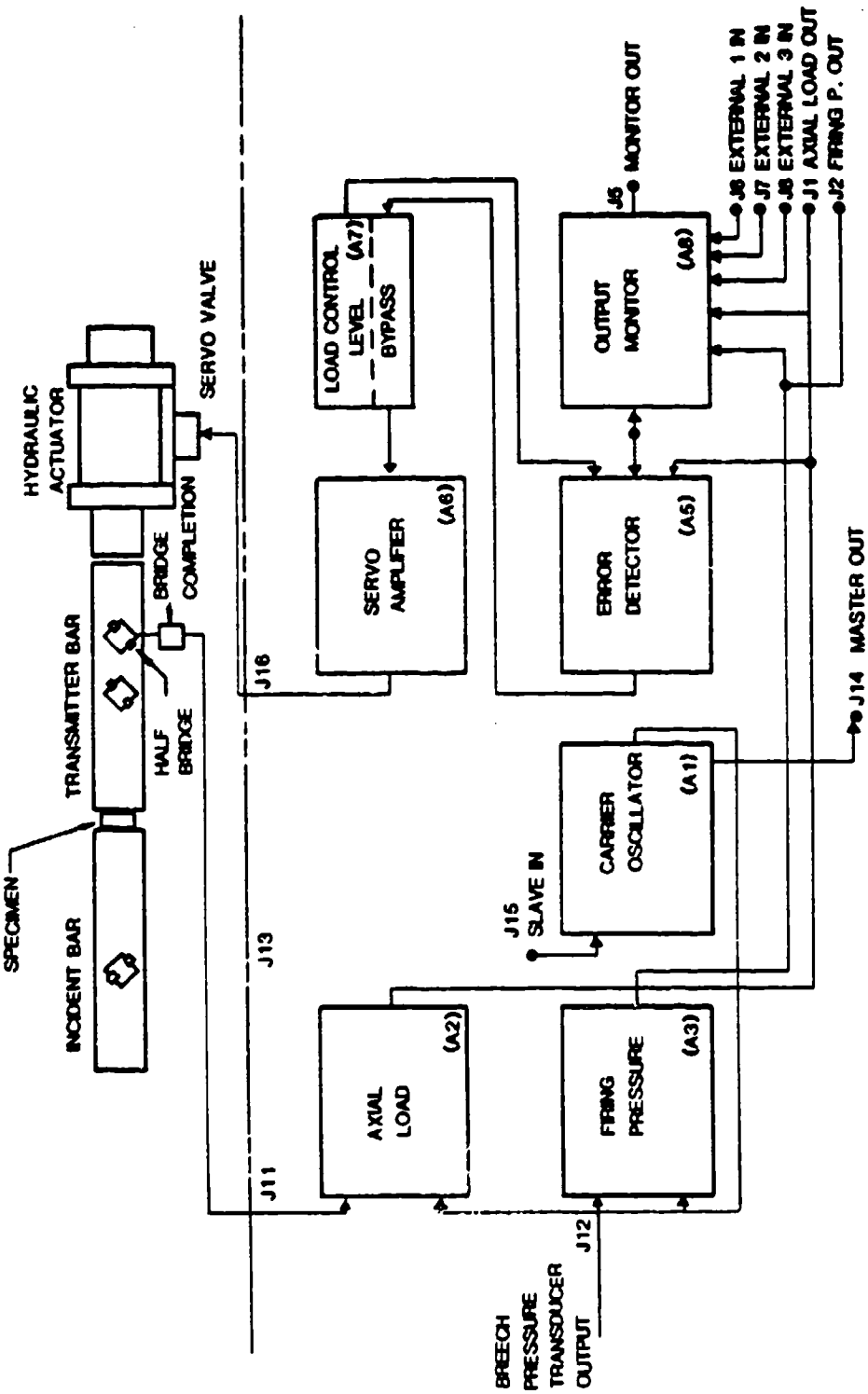

Figure B.4. Electro-hydraulic control block diagram and monitor unit circuits (Nagy and Muelenhaupt, 1983).

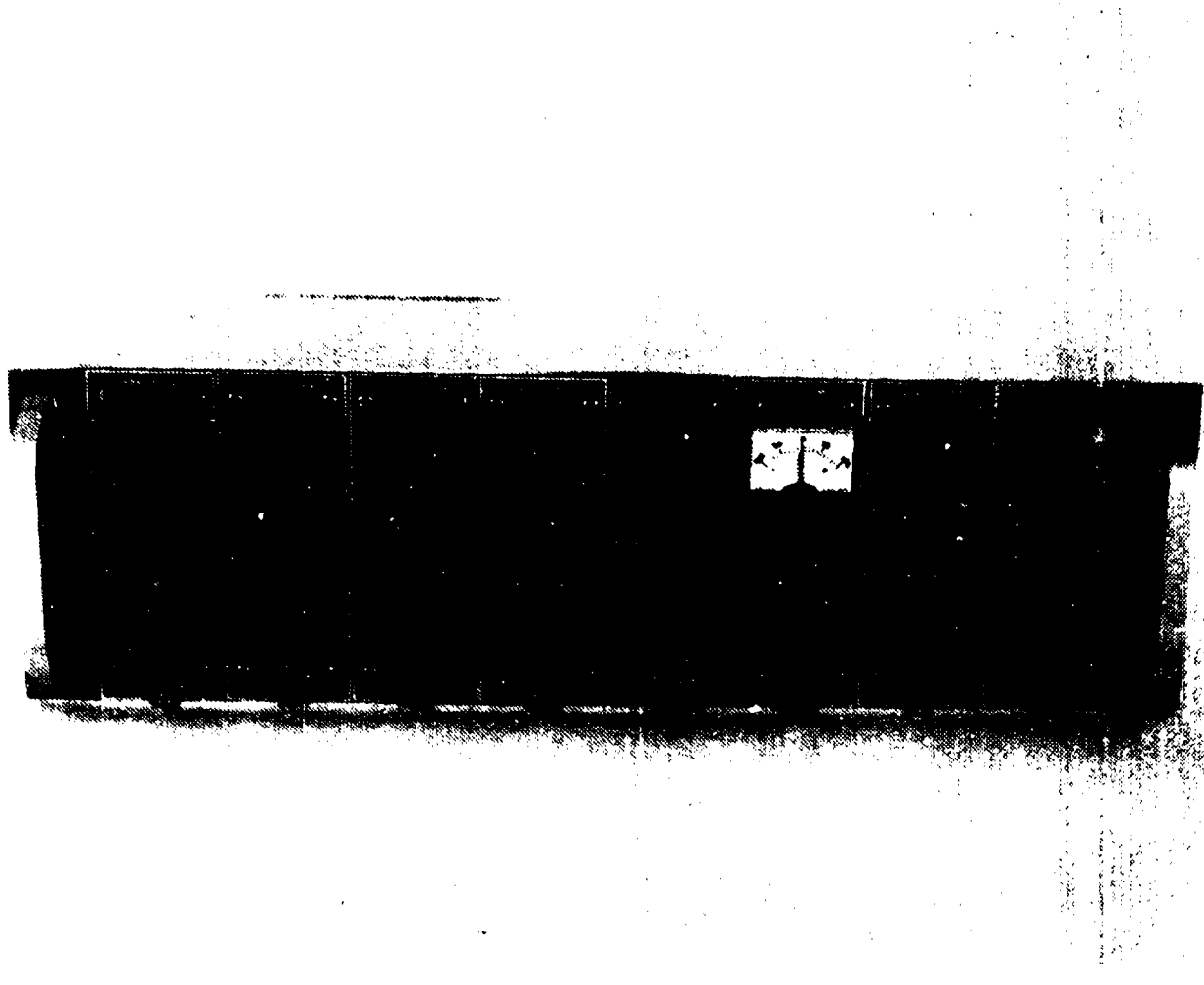

Figure B.5. Front view of electro-hydraulic control and monitor unit.

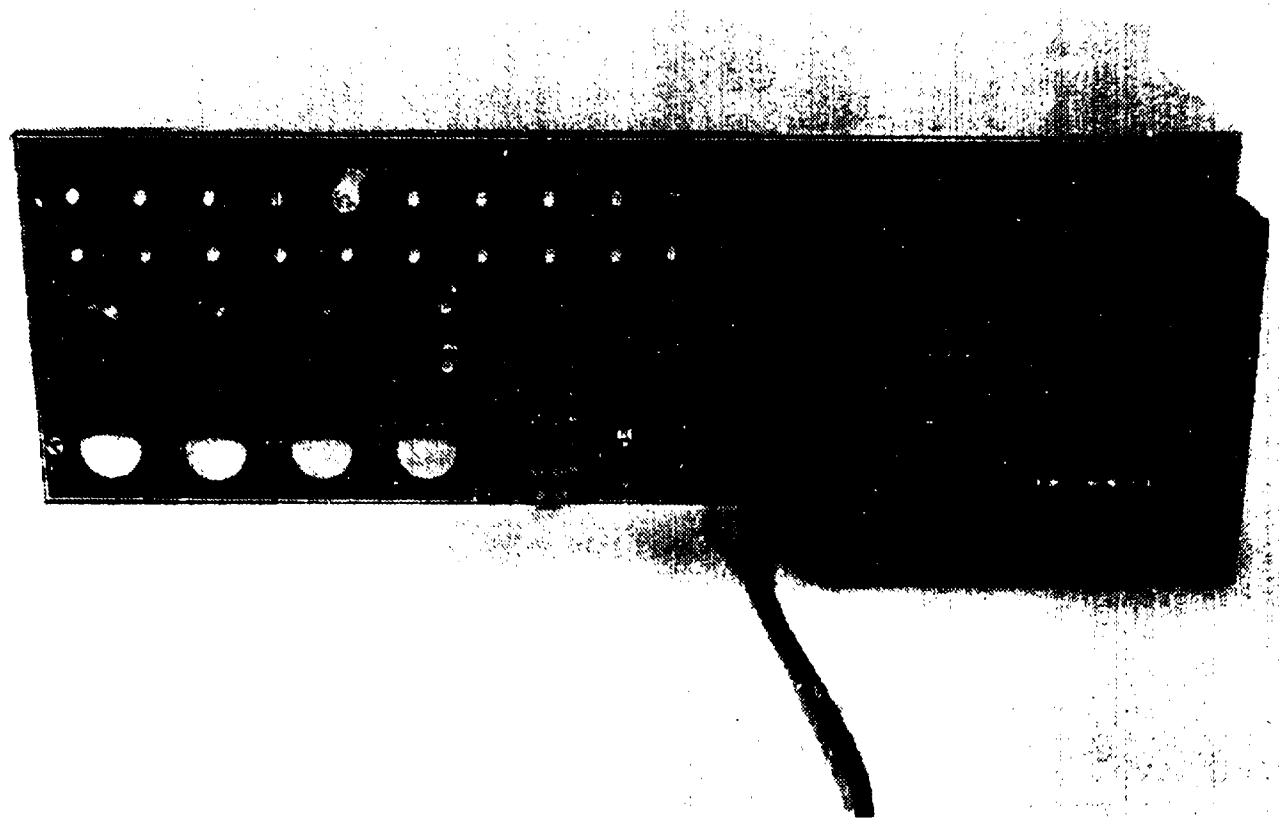

Figure B.6. Rear view of electro-hydraulic control and monitor unit.

B.4.3 Error Detector (A5)

The error detector is an integral part of the hydraulic actuator control system. The error detector continuously compares the feedback signal from the load control amplifier with the command signal and produces an appropriate error signal to be used by the servo-amplifier to drive the servo-valve (Nagy and Muelenhaupt, 1983).

B.4.4 Servo-Amplifier (A6)

The servo-amplifier controls the current to the servo-valve. The signal from the load control (A7) is summed with the error control signal and converted to a current by the servo-amplifier to drive the servo-valve.

B.4.5 Load Control (A7)

This is a manual control to adjust axial load magnitude. It is recommended that some compressive force be applied to the system with the hydraulic actuator to guarantee contact between the specimen and the pressure bars. To avoid damaging the specimen after completing the experiment, a bypass circuit has been installed to maintain control over the actuator at all times (Nagy and Muelenhaupt, 1983). The function of the bypass circuit is to prevent the actuator from applying any compressive force to the specimen after the experiment is completed.

B.4.6 Output Monitor (A8)

A multistation pushbutton switch allows monitoring of the data output from A2, A3, and A7 (Nagy and Muelenhaupt, 1983).

B.5 Dynamic Signal Conditioning System

The dynamic signal conditioning system consists of four major components:

(1) the mainframe,

(2) eight signal conditioning amplifiers,

(3) supply voltage regulation, and

(4) calibration.

B.5.1 Mainframe

The mainframe consists of a Vector Model CMA3B.20 case which houses eight modular amplifiers. Power is supplied by a LND-Y-152 Lambda Power Supply that provides the system with + 15 volts regulated power (Nagy and Muelenhaupt, 1983).

B.5.2 Signal Conditioning Amplifiers

A circuit diagram of the modular signal conditioning amplifiers is presented in figure B.7. The amplifiers are

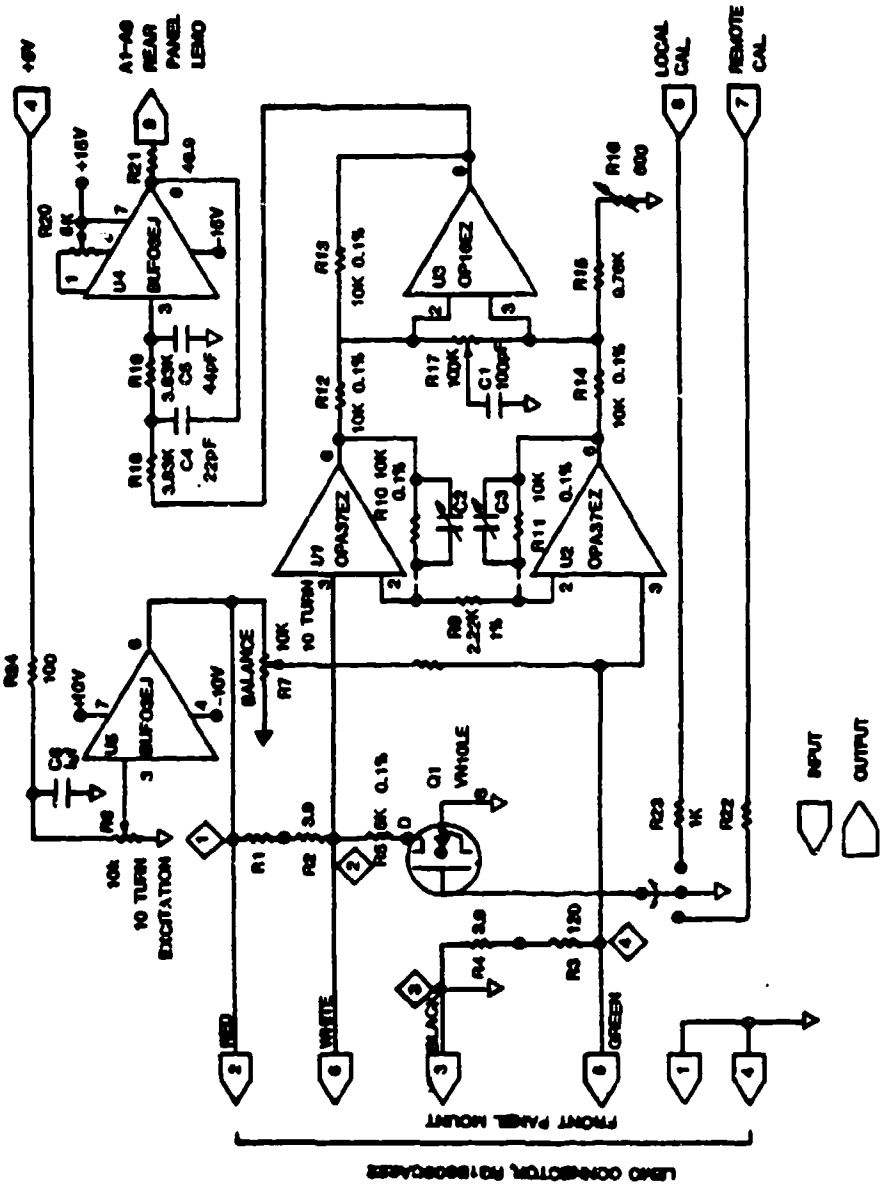

Figure B.7. Signal conditioning amplifier (Nagy and Muelenhaupt, 1983).

operated in half bridge configuration. Figure B.8 shows the wiring for the half bridge operation. The bandwidth of the amplifiers is 1 MHz, to prevent aliasing of the digital records.

B.5.3 Voltage Regulation

As the voltage output of the mainframe is + 15 volts and the requirement of the system is 10 volts, voltage regulation is necessary to assure proper system performance (Nagy and Muelenhaupt, 1983).

B.5.4 Calibration Control

The system is designed so that it is capable of switching to a calibration signal which can verify the overall gain of the data acquisition system (Nagy and Muelenhaupt, 1983).

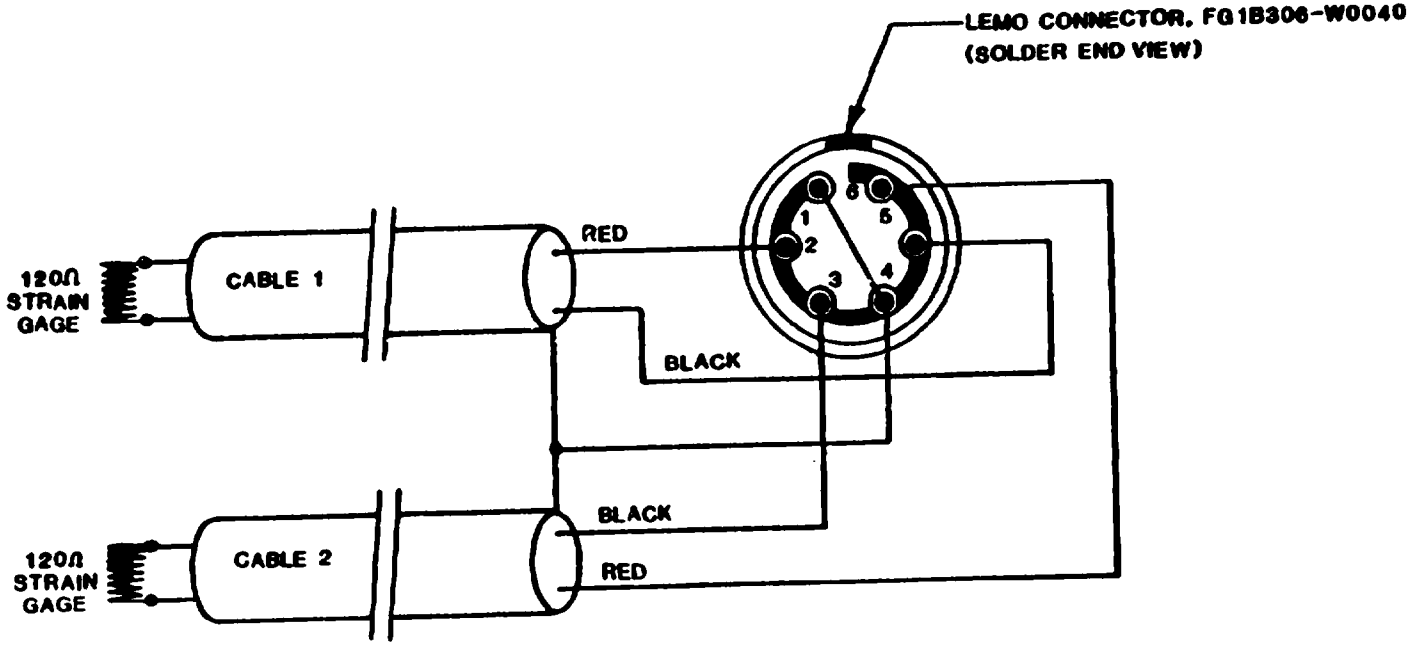

Figure B.8. Wiring diagram for signal conditioner input connector, half bridge operation (Nagy and Muelenhaupt, 1983).

APPENDIX C

DERIVATION OF THE RELATIONSHIP BETWEEN THE STRIKER BAR IMPACT VELOCITY AND THE MAGNITUDE OF THE APPLIED STRESS WAVE

The relationship between the striker bar impact velocity and the magnitude of the applied stress wave is accomplished through momentum considerations derived through Newton's second law of motion;

$$F = m\,a\ , \tag{C.1}$$

where F is force, m is mass, and a is acceleration. Equation (C.1) can be rewritten by making the following substitutions;

$$F = \sigma\,A\ , \tag{C.2}$$

$$a = \frac{dV}{dt}\ , \tag{C.3}$$

where σ is stress, A is the cross sectional area of the striker bar, V is velocity, and t is time, as;

$$A\int_0^t \sigma dt = m\int_0^V dV\ . \tag{C.4}$$

The limit of integration t, on the left side of equation (C.4) is the duration of impact between the striker bar and the incident bar. When the striker bar impacts the incident bar, a compressive wave is generated in the incident bar and striker bar as well. The compressive wave in the incident bar propagates toward the sample. The compressive wave in the striker bar propagates in the opposite direction, toward the free end of the striker bar. Upon reaching the free end, the compressive wave is

reflected as a tensile wave which returns to the impact interface. As the interface is unable to sustain tension, unloading occurs, terminating the applied stress wave. Hence, the duration of impact is the time required for a wave to traverse the length of the striker bar twice, and can be expressed as;

$$t = \frac{2\ L}{C_o} \quad , \tag{C.5}$$

where L is the length of the striker bar, and C_o is the bar velocity of the striker bar. As mentioned previously, a 0.254 m long striker bar was used in this research, hence the duration of the applied stress wave is approximately 100 microseconds. The limit of integration V, on the right side of equation (C.4) is the striker bar impact velocity. Carrying out the integration of equation (C.4) yields;

$$\frac{\sigma A\ 2\ L}{C_o} = m\ V \quad . \tag{C.6}$$

Substituting $\rho\ A\ L = m$ reduces equation (C.6) to;

$$\sigma = \frac{\rho\ C_o\ V}{2} \ . \tag{C.7}$$

The magnitude of the applied stress is therefore determined by the velocity at which the striker bar impacts the incident bar.

APPENDIX D

EXPERIMENTAL PROCEDURE CHECKLIST
(adapted from Brown, 1983)

1) Select breech pressure to produce the required striker bar impact velocity.

2) Lubricate specimen-bar interfaces with a thin film of silicon grease.

3) Measure specimen length.

4) Position specimen between pressure bars.

5) Verify that the momentum trap is attached.

6) Move momentum trap into position with hydraulic actuator.

7) Record specimen seating strain.

8) Check for continuous system contact.

9) Power and set instrumentation.

10) Lock exclusion area.

11) Turn on warning lights.

12) Open nitrogen gas bottle manual valve.

13) Open selected nitrogen gas bottle solenoid valve.

14) Open system isolation valve.

15) Retract striker bar projectile.

    a) Open firing chamber vent.
    b) Move projectile into launch tube past vent holes.
    c) Close breech vent.
    d) Close vacuum valve.
    e) Start vacuum pump.
    f) Open vacuum valve to indicated position and maintain vacuum until the striker bar bumps.
    g) Open vacuum to full open position for 5 to 10 seconds.
    h) Turn off vacuum pump.
    i) Close vacuum valve.
    j) Open breech vent to eliminate vacuum.
    k) Close breech vent.
    l) Close firing chamber vent.

16) Pressurize breech.

    a) Set "set pressure" to 300 psig.
    b) Close set pressure valves and allow pressure to stabilize.

c) Pressurize breech to desired pressure level.
d) Put on ear protection.
e) Set "firing pressure" to 200 psig.
f) Close firing pressure valves and allow pressure to stablilize.

17) Evacuate and secure exclusion area.

18) Verify instrumentation ready.

19) Fire gas gun.

a) Power fire control panel.
b) Set standby switch to "ARM" position.
c) Press "FIRE" switch.
d) Set switch to "STANDBY" position.
e) Turn fire control panel off.

20) Close nitrogen gas bottle solenoid valve.

21) Vent nitrogen gas bottle manifold.

22) Close system isolation valve.

23) Close nitrogen gas bottle manifold vent valve.

24) Enter exclusion area.

25) Close nitrogen bottle manual valve.

26) Open breech vent.

27) "SLOWLY" vent firing chamber pressure.

28) Turn off warning lights.

29) Open exclusion area.

30) Turn off laser velocity system power supply.

31) Remove specimen from between pressure bars.

32) If possible measure final specimen strain.

33) Remove portion of specimen for moisture content determination.

APPENDIX E

SUPPORTING TABLES

Table E.1

Initial Specimen Parameters

Experiment No.	Specimen Length (cm)	Moisture Content (%)	Gas Porosity (%)	Wet Density (g/cc)	Void Ratio	Degree of Saturation (%)
31	1.283	11.9	7.07	2.11	0.42	76.0
32	1.216	11.9	0.00	2.31	0.29	100.0
38	1.230	13.2	19.01	1.81	0.67	52.6
39	1.232	13.2	9.33	2.03	0.49	71.7
40	1.201	13.5	4.00	2.14	0.42	86.4
41	1.235	13.3	7.22	2.07	0.46	77.1
42	1.198	13.4	4.47	2.13	0.42	84.9
55	1.235	12.4	6.45	2.11	0.42	78.3
56	1.207	12.6	6.79	2.10	0.43	77.6
57	1.252	12.7	15.31	1.90	0.58	58.4
58	1.261	13.9	9.76	2.00	0.52	71.4
59	0.584	12.7	6.59	2.10	0.43	78.2
60	0.703	12.8	22.97	1.73	0.74	46.1
61	0.549	13.1	4.18	2.14	0.41	85.6
62	0.552	12.9	9.76	2.02	0.49	70.3
63	0.537	13.3	11.22	1.98	0.53	67.5
70	1.216	12.1	14.29	1.94	0.54	59.4
71	1.228	11.7	11.91	2.00	0.49	63.4
72	0.549	15.4	0.90	2.16	0.42	97.0
73	0.611	12.2	12.40	1.98	0.51	63.5
74	0.552	12.0	7.09	2.10	0.42	76.1
75	0.555	12.3	11.87	1.99	0.51	64.7
76	1.240	11.9	14.16	1.95	0.54	59.4
112	0.644	11.8	7.91	2.09	0.43	73.6
113	0.645	12.1	7.73	2.09	0.43	74.5
114	0.655	12.1	9.21	2.05	0.46	70.7
115	0.645	11.4	10.55	2.04	0.46	66.4
116	0.637	11.2	8.07	2.10	0.41	72.4
117	0.635	10.7	8.50	2.10	0.41	70.5
118	0.645	10.6	10.25	2.07	0.43	65.9
119	0.645	10.4	9.91	2.08	0.42	66.4
131	1.313	12.4	9.57	2.04	0.47	70.2
132	1.269	12.5	6.88	2.10	0.43	77.2
133	1.291	12.4	8.02	2.07	0.45	74.1
134	1.259	12.4	5.80	2.12	0.41	80.2
135	1.307	7.0	23.37	1.84	0.55	34.1
136	1.223	15.1	5.17	2.08	0.48	84.1
137	0.665	15.4	8.51	2.00	0.54	75.8
138	0.596	13.0	4.86	2.13	0.42	83.5
139	0.609	7.0	17.68	1.98	0.44	42.3
14[illegible]	1.265	11.8	6.23	2.13	0.40	78.3

Table E.1 cont.

Experiment No.	Specimen Length (cm)	Moisture Content (%)	Gas Porosity (%)	Wet Density (g/cc)	Void Ratio	Degree of Saturation (%)
146	1.267	11.9	6.26	2.13	0.41	78.3
147	0.636	11.9	6.64	2.12	0.41	77.2
148	0.631	14.4	7.41	2.04	0.50	77.6
162	0.629	13.0	4.44	2.14	0.41	84.7
163	0.631	12.9	4.84	2.13	0.41	83.4
164	1.298	12.9	7.49	2.07	0.45	76.0
165	1.289	12.7	7.05	2.09	0.44	77.0
166	0.624	14.0	4.42	2.12	0.44	85.5
167	0.622	14.0	4.15	2.12	0.43	86.3

Table E.2

Moisture Loss Between the Time a Specimen is Prepared and the Time it is Positioned Between the Bars

Experiment No.	MC1(a) (%)	MC2(b) (%)	Percent Difference (-)
A	13.4	12.3	8.2
B	13.0	12.2	6.2
C	12.9	12.2	5.4
D	13.0	12.7	2.3
E	13.1	12.6	3.8
F	13.2	12.6	4.5
G	13.2	12.4	6.1
H	13.3	12.4	6.8

Arithmetic mean = 5.4
Standard Deviation = 1.8

a) MC1 is the specimen moisture content at the time it was prepared.

b) MC2 is the specimen moisture content at the time it was positioned between the pressure bars.

c) The specimens for these tests were prepared following the procedure that was outlined in section 3.3. The same sequence of steps from specimen preparation to just before firing of the gas gun were followed as if an actual experiment were to be performed.

Table E.3

Experimental Results

Experiment No.	Applied Stress (MPa)	Peak Stress (MPa)	Strain at Peak Stress (%)	Strain-Rate at Peak Stress (s^{-1})
31	135	10	5.3	266
32	555	379	15.0	667
38	551	273	18.8	502
39	307	134	11.0	140
40	392	168	14.0	536
41	463	205	15.8	566
42	253	53	9.2	669
55	457	248	14.3	718
56	374	220	12.8	315
57	385	129	14.0	442
58	301	89	11.3	345
59	489	349	19.2	1070
60	509	371	14.8	781
61	260	168	14.4	537
62	270	247	10.9	150
63(a)	385	***	****	****
70(b)	629	***	****	****
71	631	340	16.2	1019
72	390	164	29.7	904
73	416	285	18.4	606
74	764	333	30.9	2159
75	281	115	18.8	1077
76	260	29	10.2	334
112	425	253	19.8	1327
113	385	247	17.4	1062
114	386	250	19.6	678
115	395	260	18.0	1051
116	243	153	14.2	424
117	268	208	14.5	294
118	244	160	14.1	313
119	246	153	14.1	389
131	387	194	12.7	440
132	375	203	10.7	673
133	368	172	12.5	472
134	399	209	12.2	696
135	385	36	15.6	382
136	397	283	11.2	408
137	249	239	6.3	90
138	251	184	11.8	579
139	249	114	17.2	347
145	269	105	10.1	150
146	523	313	13.3	867
147	237	147	13.0	585

Table E.3 cont.

Experiment No.	Applied Stress (MPa)	Peak Stress (MPa)	Strain at Peak Stress (%)	Strain-Rate at Peak Stress (s^{-1})
148	249	117	15.2	972
162	519	325	20.6	1327
163	522	425	15.3	459
164	507	309	12.4	696
165	254	76	9.3	136
166	261	124	13.3	967
167	260	151	12.6	779

a) In experiment 63 the gain setting for the transmitter bar strain gauge was incorrectly set. This caused the digitizers collecting the strain gauge data to be overdriven. As a result, only two of the required three data sets for data reduction were collected.

b) In experiment 70 a tight fit between all system components was not maintained. As a results, an irregular incident stress wave was initiated that was unsuitable for data reduction.

Table E.4

Specimen Seating Strain

Experiment No.	Preplacement Length (cm)	In-Position Length (cm)	Seating Strain (%)
112	0.673	0.644	4.3
113	0.674	0.645	4.3
114	0.723	0.655	9.4
115	0.677	0.645	4.7
116	0.715	0.637	10.9
117	0.697	0.635	8.9
118	0.694	0.645	7.1
119	0.721	0.645	10.5
131	1.349	1.313	2.7
132	1.338	1.269	5.2
133	1.367	1.291	5.6
134	1.382	1.259	8.9
135	1.337	1.307	2.2
136	1.330	1.223	8.0
137	0.670	0.665	0.7
138	0.688	0.596	13.4
139	0.728	0.609	16.3
145	1.360	1.265	7.0
146	1.316	1.267	3.7
147	0.759	0.636	16.2
162	0.646	0.629	2.6
163	0.684	0.631	7.7
164	1.362	1.298	4.7
165	1.345	1.289	4.2
166	0.687	0.624	9.2
167	0.654	0.622	4.9
A	0.727	0.641	11.8
B	0.711	0.623	12.4
C	0.715	0.631	11.7
D	1.395	1.273	8.7
E	1.364	1.275	6.5
F	1.369	1.273	7.0
G	1.335	1.273	4.6

Arithmetic mean = 7.5
Standard Deviation = 3.9

a) Experiments numbers A through G do not represent complete experiments. These were tests performed to provide additional information on seating strains and moisture loss.

Table E.5

Computed Radial Displacements Due to Applied Load

Experiment No.	Inside Radius of Cylinder (cm)	Displacement (cm)
31	3.017	0.0007
32	3.018	0.0264
38	3.025	0.0191
39	3.030	0.0094
40	3.059	0.0120
41	3.055	0.0147
42	3.018	0.0037
55	3.048	0.0177
56	3.030	0.0154
57	3.058	0.0093
58	3.055	0.0064
59	3.058	0.0251
60	3.028	0.0261
61	3.033	0.0118
62	3.020	0.0172
63	3.045	******
70	3.030	******
71	3.032	0.0240
72	3.063	0.0118
73	3.035	0.0201
74	3.053	0.0238
75	3.038	0.0082
76	3.018	0.0020
112	3.060	0.0182
113	3.056	0.0177
114	3.026	0.0175
115	3.060	0.0187
116	3.060	0.0111
117	3.056	0.0149
118	3.059	0.0115
119	3.040	0.0109
131	3.045	0.0138
132	3.062	0.0146
133	3.060	0.0124
134	3.055	0.0150
135	3.030	0.0025
136	3.020	0.0198
137	3.018	0.0166
138	3.025	0.0129
139	3.025	0.0080
145	3.025	0.0073
146	3.028	0.0220

Table E.5 cont.

Experiment No.	Inside Radius of Cylinder (cm)	Displacement (cm)
147	3.056	0.0105
148	3.035	0.0083
162	3.028	0.0228
163	3.023	0.0297
164	3.025	0.0217
165	3.055	0.0053
166	3.035	0.0087
167	3.028	0.0106

Table E.6

Mass of Soil Lost During the Experiment

Experiment No.	Mass Lost (g)
138	1.7
145	2.1
147	1.9
148	5.3
162	7.9
164	4.8
165	2.1
166	4.8
167	2.3

Table E.7

Measured Moisture Content Changes Before and After the Experiment

Experiment No.	Preexperiment - Moisture Content (%)	Postexperiment Moisture Content (%)	Percent Difference (-)
31	11.9	10.0	16.0
32	11.9	10.8	9.2
38	13.2	12.2	7.6
39	13.2	12.9	2.3
40	13.5	13.1	3.0
41	13.3	10.7	19.5
42	13.4	9.7	27.6
55	12.4	****	****
56	12.6	****	****
57	12.7	****	****
58	13.9	****	****
59	12.7	****	****
60	12.8	****	****
61	13.1	****	****
62	12.9	****	****
63	13.3	****	****
70	12.1	10.3	14.9
71	11.7	9.2	21.4
72	15.4	8.5	44.8
73	12.2	10.5	13.9
74	12.0	11.8	1.7
75	12.3	10.0	18.7
76	11.9	10.3	13.4
112	11.8	10.4	11.9
113	12.1	10.0	17.4
114	12.1	10.1	16.5
115	11.4	10.2	10.5
116	11.2	9.8	12.5
117	10.7	9.9	7.5
118	10.6	9.6	9.4
119	10.4	9.5	8.7
131	12.4	11.4	8.1
132	12.5	11.7	6.4
133	12.5	11.0	12.0
134	12.4	11.4	8.1
135	7.0	6.2	11.4
136	15.1	11.5	23.8
137	15.4	12.1	21.4
138	13.0	12.0	7.7
139	7.0	6.3	10.0
145	11.8	11.3(4.6)	4.2
146	11.9	11.1(6.2)	6.7
147	11.9	10.7(6.4)	10.1

Table E.7 cont.

Experiment No.	Preexperiment Moisture Content (%)	Postexperiment Moisture Content (%)	Percent Difference (-)
148	14.4	12.8(11.4)	11.1
162	13.0	11.7(6.6)	10.0
163	12.9	11.9	7.8
164	12.9	11.9(7.4)	7.8
165	12.7	12.1(11.1)	4.7
166	14.0	12.7(11.5)	9.3
167	14.0	12.7(11.0)	9.3

a) The numbers in parentheses beside the post experiment moisture content percentages are moisture contents (in percent) of the material scraped from the region where the bars and confining cylinder overlap (see figure 3.8).

APPENDIX F

PROCEDURE AND RESULTS OF MOISTURE/DENSITY VARIATION STUDY

The soil used for this study was the same as that used in the SHPB experiments. The specimens were prepared at moisture/density conditions near optimum as determined from the Harvard miniature compaction procedure (see figure 3.5). The specimens for this study were prepared following the same procedures outlined in section 3.3.

The specimens were compacted in stainless steel cylinders with the nominal dimensions of 12 cm in length and 6 cm inside diameter. Static compaction of the specimen was performed from both ends of the cylinder. Four lifts of soil were used to complete the compaction processs. After compaction, the specimen was extruded from the cylinder and sliced into 1 cm sections.

The density variation over the specimen length was determined by immersing a piece of each 1 cm section in a known volume of mercury, and measuring the volume of mercury the specimen displaced. Moisture content was determined according to the standard method (ASTM D-2216-80). The results of the study are presented in figures F.1 through F.6.

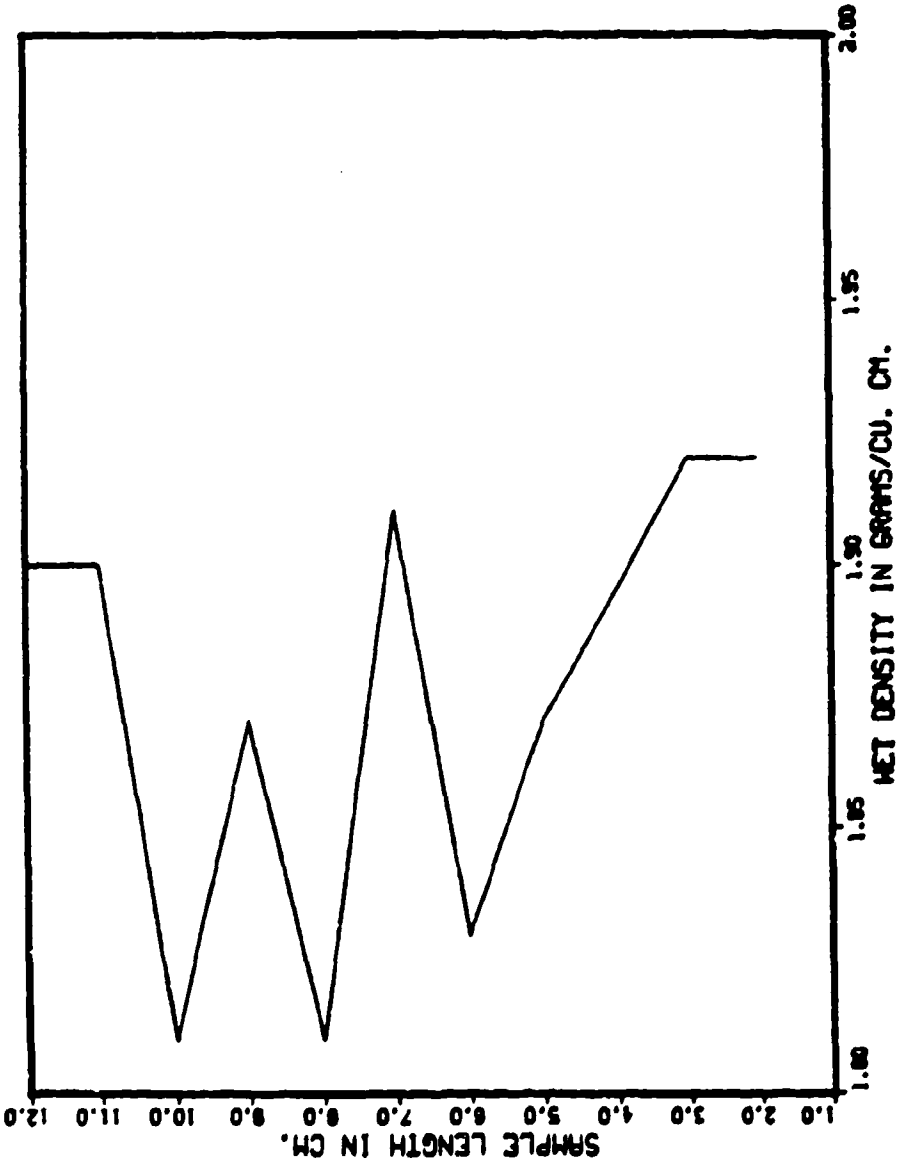

Figure F.1. Density variation for specimen 1.

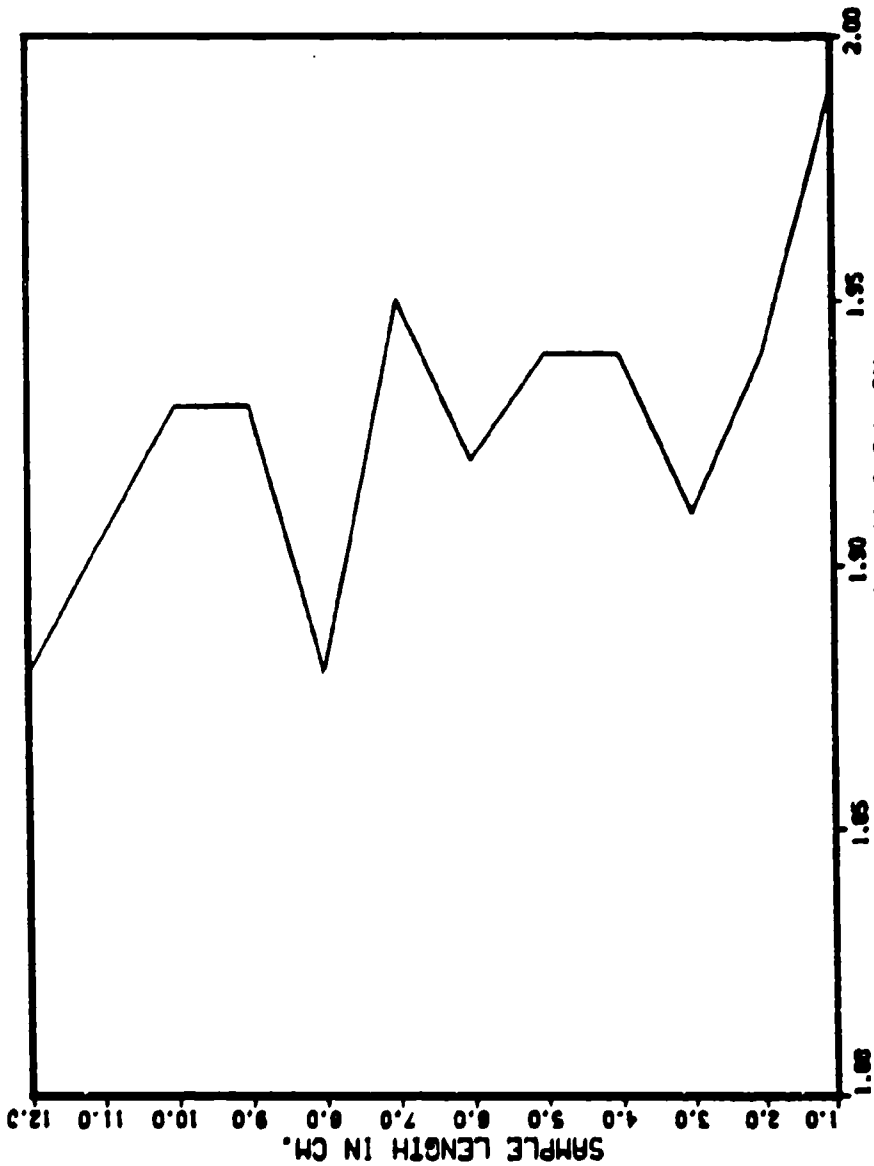

Figure F.2. Density variation for specimen 2.

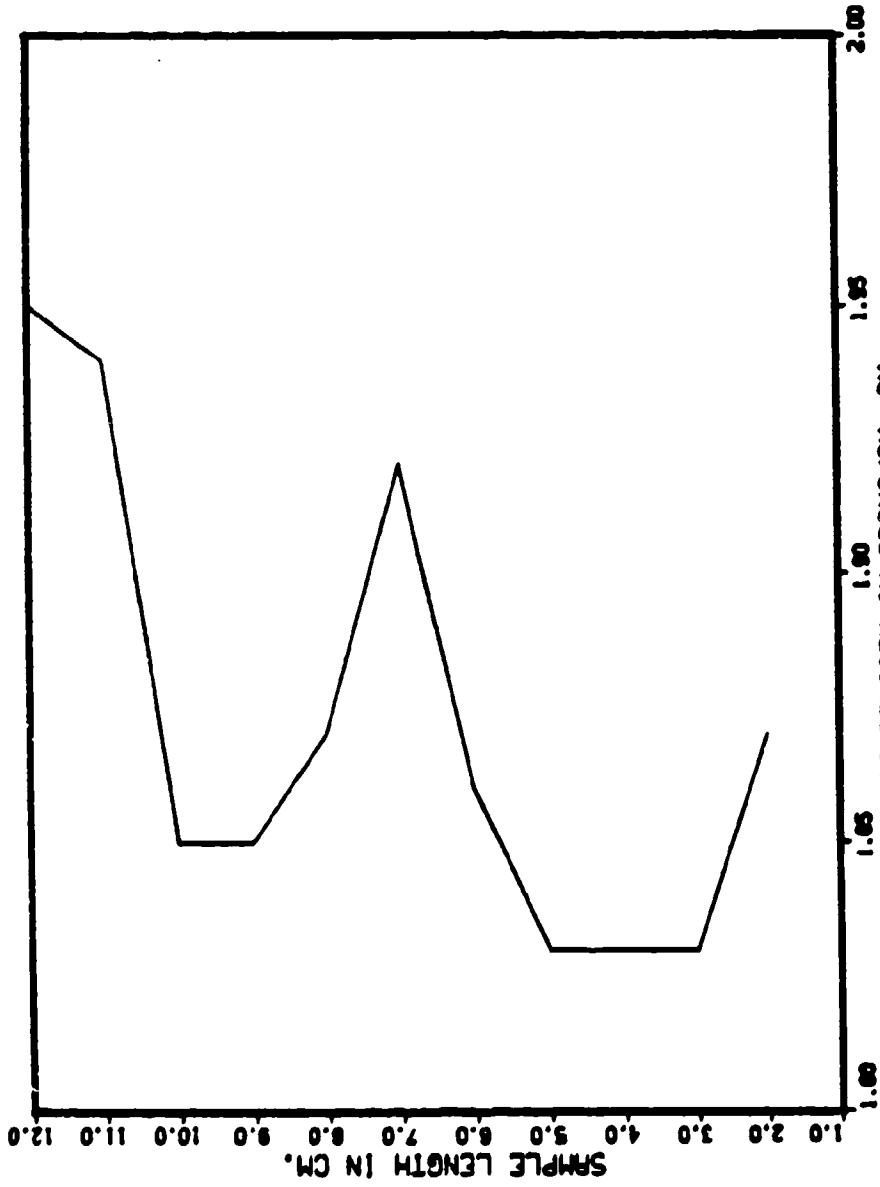

Figure F.3. Density variation for specimen 3.

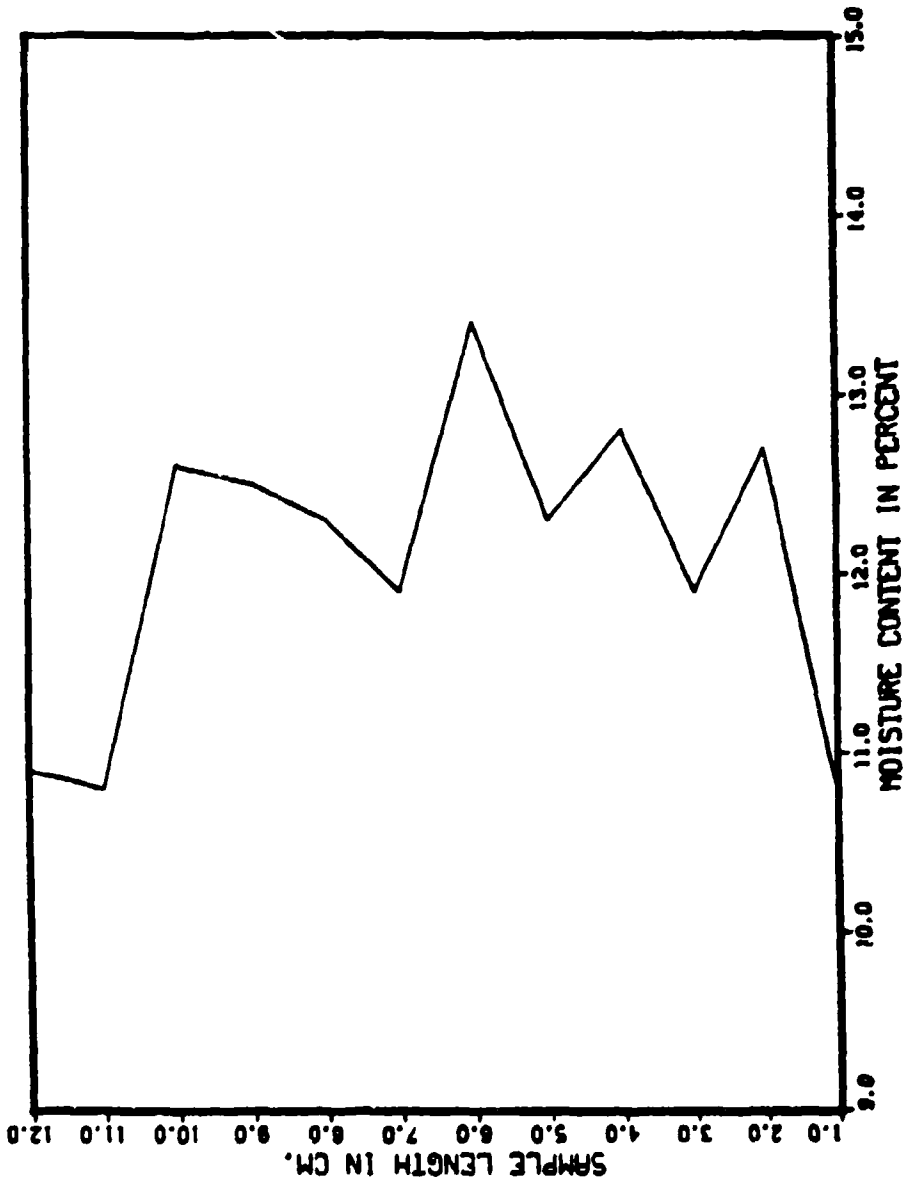

Figure F.4. Moisture variation for specimen 1.

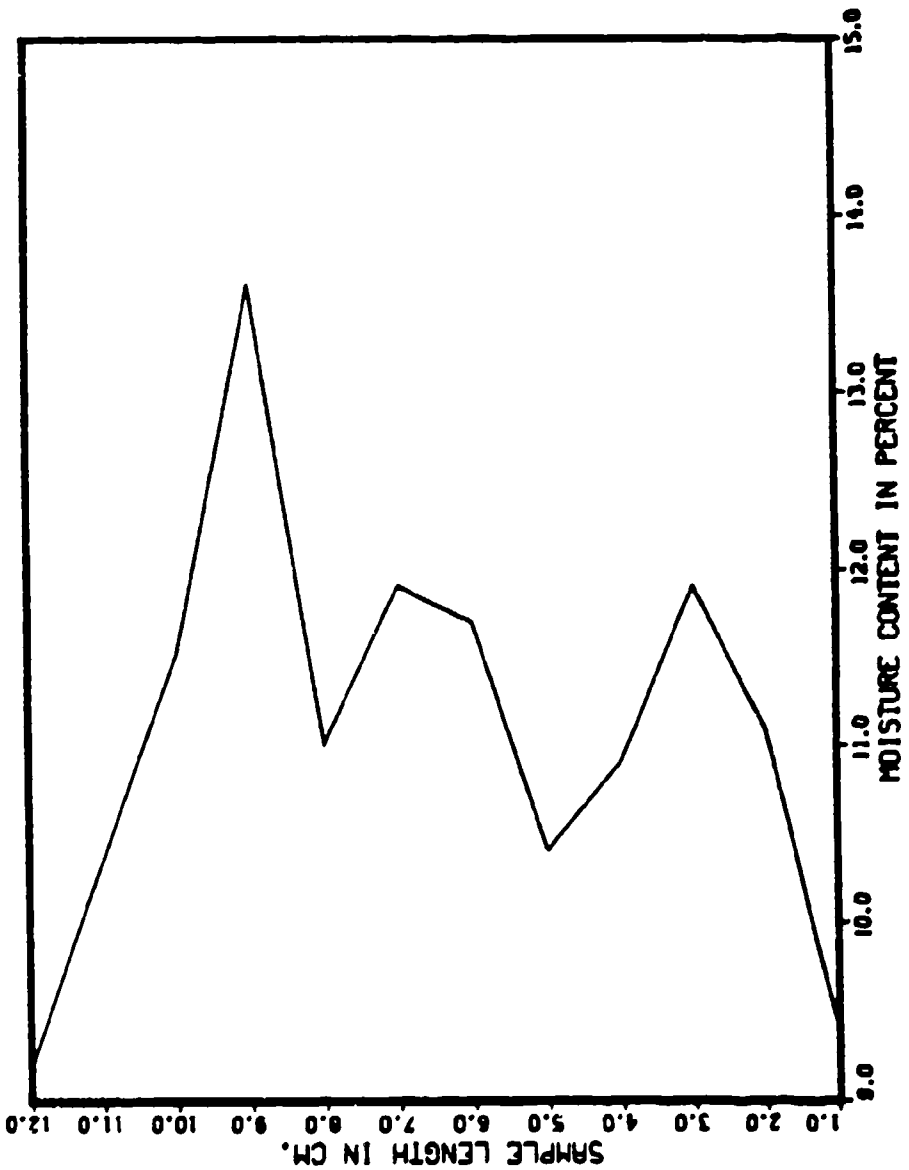

Figure F.5. Moisture variation for specimen 2.

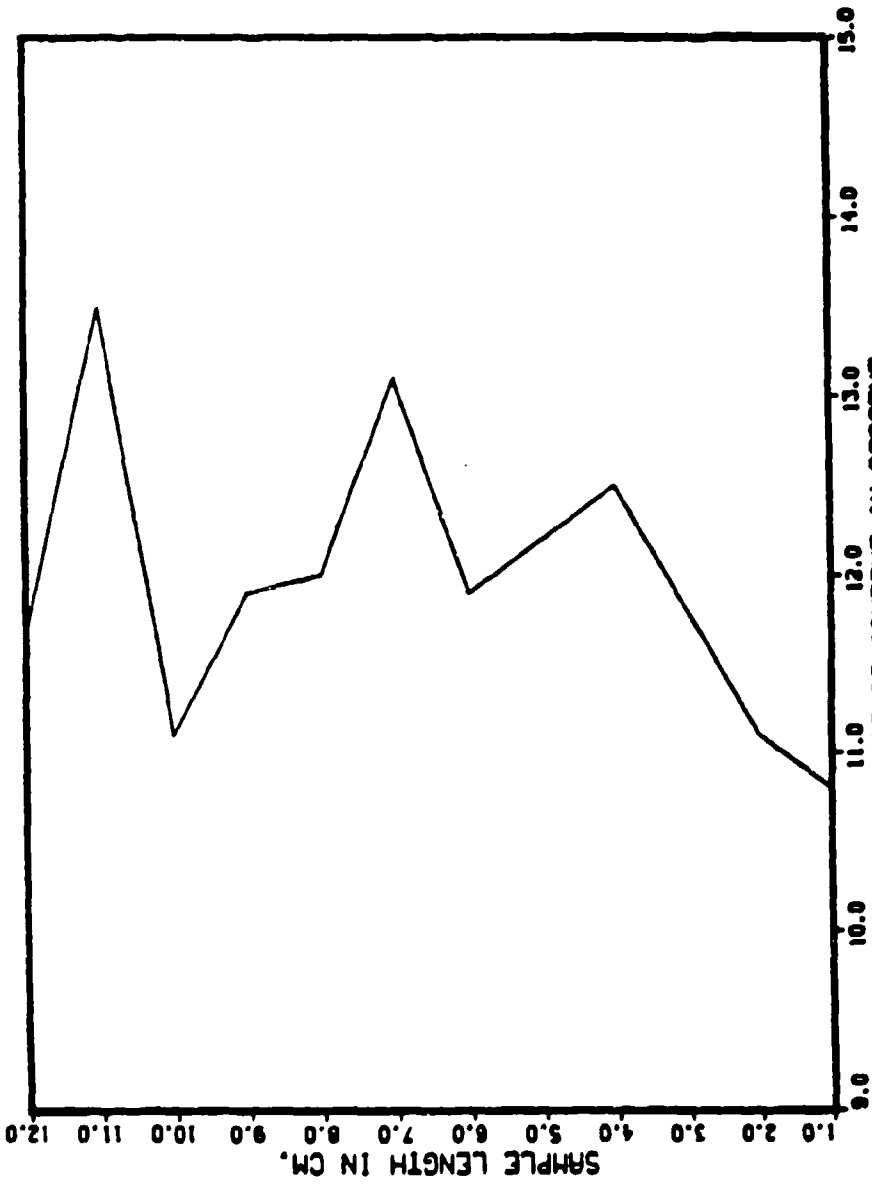

Figure F.6. Moisture variation for specimen 3.

APPENDIX G

REDUCE CODE

G.1 Flowchart for REDUCE

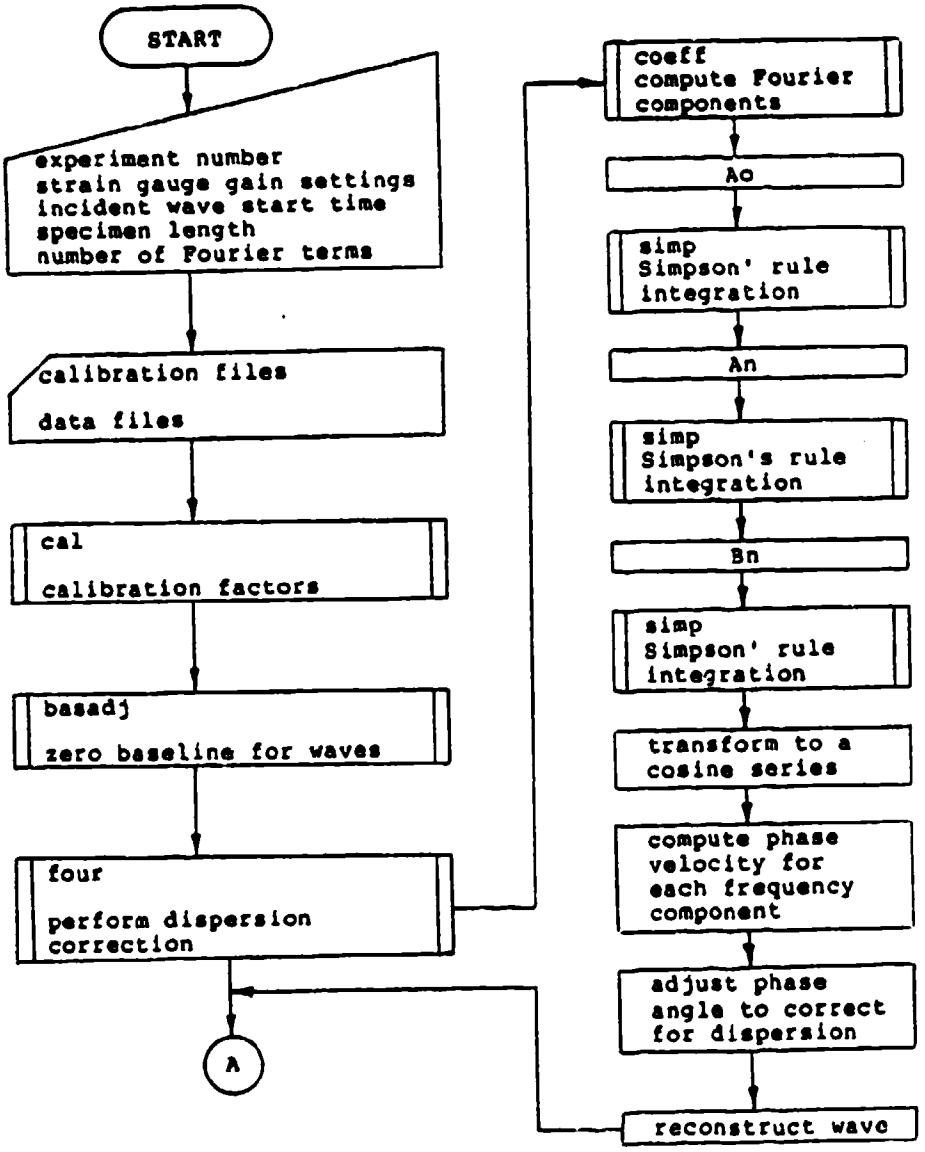

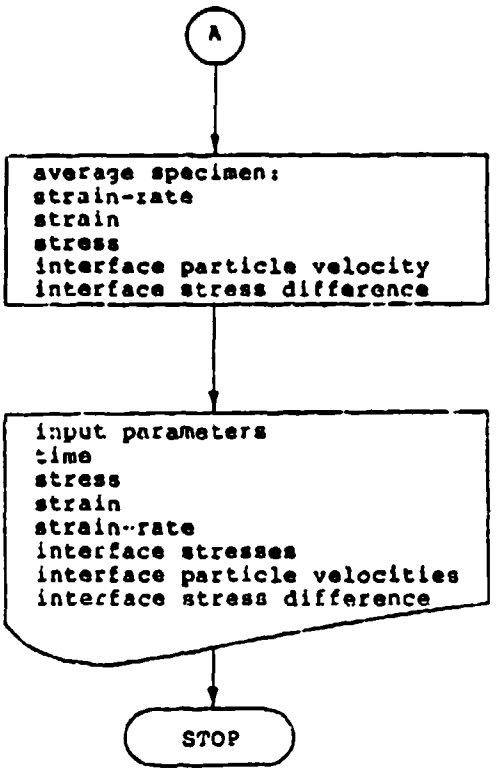
A
average specimen:
strain-rate
strain
stress
interface particle velocity
interface stress difference
input parameters
time
stress
strain
strain-rate
interface stresses
interface particle velocities
interface stress difference
STOP

G.2 Program Listing

```
c*****************************************************************
c*                                                               *
c*                      REDUCE CODE LISTING                      *
c*                                                               *
c*****************************************************************
c
c
c
c     This program is used to process the data obtained
c     from a split-Hopkinson pressure bar experiment. Two
c     sources of input data are required.
c
c       1) The incident and transmitter bar strain gauge
c          records hbxxxi and hbxxxt and the calibration
c          records calxxi and calxxt. These files will be
c          read in from storage.
c       2) The experiment number, gain settings, incident
c          wave start time, initial specimen length, and the
c          number of Fourier terms to be used in the
c          computations. These data are supplied manually by
c          the operator.
c
c     The output of the program is the average specimen
c     strain-rate-time, strain-time, and stress-time
c     histories. In addition, the particle velocities at
c     specimen-bar interfaces and stress difference between
c     the interfaces are computed. These data are formated
c     for output to a printer. The results are also plotted
c     using the DISSPLA 9.0 graphics package. The
c     graphic subroutines and their calls have been removed
c     from this listing.
c
c
c*****************************************************************
c*                                                               *
c*          MAIN PROGRAM PARAMETER IDENTIFICATION                *
c*                                                               *
c*****************************************************************
c
c
c              *********** ARRAYS ***********
c
c     cali - incident bar strain gauge calibration storage
c            file
c     calt - transmitter bar strain gauge calibration
c            storage file
c      hbi - incident bar strain gauge data storage file
c      hbt - transmitter bar strain gauge data storage file
c   barinc - incident and reflected wave stress-time
c            history
```

```
c    trsbar - transmitted wave stress-time history
c      diff - incident stress - (- reflected stress)
c       sum - incident stress + (- reflected stress)
c      xint - average specimen strain-time history
c     xrate - average specimen strain-rate-time history
c    xstres - average specimen stress-time history
c    barref - reflected wave stress-time history
c     velin - particle velocity at specimen-incident bar
c             interface
c    velout - particle velocity at specimen-transmitter bar
c             interface
c    stadel - interface stress difference
c
c            ********** OUTPUT FILES **********
c
c    hopout - output data
c    hopxxi - uncorrected incident wave stress-time history
c    hopxxf - uncorrected reflected wave stress-time history
c    hopxxt - uncorrected transmitted wave stress-time
c             history
c   hopxxif - corrected incident wave stress-time history
c   hopxxrf - corrected reflected wave stress-time history
c   hopxxtf - corrected transmitted wave stress-time history
c    straxx - strain-time history
c    strtxx - strain-rate-time history
c    strsxx - stress-time response
c    sssrxx - stress-strain response
c
c               ********** SYMBOLS **********
c
c     gaini - gain for incident bar strain gauge
c     gaint - gain for transmitter bar strain gauge
c    sttime - incident wave start time in microseconds
c    srtime - reflected wave start time in microseconds
c    tstime - transmitted wave start time in microseconds
c      test - experiment identification
c    expnam - output experiment identification
c    scfaci - incident bar strain gauge scale factor
c    scfact - transmitter bar strain gauge scale factor
c      slen - initial specimen length
c        mm - number of Fourier terms
c    velocb - pressure bar rod velocity
c     densb - density of pressure bar
c       dia - diameter of pressure bar
c     areab - area of pressure bar
c       dzi - distance from strain gauge to
c             specimen-incident bar interface
c       dzr - (-) dzi
c       dzt - distance from strain gauge to
c             specimen-transmitter bar interface
c     tstep - data collection interval
c       ndp - number of data points needed for computations
c        tc - 1/tstep
```

```
c   deltat - 2 times the wave travel time between the
c             strain gauge and specimen-bar interface
c     ibeg - incident wave start time in data
c    ibegr - reflected wave start time in data
c    ibegt - transmitted wave start time in data
c     nlbi - incident wave baseline
c     nlbr - reflected wave baseline
c     nlbt - transmitted wave baseline
c    ibegi - ibeg - nlbi
c   ibegrr - ibegr - nlbr
c   ibegtt - ibegt - nlbt
c     iend - incident wave stop time in data
c    iendr - reflected wave stop time in data
c    iendt - transmitted wave stop time in data
c      tip - duration of incident wave
c      trp - duration of reflected wave
c      ttp - duration of transmitted wave
c       ni - period of incident wave for dispersion
c            correction
c       nr - period of reflected wave for dispersion
c            correction
c       nt - period of transmitted wave for dispersion
c            correction
c    const - integration constant
c
c          ********** SUBROUTINES **********
c
c      cal - computes scale factors
c   basadj - zeros wave baseline
c     four - performs dispersion correction
c
c*****************************************************************
c*                          MAIN PROGRAM                         *
c*****************************************************************
c
      program xx(tty,input=tty,output=tty,cali,calt,
     1hbi,hbt,tape11=cali,tape12=calt,tape13=hbi,
     1tape14=hbt,tape99)
c
      dimension calt(4000),cali(4000),barinc(25000),
     1trsbar(25000),diff(2500),sum(2500),xint(2500),
     1xrate(2500),xstres(2500),barref(25000),velin(2500),
     1velout(2500),stsdel(2500)
c
 1003 format(a)
 1006 format(f12.4,1h,f12.6)
 1007 format('1 **** hopkinson bar data reduction code
     1output ****')
 1009 format(12(1x,f9.4))
 1010 format('1 **** processed hopkinson bar data ****')
 1011 format(f10.1,8x,f5.1,3x,f4.1,3x,f6.1,4x,f5.1,
     13x,f4.1,3x,f5.1,2x,f4.1,2x,f5.1)
      character*20   hopxxi,   hopxxr,    hopxxt,    hopxxif,
```

```
     1hopxxrf, hopxxtf,straxx, strtxx, strsxx, sssrxx,
      lexpnam, hopout
       character*4 test
c
c*****************************************************************
c       ********** operator supplied input **********
c
       print*,'input experiment identification number'
       read 1003,test
       print*
       print*,'gain for the incident and transmitter bar
      1strain gauges'
       read*,gaini,gaint
       print*
       print*,'initial start time for incident pulse
      1(microseconds)'
       read*,sttime
       print*
       print*,'initial specimen length (m)'
       read*,slen
       print*
       print*,'input the number of terms to be used in'
       print*,'the Fourier analysis'
       read*,mm
c
c*****************************************************************
c       ******* set file names names for storage *******
c
       hopxxi='hp'//test//'i'
       hopxxr='hp'//test//'r'
       hopxxt='hp'//test//'t'
       hopxxif='hp'//test//'if'
       hopxxrf='hp'//test//'rf'
       hopxxtf='hp'//test//'tf'
       straxx='str'//test//'time'
       strtxx='rat'//test//'time'
       strsxx='sts'//test//'time'
       sssrxx='prs'//test//'strain'
       expnam='hb'//test//'x'
       hopout='hp'//test//'out'
c
c*****************************************************************
c       ********** set parameter values **********
c
       velocb=4886.
       densb=8090.
       dia=0.06033
       areab=(3.14159*(dia**2))/4.0
       dzi=0.6033
       dzr=-dzi
       dzt=dzr
       tstep=0.5
       ndp=15000
```

```
      tip=240
      trp=tip
      ttp=tip
      deltat=2.*dzi/velocb
      srtime=sttime+deltat*1e+6
      tstime=srtime
      tc=1/tstep
c
c*****************************************************************
c  ******* read in the calibration and data files *******
c
      read(11,*)(cali(i),i=1,4000)
      read(12,*)(calt(i),i=1,4000)
      read(13,*)(barinc(i),i=1,ndp)
      read(14,*)(trsbar(i),i=1,ndp)
c
c*****************************************************************
c *** calculate the scale factor from calibration data ***
c
      call cal(cali,gaini,scfaci,4000)
      call cal(calt,gaint,scfact,4000)
c
c*****************************************************************
c   **** compute starting time of waves in the data ****
c
      ibeg=tc*sttime+1
      ibegr=tc*srtime+1
      ibegt=tc*tstime+1
c
c*****************************************************************
c   ***** compute stop times of waves in the data*****
c
      iend=tc*(sttime+tip)+1
      iendr=tc*(srtime+trp)+1
      iendt=tc*(tstime+ttp)+1
c
c*****************************************************************
c     ******* length of baseline for each wave *******
c
      nlbi=50
      nlbr=20
      nlbt=50
c
c*****************************************************************
c      ******** compute baseline start-times ********
c
      ibegi=ibeg-nlbi
      ibegrr=ibegr-nlbr
      ibegtt=ibegt-nlbt
c
c*****************************************************************
c         ******* zero wave baseline ********
c
```

```
      call basadj(barinc,scfaci,ibegi,iendr,nlbi,base)
      call basadj(trsbar,scfact,ibegtt,iendt,nlbt,base)
c
c*****************************************************************
c ** creating a separate array to store reflected pulse **
c
      do 25 i=iend,iendr
       barref(i)=barinc(i)
   25 continue
c
c*****************************************************************
c            ******* store raw data *******
c
      xi=(ibeg-1)*tstep
      xr=(ibegrr-1)*tstep
      xt=(ibegtt-1)*tstep
c
      open(unit=15,file=hopxxi)
      open(unit=16,file=hopxxr)
      open(unit=17,file=hopxxt)
c
      do 30 i=ibegi,iend
       write(15,1006)xi,barinc(i)/1e+6
       xi=xi+tstep
   30 continue
c
      do 35 i=ibegrr,iendr
       write(16,1006)xr,barref(i)/1e+6
       xr=xr+tstep
   35 continue
c
      do 40 i=ibegtt,iendt
       write(17,1006)xt,trsbar(i)/1e+6
       xt=xt+tstep
   40 continue
c
      close(15)
      close(16)
      close(17)
c
c*****************************************************************
c * perform dispersion correction on each wave separatly *
c
      nr=(iendr-iend+50)*2
      call four(barref,tstep,dia,velocb,nr,dzr,iend,mm)
c
      ni=(iend-ibegi)*2
      call four(barinc,tstep,dia,velocb,ni,dzi,ibegi,mm)
c
      nt=(iendt-ibegtt)*2
      call four(trsbar,tstep,dia,velocb,nt,dzt,ibegtt,mm)
c
c*****************************************************************
```

```
c       ******* store dispersion correction data *******
c
  42   xi=(ibegi-1)*tstep
       xr=(ibegrr-1)*tstep
       xt=(ibegtt-1)*tstep
c
       open(unit=18,file=hopxxif)
       open(unit=19,file=hopxxrf)
       open(unit=20,file=hopxxtf)
c
       do 45 i=ibegi,iend
        write(18,1006)xi,barinc(i)/le+6
        xi=xi+tstep
   45  continue
c
       do 47 i=ibegrr,iendr
        write(19,1006)xr,barref(i)/le+6
        xr=xr+tstep
   47  continue
c
       do 48 i=ibegtt,iendt
        write(20,1006)xt,trsbar(i)/le+6
        xt=xt+tstep
   48  continue
c
       close(18)
       close(19)
       close(20)
c
c*****************************************************************
c     *****  compute the following: *****
c              1) strain,
c              2) strain-rate,
c              3) stress,
c              4) particle velocity,
c              5) interface stress difference
c
       j=ibegr
       ib=1
       do 50 i=ibeg,iend
        diff(ib)=barinc(i)-barref(j)
        sum(ib)=barinc(i)+barref(j)
        j=j+1
        ib=ib+1
   50  continue
c
       const=1/(slen*densb*velocb)
c
       ipoint=iend-ibeg
       xint(1)=0.0
       xrate(1)=0.0
       tstepi=tstep*1.0e-6
       ic=2
```

```
      j=ibegt+1
      do 100 i=ic,ipoint
       n=i-1
       k=j-1
       xrate(i)=(diff(n)-trsbar(k))*const
       xint(i)=xint(n)+(tstepi*0.5*(xrate(i)+xrate(n)))
       j=j+1
  100 continue
c
      j=ibegt
      do 120 i=1,ipoint
       xstres(i)=(sum(i)+trsbar(j))/2.0
       j=j+1
  120 continue
c
      do 127 i=1,ipoint
         n=i-1
         velin(i)=((diff(i))/(densb*velocb))
         velout(i)=((trsbar(ibegt+n))/(densb*velocb))
  127 continue
c
      do 128 i=1,ipoint
       n=i-1
       stsdel(i)=(sum(i)-trsbar(ibegt+n))/1e+6
  128 continue
c
c*****************************************************************
c        ******* write output files *******
c
      open(unit=21,file=straxx)
      open(unit=22,file=strtxx)
      open(unit=23,file=strsxx)
      open(unit=24,file=sssrxx)
      t=0.0
      do 130 i=1,ipoint
       xstres(i)=xstres(i)/1e+6
       xint(i)=xint(i)*100.
       write(21,1006)t,xint(i)
       write(22,1006)t,xrate(i)
       write(23,1006)t,xstres(i)
       write(24,1006)xint(i),xstres(i)
       t=t+tstep
  130 continue
      close(21)
      close(22)
      close(23)
      close(24)
c
c*****************************************************************
c                  ******* output *******
c
      xi=(ibeg-1)*tstep
      xr=(ibegr-1)*tstep
```

```
      xt=(ibegt-1)*tstep
c
      open(unit=27,file=hopout)
      write(27,1007)
      write(27,*)' '
      write(27,*)' '
      write(27,*)' '
      write(27,*)'  *** input parameters ***'
      write(27,*)' '
      write(27,*)' '
      write(27,*)'experimental identification number
     1--------  ',expnam
      write(27,*)' '
      write(27,*)'gain for incident bar strain gauge
     1--------  ',gaini
      write(27,*)' '
      write(27,*)'gaint for transmitter bar strain gauge
     1----  ',gaint
      write(27,*)' '
      write(27,*)'incident wave starttime (microseconds)
     1----  ',xi
      write(27,*)' '
      write(27,*)'reflected wave starttime (microseconds)
     1---  ',xr
      write(27,*)' '
      write(27,*)'transmitted wave starttime (microseconds)
     1-  ',xt
      write(27,*)' '
      write(27,*)'initial specimen length (m)
     1--------------  ',slen
      write(27,*)' '
      write(27,*)'number of terms used in fourier analysis
     1--  ',mm
      write(27,*)' '
      write(27,*)'dispersion bar correction length(m)
     1-------  ',dzi
      write(27,*)' '
      write(27,*)'incident bar calibration factor
     1----------  ',scfaci
      write(27,*)' '
      write(27,*)'transmitter bar calibration factor
     1--------  ',scfact
c
      write(27,1010)
      write(27,*)' '
      write(27,*)' '
      write(27,*)' '
      write(27,*)'      time      stress strain strainrate
     1infl1  vel1  infl2  vel2  stsdif'
      write(27,*)'(microseconds)  (mpa)   (%)     (1/sec)
     1(mpa)  (m/s)   (mpa)  (m/s)  (mpa)'
      write(27,*)' '
c
```

```
      ti=0
      do 137 i=1,ipoint
       n=i-1
       write(27,1011)ti,xstres(i),xint(i),xrate(i),
     lsum(i)/le+6,velin(i),trsbar(ibegt+n)/le+6,
     lvelout(i),stsdel(i)
       ti=ti+tstep
  137 continue
c
      close(27)
c
14    end
c
c**********************************************************************
c**********************************************************************
c*                        END MAIN PROGRAM                            *
c**********************************************************************
c
c
c**********************************************************************
c*                          SUBROUTINES                               *
c**********************************************************************
c
c
c     This subroutine is used to compute scale factors
c     that are used to transform the digitized numbers
c     to stress-time data
c
c
      subroutine cal(blk,gain,sclfac,ndp)
      dimension blk(4000)
      calmax=0.0
      calzer=0.0
      ncalmx=0
      ncalze=0
      ibeg=1
      if(blk(1).gt.164) goto 130
  100 do 105 i=ibeg+1,ndp
        if(blk(i).gt.164) then
          iend=i
          goto 110
        endif
  105 continue
      iend=ndp
  110 if((iend-ibeg).gt.8) then
        do 115 i=ibeg+4,iend-4
          calzer=calzer+blk(i)
  115 continue
        ncalze=ncalze+iend-ibeg-7
      endif
      ibeg=iend
      if(ibeg.ge.ndp) goto 190
  130 do 135 i=ibeg+1,ndp
```

```
          if(blk(i).lt.164) then
            iend=i
            goto 140
          endif
  135   continue
         iend=ndp
  140   if((iend-ibeg).gt.8) then
          do 145 i=ibeg+4,iend-4
            calmax=calmax+blk(i)
  145     continue
          ncalmx=ncalmx+iend-ibeg-7
        endif
        ibeg=iend
        if(ibeg.ge.ndp) goto 190
        goto 100
c
  190   calmax=calmax/ncalmx
        calzer=calzer/ncalze
        sclfac=1.2611e+9/gain/(calmax-calzer)
c
        return
        end
c
c
c*****************************************************************
c
c
c     This subroutine perform the dispersion correction
c
c
      subroutine four(fct,tstep,dia,velocb,nn,dz,
     libegin,mm)
c
c             ********** SYMBOLS **********
c
c    fct(i) = array holding wave data
c        nn = period of the wave being analyzed
c         a = array to store An Fourier coefficient values
c         b = array to store Bn Fourier coefficient values
c         t = array to store phase angle values
c         c = array that holds the phase velocity at each
c             frequency
c   equa(i) = dummy array for computational purposes
c         v = bar radius/wavelength
c        wo = wave frequency
c        ao = value of Ao Fourier coefficient
c         d = array to store the value of Cn after
c             transformation to a cosine series
c        co = longitudinal wave velocity of bar
c
c            ******* SUBROUTINES *******
c
c     coeff - computes the Fourier coefficients Ao, An,
```

```
c             and Bn
c      simp - performs Simpson' rule integration
c
c
       dimension fct(25000),a(100),b(100),c(100),
      1d(100),t(100)
c
c      function statement; phase velocity verses r/lambda
c
        cp(v)=.5764+(.4236/(22.*v**4+12.8*v**3-2.77*v**2+
      1.92*v**1.5+1.0))
c
       freq=1.0/(tstep*1.0e-6)
c
       do 20 j=1,nn
        n=j-1
        fct(j)=fct(ibegin+n)
   20  continue
       pi=3.14159
       wo=2*pi/nn
c
       call coeff(mm,nn,wo,fct,ao,a,b)
c
       do 60 j=1,mm
        d(j)=sqrt(a(j)**2+b(j)**2)
        t(j)=acos(a(j)/d(j))
        if(b(j)-0.0) 55,60,60
   55   t(j)=-1.0*t(j)
   60  continue
c
69     w=(dia/2.0)*wo*freq/velocb
       v=0.0
       i=0
   70  i=i+1
       x=i*w
   80  v=v+0.0001
       xp=2.0*pi*cp(v)*v
   83  if(xp-x) 80,85,85
   85  c(i)=cp(v)
   88  if(i-mm)70,90,90
c
   90  do 100 i=1,mm
        c(i)=c(i)*velocb
  100  continue
c
       do 120 i=1,mm
        ak=i*wo/velocb*(velocb/c(i)-1.0)*freq
        t(i)=t(i)+ak*dz
  120  continue
c
c      perform wave reconstruction
c
13     do 150 i=1,nn
```

```
      fct(i)=ao/2.0
      do 150 j=1,mm
      fct(i)=fct(i)+d(j)*cos((j*wo*i)-t(j))
  150 continue
  c
      do 160 j=1,nn
       n=j-1
       fct(ibegin+n)=fct(j)
  160 continue
c
      return
      end
c
c
c*****************************************************************
c
c
      subroutine coeff(mm,nn,wo,fct,ao,a,b)
c
c     this routine will compute the Fourier coefficients
c     for each term in the series
c
      dimension equa(6000),a(100),b(100),fct(25000)
c
c     computing the integration limit; t/2
c
      n=nn/2
      do 10 i=1,nn
       equa(i)=fct(i)
   10 continue
c
c     Simpson's rule integration will be performed to
c     evaluate each of the coefficients; Ao,An,Bn
c
c     computing Ao
c
      call simp(equa,nn,result)
c
      ao=result/n
c
c     compute An
c
      do 30 j=1,mm
       do 20 i=1,nn
        equa(i)=fct(i)*cos(i*j*wo)
   20  continue
       call simp(equa,nn,result)
       a(j)=result/n
   30 continue
c
c     compute Bn
c
      do 50 j=1,mm
```

```
      do 40 i=1,nn
       equa(i)=fct(i)*sin(i*j*wo)
   40 continue
      call simp(equa,nn,result)
      b(j)=result/n
   50 continue
c
      return
      end
c
c
c*****************************************************************
c
c
      subroutine simp(equa,nn,result)
      dimension f(6000),equa(6000)
c
      do 2 i=1,nn
       f(i)=equa(i)
    2 continue
c
      n=nn/2
c
c     this subroutine performs simpson's rule integration
c
c     parameters
c
c     f: integration points
c     n: number of data points
c     h: spacing between data points
cresult: estimate of integral returned to caller
c
c     check to see if the number of panels is even
c
c     n-1: number of panels
c
      npanel=n-1
      nhalf=npanel/2
      nbegin=1
      result=0.0
      h=1
      if((npanel-2*nhalf).eq.0) go to 5
c
c     if the number of panels is odd use 3/8 rule for the
c     first four points then continue using the 1/3 rule
c     if the numbers of panels is even then the 1/3 rule
c     will be used exclusively
c
      result=3.0*h/8.0*(f(1)+3.0*f(2)+3.0*f(3)+f(4))
      nbegin=4
c
c     apply 1/3 rule, add in the first,second, and last
c     values
```

```
c
     5 result=result+h/3.0*(f(nbegin)+
      14.0*f(nbegin+1)+f(n))
        nbegin=nbegin+2
        if(nbegin.eq.n) go to 15
c
c       the pattern after nbegin+2 is repetitive
c
        nend=n-2
        do 10 i=nbegin,nend,2
         result=result+h/3.0*(2.0*f(i)+4.0*f(i+1))
    10  continue
c
    15  return
        end
c
c
c*****************************************************************
c
c
        subroutine basadj(blk,sclfac,nbeg,nend,n,base)
        dimension blk(25000)
c
    50  k=nbeg+0.8*float(n)
        base=0.0
        count=0.0
        do 100 i=nbeg,k
         count=count+1
         base=base+blk(i)
   100  continue
c
        base=base/count
c
c       adjust data for baseline and apply scalefactor
c
   150  do 200 i=nbeg,nend
         blk(i)=(blk(i)-base)*sclfac
   200  continue
c
        return
        end
c
c
c*****************************************************************
c*****************************************************************
c*                              END                              *
c*****************************************************************
```

G.3 Computer Output for Experiment 134

The following abbreviations have been used in the computer output (see also figure 2.5):

infl1 : stress at interface 1,

vel1 : particle velocity at interface 1

infl2 : stress at interface 2

vel2 : particle velocity ar interface 2

stsdif : stress difference between interface 1 and interface 2.

**** hopkinson bar data reduction code output ****

*** input parameters ***

experimental identification number --------	hb134ax
gain for incident bar strain gauge --------	2.5
gaint for transmitter bar strain gauge ----	5.
incident wave starttime (microseconds) ----	2519.
reflected wave starttime (microseconds) ---	2765.5
transmitted wave starttime (microseconds) -	2765.5
initial specimen length (m) ---------------	1.26e-2
number of terms used in fourier analysis --	20
dispersion bar correction length(m) -------	0.6033
incident bar calibration factor -----------	7630275.099424
transmitter bar calibration factor --------	3816424.365323

**** processed hopkinson bar data ****

time (microseconds)	stress (mpa)	strain (%)	strainrate (1/sec)	infl1 (mpa)	vel1 (m/s)	infl2 (mpa)	vel2 (m/s)	stsdif (mpa)
0.0	10.2	0.0	0.0	21.7	-0.3	-1.4	0.0	23.1
0.5	10.2	0.0	-21.1	21.6	-0.3	-1.3	0.0	22.9
1.0	10.1	0.0	-18.2	21.5	-0.2	-1.2	0.0	22.7
1.5	10.1	0.0	-14.9	21.3	-0.2	-1.1	0.0	22.4
2.0	10.0	0.0	-11.1	21.0	-0.1	-1.0	0.0	22.1
2.5	9.9	0.0	-6.8	20.7	0.0	-0.9	0.0	21.7
3.0	9.7	0.0	-2.1	20.4	0.0	-0.9	0.0	21.2
3.5	9.6	0.0	3.2	19.9	0.1	-0.8	0.0	20.7
4.0	9.4	0.0	9.1	19.5	0.2	-0.7	0.0	20.2
4.5	9.1	0.0	15.5	18.9	0.3	-0.7	0.0	19.6
5.0	8.9	0.0	22.4	18.4	0.4	-0.6	0.0	19.0
5.5	8.6	0.0	30.0	17.8	0.5	-0.6	0.0	18.4
6.0	8.3	0.0	38.2	17.2	0.6	-0.5	0.0	17.7
6.5	8.0	0.0	47.0	16.5	0.7	-0.5	0.0	17.0
7.0	7.7	0.0	56.5	15.9	0.8	-0.5	0.0	16.4
7.5	7.4	0.0	66.6	15.2	1.0	-0.5	0.0	15.7
8.0	7.0	0.0	77.5	14.5	1.1	-0.5	0.0	15.0
8.5	6.7	0.0	89.0	13.8	1.3	-0.5	0.0	14.4
9.0	6.3	0.0	101.1	13.2	1.4	-0.5	0.0	13.7
9.5	6.0	0.0	114.1	12.5	1.6	-0.6	0.0	13.0
10.0	5.6	0.0	127.7	11.8	1.8	-0.6	0.0	12.4
10.5	5.3	0.0	142.0	11.2	2.0	-0.6	0.0	11.8
11.0	4.9	0.0	157.1	10.5	2.2	-0.7	0.0	11.2
11.5	4.6	0.1	173.0	9.9	2.4	-0.7	0.0	10.7
12.0	4.3	0.1	189.6	9.3	2.6	-0.8	0.0	10.1
12.5	4.0	0.1	206.9	8.8	2.8	-0.8	0.0	9.6
13.0	3.7	0.1	225.0	8.3	3.0	-0.9	0.0	9.2
13.5	3.4	0.1	243.8	7.8	3.3	-0.9	0.0	8.7
14.0	3.2	0.1	263.4	7.3	3.6	-1.0	0.0	8.3
14.5	2.9	0.1	283.8	6.9	3.8	-1.0	0.0	8.0
15.0	2.7	0.1	304.9	6.6	4.1	-1.1	0.0	7.6
15.5	2.6	0.2	326.7	6.2	4.4	-1.1	0.0	7.3
16.0	2.4	0.2	349.3	5.9	4.7	-1.1	0.0	7.0
16.5	2.3	0.2	372.6	5.7	5.0	-1.1	0.0	6.8
17.0	2.2	0.2	396.7	5.5	5.3	-1.1	0.0	6.6
17.5	2.1	0.2	421.4	5.3	5.6	-1.1	0.0	6.4
18.0	2.0	0.3	446.9	5.2	5.9	-1.1	0.0	6.3
18.5	2.0	0.3	473.1	5.1	6.3	-1.1	0.0	6.1
19.0	2.0	0.3	499.9	5.0	6.6	-1.0	0.0	6.0
19.5	2.0	0.3	527.4	5.0	7.0	-1.0	0.0	5.9
20.0	2.0	0.4	555.5	5.0	7.3	-0.9	0.0	5.9
20.5	2.1	0.4	584.3	5.0	7.7	-0.8	0.0	5.8
21.0	2.2	0.4	613.6	5.0	8.1	-0.7	0.0	5.8
21.5	2.3	0.4	643.5	5.1	8.5	-0.6	0.0	5.7
22.0	2.4	0.5	674.0	5.2	8.9	-0.5	0.0	5.7
22.5	2.5	0.5	704.9	5.3	9.3	-0.4	0.0	5.7
23.0	2.6	0.5	736.4	5.5	9.7	-0.3	0.0	5.7
23.5	2.7	0.6	768.2	5.6	10.1	-0.1	0.0	5.7
24.0	2.9	0.6	800.5	5.8	10.5	0.0	0.0	5.8
24.5	3.0	0.7	833.2	5.9	10.9	0.2	0.0	5.8
25.0	3.2	0.7	866.2	6.1	11.3	0.3	0.0	5.8
25.5	3.4	0.7	899.4	6.3	11.8	0.4	0.0	5.8
26.0	3.5	0.8	932.9	6.5	12.2	0.6	0.0	5.9

26.5	3.7	0.8	966.5	6.6	12.6	0.7	0.0	5.9
27.0	3.8	0.9	1000.3	6.8	13.1	0.9	0.0	5.9
27.5	4.0	0.9	1034.2	7.0	13.5	1.0	0.0	6.0
28.0	4.1	1.0	1068.0	7.1	13.9	1.1	0.0	6.0
28.5	4.3	1.0	1101.8	7.3	14.3	1.2	0.0	6.1
29.0	4.4	1.1	1135.5	7.5	14.8	1.4	0.0	6.1
29.5	4.5	1.2	1169.1	7.6	15.2	1.5	0.0	6.1
30.0	4.6	1.2	1202.3	7.7	15.6	1.5	0.0	6.2
30.5	4.7	1.3	1235.3	7.9	16.0	1.6	0.0	6.2
31.0	4.8	1.3	1267.9	8.0	16.4	1.7	0.0	6.3
31.5	4.9	1.4	1300.0	8.1	16.8	1.8	0.0	6.3
32.0	5.0	1.5	1331.6	8.2	17.2	1.8	0.0	6.4
32.5	5.1	1.5	1362.6	8.3	17.6	1.8	0.0	6.4
33.0	5.1	1.6	1392.9	8.4	18.0	1.9	0.0	6.5
33.5	5.2	1.7	1422.5	8.5	18.3	1.9	0.0	6.6
34.0	5.2	1.8	1451.2	8.6	18.7	1.9	0.0	6.6
34.5	5.3	1.8	1479.1	8.6	19.0	1.9	0.0	6.7
35.0	5.3	1.9	1506.0	8.7	19.3	1.9	0.0	6.8
35.5	5.4	2.0	1531.8	8.8	19.7	1.9	0.0	6.8
36.0	5.4	2.1	1556.6	8.8	20.0	1.9	0.0	6.9
36.5	5.4	2.1	1580.2	8.9	20.2	1.9	0.0	6.9
37.0	5.5	2.2	1602.6	9.0	20.5	2.0	0.0	7.0
37.5	5.5	2.3	1623.7	9.0	20.8	2.0	0.0	7.0
38.0	5.5	2.4	1643.5	9.1	21.0	2.0	0.1	7.1
38.5	5.6	2.5	1661.9	9.1	21.2	2.0	0.1	7.1
39.0	5.6	2.5	1678.9	9.2	21.4	2.1	0.1	7.1
39.5	5.7	2.6	1694.4	9.3	21.6	2.1	0.1	7.1
40.0	5.8	2.7	1708.4	9.3	21.7	2.2	0.1	7.1
40.5	5.9	2.8	1720.9	9.4	21.9	2.3	0.1	7.1
41.0	6.0	2.9	1731.9	9.5	22.0	2.5	0.1	7.0
41.5	6.1	3.0	1741.3	9.5	22.1	2.6	0.1	6.9
42.0	6.2	3.1	1749.1	9.6	22.2	2.8	0.1	6.8
42.5	6.3	3.1	1755.4	9.7	22.3	3.0	0.1	6.7
43.0	6.5	3.2	1760.2	9.7	22.3	3.2	0.1	6.5
43.5	6.7	3.3	1763.4	9.8	22.3	3.5	0.1	6.3
44.0	6.8	3.4	1765.1	9.9	22.3	3.8	0.1	6.0
44.5	7.0	3.5	1765.3	9.9	22.3	4.2	0.1	5.8
45.0	7.3	3.6	1764.1	10.0	22.3	4.5	0.1	5.5
45.5	7.5	3.7	1761.5	10.0	22.3	4.9	0.1	5.1
46.0	7.7	3.8	1757.5	10.1	22.2	5.4	0.1	4.7
46.5	8.0	3.8	1752.2	10.1	22.1	5.8	0.1	4.3
47.0	8.2	3.9	1745.8	10.2	22.1	6.3	0.2	3.8
47.5	8.5	4.0	1738.2	10.2	22.0	6.8	0.2	3.3
48.0	8.8	4.1	1729.5	10.2	21.9	7.4	0.2	2.8
48.5	9.1	4.2	1719.8	10.2	21.7	8.0	0.2	2.2
49.0	9.4	4.3	1709.3	10.2	21.6	8.6	0.2	1.7
49.5	9.7	4.4	1698.0	10.2	21.5	9.2	0.2	1.0
50.0	10.0	4.5	1685.9	10.2	21.3	9.8	0.2	0.4
50.5	10.3	4.5	1673.3	10.2	21.2	10.5	0.3	-0.3
51.0	10.7	4.6	1660.2	10.2	21.0	11.2	0.3	-1.0
51.5	11.0	4.7	1646.6	10.2	20.9	11.8	0.3	-1.7
52.0	11.3	4.8	1632.9	10.1	20.7	12.5	0.3	-2.4
52.5	11.6	4.9	1618.9	10.1	20.6	13.2	0.3	-3.1
53.0	12.0	4.9	1604.9	10.1	20.4	13.9	0.4	-3.8
53.5	12.3	5.0	1590.9	10.0	20.2	14.5	0.4	-4.5
54.0	12.6	5.1	1577.0	10.0	20.1	15.2	0.4	-5.2
54.5	12.9	5.2	1563.4	10.0	19.9	15.9	0.4	-5.9
55.0	13.2	5.3	1550.1	10.0	19.8	16.5	0.4	-6.5
55.5	13.6	5.3	1537.3	10.0	19.6	17.1	0.4	-7.2
56.0	13.9	5.4	1524.9	10.0	19.5	17.8	0.4	-7.8

56.5	14.2	5.5	1513.2	10.0	19.4	18.3	0.5	-8.3
57.0	14.5	5.6	1502.2	10.1	19.3	18.9	0.5	-8.8
57.5	14.8	5.6	1491.8	10.1	19.2	19.4	0.5	-9.3
58.0	15.1	5.7	1482.3	10.2	19.1	20.0	0.5	-9.7
58.5	15.4	5.8	1473.7	10.4	19.0	20.4	0.5	-10.1
59.0	15.7	5.9	1465.9	10.5	18.9	20.9	0.5	-10.4
59.5	16.0	5.9	1459.1	10.7	18.9	21.3	0.5	-10.6
60.0	16.4	6.0	1453.2	11.0	18.8	21.8	0.6	-10.8
60.5	16.7	6.1	1448.3	11.3	18.8	22.1	0.6	-10.9
61.0	17.1	6.2	1444.4	11.6	18.7	22.5	0.6	-10.9
61.5	17.4	6.2	1441.5	12.0	18.7	22.9	0.6	-10.9
62.0	17.8	6.3	1439.6	12.4	18.7	23.2	0.6	-10.8
62.5	18.2	6.4	1438.6	12.9	18.7	23.5	0.6	-10.6
63.0	18.6	6.4	1438.5	13.5	18.7	23.8	0.6	-10.3
63.5	19.1	6.5	1439.3	14.1	18.8	24.1	0.6	-10.0
64.0	19.6	6.6	1441.0	14.7	18.8	24.4	0.6	-9.6
64.5	20.1	6.7	1443.4	15.5	18.9	24.7	0.6	-9.2
65.0	20.6	6.7	1446.5	16.3	18.9	25.0	0.6	-8.7
65.5	21.2	6.8	1450.3	17.1	19.0	25.3	0.6	-8.2
66.0	21.8	6.9	1454.7	18.0	19.0	25.6	0.6	-7.6
66.5	22.5	6.9	1459.6	19.0	19.1	26.0	0.7	-6.9
67.0	23.2	7.0	1464.8	20.1	19.2	26.3	0.7	-6.2
67.5	24.0	7.1	1470.4	21.2	19.3	26.7	0.7	-5.5
68.0	24.8	7.2	1476.2	22.4	19.4	27.2	0.7	-4.8
68.5	25.7	7.2	1482.1	23.7	19.5	27.7	0.7	-4.0
69.0	26.6	7.3	1488.1	25.0	19.5	28.2	0.7	-3.3
69.5	27.6	7.4	1494.0	26.4	19.6	28.8	0.7	-2.5
70.0	28.7	7.5	1499.7	27.8	19.7	29.5	0.7	-1.7
70.5	29.8	7.5	1505.2	29.3	19.8	30.3	0.8	-0.9
71.0	31.0	7.6	1510.3	30.9	19.9	31.1	0.8	-0.2
71.5	32.2	7.7	1514.9	32.5	19.9	31.9	0.8	0.5
72.0	33.5	7.8	1519.1	34.2	20.0	32.9	0.8	1.3
72.5	34.9	7.8	1522.6	35.9	20.1	34.0	0.9	1.9
73.0	36.4	7.9	1525.4	37.7	20.1	35.1	0.9	2.6
73.5	37.9	8.0	1527.4	39.5	20.2	36.3	0.9	3.2
74.0	39.5	8.1	1528.5	41.4	20.2	37.6	1.0	3.7
74.5	41.2	8.1	1528.8	43.3	20.2	39.1	1.0	4.2
75.0	42.9	8.2	1528.2	45.3	20.3	40.6	1.0	4.7
75.5	44.7	8.3	1526.5	47.3	20.3	42.2	1.1	5.1
76.0	46.6	8.4	1523.8	49.3	20.3	43.9	1.1	5.4
76.5	48.6	8.5	1520.0	51.4	20.2	45.7	1.2	5.7
77.0	50.6	8.5	1515.2	53.5	20.2	47.6	1.2	5.9
77.5	52.7	8.6	1509.2	55.7	20.2	49.6	1.3	6.1
78.0	54.8	8.7	1502.2	57.9	20.1	51.7	1.3	6.2
78.5	57.0	8.8	1494.1	60.1	20.1	53.9	1.4	6.2
79.0	59.3	8.8	1484.9	62.4	20.0	56.2	1.4	6.2
79.5	61.6	8.9	1474.7	64.7	19.9	58.6	1.5	6.1
80.0	64.0	9.0	1463.4	67.0	19.8	61.0	1.5	6.0
80.5	66.5	9.0	1451.2	69.4	19.7	63.6	1.6	5.9
81.0	69.0	9.1	1438.1	71.8	19.6	66.2	1.7	5.6
81.5	71.6	9.2	1424.1	74.3	19.5	68.9	1.7	5.4
82.0	74.2	9.3	1409.2	76.7	19.4	71.6	1.8	5.1
82.5	76.8	9.3	1393.7	79.2	19.2	74.4	1.9	4.8
83.0	79.5	9.4	1377.4	81.8	19.1	77.3	2.0	4.5
83.5	82.3	9.5	1360.6	84.3	19.0	80.2	2.0	4.1
84.0	85.1	9.5	1343.2	87.0	18.8	83.2	2.1	3.8
84.5	87.9	9.6	1325.3	89.6	18.7	86.2	2.2	3.4
85.0	90.8	9.7	1307.1	92.3	18.5	89.3	2.3	3.0
85.5	93.7	9.7	1288.6	95.0	18.3	92.3	2.3	2.7
86.0	96.6	9.8	1269.9	97.8	18.2	95.5	2.4	2.3

86.5	99.6	9.9	1251.1	100.6	18.0	98.6	2.5	2.0
87.0	102.6	9.9	1232.3	103.4	17.9	101.7	2.6	1.7
87.5	105.6	10.0	1213.4	106.3	17.7	104.9	2.7	1.4
88.0	108.6	10.0	1194.7	109.2	17.6	108.1	2.7	1.1
88.5	111.7	10.1	1176.2	112.1	17.4	111.2	2.8	0.9
89.0	114.8	10.2	1157.9	115.1	17.3	114.4	2.9	0.7
89.5	117.9	10.2	1139.9	118.1	17.1	117.6	3.0	0.6
90.0	121.0	10.3	1122.3	121.2	17.0	120.7	3.1	0.5
90.5	124.1	10.3	1105.2	124.3	16.8	123.9	3.1	0.4
91.0	127.2	10.4	1088.5	127.4	16.7	127.0	3.2	0.4
91.5	130.3	10.4	1072.3	130.5	16.6	130.1	3.3	0.4
92.0	133.4	10.5	1056.6	133.6	16.5	133.1	3.4	0.5
92.5	136.5	10.5	1041.6	136.8	16.4	136.2	3.4	0.6
93.0	139.6	10.6	1027.1	139.9	16.3	139.2	3.5	0.7
93.5	142.6	10.7	1013.2	143.1	16.2	142.2	3.6	0.9
94.0	145.7	10.7	1000.0	146.3	16.1	145.1	3.7	1.1
94.5	148.7	10.8	987.4	149.4	16.0	148.0	3.7	1.4
95.0	151.7	10.8	975.4	152.6	16.0	150.9	3.8	1.7
95.5	154.7	10.8	964.0	155.7	15.9	153.7	3.9	2.0
96.0	157.6	10.9	953.1	158.8	15.8	156.4	4.0	2.4
96.5	160.5	10.9	942.9	161.9	15.8	159.1	4.0	2.7
97.0	163.4	11.0	933.1	164.9	15.7	161.8	4.1	3.1
97.5	166.2	11.0	923.9	167.9	15.7	164.4	4.2	3.5
98.0	168.9	11.1	915.2	170.9	15.6	167.0	4.2	3.9
98.5	171.6	11.1	906.8	173.8	15.6	169.4	4.3	4.3
99.0	174.2	11.2	898.9	176.6	15.6	171.9	4.3	4.8
99.5	176.8	11.2	891.3	179.4	15.5	174.2	4.4	5.2
100.0	179.3	11.3	884.0	182.1	15.5	176.5	4.5	5.6
100.5	181.7	11.3	877.0	184.7	15.5	178.7	4.5	6.0
101.0	184.0	11.4	870.1	187.2	15.5	180.9	4.6	6.3
101.5	186.3	11.4	863.4	189.6	15.4	182.9	4.6	6.7
102.0	188.4	11.4	856.8	191.9	15.4	184.9	4.7	7.0
102.5	190.5	11.5	850.3	194.2	15.4	186.8	4.7	7.3
103.0	192.5	11.5	843.8	196.3	15.3	188.7	4.8	7.6
103.5	194.3	11.6	837.2	198.3	15.3	190.4	4.8	7.9
104.0	196.1	11.6	830.6	200.1	15.2	192.1	4.9	8.1
104.5	197.7	11.6	823.9	201.9	15.2	193.6	4.9	8.3
105.0	199.3	11.7	817.0	203.5	15.1	195.1	4.9	8.4
105.5	200.7	11.7	810.0	205.0	15.1	196.4	5.0	8.6
106.0	202.1	11.8	802.7	206.4	15.0	197.7	5.0	8.7
106.5	203.3	11.8	795.2	207.7	15.0	198.9	5.0	8.8
107.0	204.4	11.8	787.5	208.8	14.9	199.9	5.1	8.8
107.5	205.3	11.9	779.6	209.8	14.8	200.9	5.1	8.9
108.0	206.2	11.9	771.3	210.6	14.7	201.7	5.1	8.9
108.5	206.9	12.0	762.8	211.4	14.6	202.5	5.1	8.9
109.0	207.5	12.0	754.0	212.0	14.5	203.1	5.1	8.9
109.5	208.0	12.0	745.0	212.5	14.4	203.6	5.2	8.8
110.0	208.4	12.1	735.6	212.8	14.3	204.0	5.2	8.8
110.5	208.7	12.1	726.0	213.1	14.2	204.3	5.2	8.7
111.0	208.9	12.2	716.2	213.2	14.1	204.5	5.2	8.7
111.5	208.9	12.2	706.0	213.2	13.9	204.6	5.2	8.6
112.0	208.9	12.2	695.7	213.1	13.8	204.6	5.2	8.6
112.5	208.7	12.3	685.2	213.0	13.7	204.4	5.2	8.5
113.0	208.4	12.3	674.4	212.7	13.5	204.2	5.2	8.5
113.5	208.1	12.3	663.5	212.3	13.4	203.8	5.2	8.4
114.0	207.6	12.4	652.5	211.8	13.2	203.4	5.1	8.4
114.5	207.0	12.4	641.3	211.2	13.1	202.8	5.1	8.4
115.0	206.4	12.4	630.1	210.6	12.9	202.2	5.1	8.4
115.5	205.7	12.5	618.7	209.9	12.7	201.5	5.1	8.4
116.0	204.9	12.5	607.3	209.1	12.6	200.6	5.1	8.4

116.5	204.0	12.5	595.8	208.2	12.4	199.7	5.1	8.5
117.0	203.0	12.5	584.4	207.3	12.2	198.7	5.0	8.6
117.5	202.0	12.6	572.9	206.3	12.1	197.7	5.0	8.6
118.0	200.9	12.6	561.4	205.3	11.9	196.5	5.0	8.7
118.5	199.8	12.6	550.0	204.2	11.7	195.3	4.9	8.8
119.0	198.6	12.7	538.6	203.0	11.6	194.1	4.9	8.9
119.5	197.3	12.7	527.2	201.8	11.4	192.8	4.9	9.0
120.0	196.0	12.7	515.9	200.6	11.2	191.4	4.8	9.2
120.5	194.7	12.7	504.6	199.3	11.0	190.0	4.8	9.3
121.0	193.3	12.8	493.3	198.0	10.8	188.6	4.8	9.4
121.5	191.8	12.8	482.1	196.6	10.7	187.1	4.7	9.5
122.0	190.4	12.8	470.9	195.2	10.5	185.6	4.7	9.6
122.5	188.9	12.8	459.8	193.8	10.3	184.0	4.7	9.7
123.0	187.4	12.9	448.6	192.3	10.1	182.5	4.6	9.8
123.5	185.8	12.9	437.4	190.8	9.9	180.9	4.6	9.9
124.0	184.3	12.9	426.2	189.2	9.8	179.3	4.5	9.9
124.5	182.7	12.9	414.9	187.7	9.6	177.7	4.5	9.9
125.0	181.1	12.9	403.6	186.0	9.4	176.1	4.5	9.9
125.5	179.4	13.0	392.2	184.4	9.2	174.5	4.4	9.9
126.0	177.8	13.0	380.7	182.7	9.0	172.9	4.4	9.8
126.5	176.1	13.0	369.0	181.0	8.8	171.3	4.3	9.7
127.0	174.4	13.0	357.2	179.2	8.6	169.7	4.3	9.5
127.5	172.7	13.0	345.1	177.4	8.4	168.0	4.3	9.3
128.0	171.0	13.0	332.9	175.5	8.2	166.4	4.2	9.1
128.5	169.2	13.1	320.5	173.7	8.0	164.8	4.2	8.8
129.0	167.5	13.1	307.8	171.7	7.8	163.2	4.1	8.5
129.5	165.7	13.1	294.8	169.8	7.6	161.6	4.1	8.2
130.0	163.9	13.1	281.6	167.8	7.4	160.0	4.0	7.8
130.5	162.1	13.1	268.0	165.8	7.2	158.4	4.0	7.3
131.0	160.3	13.1	254.2	163.7	7.0	156.8	4.0	6.9
131.5	158.4	13.1	240.0	161.6	6.8	155.2	3.9	6.4
132.0	156.6	13.2	225.5	159.5	6.5	153.6	3.9	5.8
132.5	154.7	13.2	210.8	157.3	6.3	152.0	3.8	5.3
133.0	152.8	13.2	195.7	155.1	6.1	150.4	3.8	4.7
133.5	150.8	13.2	180.3	152.9	5.8	148.8	3.8	4.1
134.0	148.9	13.2	164.6	150.7	5.6	147.1	3.7	3.5
134.5	147.0	13.2	148.6	148.4	5.3	145.5	3.7	2.9
135.0	145.0	13.2	132.4	146.1	5.1	143.8	3.6	2.3
135.5	143.0	13.2	116.0	143.9	4.8	142.1	3.6	1.8
136.0	141.0	13.2	99.4	141.6	4.6	140.4	3.6	1.2
136.5	139.0	13.2	82.6	139.3	4.3	138.7	3.5	0.6
137.0	136.9	13.2	65.7	137.0	4.1	136.9	3.5	0.1
137.5	134.9	13.2	48.7	134.7	3.8	135.1	3.4	-0.4
138.0	132.8	13.2	31.6	132.4	3.6	133.3	3.4	-0.9
138.5	130.8	13.2	14.5	130.1	3.3	131.4	3.3	-1.3
139.0	128.7	13.2	-2.5	127.9	3.0	129.6	3.3	-1.7
139.5	126.7	13.2	-19.4	125.7	2.8	127.7	3.2	-2.0
140.0	124.6	13.2	-36.2	123.5	2.5	125.8	3.2	-2.3
140.5	122.6	13.2	-52.8	121.3	2.3	123.8	3.1	-2.5
141.0	120.5	13.2	-69.1	119.2	2.0	121.9	3.1	-2.7
141.5	118.5	13.2	-85.2	117.1	1.8	119.9	3.0	-2.8
142.0	116.5	13.2	-100.8	115.1	1.5	117.9	3.0	-2.8
142.5	114.5	13.2	-116.1	113.1	1.3	115.9	2.9	-2.8
143.0	112.5	13.2	-130.9	111.1	1.1	113.9	2.9	-2.7
143.5	110.6	13.2	-145.3	109.3	0.8	111.8	2.8	-2.6
144.0	108.6	13.2	-159.0	107.5	0.6	109.8	2.8	-2.4
144.5	106.7	13.2	-172.2	105.7	0.4	107.8	2.7	-2.1
145.0	104.9	13.2	-184.7	104.0	0.2	105.8	2.7	-1.8
145.5	103.1	13.2	-196.6	102.4	0.0	103.8	2.6	-1.4
146.0	101.3	13.2	-207.7	100.8	-0.2	101.8	2.6	-0.9

146.5	99.6	13.2	-218.2	99.4	-0.3	99.8	2.5	-0.5
147.0	97.9	13.1	-227.8	97.9	-0.5	97.9	2.5	0.0
147.5	96.3	13.1	-236.7	96.6	-0.7	96.0	2.4	0.6
148.0	94.7	13.1	-244.7	95.3	-0.8	94.1	2.4	1.2
148.5	93.2	13.1	-251.9	94.1	-0.9	92.3	2.3	1.8
149.0	91.8	13.1	-258.3	92.9	-1.0	90.6	2.3	2.4
149.5	90.4	13.1	-263.9	91.9	-1.1	88.9	2.2	3.0
150.0	89.0	13.1	-268.6	90.8	-1.2	87.2	2.2	3.6
150.5	87.7	13.1	-272.5	89.9	-1.3	85.6	2.2	4.2
151.0	86.5	13.0	-275.6	88.9	-1.4	84.1	2.1	4.8
151.5	85.4	13.0	-277.8	88.1	-1.4	82.7	2.1	5.4
152.0	84.3	13.0	-279.3	87.3	-1.5	81.3	2.1	6.0
152.5	83.2	13.0	-280.1	86.5	-1.5	80.0	2.0	6.5
153.0	82.3	13.0	-280.1	85.8	-1.5	78.8	2.0	7.0
153.5	81.4	13.0	-279.4	85.1	-1.5	77.6	2.0	7.4
154.0	80.5	13.0	-278.0	84.4	-1.5	76.6	1.9	7.8
154.5	79.7	12.9	-276.0	83.8	-1.5	75.6	1.9	8.1
155.0	78.9	12.9	-273.4	83.1	-1.5	74.7	1.9	8.4
155.5	78.2	12.9	-270.3	82.5	-1.5	73.9	1.9	8.6
156.0	77.6	12.9	-266.7	82.0	-1.5	73.2	1.9	8.8
156.5	77.0	12.9	-262.6	81.4	-1.4	72.5	1.8	8.9
157.0	76.4	12.9	-258.1	80.8	-1.4	71.9	1.8	8.9
157.5	75.9	12.9	-253.2	80.3	-1.3	71.4	1.8	8.9
158.0	75.3	12.8	-248.1	79.7	-1.3	71.0	1.8	8.7
158.5	74.9	12.8	-242.6	79.2	-1.2	70.6	1.8	8.6
159.0	74.4	12.8	-237.0	78.6	-1.1	70.3	1.8	8.3
159.5	74.0	12.8	-231.2	78.0	-1.1	70.0	1.8	8.1
160.0	73.6	12.8	-225.2	77.5	-1.0	69.8	1.8	7.7
160.5	73.2	12.8	-219.2	76.9	-0.9	69.6	1.8	7.3
161.0	72.9	12.8	-213.2	76.3	-0.9	69.4	1.8	6.9
161.5	72.5	12.8	-207.1	75.7	-0.8	69.3	1.8	6.4
162.0	72.2	12.8	-201.1	75.1	-0.7	69.2	1.8	5.9
162.5	71.8	12.7	-195.2	74.5	-0.6	69.2	1.7	5.3
163.0	71.5	12.7	-189.4	73.8	-0.6	69.1	1.7	4.7
163.5	71.1	12.7	-183.7	73.2	-0.5	69.0	1.7	4.2
164.0	70.8	12.7	-178.3	72.5	-0.4	69.0	1.7	3.6
164.5	70.4	12.7	-173.0	71.9	-0.4	68.9	1.7	3.0
165.0	70.0	12.7	-167.9	71.2	-0.3	68.8	1.7	2.4
165.5	69.6	12.7	-163.1	70.5	-0.3	68.8	1.7	1.8
166.0	69.2	12.7	-158.6	69.8	-0.2	68.6	1.7	1.2
166.5	68.8	12.7	-154.3	69.1	-0.2	68.5	1.7	0.6
167.0	68.4	12.7	-150.3	68.5	-0.1	68.3	1.7	0.1
167.5	68.0	12.7	-146.6	67.8	-0.1	68.1	1.7	-0.4
168.0	67.5	12.7	-143.2	67.1	0.0	67.9	1.7	-0.8
168.5	67.0	12.6	-140.0	66.4	0.0	67.7	1.7	-1.3
169.0	66.5	12.6	-137.2	65.7	0.0	67.3	1.7	-1.6
169.5	66.0	12.6	-134.7	65.0	0.0	67.0	1.7	-1.9
170.0	65.5	12.6	-132.5	64.4	0.0	66.6	1.7	-2.2
170.5	65.0	12.6	-130.5	63.7	0.1	66.2	1.7	-2.4
171.0	64.4	12.6	-128.9	63.1	0.1	65.7	1.7	-2.6
171.5	63.8	12.6	-127.4	62.5	0.1	65.2	1.6	-2.7
172.0	63.2	12.6	-126.3	61.8	0.1	64.6	1.6	-2.8
172.5	62.6	12.6	-125.4	61.2	0.0	64.0	1.6	-2.8
173.0	62.0	12.6	-124.7	60.6	0.0	63.4	1.6	-2.8
173.5	61.4	12.6	-124.2	60.1	0.0	62.8	1.6	-2.7
174.0	60.8	12.6	-123.9	59.5	0.0	62.1	1.6	-2.6
174.5	60.1	12.6	-123.7	58.9	0.0	61.4	1.6	-2.4
175.0	59.5	12.6	-123.8	58.4	0.0	60.6	1.5	-2.2
175.5	58.9	12.6	-123.9	57.9	-0.1	59.9	1.5	-2.0
176.0	58.2	12.6	-124.2	57.3	-0.1	59.1	1.5	-1.7

APPENDIX H

SPECIMEN MOISTURE/DENSITY RELATIONSHIPS TO THE HARVARD MINIATURE COMPACTION CURVE

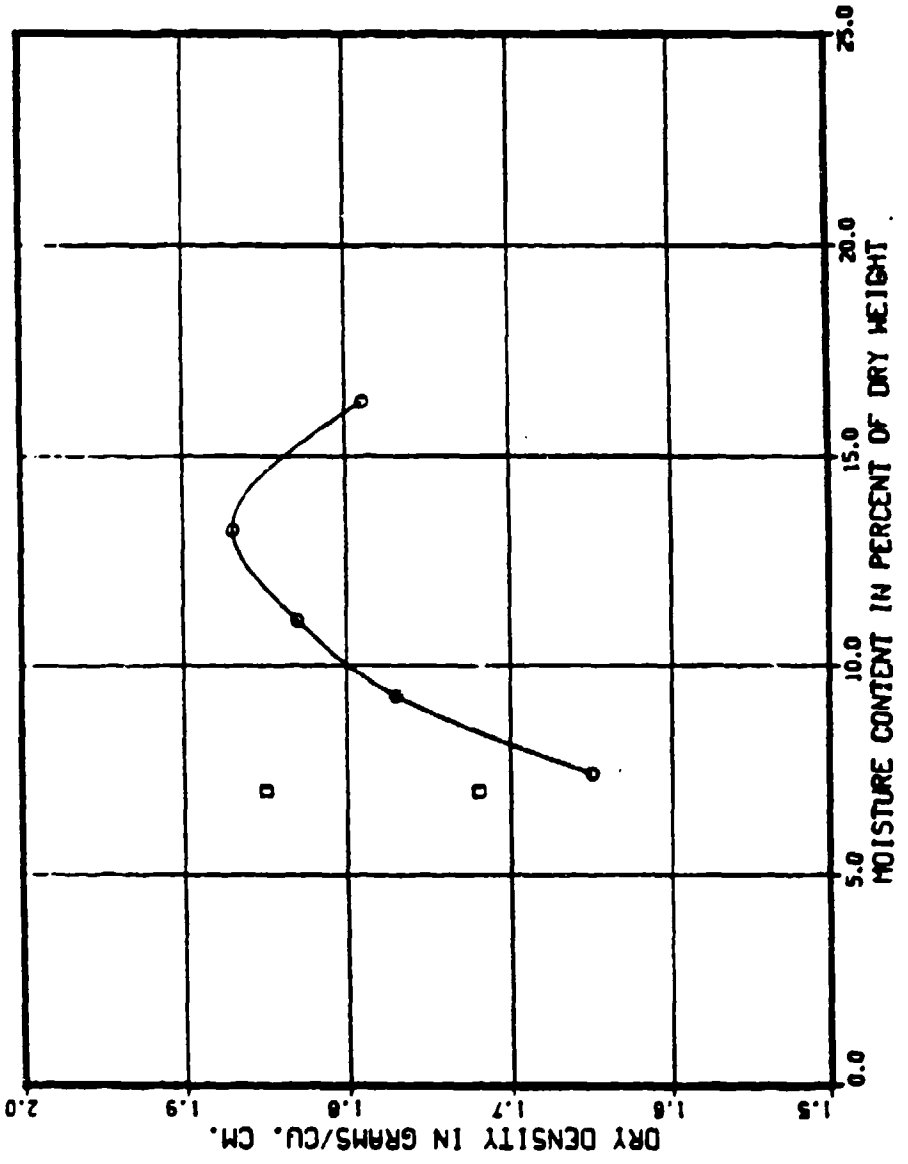

Figure H.1. Moisture/density relationship to the Harvard miniature compaction curve for specimens compacted dry of optimum.

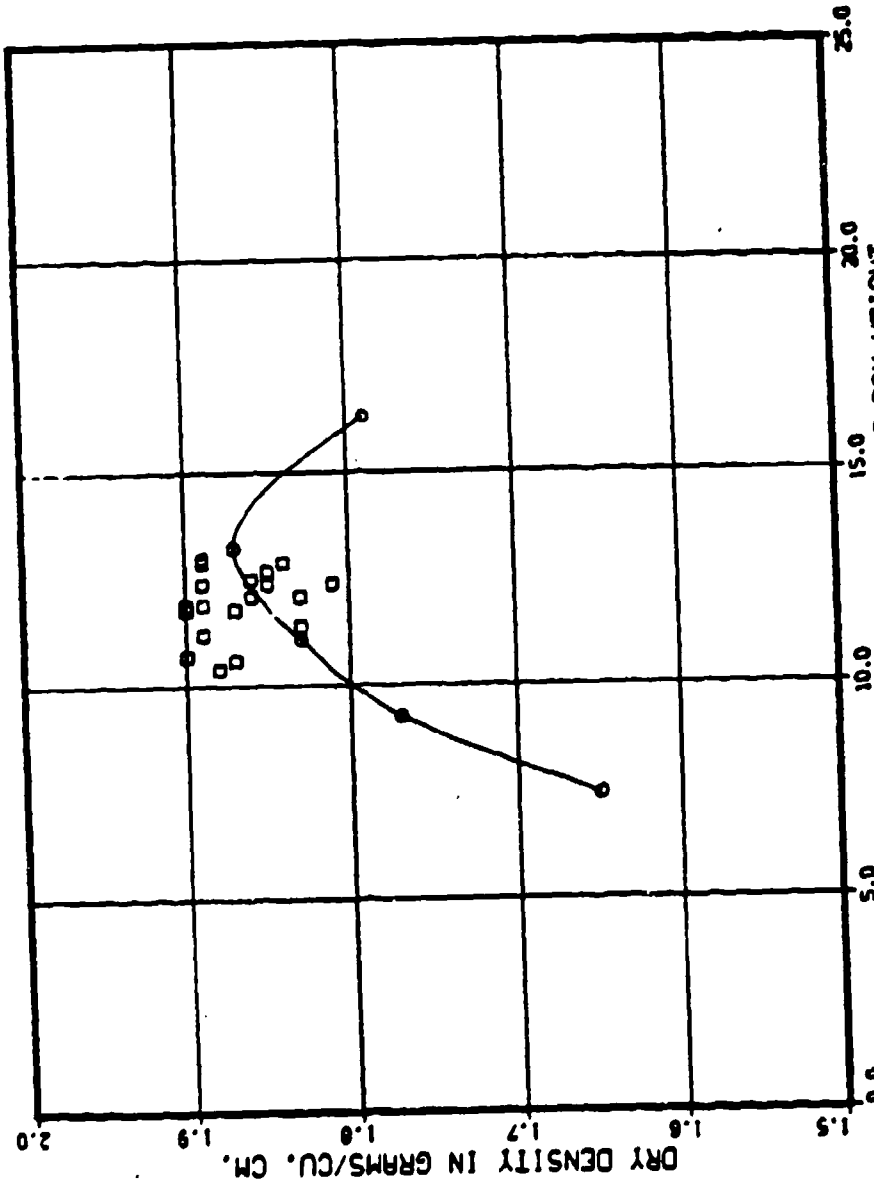

Figure H.2. Moisture/density relationship to the Harvard miniature compaction curve for specimens compacted near optimum.

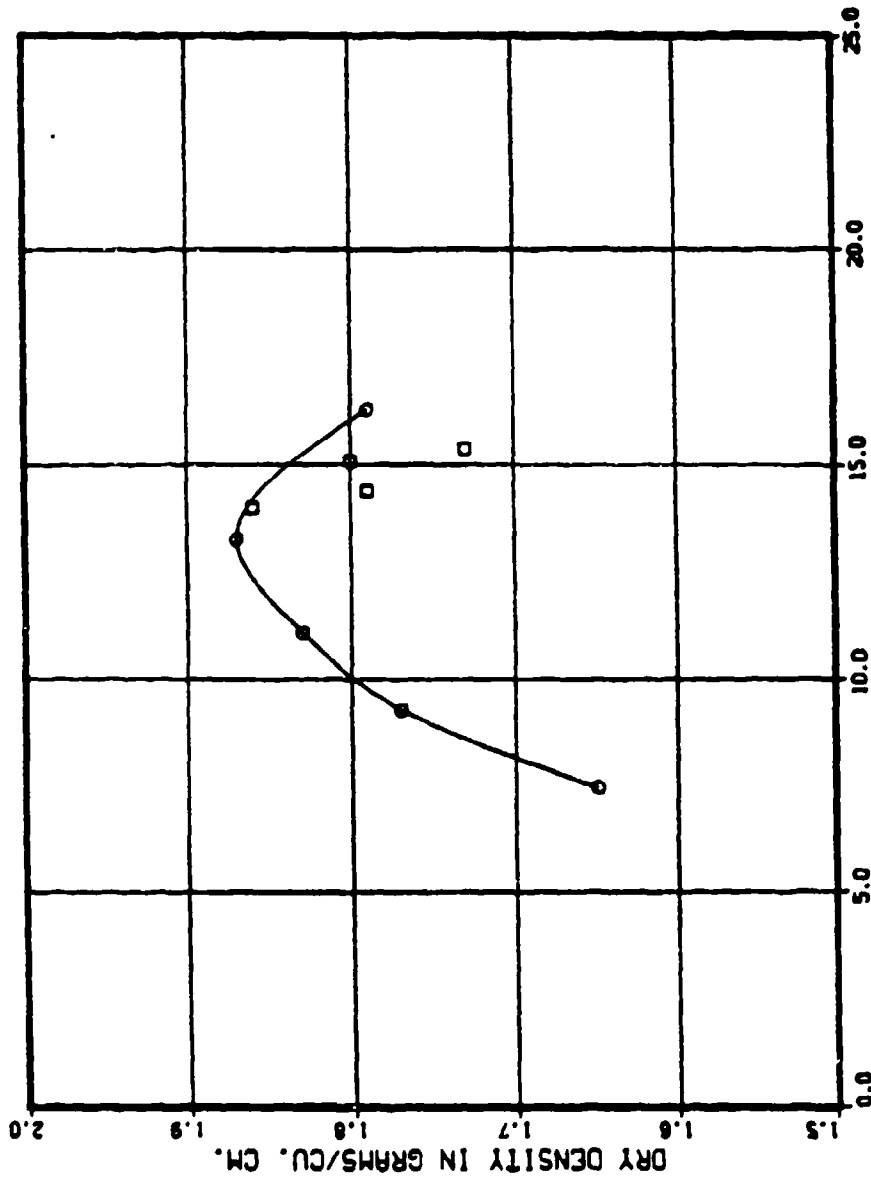

Figure H.3. Moisture/density relationship to the Harvard miniature compaction curve for specimens compacted wet of optimum.

APPENDIX I

PLOTTED EXPERIMENTAL RESULTS WITH SUMMARY DATA

The following nomenclature has been used in the presentation of the summary data:

σ_a = magnitude of applied stress wave,

$\dot{\varepsilon}_{max}$ = maximum average strain-rate,

$\dot{\varepsilon}_{avg}$ = average strain-rate over the duration of the experiment,

l = specimen length after seating has been applied,

ε_s = seating strain,

w = initial specimen moisture content,

w_l = percentage if initial moisture lost during the experiment,

e = void ratio based on specimen length l,

n_g = initial gas porosity,

V_t = specimen total volume,

γ_t = wet density,

S = degree of saturation.

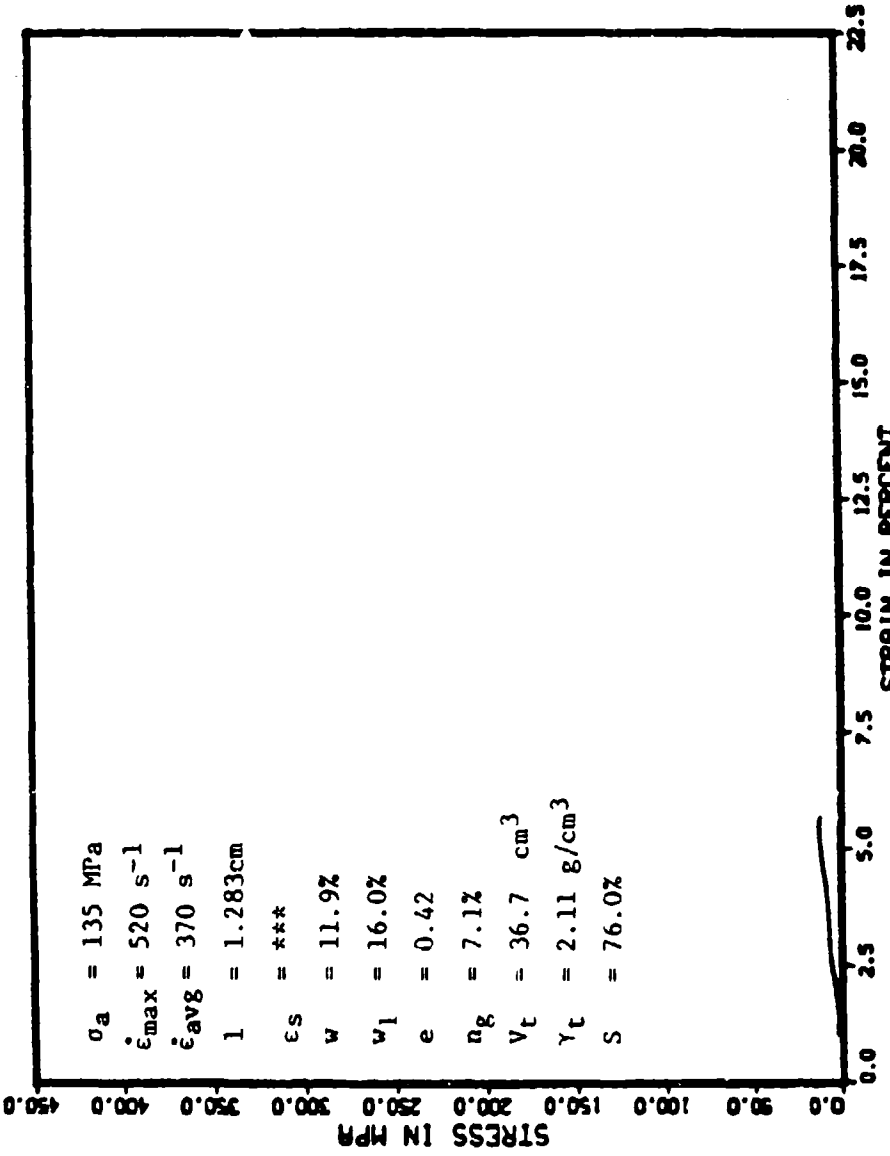

Figure I.1. Stress-strain response for experiment 31.

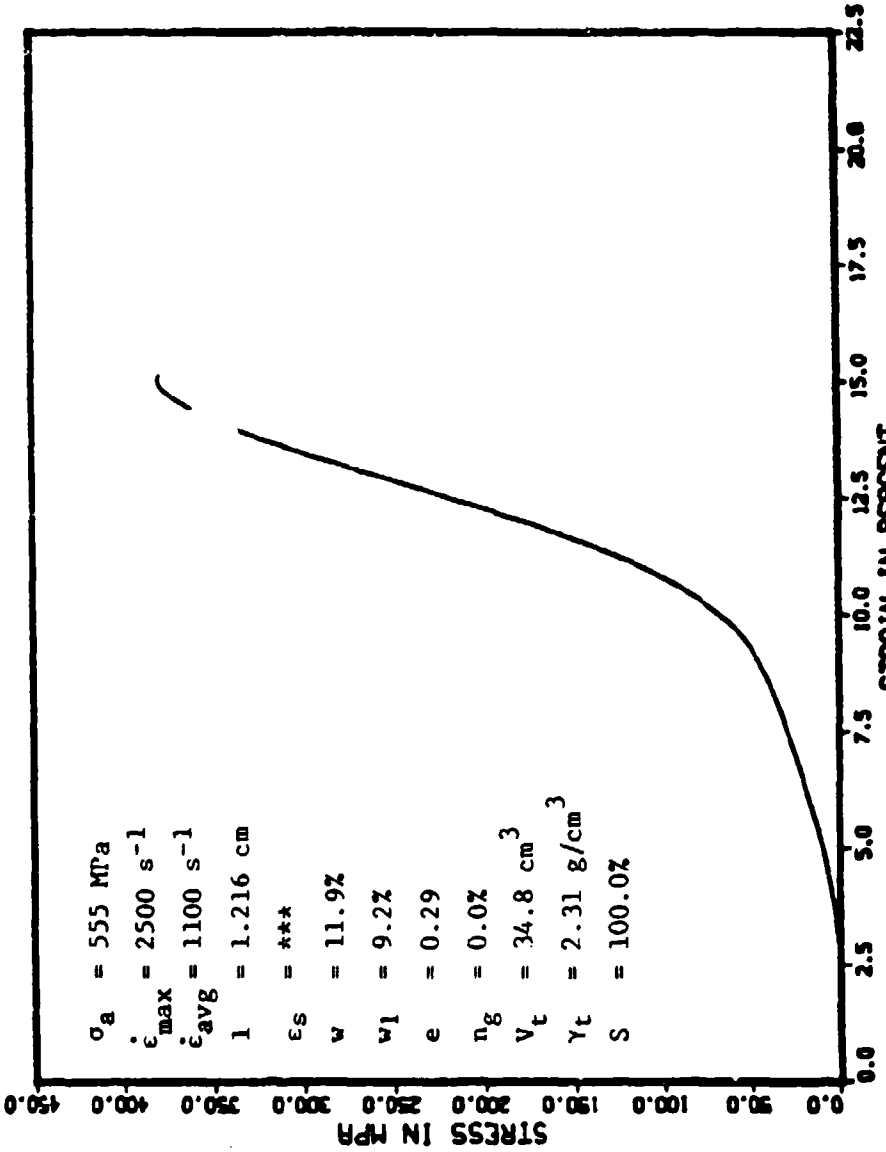

Figure I.2. Stress-strain response for experiment 32.

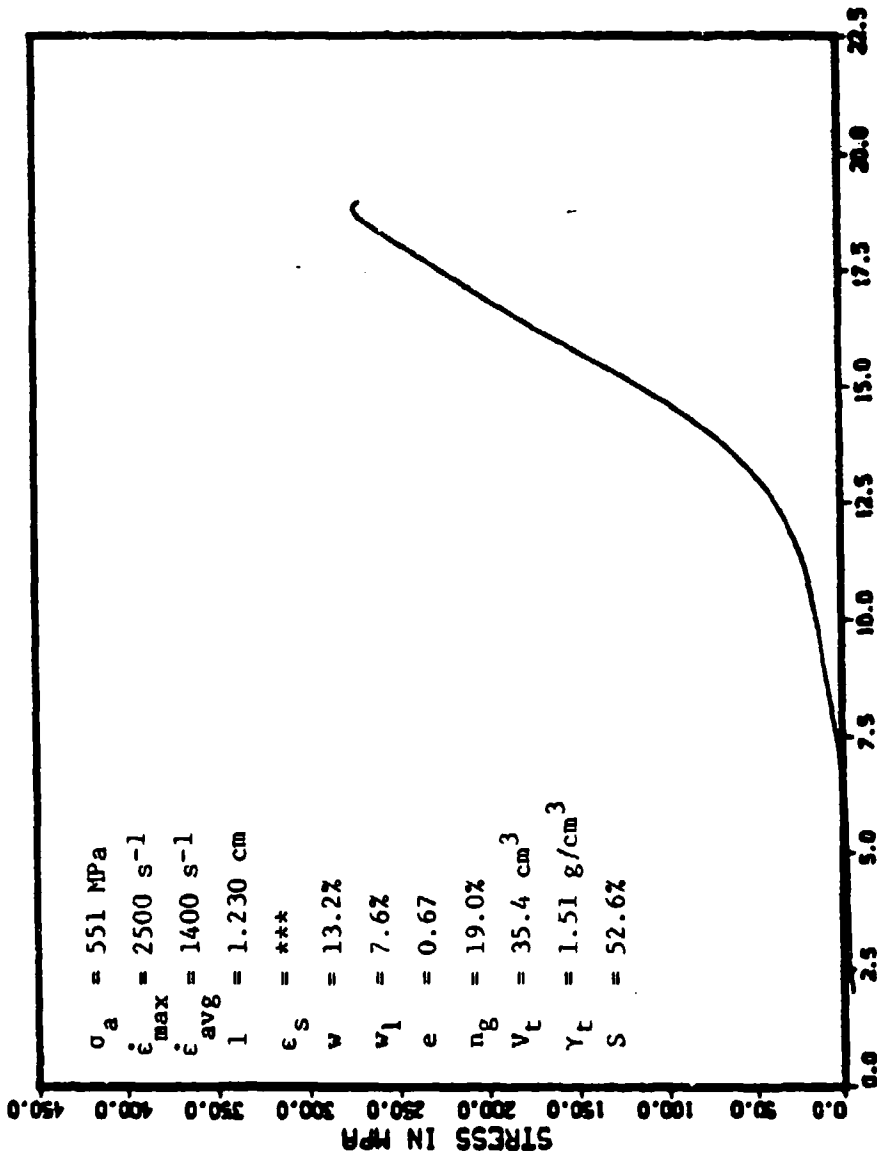

Figure I.3. Stress-strain response for experiment 38.

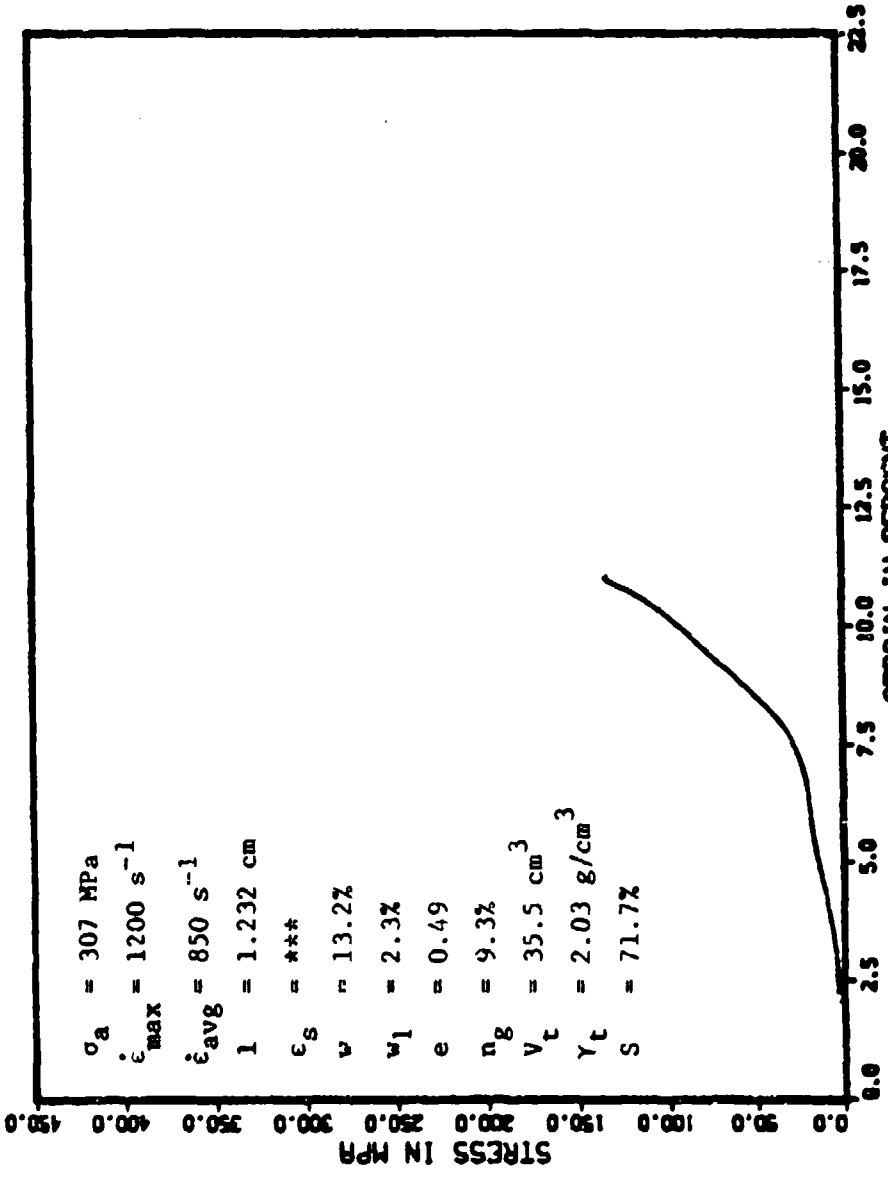

Figure I.4. Stress-strain response for experiment 39.

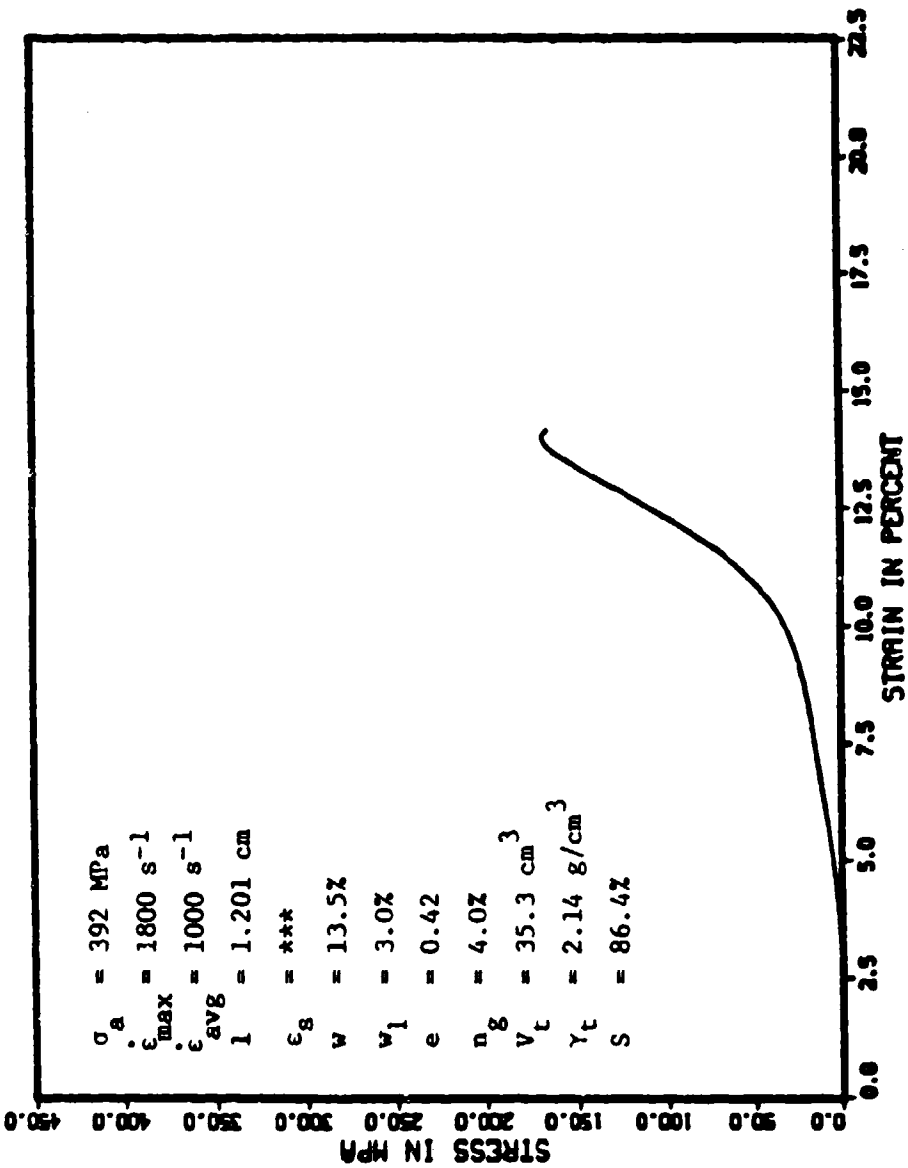

Figure I.5. Stress-strain response for experiment 40.

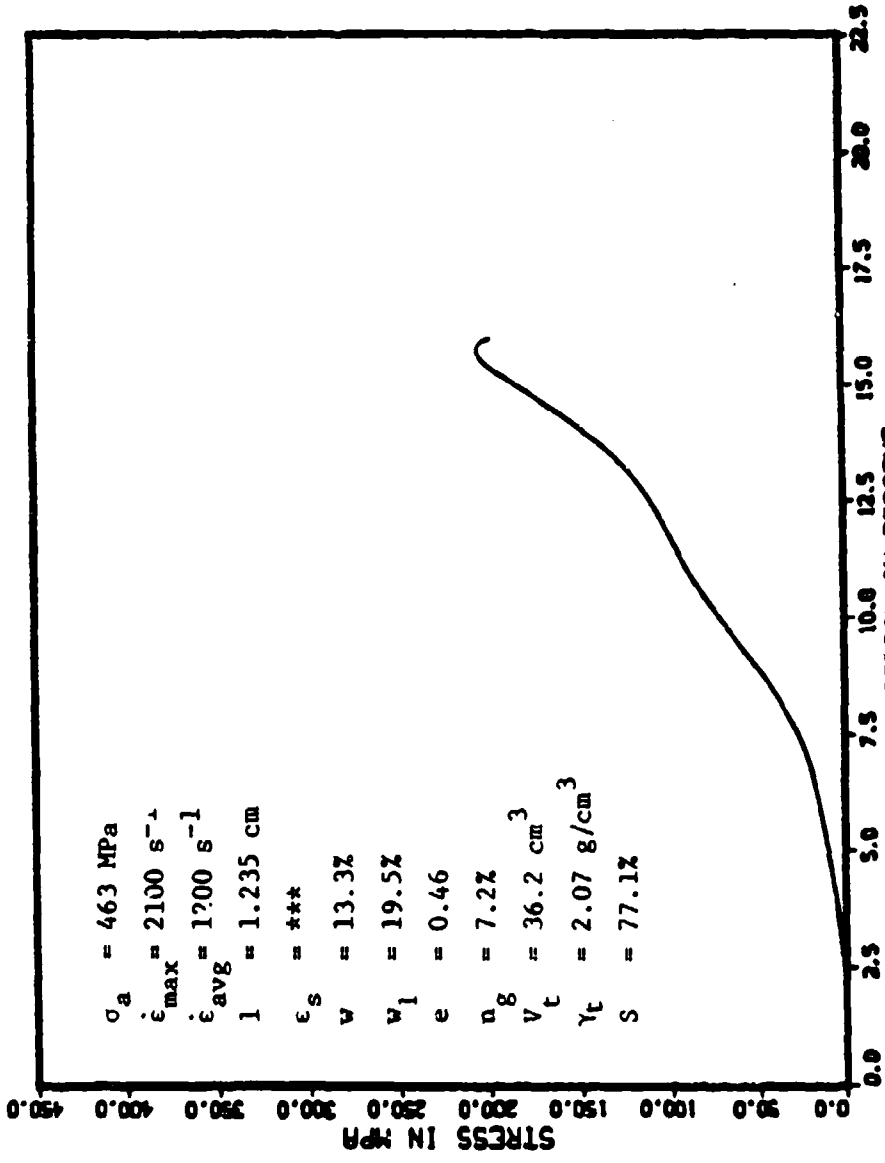

Figure I.6. Stress-strain response for experiment 41.

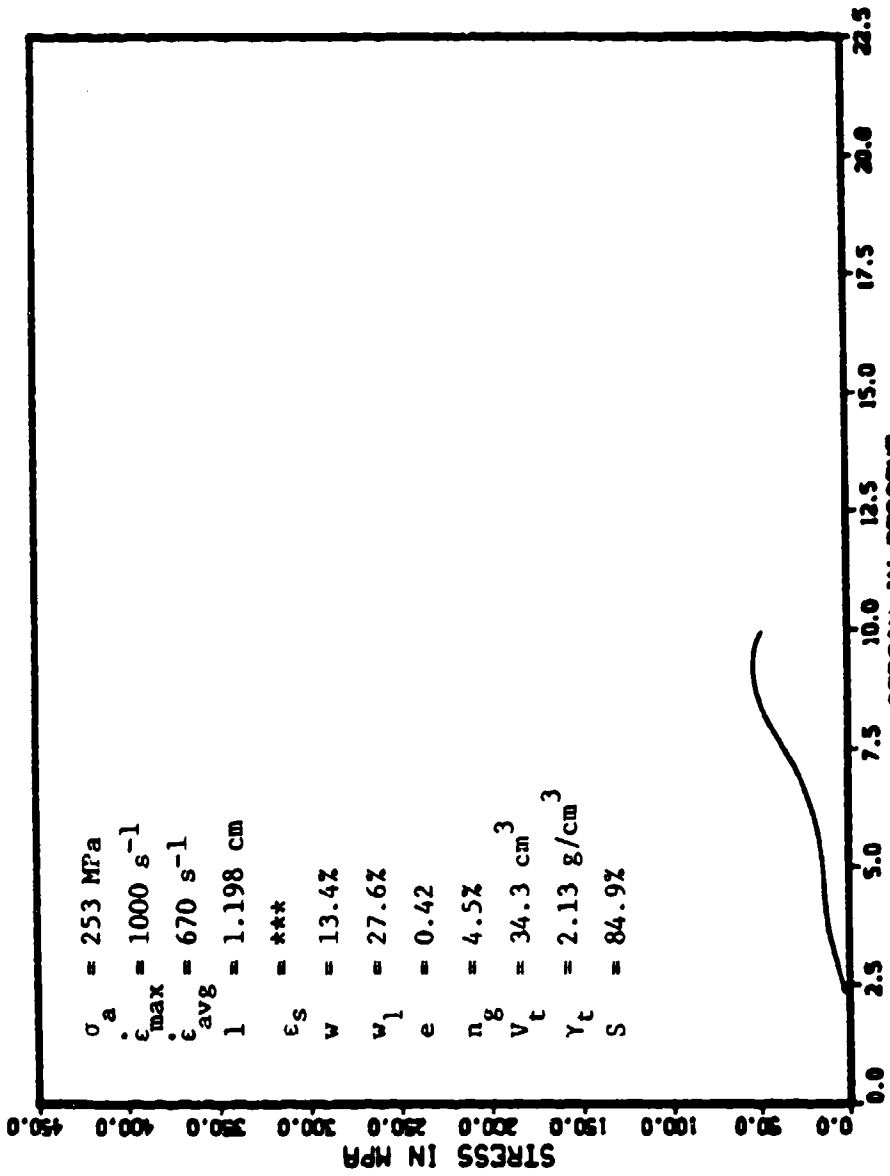

Figure I.7. Stress-strain response for experiment 42.

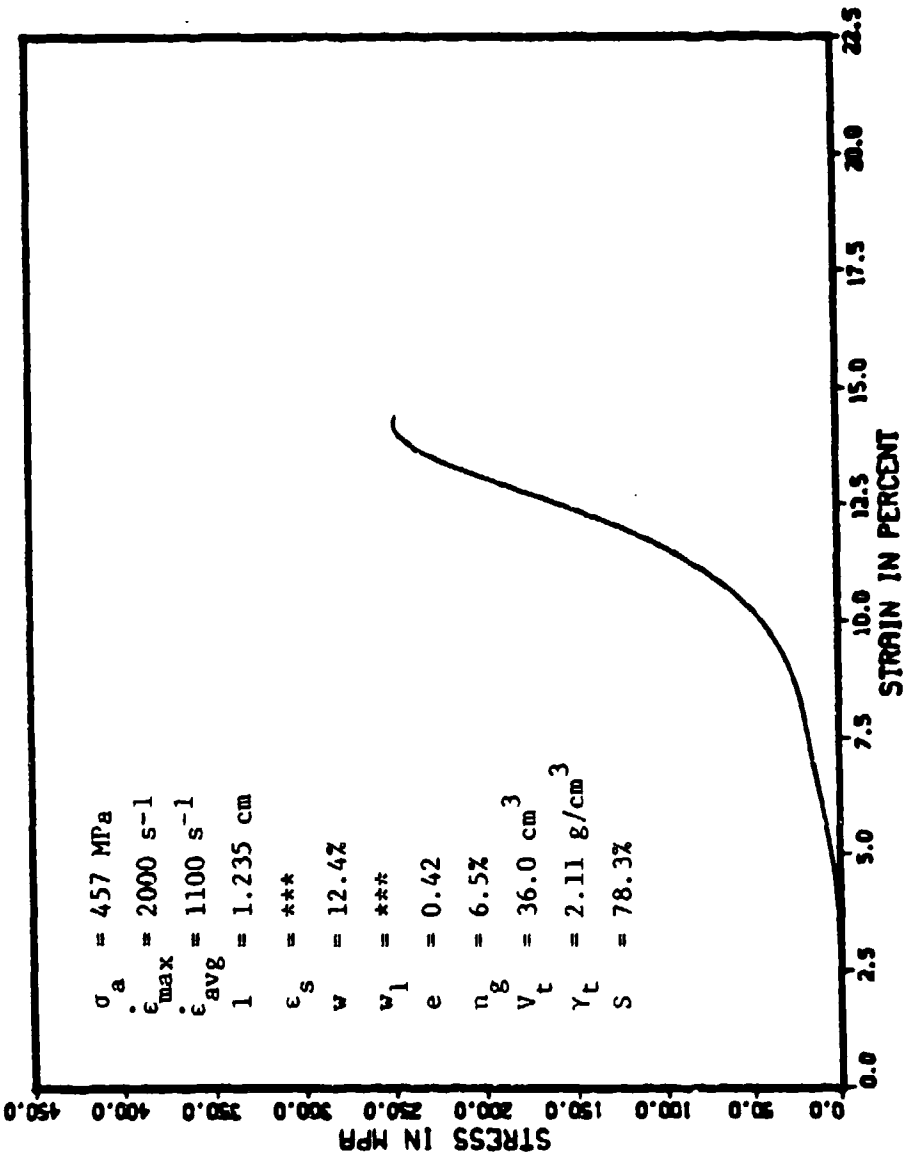

Figure I.8. Stress-strain response for experiment 55.

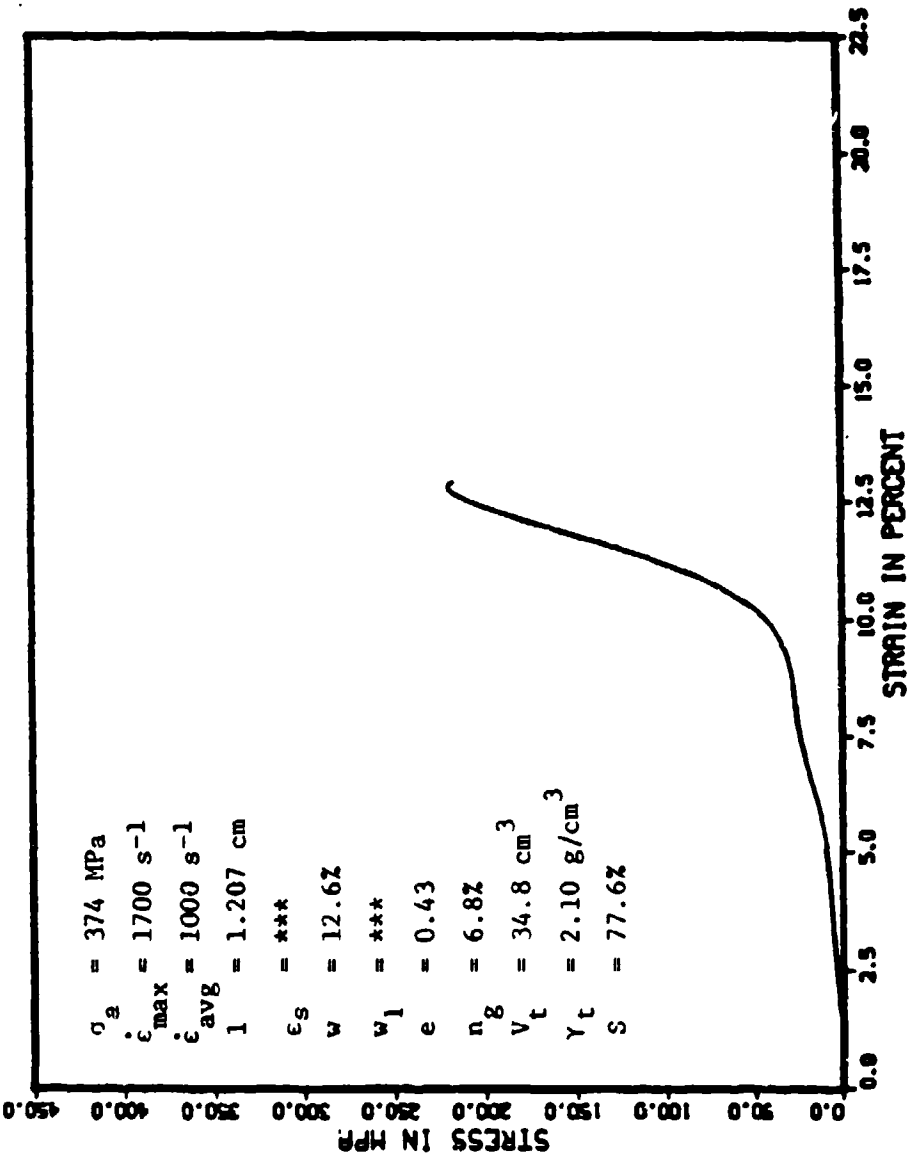

Figure I.9. Stress-strain response for experiment 56.

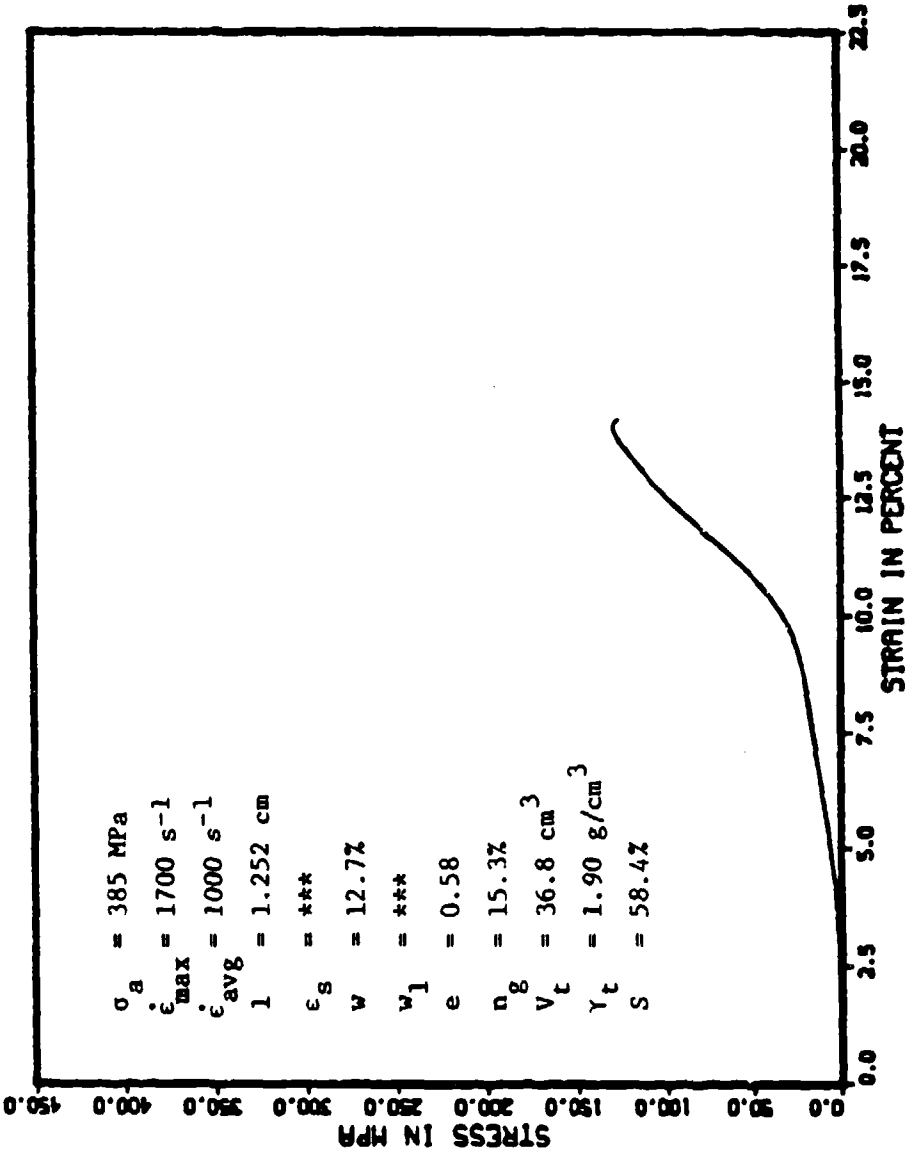

Figure I.10. Stress-strain response for experiment 57.

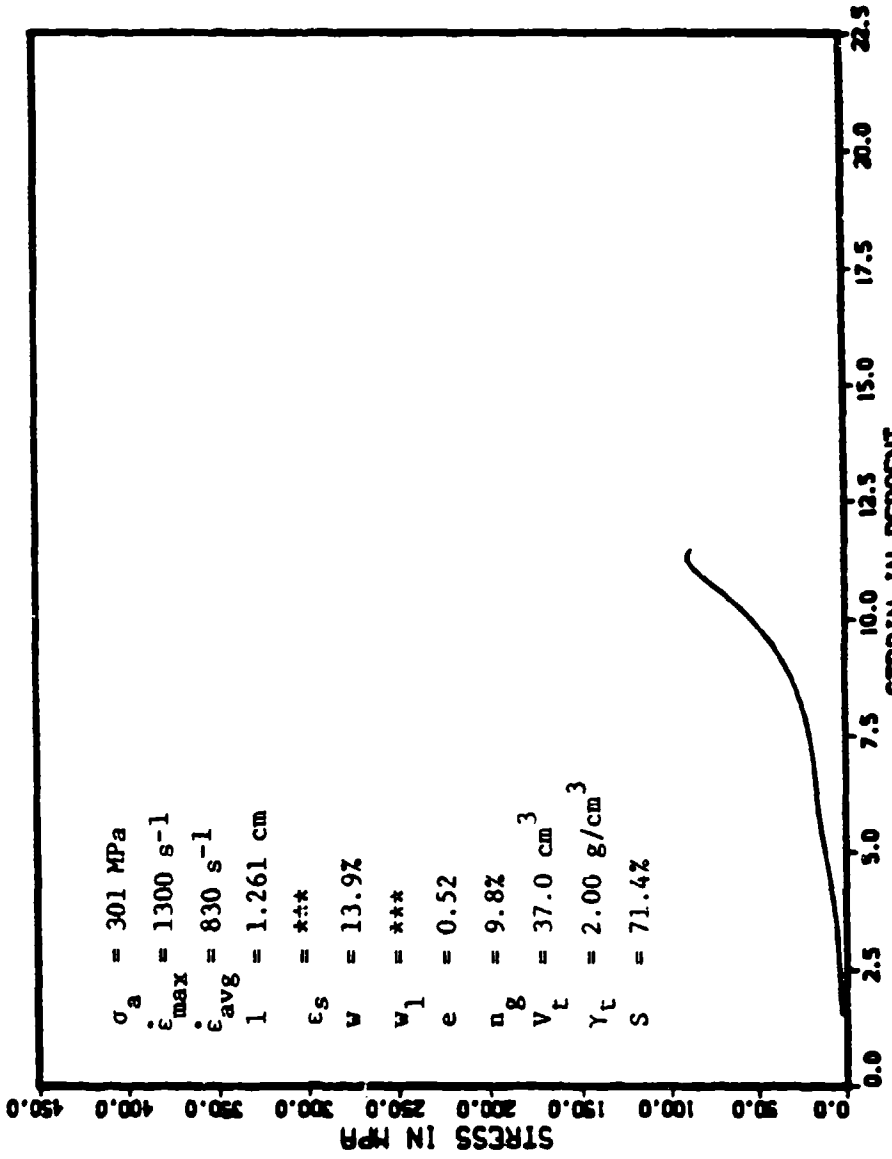

Figure I.11. Stress-strain response for experiment 58.

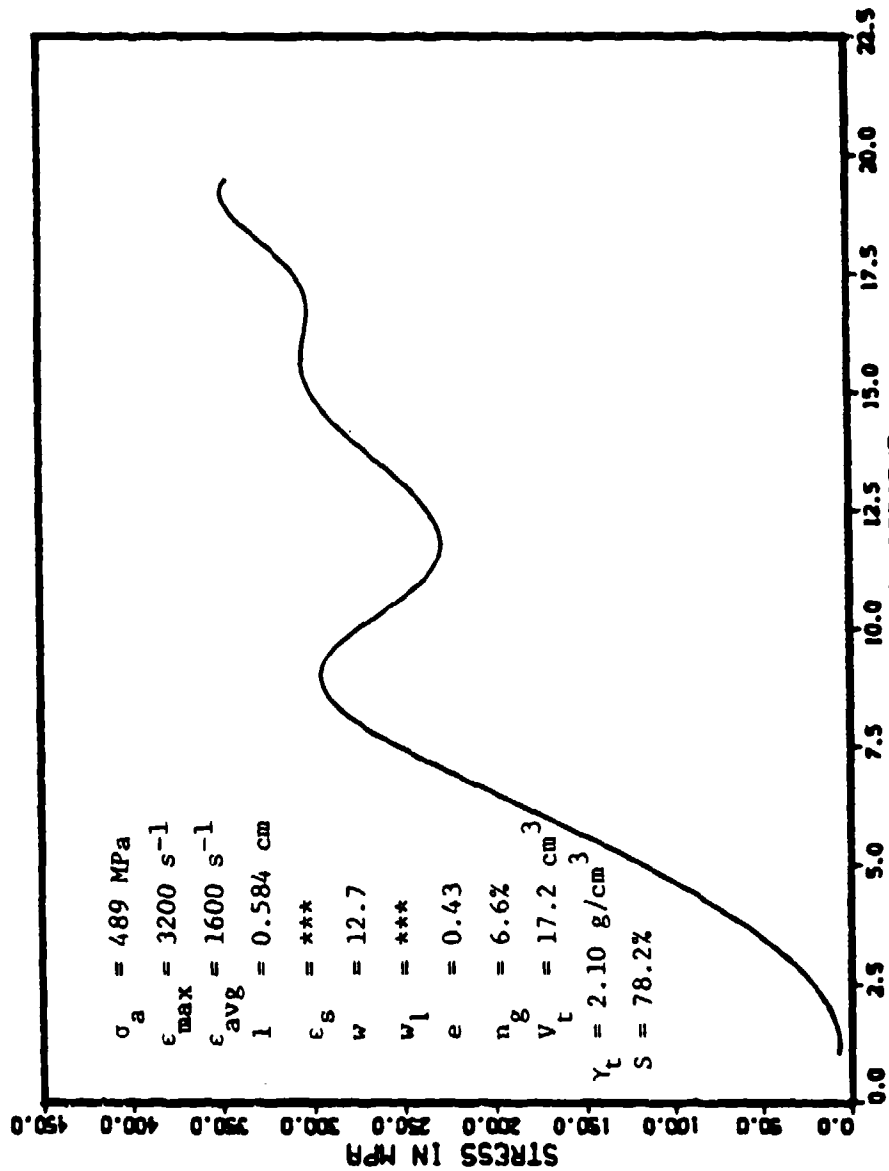

Figure I.12. Stress-strain response for experiment 59.

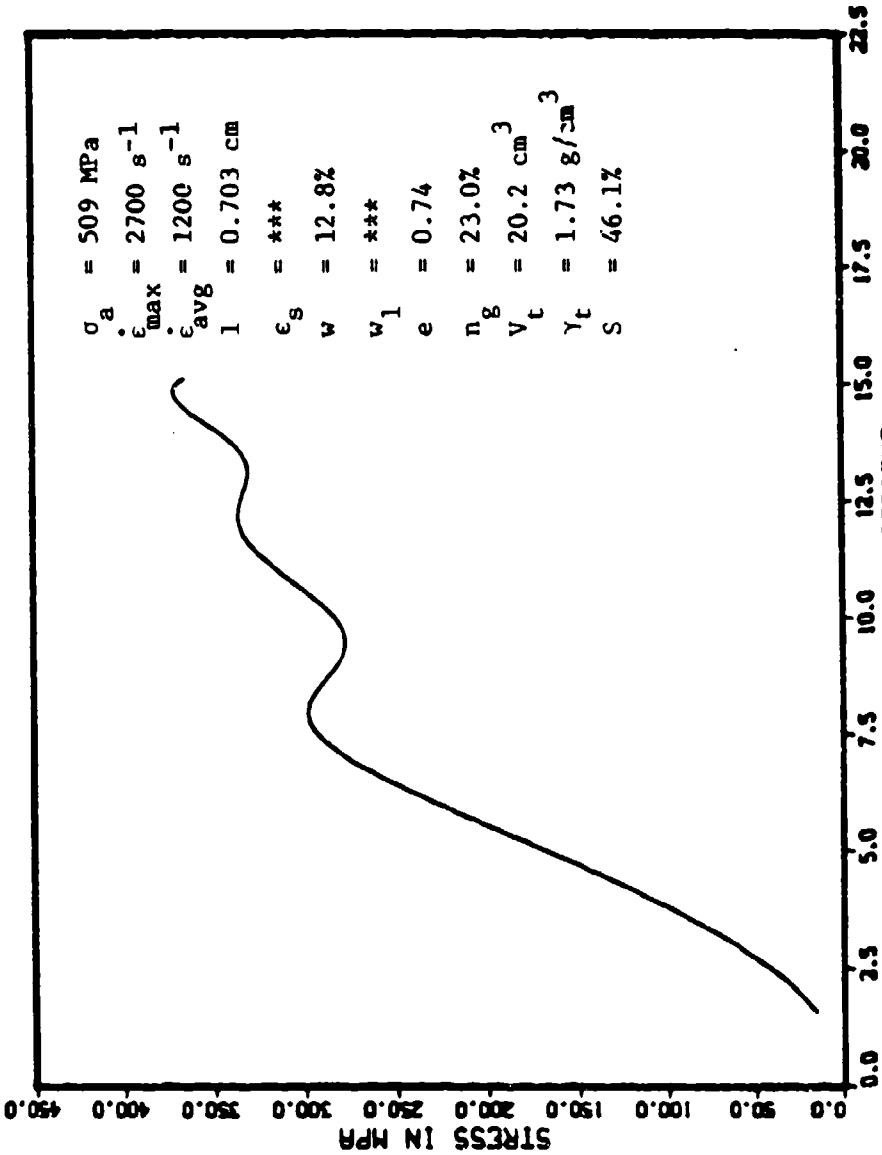

Figure I.13. Stress-strain response for experiment 60.

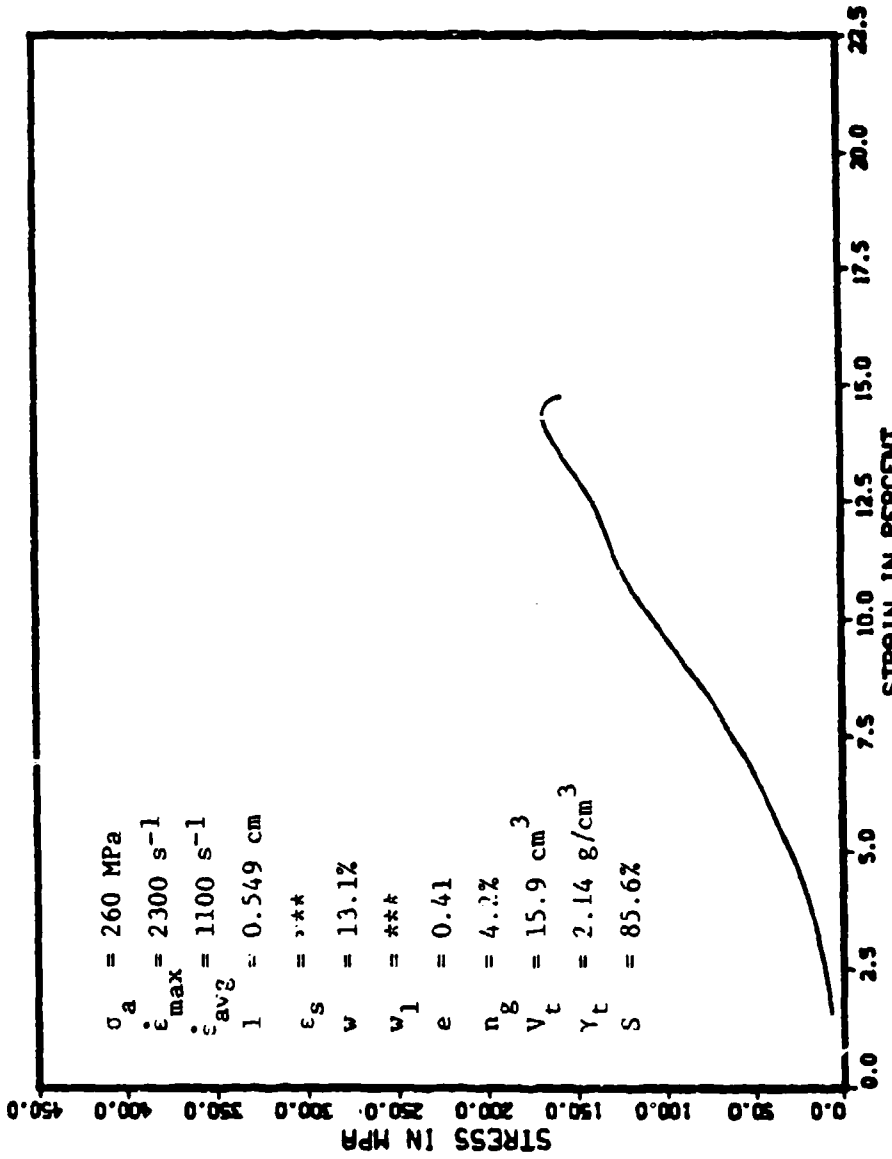

Figure I.14. Stress-strain response for experiment 61.

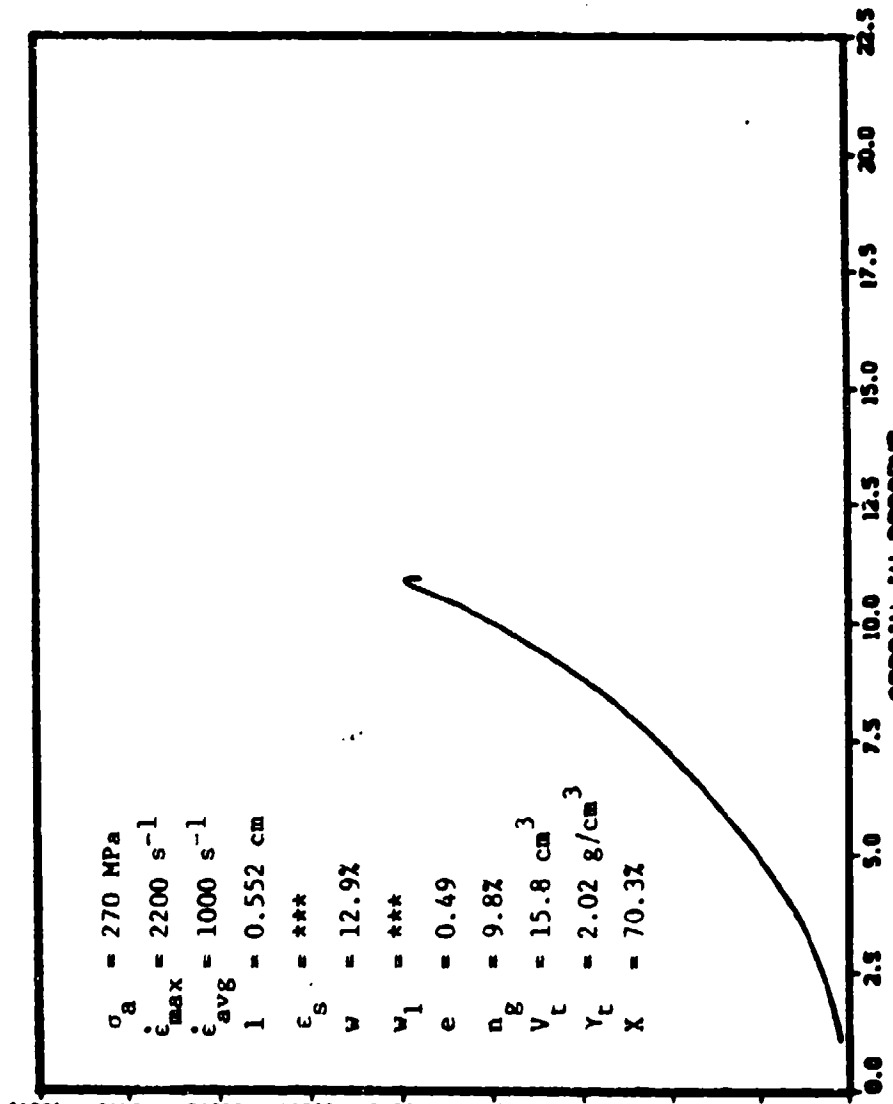

Figure I.15. Stress-strain response for experiment 62.

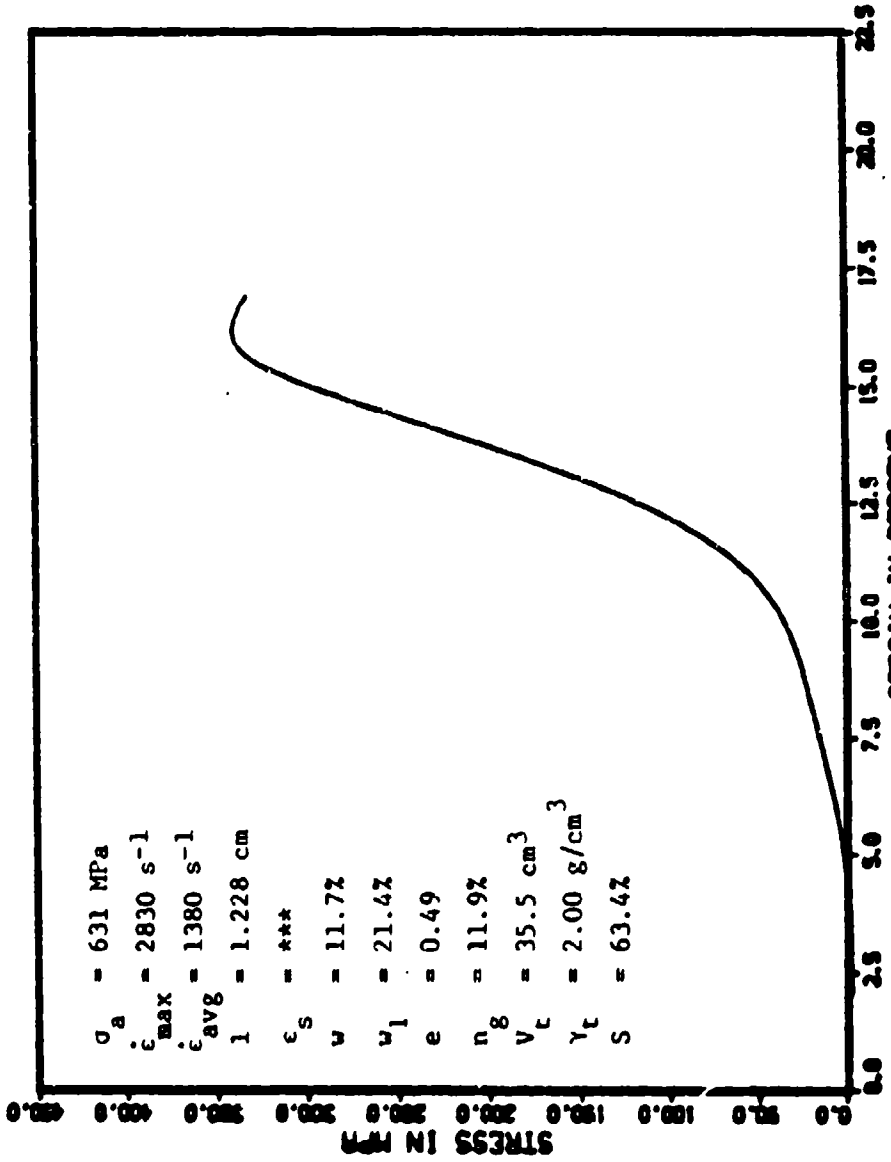

Figure I.16. Stress-strain response for experiment 71.

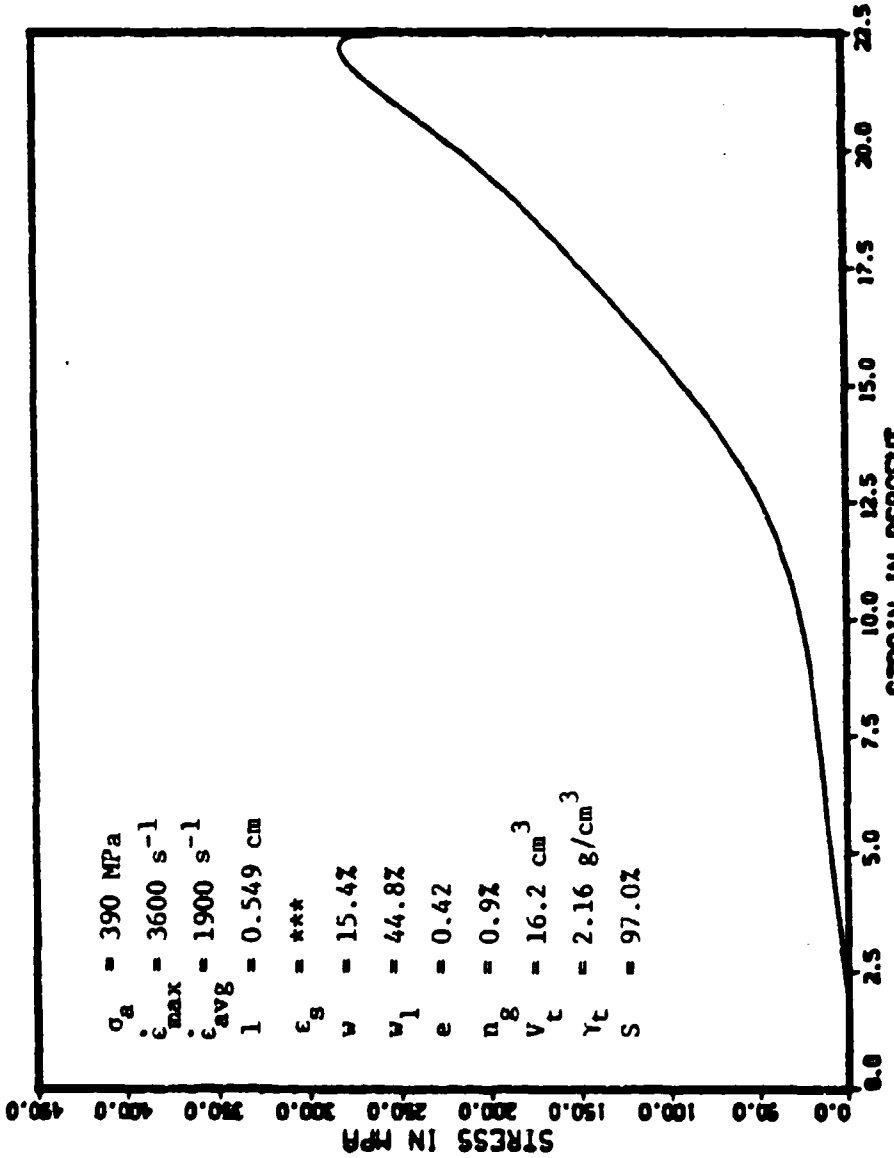

Figure I.17. Stress-strain response for experiment 72.

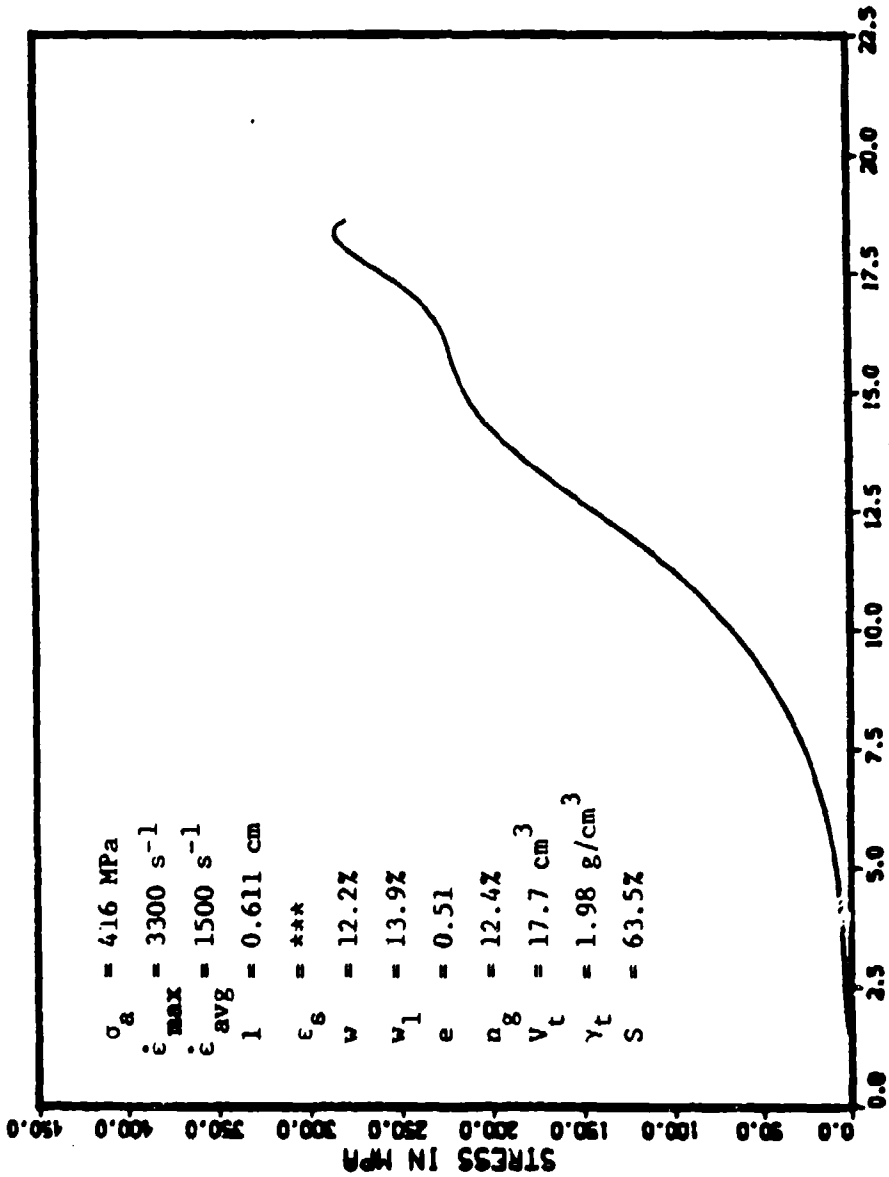

Figure I.18. Stress-strain response for experiment 73.

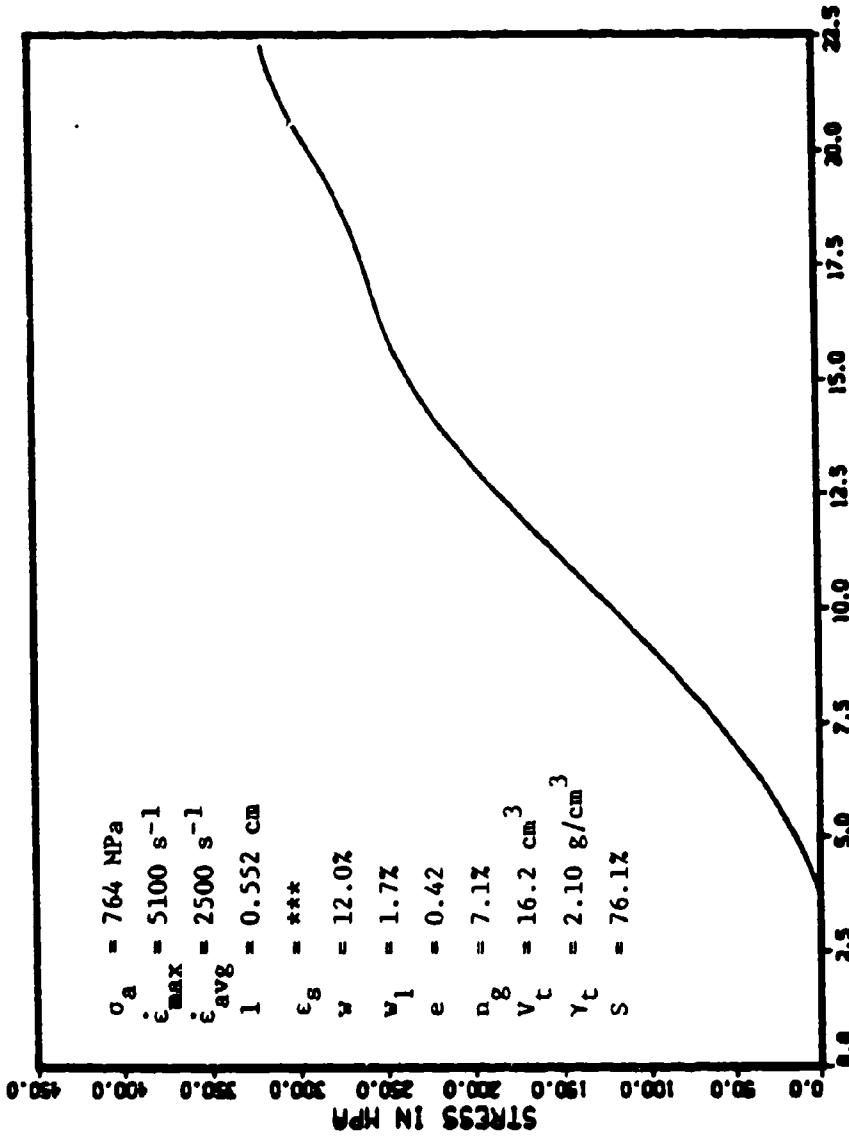

Figure I.19. Stress-strain response for experiment 74.

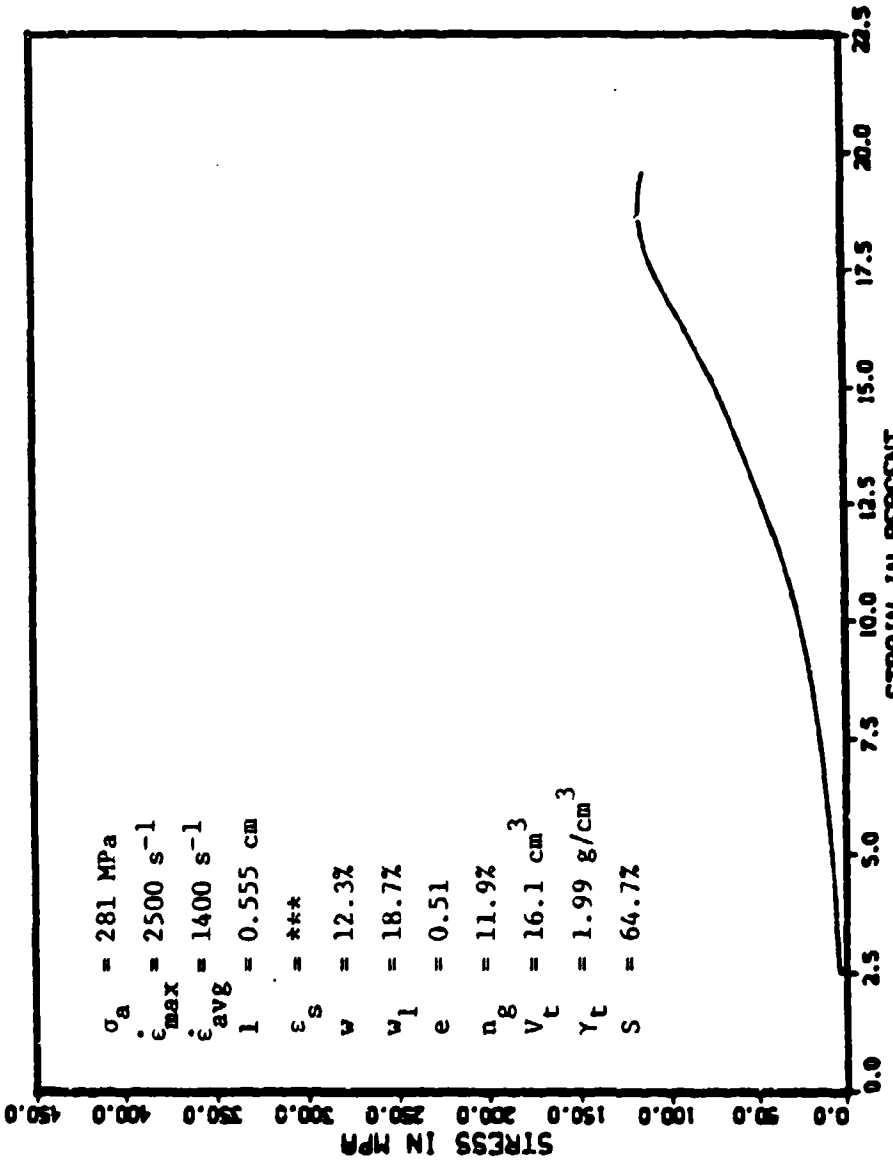

Figure I.20. Stress-strain response for experiment 75.

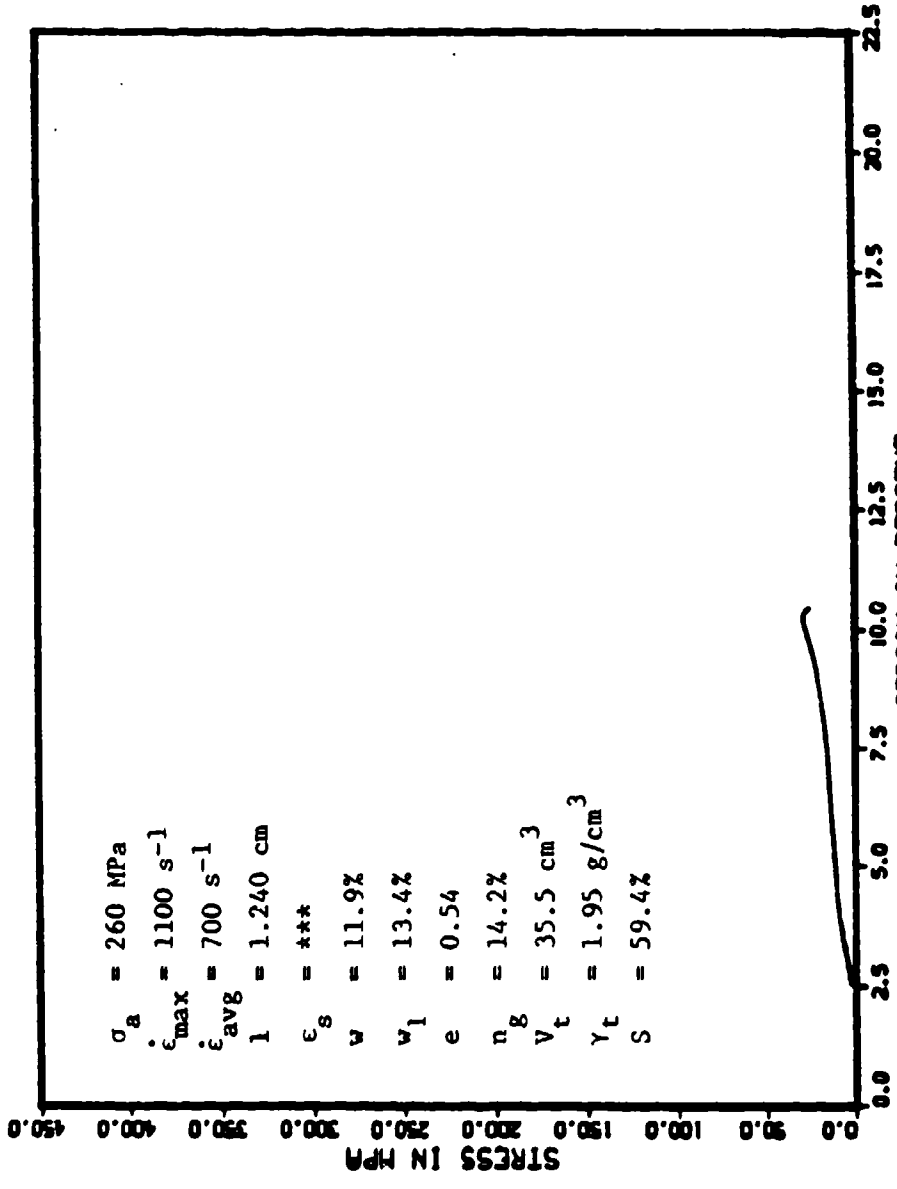

Figure I.21. Stress-strain response for experiment 76.

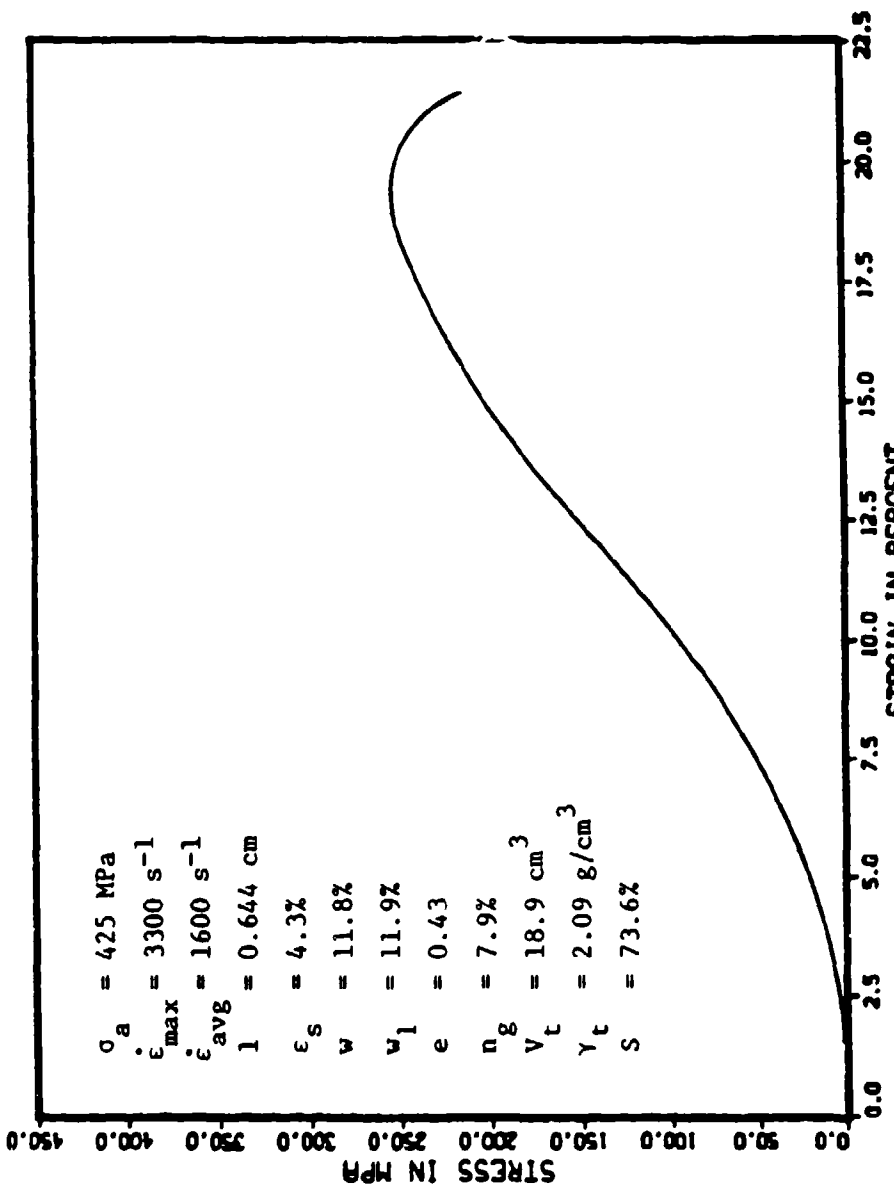

Figure I.22. Stress-strain response for experiment 112.

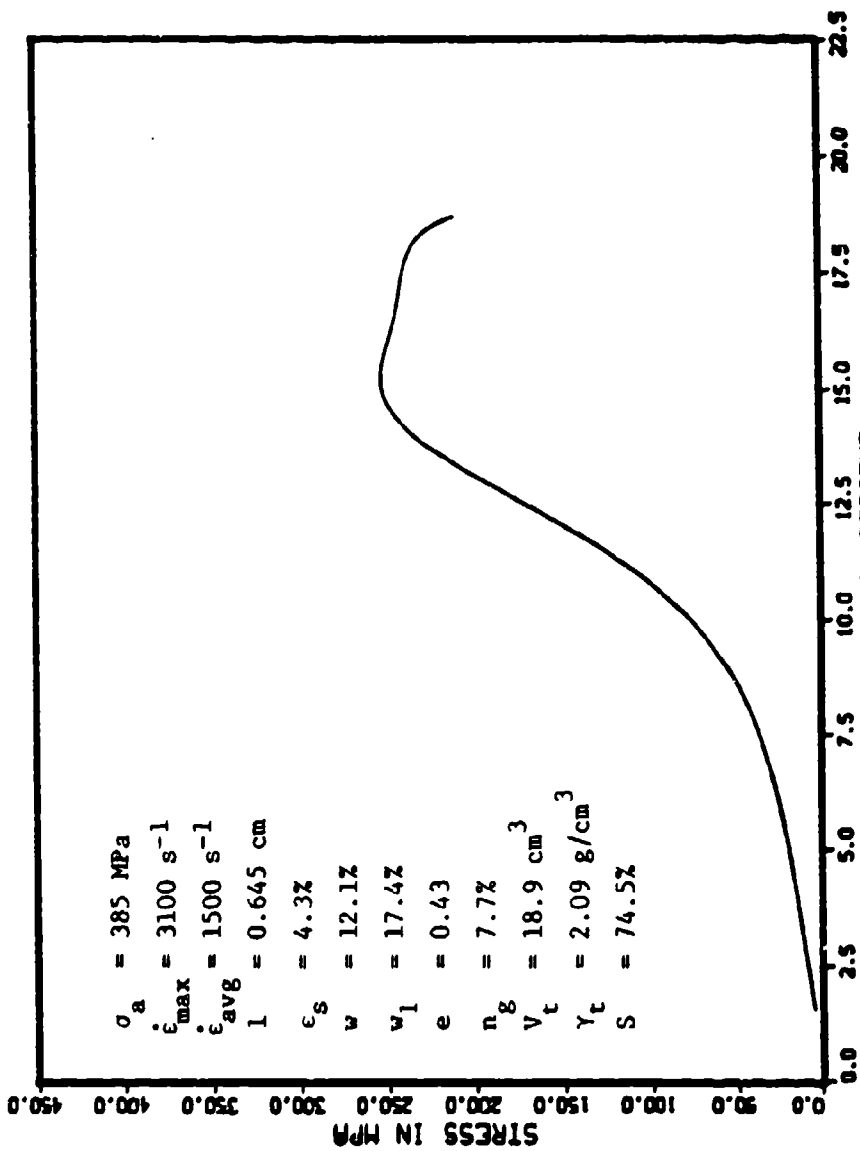

Figure I.23. Stress-strain response for experiment 113.

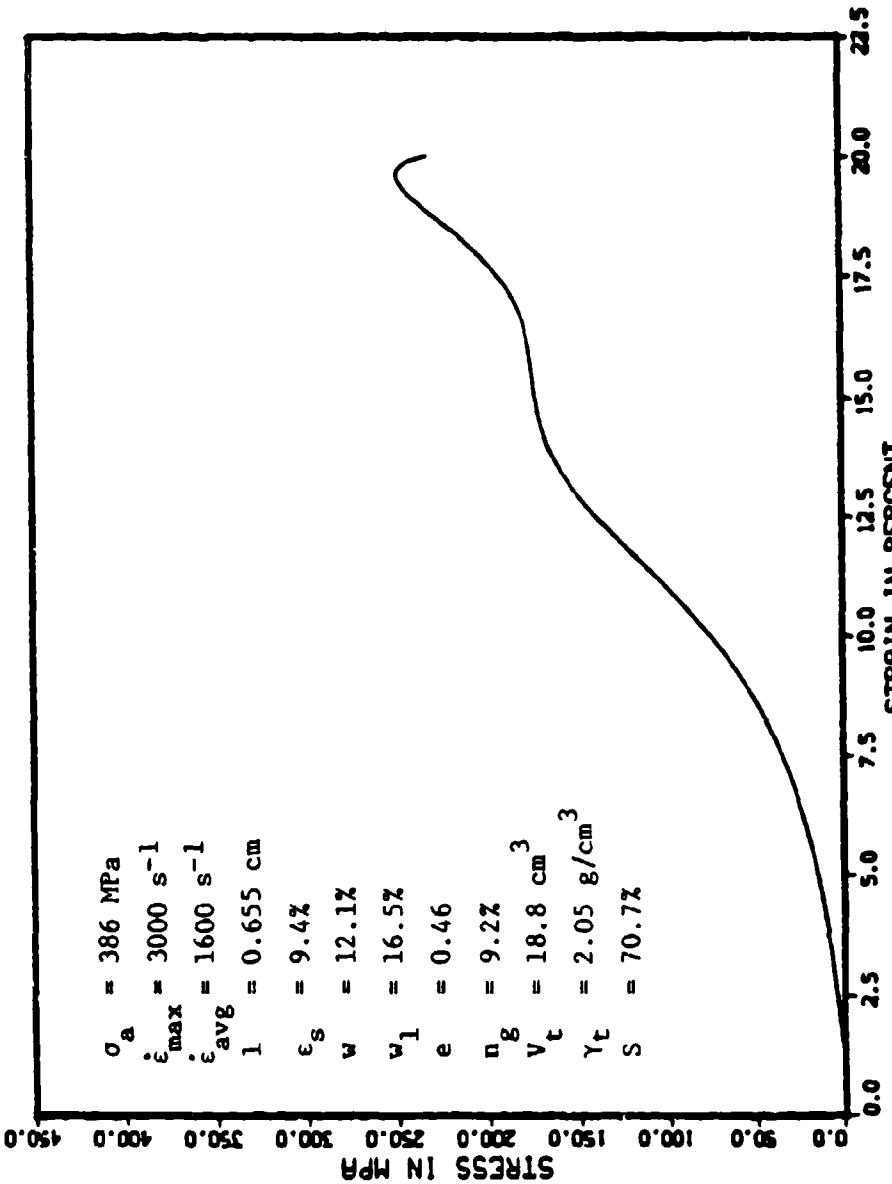

Figure I.24. Stress-strain response for experiment 114.

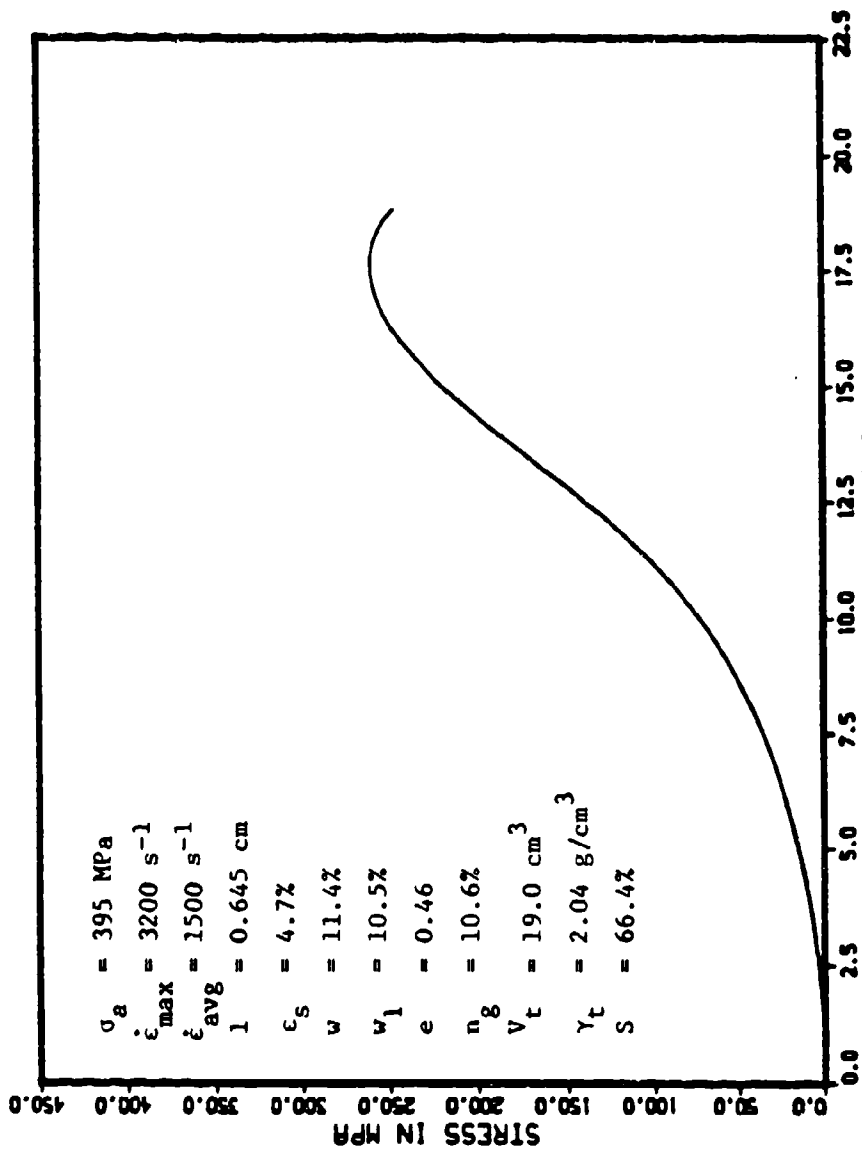

Figure I.25. Stress-strain response for experiment 115.

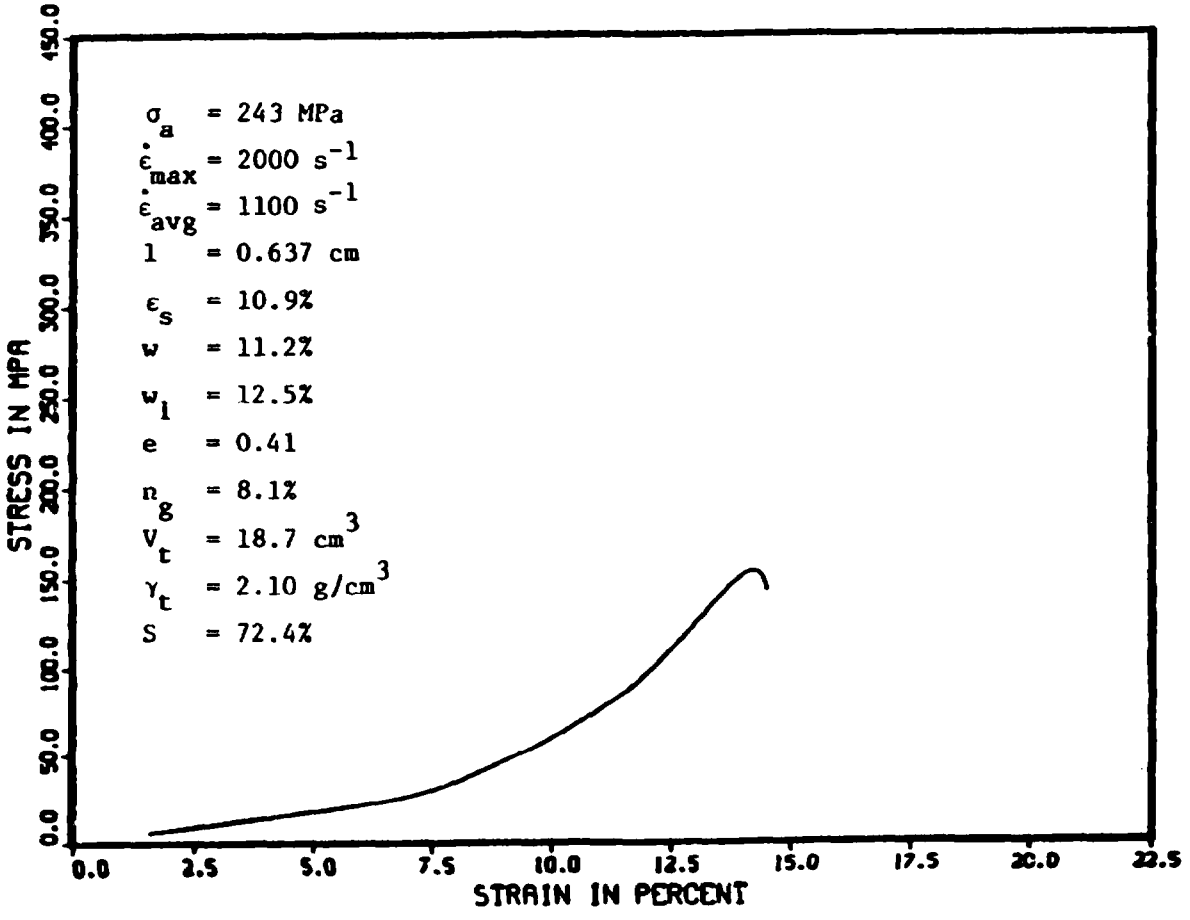

Figure I.26. Stress-strain response for experiment 116.

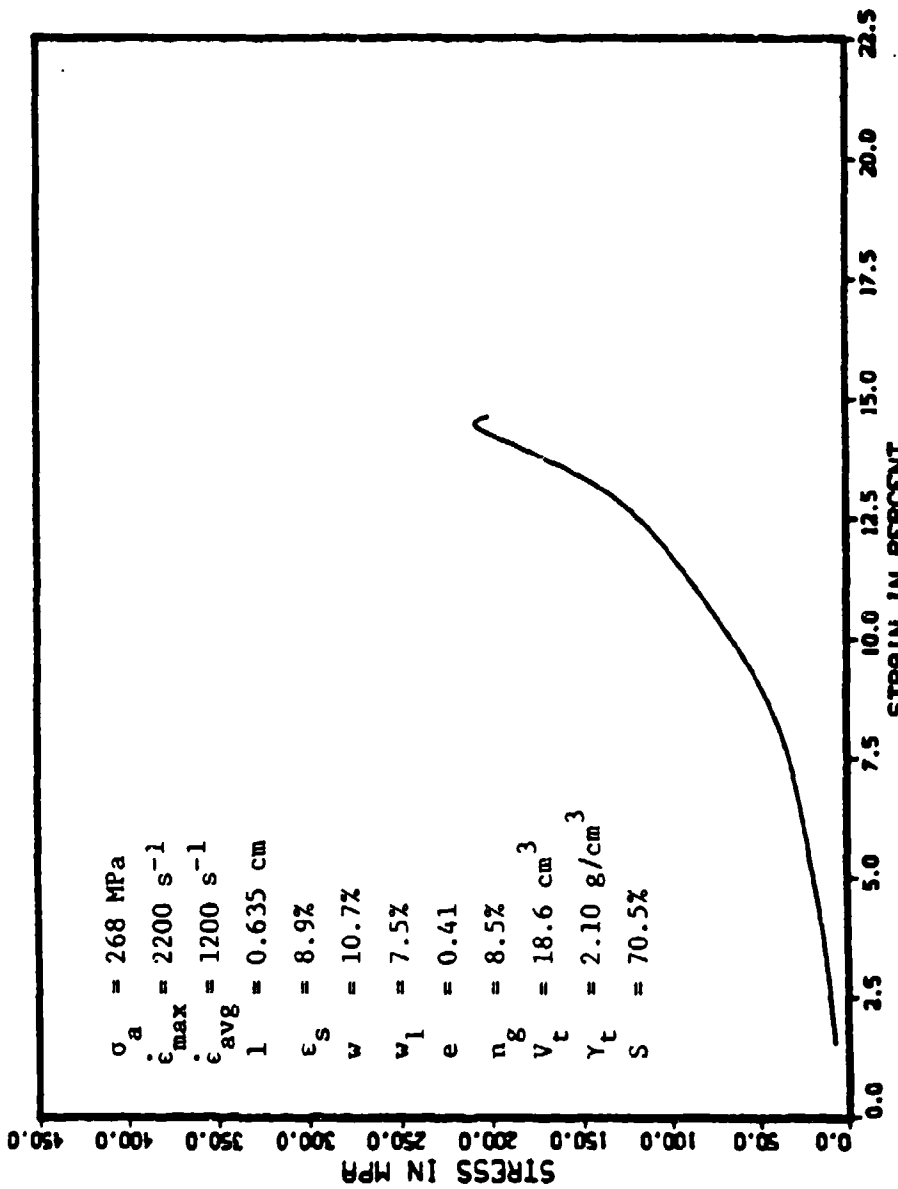

Figure I.27. Stress-strain response for experiment 117.

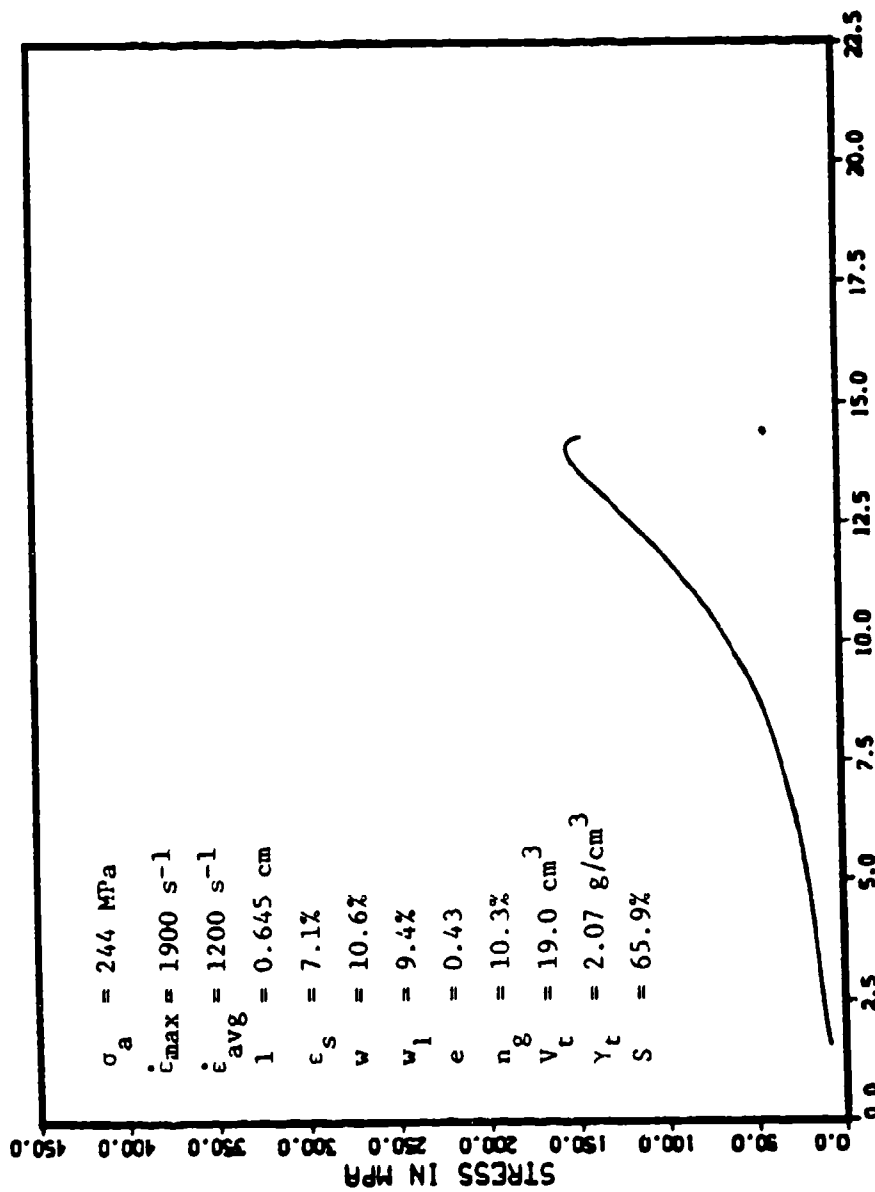

Figure I.28. Stress-strain response for experiment 118.

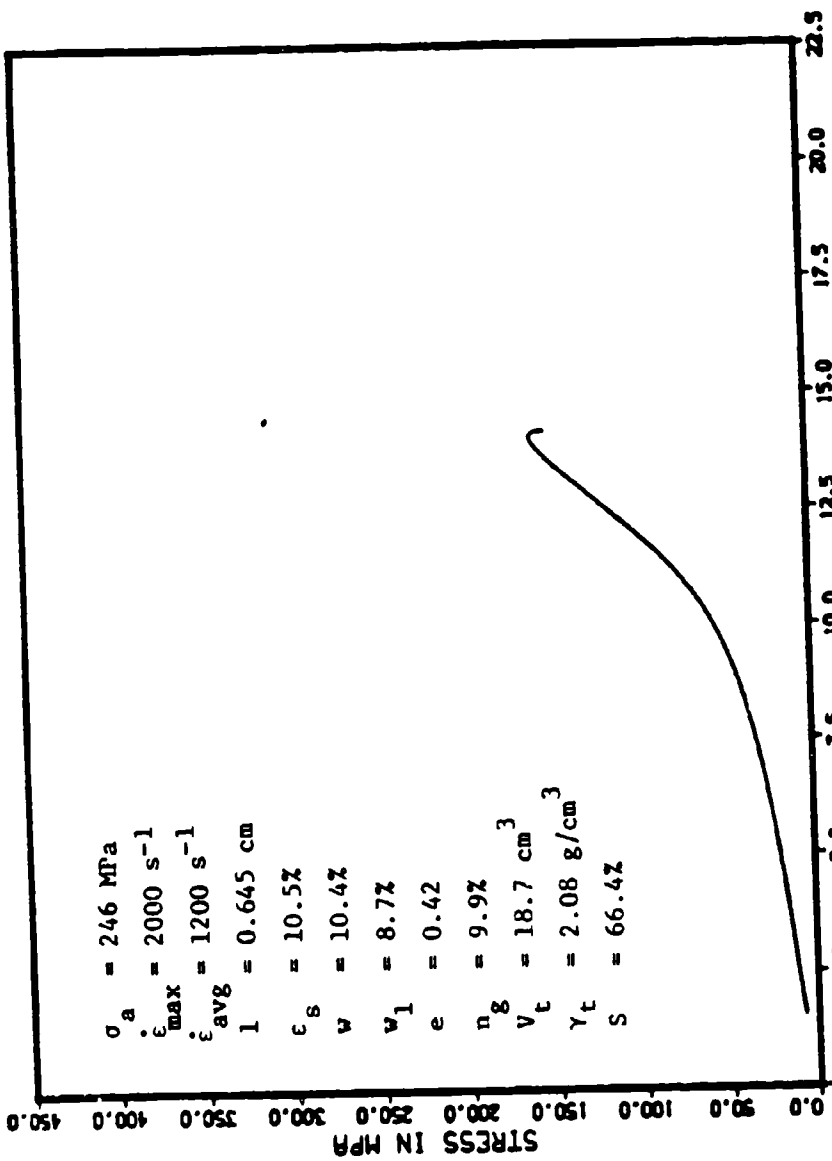

Figure I.29. Stress-strain response for experiment 119.

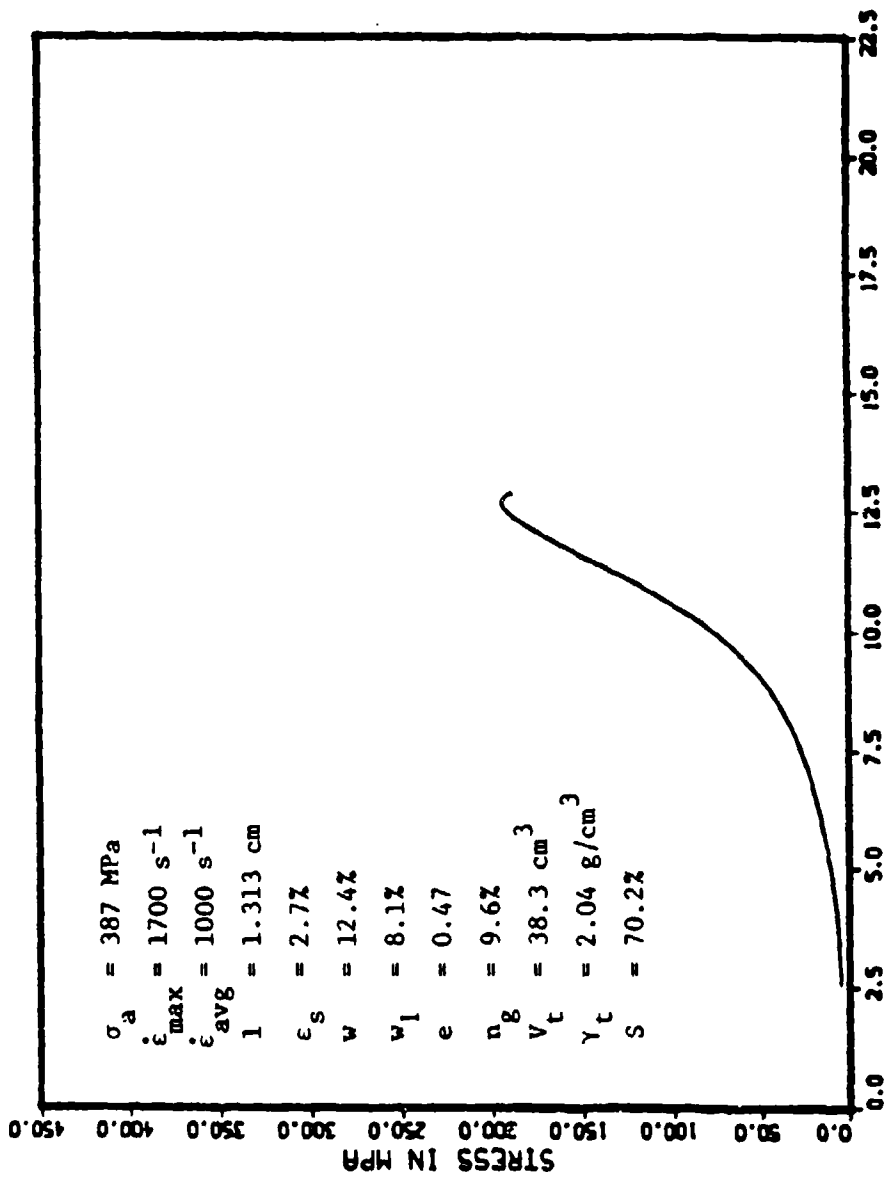

Figure I.30. Stress-strain response for experiment 131.

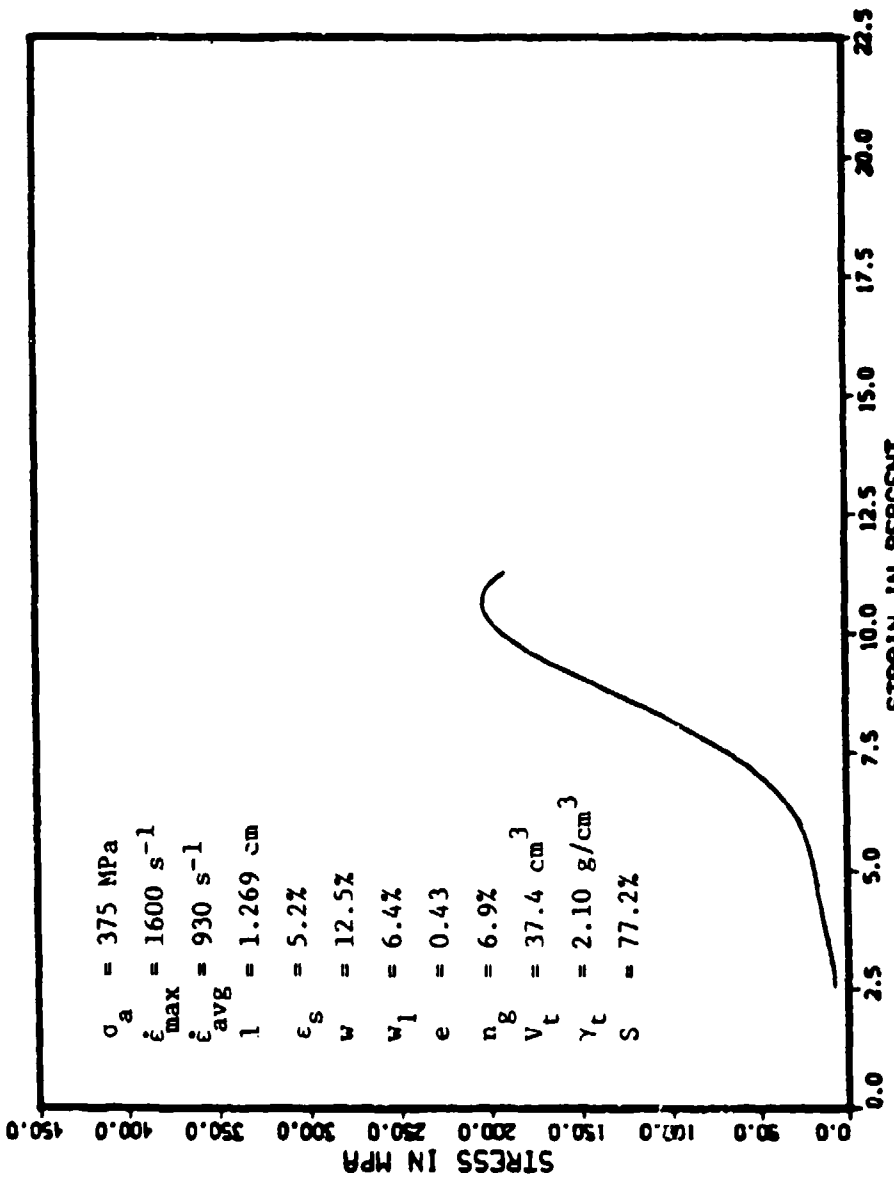

Figure I.31. Stress-strain response for experiment 132.

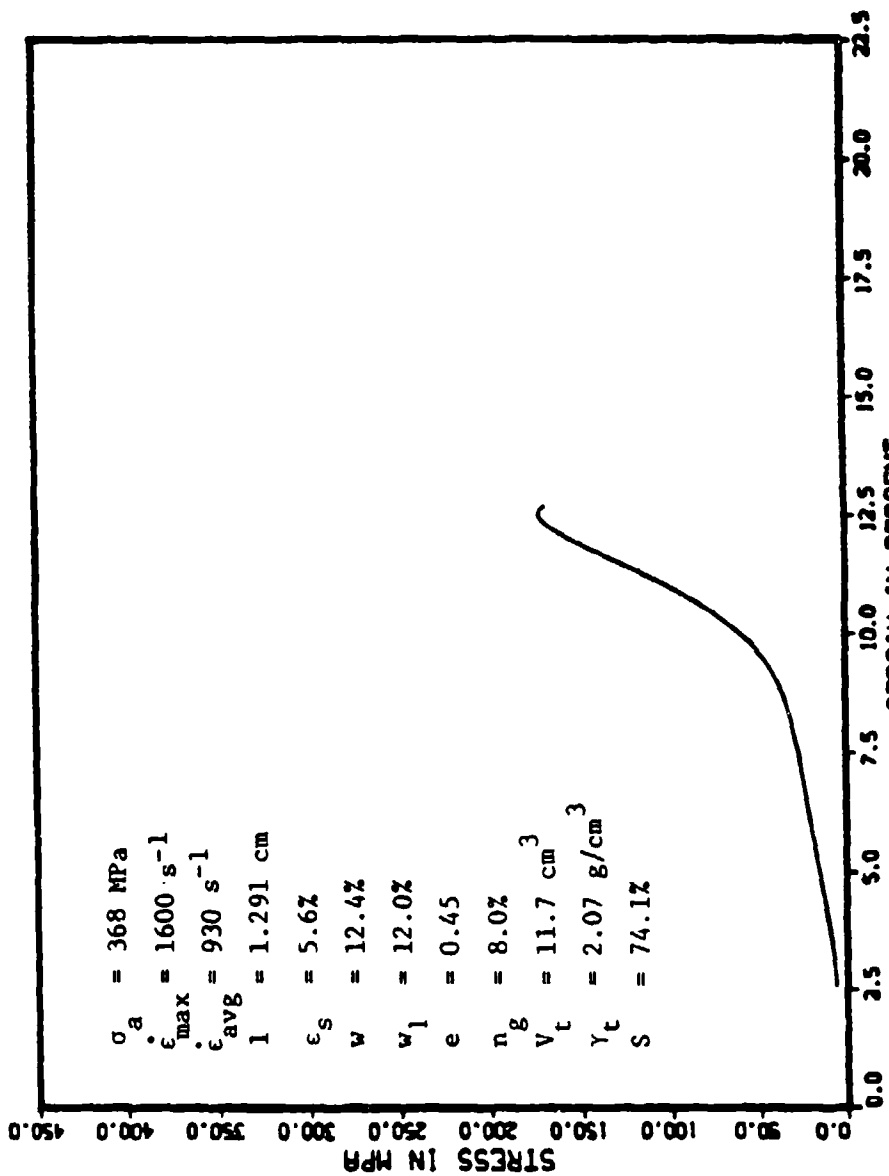

Figure I.32. Stress-strain response for experiment 133.

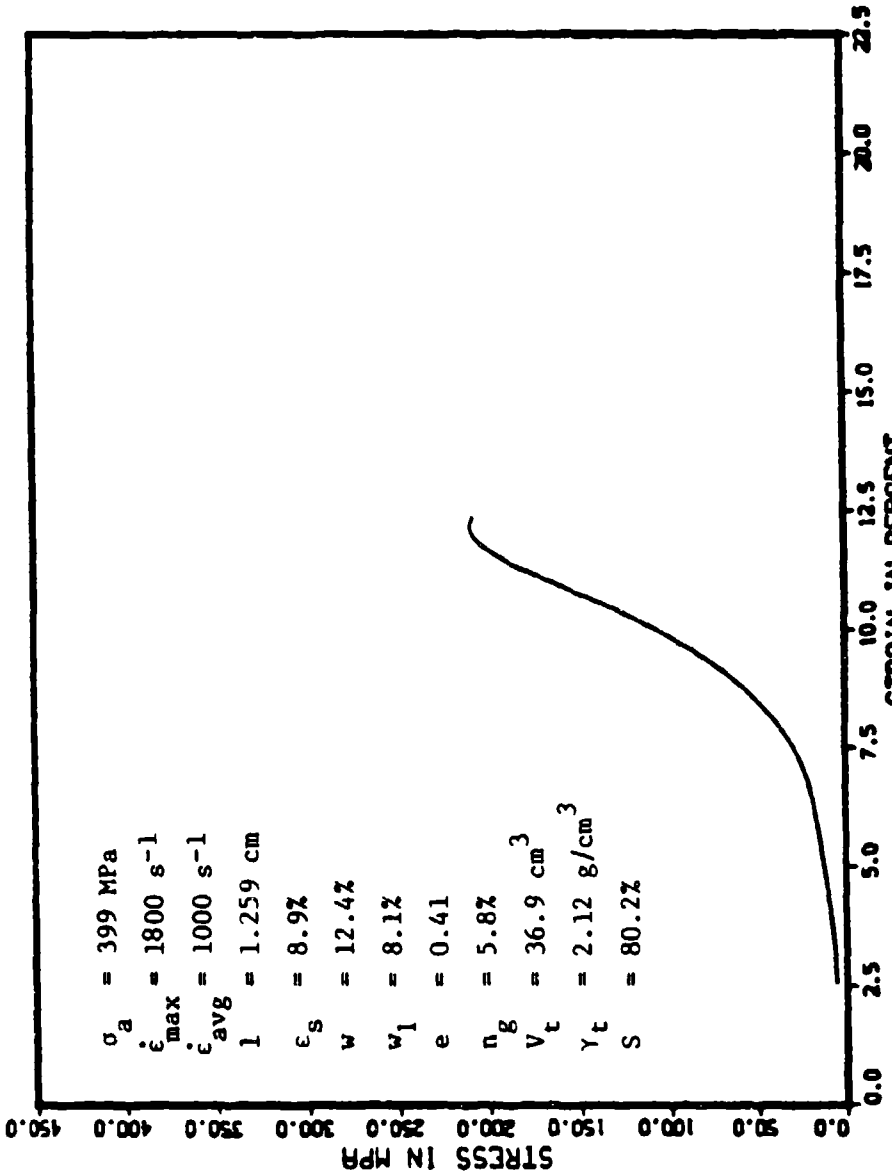

Figure I.33. Stress-strain response for experiment 134.

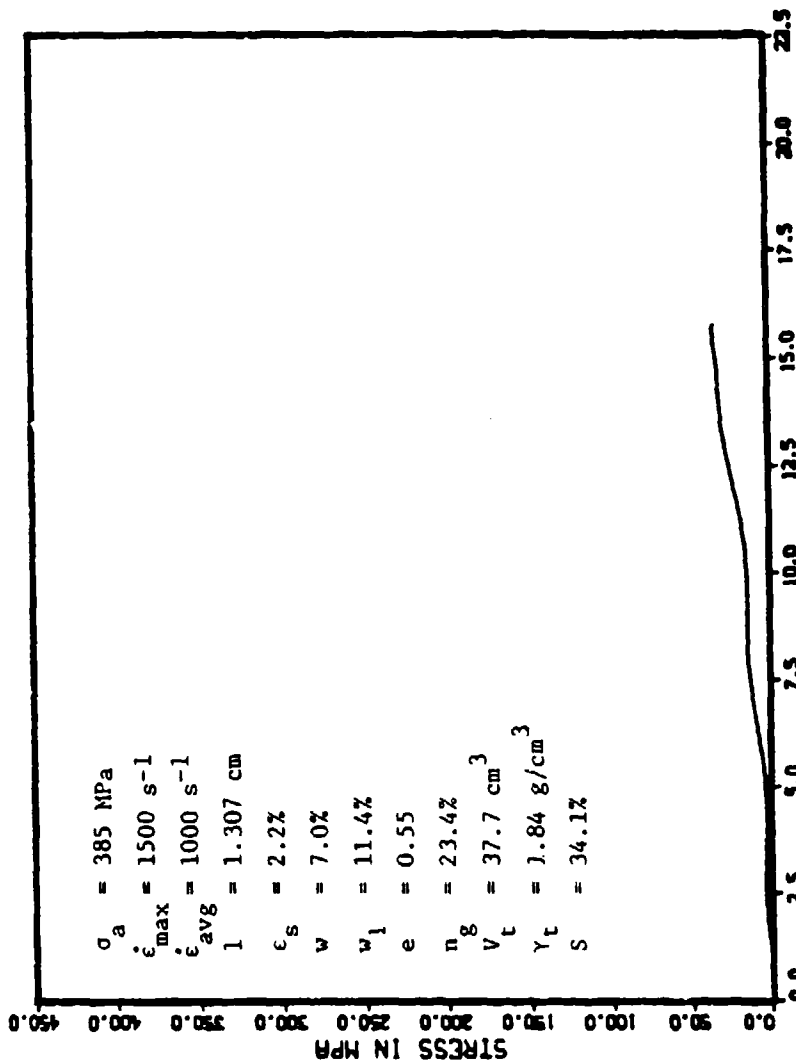

Figure I.34. Stress-strain response for experiment 135.

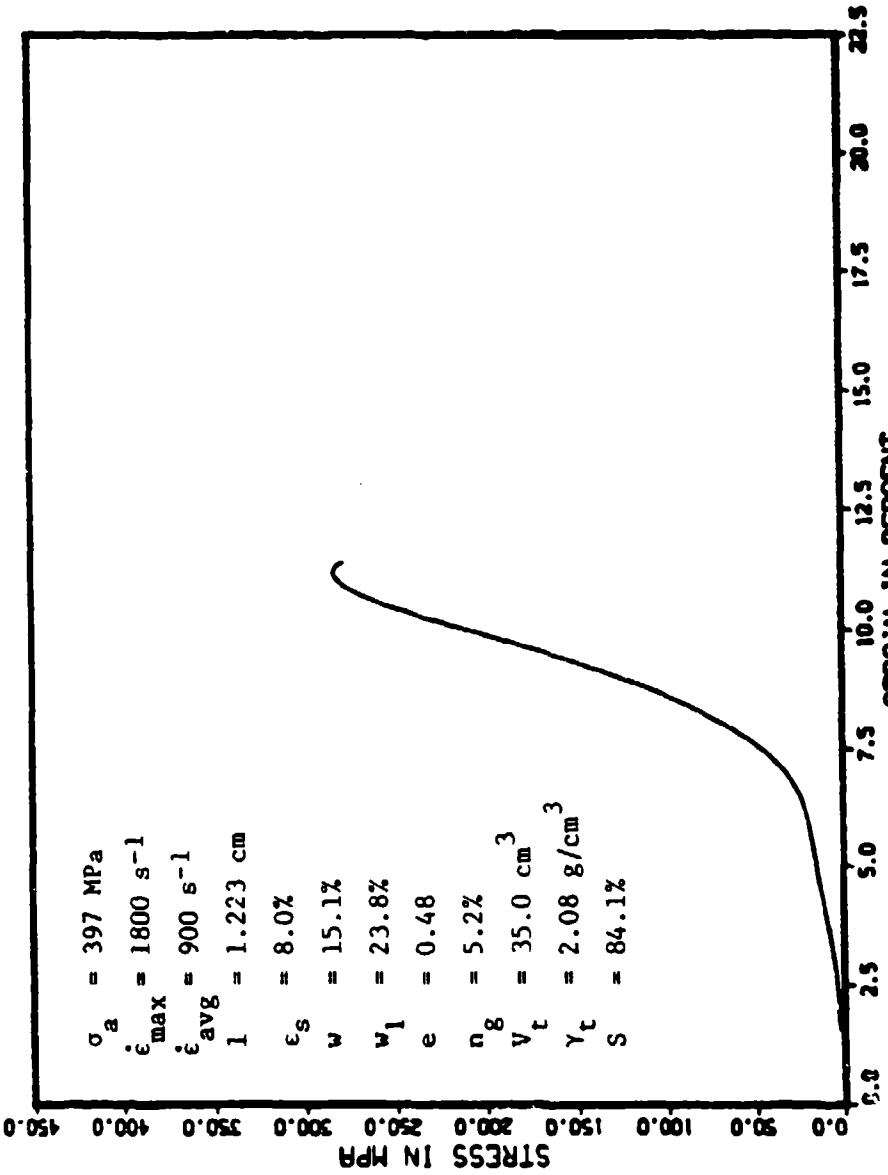

Figure I.35. Stress-strain response for experiment 136.

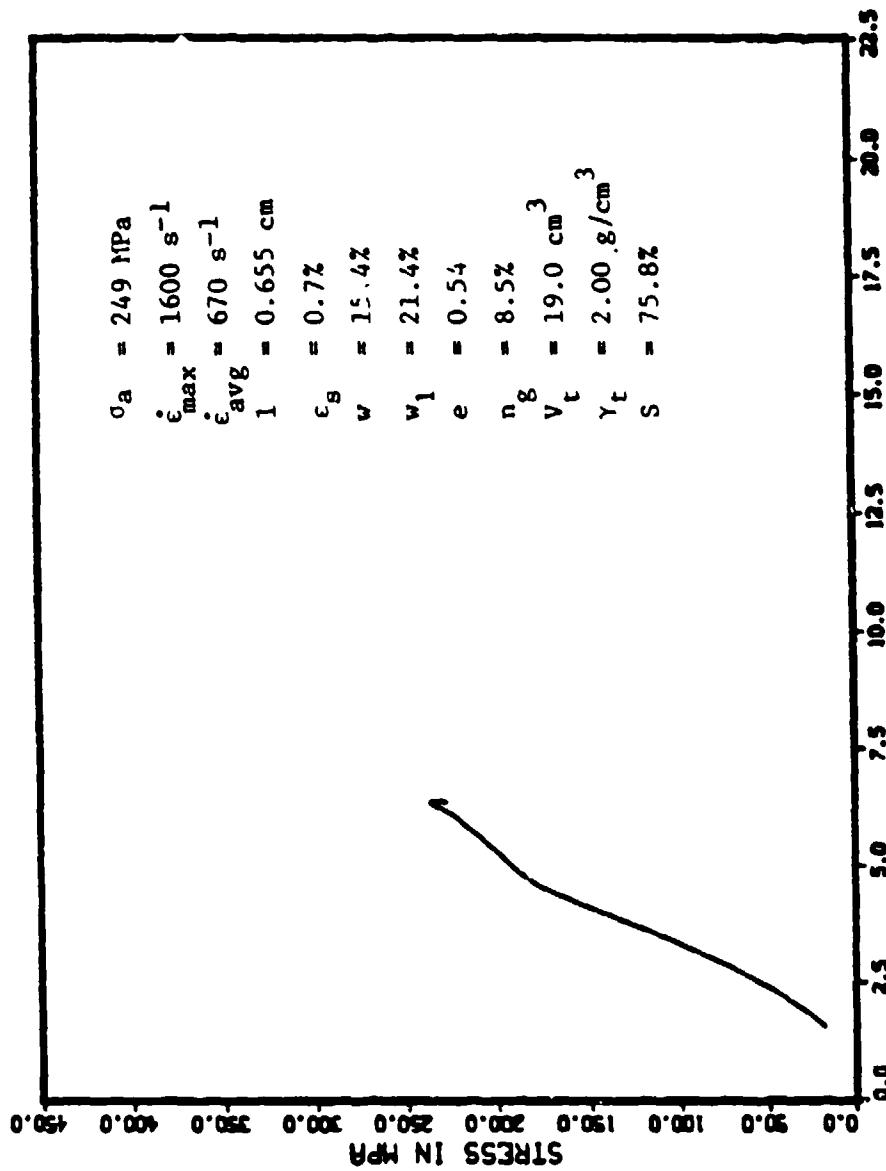

Figure I.36. Stress-strain response for experiment 137.

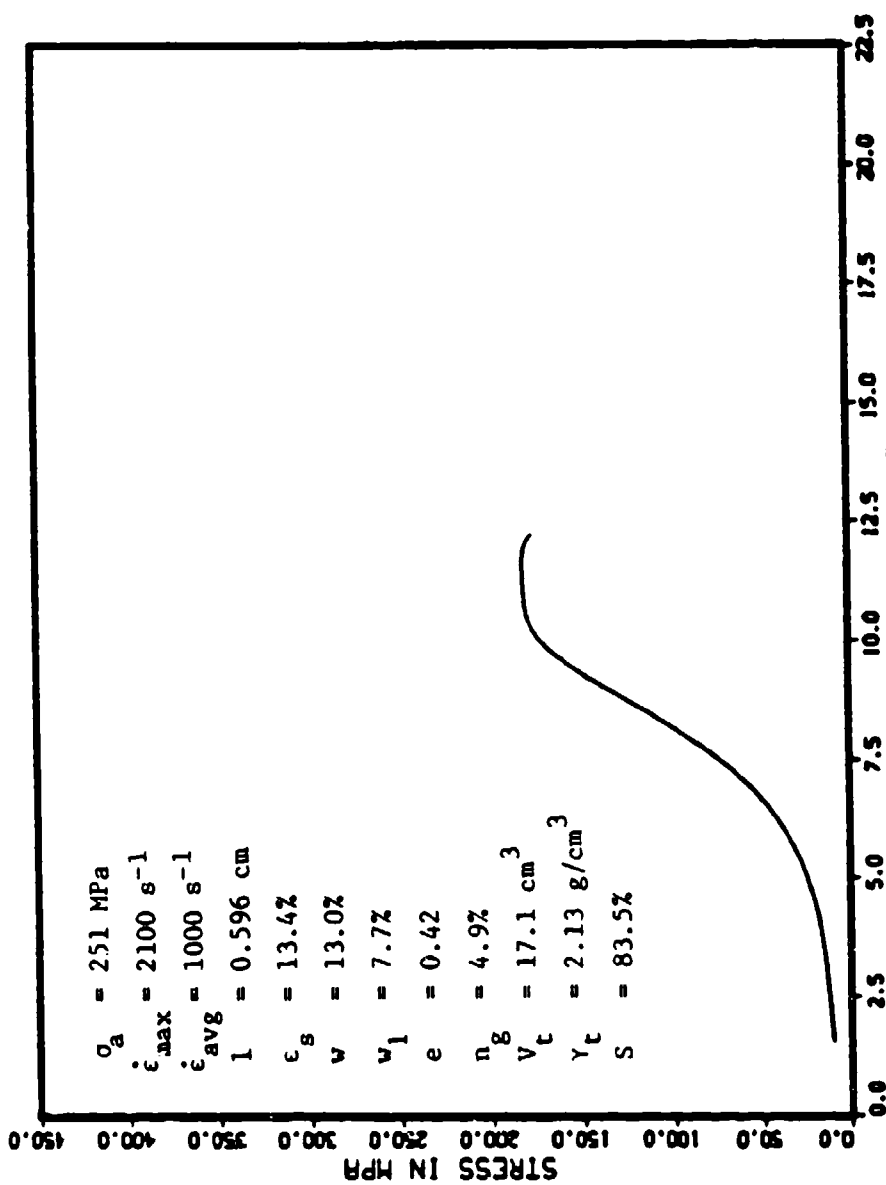

Figure I.37. Stress-strain response for experiment 138.

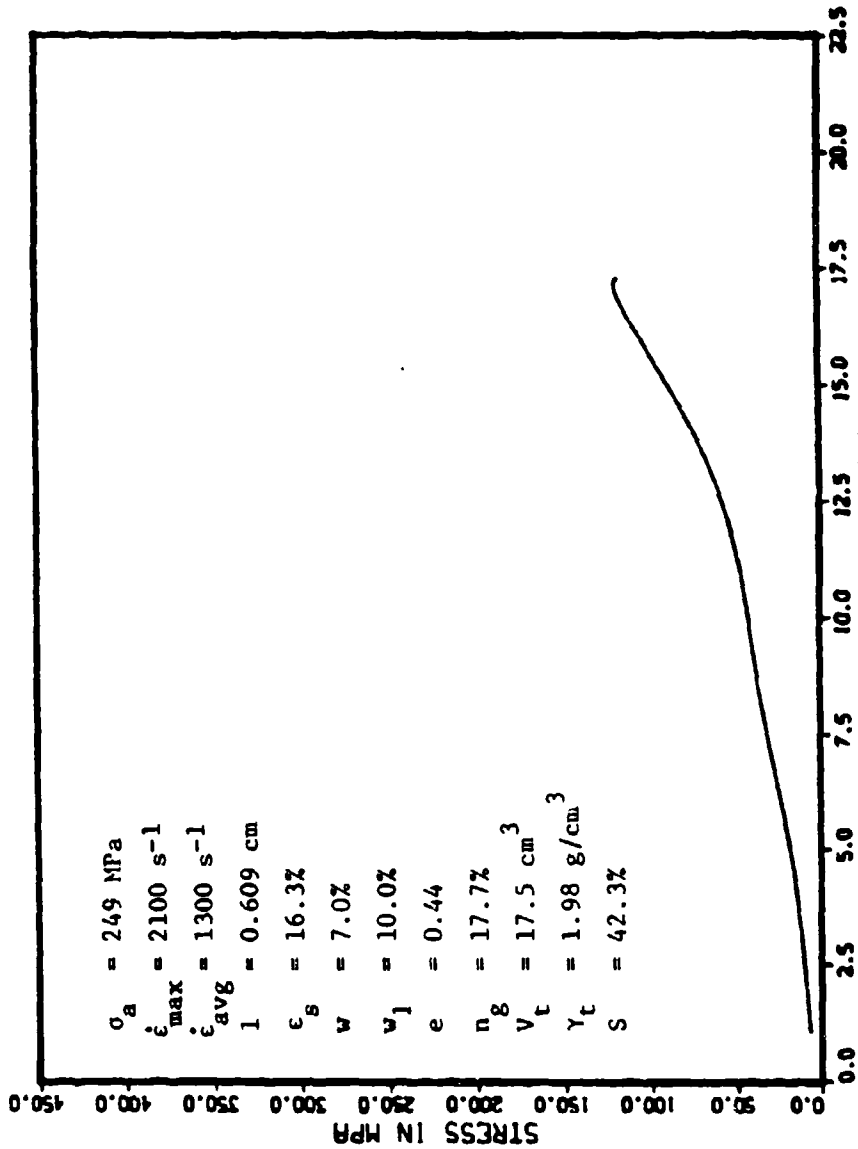

Figure I.38. Stress-strain response for experiment 139.

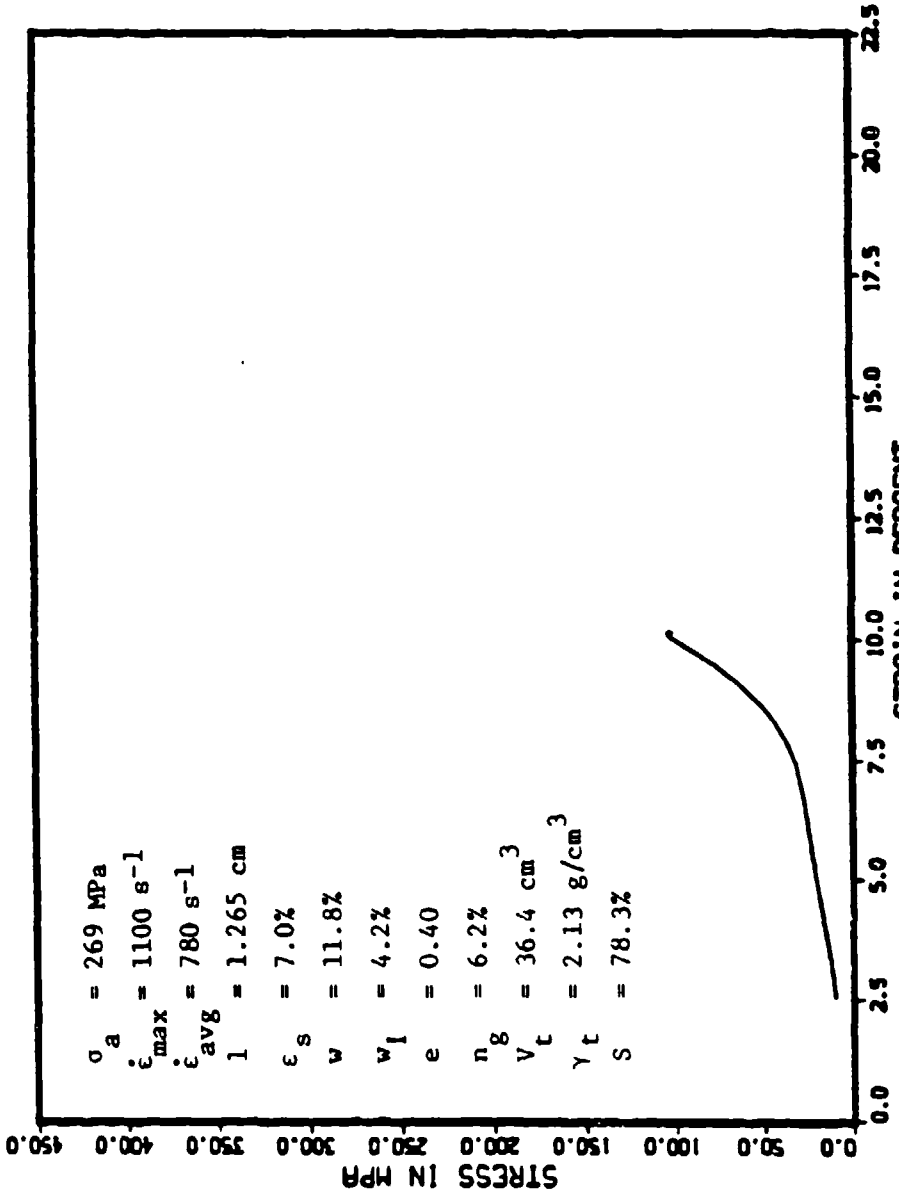

Figure I.39. Stress-strain response for experiment 145.

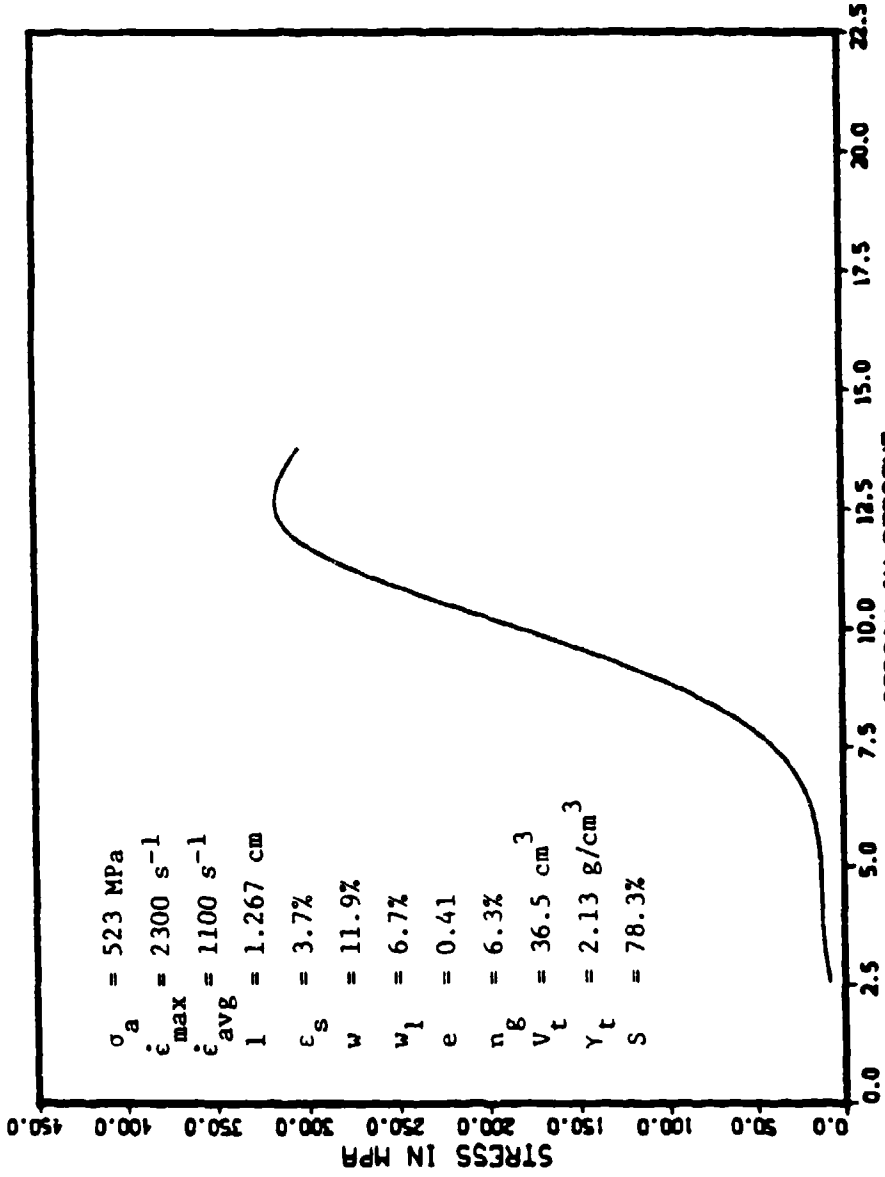

Figure I.40. Stress-strain response for experiment 146.

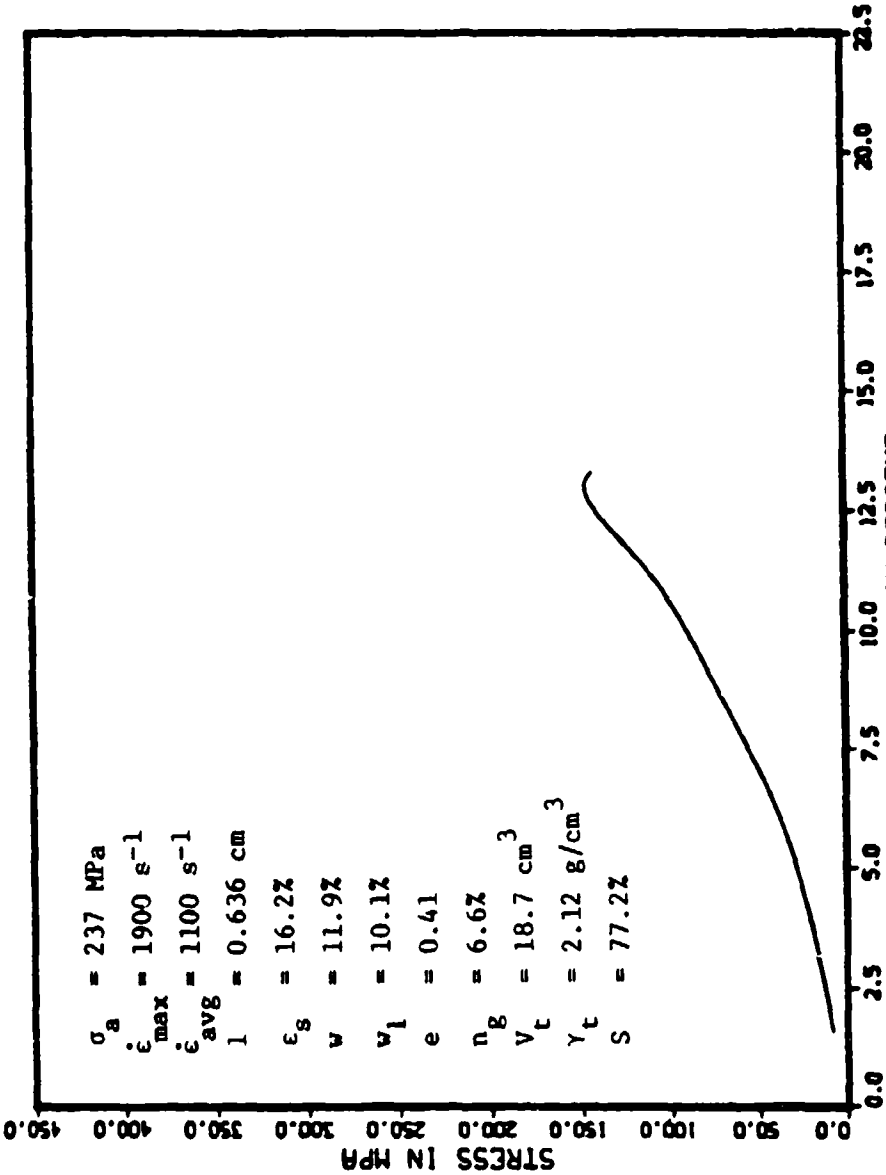

Figure I.41. Stress-strain response for experiment 147.

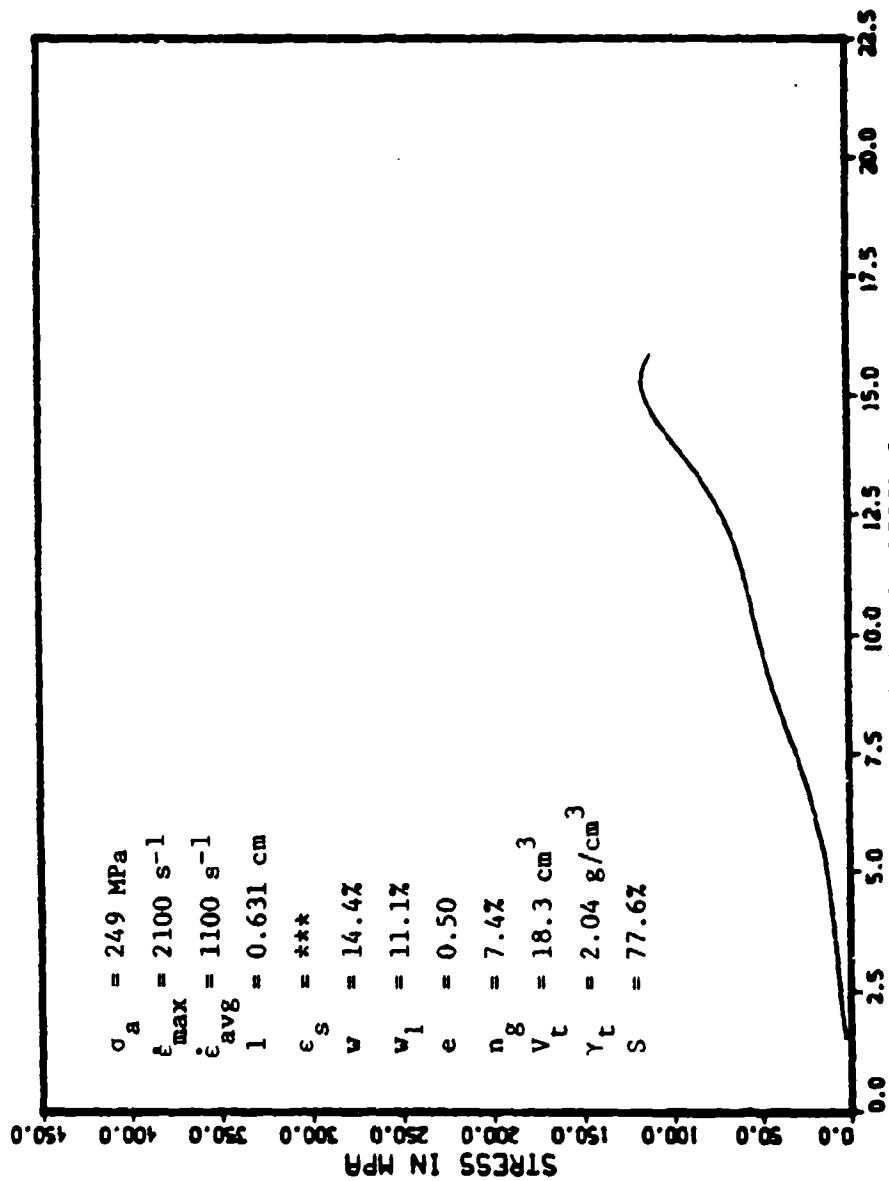

Figure I.42. Stress-strain response for experiment 148.

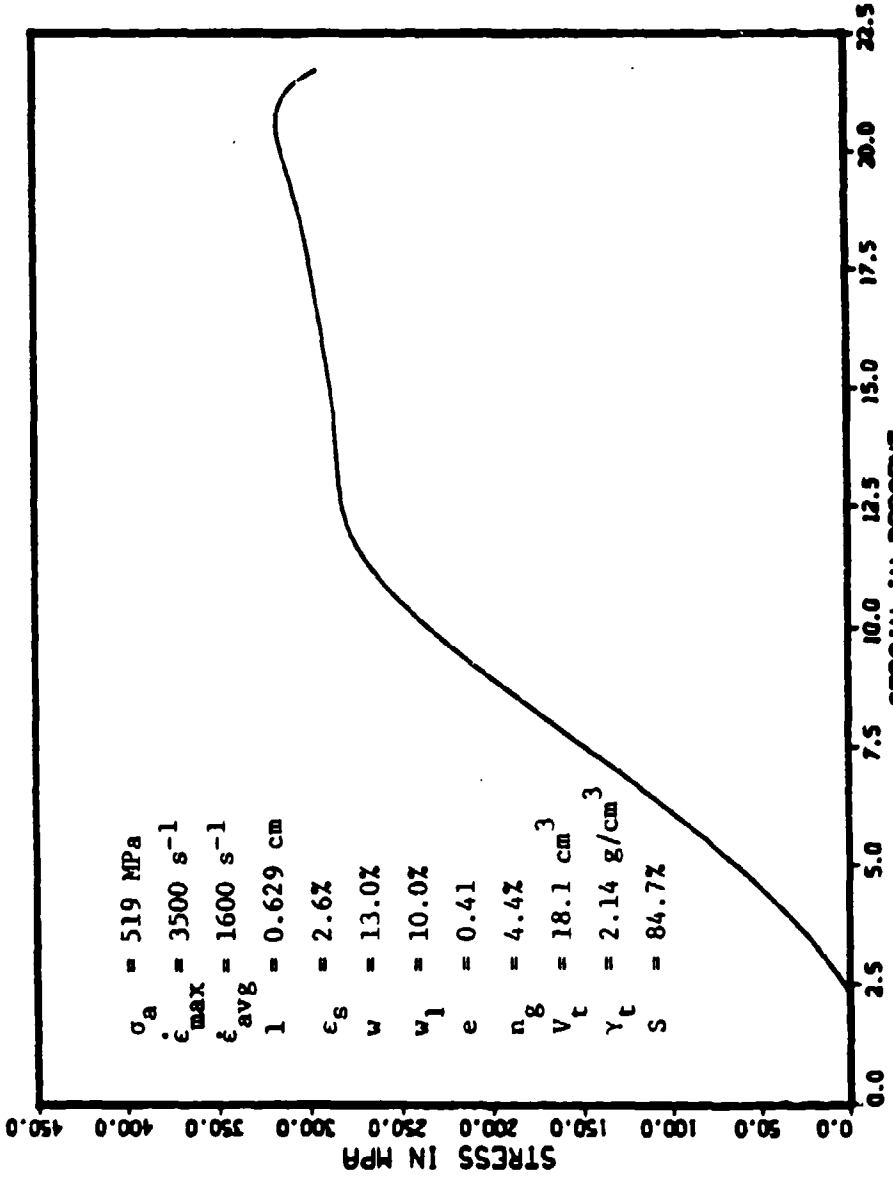

Figure I.43. Stress-strain response for experiment 162.

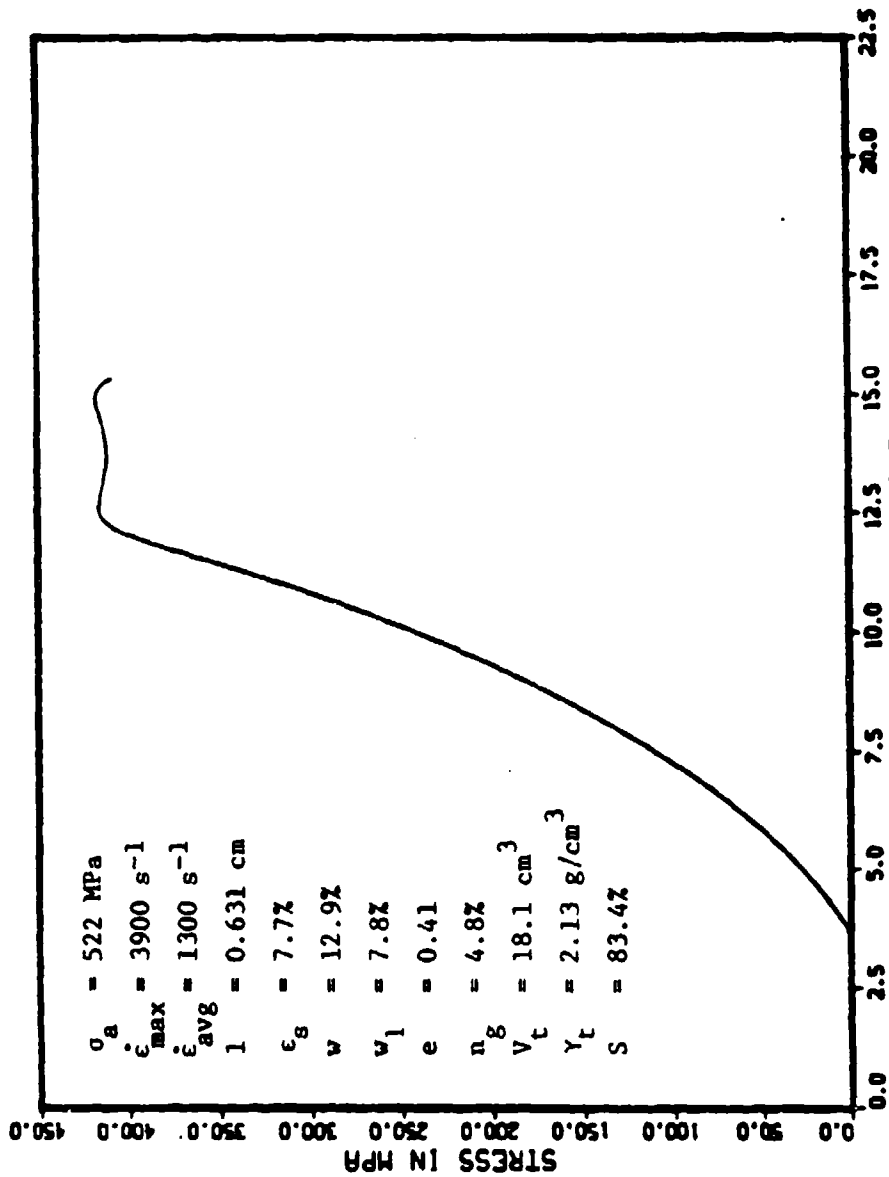

Figure I.44. Stress-strain response for experiment 163.

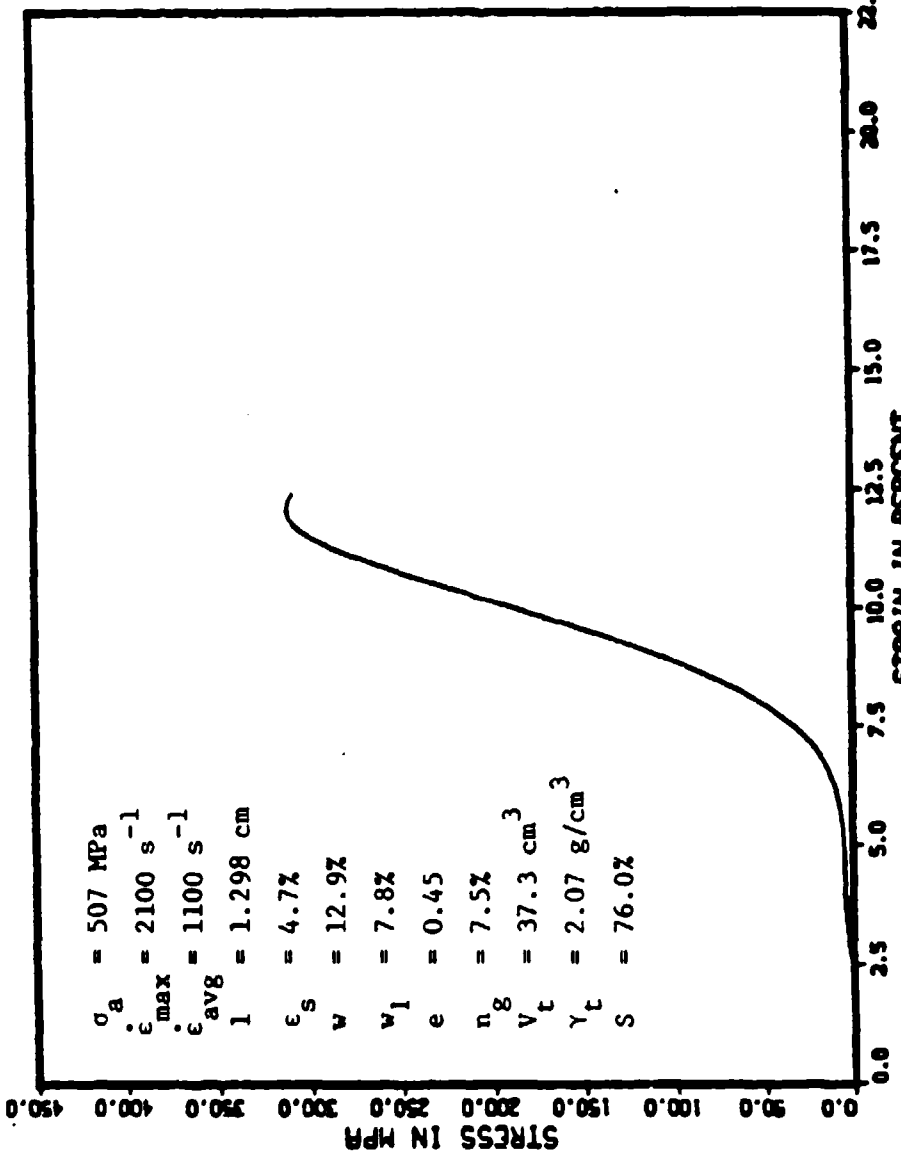

Figure I.45. Stress-strain response for experiment 164.

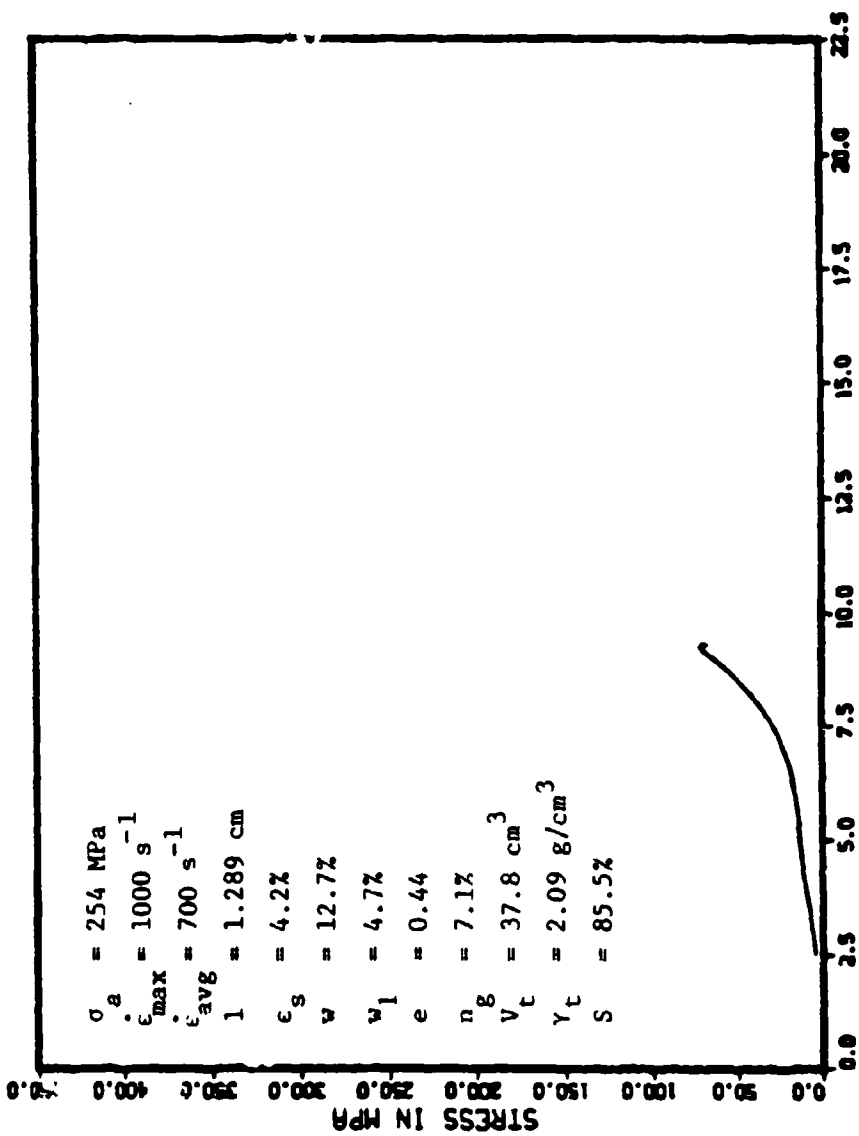

Figure I.46. Stress-strain response for experiment 165.

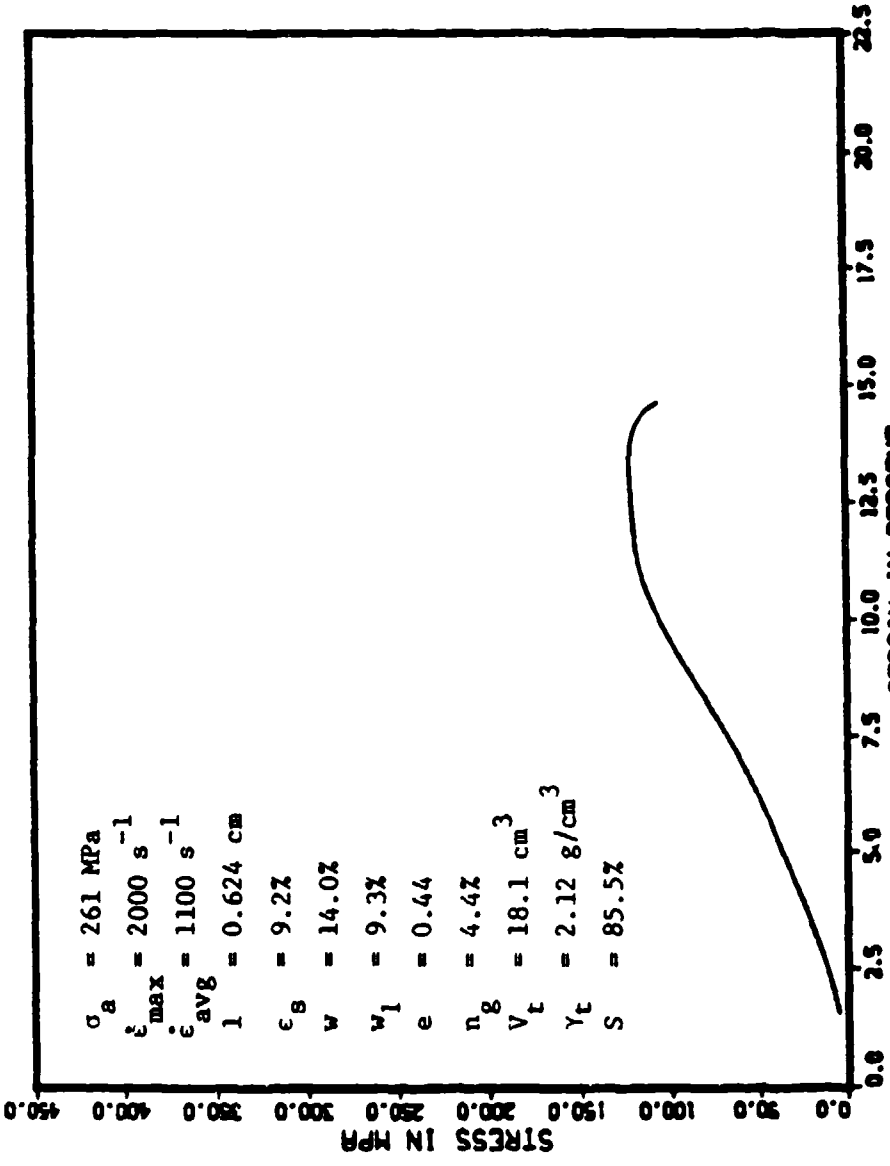

Figure I.47. Stress-strain response for experiment 166.

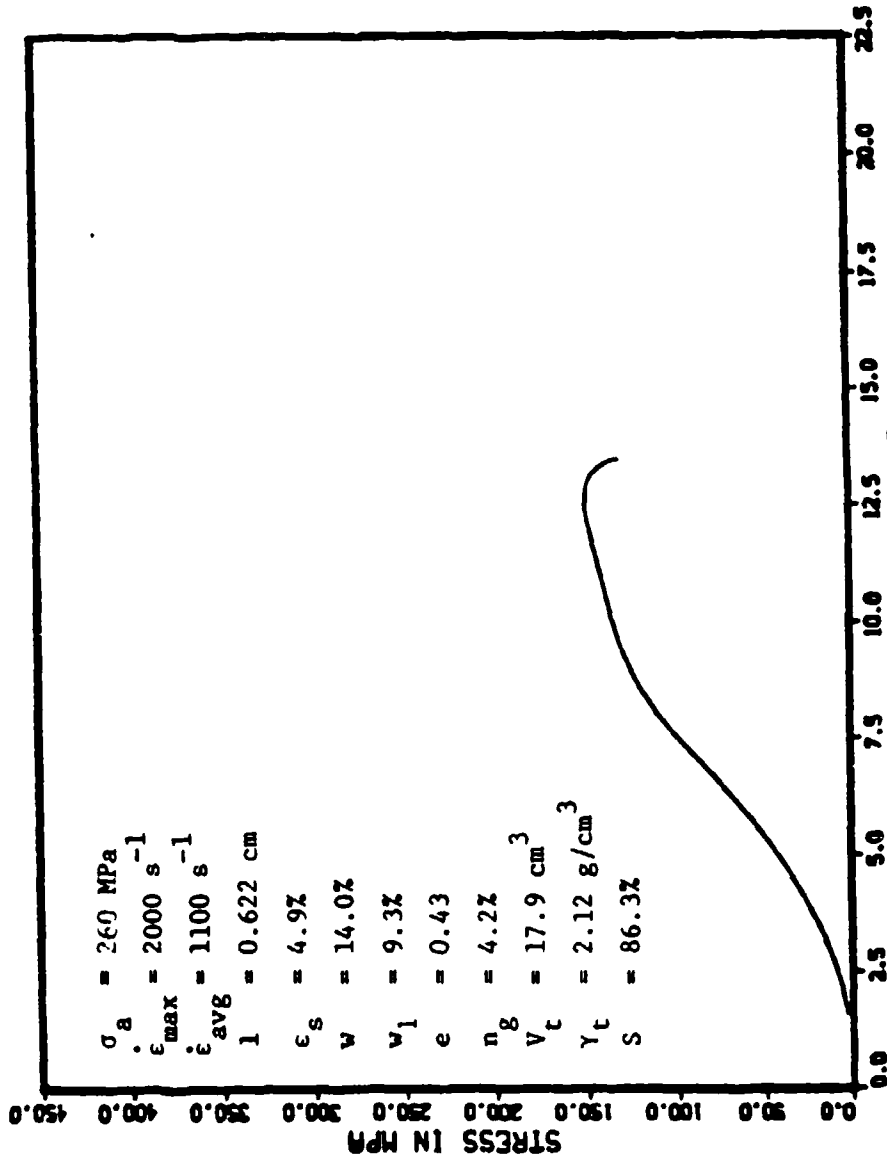

Figure I.48. Stress-strain response for experiment 167.

APPENDIX J

GROSS STRAIN CORRECTION

Due to the uncertainty in the evaluation of the strain contributions from factors discussed in section 6.4, a gross strain adjustment, to account for the excess between strain at peak stress, and the initial gas porosity has been computed. This was accomplished by plotting the difference between the strain at peak stress and the initial gas porosity against the average force felt by the specimen. The average force is computed as the peak stress multiplied by the area of the specimen. A linear regression line was then fit to the data for specimens prepared near the optimum compaction conditions. The linear regression line was computed with the dependent variable (Y) taken as the difference between the initial gas porosity and the strain at peak stress and the independent variable (X) taken as the maximum force felt by the specimen. The equation of the linear regression line is;

$$Y = 0.98X + 0.56 \ . \qquad \text{(J.1)}$$

The resulting plot is shown in figure J.1. The data used to prepare figure J.1 are presented in table J.1.

Using the regression line and the average force sustained by the specimen, a strain correction was computed for each specimen. The strain correction is added to the initial gas porosity and the sum compared to the strain at peak stress. The balance can then be used to

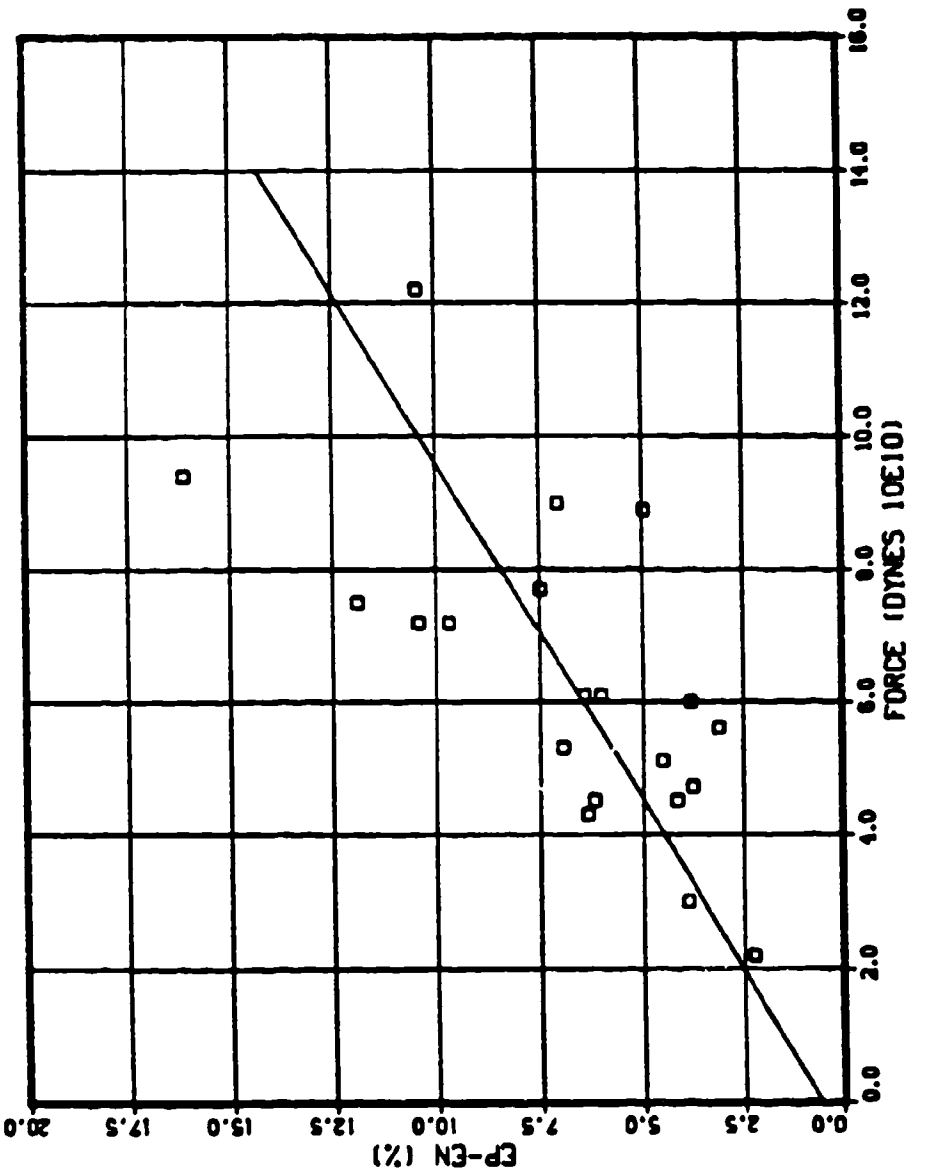

Figure J.1. Linear regression fit to data for specimens compacted at conditions near optimum.

Table J.1

Strain Correction Data

Experiment No.	Strain - Gas Porosity (%)	Force (dynes 10E10)
112	11.9	7.5
113	9.7	7.2
114	10.4	7.2
115	7.5	7.7
116	6.2	4.5
117	6.0	6.1
118	3.8	4.7
119	4.2	4.5
131	3.1	5.6
132	3.8	6.0
133	4.5	5.1
134	6.4	6.1
138	6.9	5.3
145	3.9	3.0
146	7.0	9.0
147	6.3	4.3
162	16.2	9.4
163	10.4	12.2
164	4.9	8.9
165	2.2	2.2

a) Strain is taken as the strain at peak stress.

gauge the success of the correction. The results of the correction procedure are tabulated in table J.2.

This procedure requires none of the assumptions made in the computations of strain contribution from moisture loss, pore water compression, or radial expansion. It is based solely on the peak stress sustained by the specimen. In addition, the strain contribution of soil loss is also included.

Table J.2

Strain Correction Results

Experiment No.	Gas Porosity (%)	Strain Correction (%)	Sum (%)	Strain at Peak Stress (%)	Balance (%)
112	7.91	7.87	15.78	19.79	4.01
113	7.73	7.67	15.40	17.40	2.00
114	9.21	7.61	16.82	19.60	2.78
115	10.55	8.07	18.62	18.03	-0.59
116	8.07	4.98	13.05	14.24	1.19
117	8.50	6.54	15.04	14.50	-0.54
118	10.25	5.18	15.43	14.06	-1.37
119	9.91	4.93	14.84	14.07	-0.77
131	9.57	6.10	15.67	12.68	-2.99
132	6.88	6.43	13.31	10.67	-2.64
133	8.02	5.52	13.54	12.52	-1.02
134	5.80	6.57	12.37	12.22	-0.15
138	4.86	5.75	10.61	11.80	1.19
145	6.23	3.51	9.74	10.12	0.38
146	6.26	9.41	15.67	13.30	-2.37
147	6.64	4.78	11.42	12.99	1.57
162	4.44	9.74	14.18	20.60	6.42
163	4.84	12.52	17.36	15.27	-2.09
164	7.49	9.28	16.77	12.43	-4.34
165	7.05	2.70	9.75	9.27	-0.48

REFERENCES

1) American Society for Testing and Materials, "Annual Book of Standards: Soil and Rock; Building Stones," Part 19, American Society for Testing and Materials, Philadelphia, Pennsylvania., 1982.

2) Bedsun, D. A., Summary of Geotechnical Testing and Material Models for Subsurface Soil Conditions at McCormick Ranch, Kirtland Air Force Base, New Mexico, NMERI 7.11-TA7-20, New Mexico Engineering Research Institute, University of New Mexico, Albuquerque, New Mexico, September 1983.

3) Bertholf, L. D. and Benzley, S. E., TOODY II - A Computer Program for Two Dimensional Wave Propagation, SC-RR-68-41, Sandia National Laboratory, Albuquerque, New Mexico, 1968.

4) Bertholf, L. D. and Karnes, C. H., "Two-Dimensional Analysis of the Split Hopkinson Pressuse Bar System," Journal of the Mechanics and Physics of Solids, Vol. 23, 1975, pp. 1-19.

5) Bhushan, B. and Jahsman, W. E., "Measurment of Dynamic Material Behavior Under Nearly Uniaxial Strain Conditions," International Journal of Solids and Structures, Vol. 14, 1978, pp. 739-753.

6) Brode, H. L., Airblast from Nuclear Bursts-Analytical Approximations, PSR Report 1419, Pacific Sierra Research Corporation, Los Angeles, California, 1984.

7) Brown, J. A., HSE-Division Review of SOP: 60-mm Split Hopkinson Pressure Bar System, Office Memorandum, Los Alamos National Laboratory, Los Alamos, New Mexico, October 17, 1983.

8) Calhoun, D. E. and Kraft, D. C., An Investigation of the Dynamic Behavior of a Partially Saturated Silt with Applications to Shock-Wave Propagation, AFWL-TR-65-176, Air Force Weapons Laboratory, Kirtland AFB, New Mexico, May 1966.

9) Chree, C., "The Equations of an Isotropic Elastic Solid in Polar and Cylindrical Coordinates, their Solutions and Applications," Transactions of the Cambridge Philosophical Society, Vol. 14, 1889, pp. 250-369.

10) Christensen, R. J., Swanson, S. R., and Brown, W. S., "Split-Hopkinson-bar Tests on Rocks under Confining Pressure," Experimental Mechanics, Vol. 12, No. 11, November, 1972, pp. 508-513.

11) Crawford R. E., Higgins, C. J., and Bultmann, E. H., The Air Force Manual for Design and Analysis of Hardened Structures, AFWL-TR-74-102, Air Force Weapons Laboratory, Kirtland AFB, New Mexico, October 1974.

12) Curtis, C. W., "Propagation of an Elastic Pulse in a Semi-Infinite Bar," in International Symposium on Stress Wave Propagation in Materials, N. Davids, Ed., Interscience, New York, 1960, pp. 15-43.

13) Dass, W. C. and Bratton, J. L., "Soil Element Model Evaluation Under Dynamic Loadings," in Symposium on the Interaction of Non-nuclear Munitions with Structures, U.S. Air Force Academy, Colorado, May 10-13, 1983.

14) Davies, E. D. and Hunter, S. C., "The Dynamic Compression Testing of Solids by the Method of the Split Hopkinson Pressure Bar," Journal of the Mechanics and Physics of Solids, Vol. 11, 1963, pp. 155-179.

15) Davies, R. M., 1948. "A Critical Study of the Hopkinson Pressure Bar," Philosophical Transactions of the Royal Society of London, Series A, Vol. 240, January, 1948, pp. 375-457.

16) Fletcher, E. B. and Poorooshab, H. B., "Response of a Clay Sample to Low Magnitude Loads Applied at a High Rate," in Proceedings of the International Symposium on Wave Propagation and Dynamic Properties of Earth Materials, University of New Mexico Press, Albuquerque, New Mexico, August 1968, pp. 781-786.

17) Follansbee, P. S. and Frantz, C. E., "Wave Propagation in the Split Hopkinson Pressure Bar," Journal of Engineering Materials and Technology, Vol. 105, January, 1983, pp. 61-66.

18) Follansbee, P. S., and C. E. Frantz, "Experimental Techniques with the Split-Hopkinson Pressure Bar," in High Energy Rate Fabrication, Book No. H00318, ASME, I. Berman and J. W. Schroeder, Ed., 1984, pp. 229-236.

19) Gaffney, E. S. and Brown, J. A., Dynamic Material Properties for Dry CARES Alluvium, LA-UR-84-3795, Los Alamos National Laboratory, Los Alamos, New Mexico, 1984.

20) Gaffney, E. S., J. A. Brown, and C. W. Felice, "Soils as Samples for the Split Hopkinson Bar," in 2nd Symposium on the Interaction of Non-nuclear Munitions with Structures, Panama City Beach, Florida, April 15-18, 1985.

21) Green, S. J. and Perkins, R. D., Uniaxial Compression Tests at Strain Rates from 10^{-3}/sec. to 10^{3}/sec. on Three Geologic Materials, DASA-2199, Defense Atomic Support Agency, Washington, D.C., January, 1969.

22) Hauser, F. E., Simmons, J. A., and Dorn, J. E., "Strain Rate Effects in Wave Propagation," in Response of Metals to High Velocity Deformation, Metallurgical Society Conferences, Vol. 9, P. G. Shewmon and V. F. Zacky, Ed., Interscience, New York, 1961, pp. 93-110.

23) Hendron, A. J. and Auld, H. E., The Effect of Soil Properties on the Attenuation of Airblast-Induced Ground Motion, in Proceedings of the International Symposium on Wave Propagation and Dynamic Properties of Earth Materials, University of New Mexico Press, Albuquerque, New Mexico, August, 1968, pp. 29-47.

24) Hodge, K. G. and Wasley, R. J., "Dynamic Compressive Behavior of Various Foam Materials," in High Speed Testing, Vol. 6, Interscience, New York, 1969, pp. 97-109.

25) Hopkinson, B., 1914. "A Method of Measuring the Pressure Produced in the Detonation of High Explosives or by the Impact of Bullets," Philosophical Transactions of the Royal Society of London, Series A, Vol. 213, 1914, pp. 437-456.

26) Jackson, J. G. Jr., Factors that Influence the Development of Constitutive Relations, Mics. Paper No. 4-980, U.S. Army Engineer Waterways Experiment Station, Vicksburg, Mississippi, July, 1968.

27) Jackson, J. G. Jr., Ehgott, J. Q., and Rohani, B., "Loading Rate Effects on Compressibility of Sand," Journal of the Geotechinal Engineering Division, ASCE, Vol. 108, No. GT8, August, 1980, pp. 839-852.

28) Karman, T. v., On the Propagation of Plastic Deformation in Solids, National Defense Research Committee Report No. A-29, 1942.

29) Kolsky, H., "An Investigation of the Mechanical Properties of Materials at Very High Rates of Loading," Proceedings of the Physical Society, Section B, Vol. 62, 1949, pp. 676-700.

30) Kolsky, H., Stress Waves in Solids, Dover Publications, New York, 1963.

31) Lindholm, U. S., "Some Experiments with the Split Hopkinson Pressure Bar," Journal of the Mechanics and Physics of Solids, Vol. 12, 1964, pp. 317-335.

32) Mazanti B. B., and Holland, C. N., Study of Soil Behavior Under High Pressure, Contract Report S-70-2, U.S. Army Engineer Waterways Experiment Station, Vicksburg, Mississippi, February 1970.

33) Nagy, A. and Muelenhaupt, H. J., Description and Operating Manual for the 2.375 Inch Split Pressure Bar System for Dynamic Material Testing in Compression, Contract No. N68-6525G-1, Prepared for the In Situ Science Group, Los Alamos National Laboratory, Los Alamos, New Mexico, by The Department of Materials Sciences, Southwest Research Institute, 1983.

34) Nelson, I., Baron M. L., and Sandler, I, "Mathematical Models for Geological Materials for Wave Propagation Studies," in Shock Waves and the Mechanical Properties of Solids, Syracuse University Press, Syracuse, New York, 1971.

35) Pochhammer, L., "On the Propagation Velocities of Small Oscillations in an Unlimited Isotropic Circular Cylinder," Journal für die Reine und Angewandte Mathematik, Vol. 81, 1876, pp. 324-326.

36) Rand, J. L., "An Analysis of the Split Hopkinson Pressure Bar," dissertation, presented to the University of Maryland, in 1967, in partial fulfillment of the requirements for the degree of Doctor of Philosophy.

37) Rubin, D. and Sandler, I., Development of a High Pressure CAP Model for Use in Computations of Ground Shock from Subsurface Explosions, Contract Report S-77-2, U.S. Army Engineer Waterways Experiment Station, Vicksburg, Mississippi, July 1977.

38) Rinehart, J. S., Stress Transients in Solids, HyperDynamics, Santa Fe, New Mexico, 1975.

39) Seely, F. B. and Smith, J. O., Advanced Mechanics of Materials, John Wiley and Sons, Inc., New York, 1959.

40) Schindler L., "An Improved Facility for Testing Soils in One-Dimensional Compression," in Proceedings of the International Symposium on Wave Propagation and Dynamic Properties of Earth Materials, University of New Mexico Press, Albuquerque, New Mexico, August, 1968, pp. 847-860.

41) Selby, S. M. ed., Standard Mathematical Tables, 23rd ed., CRC Press, Inc., Cleveland, Ohio, 1975.

42) Sydney, C. P., Jr., ed., Handbook of Physical Constants, The Geological Society of America, Mem. 97, 1966.

43) Taylor, G. I., "The Plastic Wave in a Wire Extended by an Impact Load," in The Scientific Papers of G. I. Taylor, Vol. 1, G. Batchelor, Ed., Cambridge University Press, 1958, pp. 467-479.

44) Timoshenko, S. P. and Goodier, J. N., Theory of Elasticity, 3rd ed., McGraw-Hill Book Company, New York, 1970.

45) Wasley, R. J., Stress Wave Propagation in Solids An Introduction, Marcel Dekker, Inc., New York, 1973.

46) Whitman, R. V., The Response of Soils to Dynamic Loadings, Contract Report No. 3-26, U.S. Army Engineer Waterways Experiment Station, Vicksburg, Mississippi, May 1970.

47) Wiley C. R., and Barrett, L. C., Advanced Engineering Mathematics, McGraw-Hill Book Company, New York, 1982.

48) Yeung Wye Kong, Y. C. T., B. Parsons, and B. N. Cole, 1974. "The Dispersive Nature of a Hopkinson Pressure Bar in Material Property Tests," in Mechanical Properties at High Rates of Strain, Institute of Physics Conference Series, No. 21, 1974, pp. 33-47.

49) Zukus, J. A., T. Nicholas, H. F. Swift, L. B. Greszczuk, and D. R. Curran, Impact Dynamics, John Wiley and Sons, New York, 1982.